8-SUBSTITUTED-2'-DEOXYGUANOSINES AS INTERNAL PROBES FOR DNA FOLDING AND ENERGY TRANSFER

Dissertation

zur

Erlangung der naturwissenschaftlichen Doktorwürde

(Dr. sc. nat.)

vorgelegt der

Mathematisch-naturwissenschaftlichen Fakultät

der

Universität Zürich

von

Anaëlle Dumas

von

Vuisternens-devant-Romont FR

Promotionskomitee

Prof. Dr. Nathan W. Luedtke (Vorsitz)

Prof. Dr. Roland K. O. Sigel

Prof. Dr. Jay S. Siegel

Zürich, 2011

Die vorliegende Arbeit wurde von der Mathematisch-naturwissenschaftlichen Fakultät der Universität Zürich im Herbstsemester 2011 als Dissertation angenommen.

Promotionskomitee:	Prof. Dr. Nathan W. Luedtke (Vorsitz)
	Prof. Dr. Roland K. O. Sigel
	Prof. Dr. Jay S. Siegel

To my family

Table of contents

Preface

Secondary structures adopted by nucleic acids might play important roles in diverse cellular processes. Developing efficient tools for their detection can provide means to elucidate their biological roles. This work presents our efforts to develop fluorescent nucleobase analogs, 8-substituted-2'-deoxyguanosines, that can serve as internal probes for the detection of G-quadruplexes structures. This dissertation consists of 8 chapters, including 2 introductory chapters, 5 chapters presenting research results and one chapter of experimental procedures.

An overview of relevant aspects of DNA chemistry and conformations is presented in *Chapter 1*. The reader is introduced to some general characteristics of G-quadruplex structures and to strategies available for fluorescent labeling of nucleic acids. In *Chapter 2* the spectroscopic properties and potential applications of nearly all fluorescent purine analogs reported to date are reviewed.

Our strategy towards the development of new fluorescent purine analogs with improved characteristics focuses on the elaboration of 8-substituted-2'-deoxyguanosines. In *Chapter 3* the synthetic strategy developed to prepare these compounds is described. Further photophysical and conformational analysis of the resulting fluorescent nucleosides are presented in this chapter.

The structural impact and fluorescence properties of the 8-substituted guanosine derivative 8-(2-pyridyl)-2'-deoxyguanosine (**2PyG**) upon its incorporation into G-quadruplex and duplex structures is presented in *Chapter 4*. A comparative study with the commonly used fluorescent nucleobase 2-aminopurine is presented. These results were published as part of: Dumas, A. and Luedtke, N. W. *ChemBioChem,* **2011**, *12*, 2044-2051.

2PyG can act as an effective energy acceptor for unmodified guanine residues in oligonucleotides. In *Chapter 5,* the use of **2PyG** to quantify this phenomenon in G-rich sequences is presented. This property was exploited to detect DNA folding, and elucidate the direct role played by cations bound in the central cavity of G-quadruplex structures. Highly efficient energy transfer reactions are detected in G-quadruplex structures but not in

duplex or single stranded DNA. Parts of these results were published in: Dumas, A. and Luedtke, N. W. *J. Am. Chem. Soc.,* **2010**, *132*, 18004-18007.

In *Chapter 6* two alternative fluorescent guanosine analogs, 8-(2-phenylethenyl)-2'-deoxyguanosine (**StG**) and 8-[2-(pyrid-4-yl)-ethenyl]-2'-deoxyguanosine (**4PVG**) for the quantification of energy transfer and detection of G-quadruplex folding are introduced. These probes provide some potential advantages over **2PyG**. Parts of these results were published in: Dumas, A. and Luedtke, N. W. *Nucleic Acids Res.,* **2011**, *39*, 6825-6834.

2PyG is unique among all reported fluorescent purine analogs as it has the ability to selectively bind metals. *Chapter 7* describes how this property can be exploited to site-specifically localize metal ions at the *N7* position of guanosine residues.

Detailed experimental procedures are described in *Chapter 8*. An extensive collection of circular dichroism and fluorescence spectra is provided in the Appendixes section.

Acknowledgements

The realization of this work was made possible by the essential contributions of many people who accompanied and supported me all along the way. In particular, I would like to express my profound gratitude to the following Ladies and Gentlemen.

First, I thank my mentor, Prof. Dr. Nathan W. Luedtke, for his guidance and support along my Ph.D. thesis. His outstanding involvement and continuous enthusiasm strongly contributed to the fruitful realization of this project. I further thank Prof. Dr. Jay S. Siegel and Prof. Dr. Roland K. O. Sigel for serving on my thesis committee, as well as Prof. Dr. Shana J. Sturla for her expert review of my thesis. I am grateful to Professor Andrea Vasella, Dr. Fabio De Giacomo, and Dr. Thomas Steinlin for providing 8-substituted guanines for initial fluorescence studies. I would like to thank the Swiss National Science Foundation, the University of Zürich and CMSZH, for the generous financial support.

Besides numerous fruitful discussions, the present and past members of the Luedtke group, especially Martin Seyfried, Bala Vummidi, Sarah Hentschel, Anne Neef, Guillaume Mata, Joëlle Räber, Olivia Schmidt and David Oesch were responsible for the pleasant working atmosphere that surrounded me during my thesis. I would like to especially thank Dr. Jawad Alzeer for his precious advice and help in the beginning of the project. Numerous members of the Organic Chemistry Institute, especially Dr. Silvan Eichenberger and Dr. Pascal Bisegger contributed to the enjoyable time spent in- and outside of the University of Zurich. I would like to thank Dr. Laurent Bigler, for the loud and animated discussions around coffee, and the whole MS team to give me access to some of their instruments and especially Urs Stalder for his help and availability in urgent matters.

I direct my further thanks to Jean-Christophe Prost, Julien Réhault, Michaël Méret, “Les trognes”, Séverine Riggaz, Geneviève Rydlo and Isabelle Roth for their friendship. Their encouragement and plenty of funny moments spent together, have been indispensible for the realization of this work.

I am very grateful to my family, especially my parents, André and Sonia Dumas, my sister Mélanie Dumas as well as my grand-parents Marcel and Margherita Rion for their inestimable support from the very beginning and for giving me the means to realize my personal ambition, and last but certainly not least, Jan Wurzbacher for all his support, encouragement and understanding during this adventure.

8-Substituted-2'-Deoxyguanosines as Internal Probes for DNA Folding and Energy Transfer

CHAPTER 1

Introduction

1.1 DNA structures and functions

Deoxyribonucleic acid (DNA) is a linear polymer constructed from four deoxyribonucleotide units of variable sequences. Monomeric deoxyribonucleotide units consist of: (1) a nitrogenous base, (2) a pentose and (3) a phosphate. Four different nitrogenous bases define the DNA sequence: adenine (A), guanine (G), cytidine (C) and thymine (T). Each nucleobase is connected to a 2-deoxyribose sugar through a β-N-glycosidic bond, forming a nucleoside. Phosphate units bridge the nucleosides through phosphodiester bonds at the 5′-OH and 3′-OH position of the sugars, forming a phosphodiester backbone that is negatively charged at pH 7.

DNA is responsible for the storage and transfer of the genetic information known as the central dogma of biology.[1] In living systems, DNA is transcribed to RNA, which serves as an information messenger that is finally translated into proteins. Ultimately, the linear sequence formed by the four nucleobases encodes for the information necessary for the construction and function of every living organism on Earth.

In 1953, *Watson* and *Crick* described the structure of B-form duplex DNA, consisting of two anti-parallel DNA strands twisted about each other to form a right-handed double helix defined by a minor and a major groove. The negatively charged phosphate backbone points to the outside of the coil, whereas the nitrogenous bases stack on the top of each other in the center and interact in a specific pattern: guanine binds to cytidine through three hydrogen bonds, and adenine forms two hydrogen bonds with thymine. These two sets of complementary nucleobases form the so-called "*Watson & Crick* base pairs" (Figure 1.1 A).

The *Watson & Crick*'s model of duplex DNA inspired our mechanistic understanding of the replication and flow of genetic information.[1] Since then, DNA has been regarded by most as a uniform double helix and a passive library of genes. DNA is however a highly dynamic macromolecule. In addition to the double helical conformations described in the 1950's, it can fold into a variety of hairpin, triplex, G-quadruplex, and i-motif structures (Figure 1.2) held together through non-canonical base interactions (Figure 1.1 B).[2,3] Recent evidence suggests that non-duplex DNA structures may play a direct role in regulating gene expression and in important biological regulation processes.[4-6]

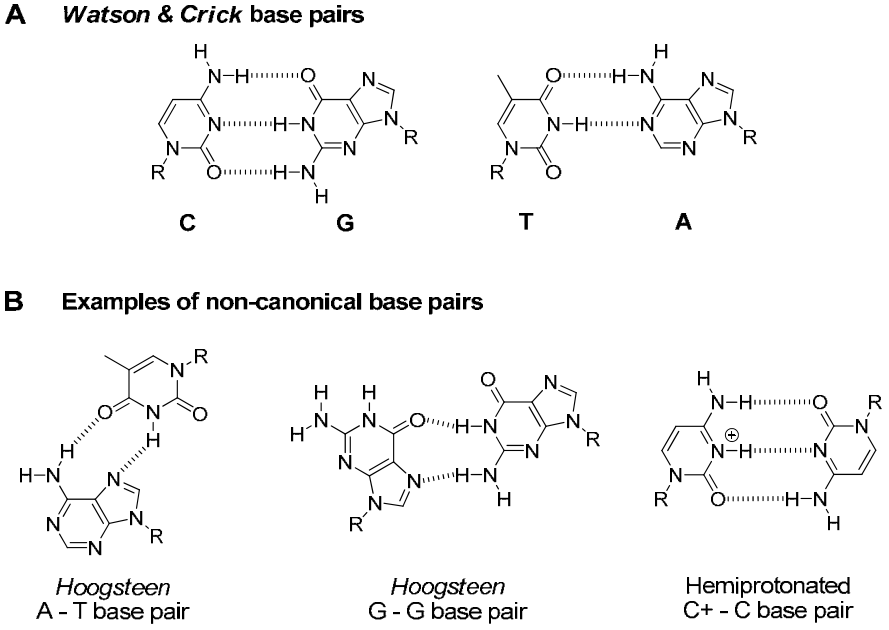

Figure 1.1: (A) Canonical *Watson & Crick* base pairs, (B) selected examples of non-canonical base pairs. R = 2'-deoxyribose.

Interestingly, protein-coding sequences represent only 2% of the human genome. The other 98%, known to carry among others pseudogenes or unfunctional copies of genes, were long considered as "garbage" or "junk" DNA.[7] This term is however outdated nowadays and strong evidence shows that an important part of the non-coding genome is functional, playing regulatory roles in the control of gene expression.[7] Non-duplex DNA structures possibly mediate these functional outcomes by modulating key protein-DNA interactions. For these reasons, the elucidation of the structure-function relationship of the non-coding portion of the genome and the development of new methods for the detection of DNA folding *in vivo* has become an important area of scientific investigation.

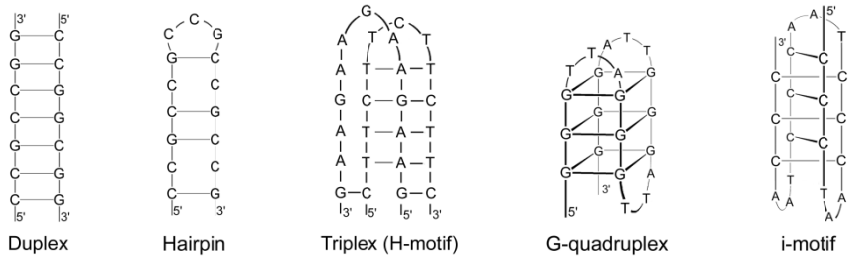

Figure 1.2: Schematic representation of selected secondary DNA structures.

1.2 G-quadruplexes

G-quadruplexes are characterized by vertical stacking of G-tetrads, arising from the association of four guanines into a cyclic *Hoogsteen* hydrogen-bonding arrangement. In this assembly, each guanine interacts through hydrogen bonds with its neighbor involving both its *Watson & Crick* and *Hoogsteen* face (*N*1 to O^6 and N^2 to *N*7) (Figure 1.3).[8,9] The formation of G-quadruplexes is promoted by monovalent cations, such as potassium or sodium coordinated to the O^6-guanine carbonyls positioned within the center of the tetrads and/or molecular crowding agents.[10,11] DNA G-quadruplexes are highly polymorphic and their structures are influenced by numerous factors such as the DNA sequence, the ions present in solution, temperature and pH. Different families of G-quadruplexes can be distinguishing according to basic geometrical factors. G-quadruplexes can form in an intra- or intermolecular fashion, and oligonucleotides containing one, two or four G-streches can form tetrameric, dimeric or monomeric G-quadruplexes respectively. The G-tracts can have parallel or anti-parallel orientations with respect to each other, and guanine residues can adopt *syn* or *anti* glycosidic bond conformations. The connecting loops have variable length and topologies, depending on the directionality of the G-tracts that they connect. G-quadruplex topologies are defined by the combination of strand directionality, loop connectivity and groove dimensions with widths and depths determined by the overall geometrical factors described (Figure 1.3).[3]

Interestingly, G-quadruplex structures display particular photophysical characteristics as compared to single stranded or duplex DNA. These include enhanced quantum yields ($\Phi_{\text{G-quadruplex}} = 4 \times 10^{-4}$; $\Phi_{\text{Duplex}} = 10^{-4}$), photo-excited lifetimes ($\tau_{f(\text{G-quadruplex})} = \sim 10$ ps; $\tau_{f(\text{Duplex})} = \sim 1$ ps) and energy transfer properties.[12-15] At the onset of our work, the origins of these unusual properties were not strictly elucidated.

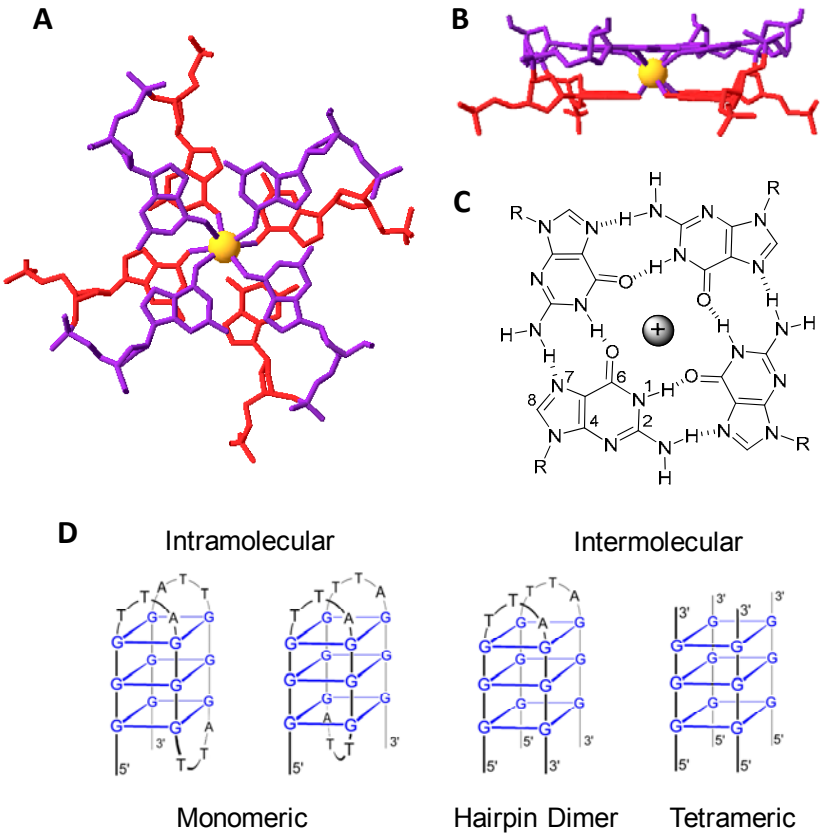

Figure 1.3: Two stacked G-tetrads from the crystal structure of the human telomeric sequence with a K^+ ion bound in the central channel, top view (A) and side view (B).[16] (C) Schematic structure of a cation-bound G-tetrad showing hydrogen bonding (R = DNA), (D) Schematic representation of different G-quadruplex topologies. From left to right, monomeric chair and basket, hairpin dimer, tetrameric G-quadruplex.

Although G-quadruplexes were considered for many years as structural curiosities, evidence is accumulating for their presence in genomic DNA and RNA.[17] As many as 376'000 putative G-quadruplex-forming motifs $(G_{3+}N_{1-7})_{4+}$ (where N = any base) are dispersed throughout the human genome.[18,19] Systematic algorithmic searches of bacterial and human genomes for guanine-rich tracts discovered an underrepresentation of these G-quadruplex forming sequences in tumor-suppressor genes and open reading-frames but an overabundance of these sequences in the promoter regions of proto-oncogenes and at the 3' telomeric ends of chromosomes (telomeres).[20,21] While the exact biological relevance of these structures remains an open question, DNA sequences with the ability to fold into G-quadruplex structures have been implicated in regulating gene transcription,[4,20,21] recombination,[22] chromosome stability,[23-25] and programmed cell death.[26]

Ligands that can stabilize G-quadruplexes potentially forming in the promoter regions of oncogenes or at the telomeric end of chromosomes are current targets of anti-cancer drug design.[5,27,28] Telomerase is an enzyme that plays a major role in maintaining cellular immortality by catalyzing telomere extension. Telomerase is upregulated in approximately 85% of human cancer cells.[29] Evidence shows that the folding of telomeres in non-linear G-quadruplex structures can inhibit telomerase activity (Figure 1.4). The stabilization of G-quadruplex structures by high affinity ligands could enhance the inhibition of telomerase *in vivo* and lead to cellular senescence.[25] Similarly, the stabilization of G-quadruplexes in promoter regions could inhibit oncogene transcription (Figure 1.4). For example, a small molecule targeting putative G-quadruplexes in the MYC proto-oncogene has been shown to inhibit transcriptional activity, encouraging the development of more selective G-quadruplex ligands.[5,30,31]

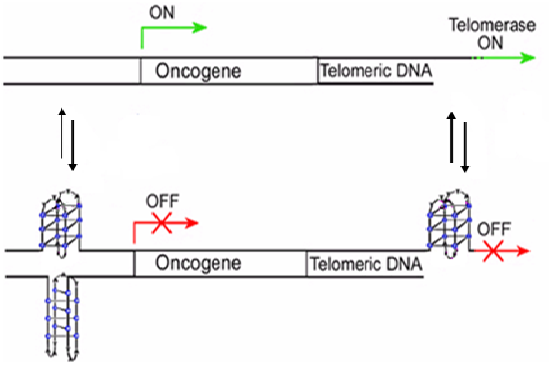

Figure 1.4: Schematic representation of the potential roles played by G-quadruplexes in the control of oncogene transcription (left) and telomerase inhibition (right).

Although there is rapidly accumulating indirect evidence for G-quadruplex structures as anti-cancer targets, there is still no direct proof for the existence of these structures in living human cells.[17] Immunostaining experiments have demonstrated the existence of G-quadruplexes *in vivo* in ciliate cells,[32] however, due to low telomere abundance, similar conclusions cannot yet be drawn for human cells, and remain an active topic of investigation. This, in combination with the numerous potential cellular roles of G-quadruplexes, strongly encourages the development of direct techniques for the sensitive and specific detection of these structures *in vitro* and *in vivo*.

1.3 *Fluorescent probes for the detection of nucleic acids folding*

A wide variety of biophysical techniques have been used to characterize DNA folding *in vitro*. These include NMR,[33-35] circular dichroism,[36] UV absorption,[37,38] X-ray crystallography,[16] FRET[39-41] and immunostaining.[32] However, most of these methods require pure DNA samples and are not compatible with conformational analyses in living cells. Fluorescence phenomena enable powerful and readily accessible technologies for probing biomolecule folding and activity.[42] Fluorescence spectroscopy benefits from excellent sensitivity, versatility, is fast, easily accessible and straightforward. Strategic labeling in combination with fluorescence microscopy can lead to biomolecule visualization in systems as complex as living cells or organisms.

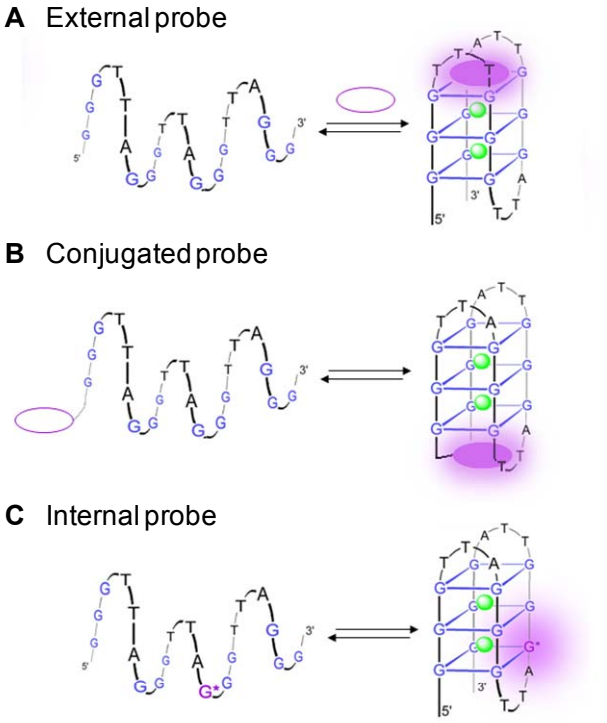

Figure 1.5: Schematic representation of fluorescence labeling strategies illustrated for G-quadruplex detection: (A) Non-covalently bound external probe, (B) conjugated external probe, (C) internal probe.

In the context of nucleic acids, the poor intrinsic fluorescence of native nucleobases requires the implementation of fluorescent labeling strategies for DNA and RNA. Three main classes of fluorescent probes will be presented: (A) external probes, not covalently linked to the nucleic acids, (B) conjugated probes, attached to nucleic acids *via* a covalent linker and (C) internal probes (Figure 1.5).

1.3.1 External probes

As a result of complementary stacking, hydrogen bonding and/or electrostatic interactions, exogenous fluorescent dyes can specifically recognize certain DNA structures. Intercalating agents such as ethidium bromide and oxazole yellow, as well as DNA groove binders such as 4',6-diamidino-2-phenylindole (DAPI) and Hoechst derivatives are commonly used for the specific visualization of duplex DNA in gel electrophoresis and cell microscopy. More recently, small molecules that can end-stack onto G-tetrads were identified as selective "turn-on" fluorescent probes for G-quadruplexes.[43,44] Fluorescent antibodies raised against specific DNA structures were also exploited as external probes for G-quadruplex recognition.[32] While fluorescence spectroscopy has the potential for conformational analyses *in vivo*, techniques involving high affinity external and conjugated probes can perturb the conformational preference of the DNA itself.[40,45,46]

1.3.2 Conjugated probes

Fluorescent moities can also be covalently linked outside the base stack, at the end or within the oligonucleotides. Many such fluorophores are commercially available and include fluorescein, boron-dipyrromethene (BODIPY), coumarin and cyanine dye derivatives. These probes are usually very bright and therefore useful for nucleic acids visualization in fluorescence microscopy as well as single-molecule experiments. *Förster* resonance energy transfer (FRET) probes and exciton pairs covalently-linked to nucleic acids can report approximate distances and provide constraints of global structural changes and DNA folding. Large probes such as pyrenes or FRET pairs like fluorescein / rhodamine derivatives were recently used for the characterization of G-quadruplex folding.[39-41,47] Data interpretation in these systems however is typically limited to large changes in probe-to-probe distances.

1.3.3 Internal probes

Internal probes are small fluorescent molecules linked to a 2-deoxyribose or ribose moiety and incorporated directly into the base-stacking interactions of folded nucleic acids thereby replacing a natural nucleobase. These fluorophores show a vast structural diversity and their impact on the structure and stability of the modified oligonucleotides is highly variable.[42]

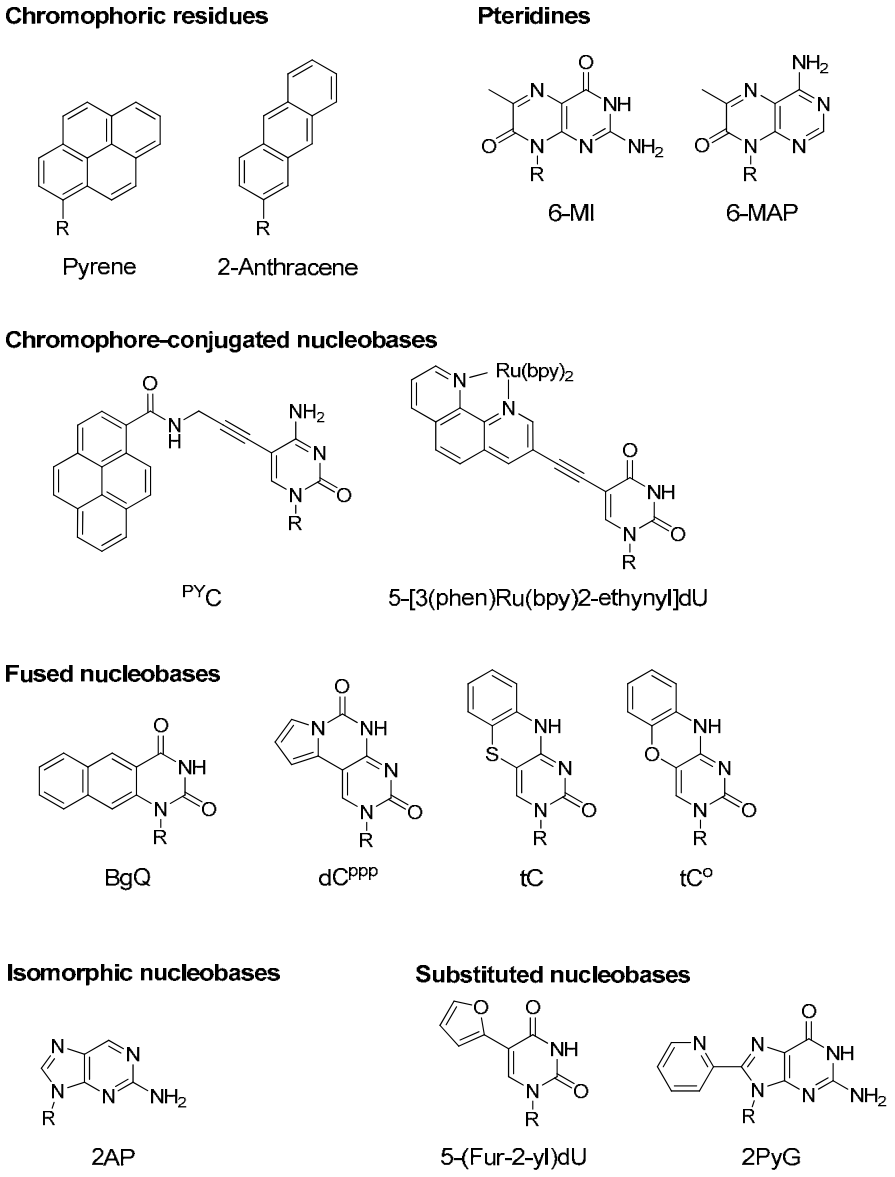

Figure 1.6: Selected examples of reported fluorescent nucleic acids internal probes. R = 2'-deoxyribose or ribose.

Nucleic acids internal probes can be classified in different families according to structural considerations (some examples are illustrated in Figure 1.6):[42,48] (1) Chromophoric Residues: fluorescent polycyclic aromatic hydrocarbons, that lack the "natural" nucleobase hydrogen bonding faces,[49] (2) Chromophore-conjugated Nucleobases: consist of a fluorescent moiety covalently linked to a natural nucleobase, (3) Pteridines: highly emissive purine analogs containing two condensed six-membered rings,[50,51] (4) Fused Nucleobases: consist of ring systems fused to a pyrimidine or purine nuclei, (5) Isomorphic

Nucleobases: closely ressemble the natural nucleoside in terms of their overall dimensions, hydrogen bonding patterns and ability to form *Watson & Crick* base pairs, (6) Substituted Nucleobases: consist of an aromatic ring conjugated to the pyrimidine or purine nuclei. Reported fluorescent purine analogs that can serve as internal probes in the context of nucleic acids are reviewed in Chapter 2.

The value of nucleoside analogs as internal fluorescent probes is highly dependent on their successful incorporation into nucleic acids. The introduction of nucleoside analogs into short oligonucleotides is routinely performed using solid-phase assisted phosphoramidite chemistry. Alternatively, nucleotides triphosphate building blocks can be assembled *in vitro* by DNA polymerase using the complementary strand as a template.[52,53] Cellular enzymes can be exploited for the incorporation of nucleosides, monophosphate analogs or pronucleotides into cellular DNA and RNA.[54-56] Another possibility is to exploit the ability of certain cell lines to extend their telomeres *via* homologous recombination to specifically incorporate fluorescent labels into telomeric repeats of chromosomes.[57] Biological and enzymes-based methods are highly sensitive to structural dissimilarities and have to be evaluated on a case by case basis.[58] Synthetic methods, in contrast, can accommodate a wide variety of structures and functional groups.

1.4 Nucleobase analogs as probes for G-quadruplex folding

"Internal" fluorescent base analogs can provide a direct readout for the folding of nucleic acids secondary structures if their photophysical properties are sensitive to global and local conformational changes. Their small size and predicatiable location can offer the ability to detect subtle changes with single nucleotide resolution. For the efficient detection of G-quadruplex folding, an internal probe should complete different requirements: (1) provide distinct responses to changes in surrounding micro-environment *via* marked differences in its basic photophysical parameters, (2) retain sufficient emission quantum efficiency in the context of nucleic acids, optimally, the fluorescence should be increased upon DNA folding into G-quadruplex, (3) display emission at specific wavelengths for particular applications involving fluorescence imaging of cellular systems, (4) induce as little perturbation of the system as possible for an unbiased report of the conformational equilibria. This last point is crucial and requires the preservation of high structural similarity to the natural nucleobases, including the retention of the *Watson & Crick* and *Hoogsteen*'s base pairing faces.

Fluorescence-based assays involving fluorescent nucleobase analogs typically assess conformational changes and/or phosphodiester bond cleavage using probes that exhibit lower quantum yields when base-stacked with neighbouring residues.[48,51,59-71] This approach is effective when large changes in base-stacking/solvation of the probe occur during the course of a reaction. Internal probes that are highly emissive in both base-stacked and solvated environments can provide an alternative and highly sensitive means to differentiate DNA/RNA structures with variable base-stacking configurations. However, only a very limited number of examples, such as the cytidine analog 1,3-diaza-2-oxophenothiazine (**tC**),[72] or 5-(fur-2-yl)-2'-deoxyuridine[73] (Figure 1.6) retain their *Watson & Crick* pairing ability and show similar or higher quantum yields in the context of nucleic acids. To the best of our knowledge, no similar example was reported for guanosine analogs. As central part of the assembly, fluorescent base analogs derived from guanosine are ideal candidates for the detection of G-quadruplex folding. Few fluorescent guanosine mimics such as 6-methylisoxanthopterin (**6-MI**) and 3-methylisoxanthopterin (**3-MI**) have been reported,[50,51,74] but are imperfect structural mimics of guanosine that destabilize G-quadruplex structures. These nucleosides are also quenched 100-fold or more by close proximity and base-stacking with purines,[74,75] resulting in non-emissive products when inserted into G-tetrad structures (Chapter 2).[76] For these reasons, the development of new guanosine analogs that are minimally disruptive and retain their emission efficiency in the context of nucleic acids is highly desirable for G-quadruplex folding studies.

1.5 Goals

In the last decade, fluorescent biomolecules labeling has revolutionized our understanding of biological processes and revealed new means to treat diseases. DNA G-quadruplexes are intriguing DNA secondary structures displaying particular photophysical properties and having a potentially strong biological relevance. However, the existence of these structures in mammalian cells remains an open question and the development of sensitive and versatile means to detect their formation *in vitro* and *in vivo* is highly desirable. Our work is focused on the development of new fluorescent tools for the study of G-quadruplex structures and can be summarized in three main objectives:

1) Develop environment-sensitive fluorescent guanosine analogs that remain highly emissive in the context of proper base pairing and stacking interactions in nucleic acids.

2) Develop fluorescence-based assays for the detection of G-quadruplex folding.

3) Address the origin of the remarkable photophysical characteristics displayed by G-quadruplex structures.

To tackle these goals, we developed environment-sensitive 8-substituted-2'-deoxyguanosine derivatives as fluorescent probes for G-quadruplex-forming DNA sequences. These compounds have provided the first family of guanine analogs that act as energy acceptors from natural nucleobases. Remarkably, these compounds retain their fluorescence efficiency in the context of nucleic acids, even when base-stacked with other purine residues in DNA. The unusual photophysical characteristics of these probes will enable other applications in the context of nucleic acids beyond the scope of specific G-quadruplexes studies presented here.

CHAPTER 2

Fluorescent Purine Analogs and Purine Mimics: Shedding Light on DNA Structures and Functions

2.1 Introduction

Due to their small size and predictable location, internal fluorescent probes offer some advantages over external and conjugated probes, including the ability to highlight subtle structural changes with single nucleotide resolution.[48,51,59-71] For this purpose, fluorescent nucleobase analogs are highly desirable, since they can retain the structural and electronic characteristics of the natural base and therefore have minimal impact on the structure and stability of nucleic acids. The development of fluorescent internal probes using emissive purine analogs can provide useful tools to elucidate DNA and RNA secondary structures within living cells, and provide a basis for understanding fundamental photophysical and electronic processes taking place within nucleic acids.

Purines are heterocyclic compounds consisting of an imidazole ring fused to a pyrimidine ring and provide the core scaffold of guanine and adenine residues (Figure 2.1). In the context of DNA, purines act as efficient energy donors,[77,78] and provide much of the energetic driving force for nucleic acids folding.[8,9,79] Due to their large aromatic surface, numerous modifications of the purine scaffold can be envisaged to design novel fluorescent purine or purine mimic residues.

In this chapter, fluorescent purine analogs and purine mimics (**P.1** – **P.108**) are reviewed. These fluorescent probes are classified in five families according to structural aspects: (1) Chromophore-conjugated purine analogs, (2) pteridines, (3) isomorphic purine analogs, (4) fused purine analogs and (5) substituted purine derivatives. An emphasis is put on their basic photophysical characteristics and spectroscopic properties. A few numbers of these have been incorporated into nucleic acids for fluorescence detection of diverse

biomolecular events. Examples are included to illustrate the potential applications of judiciously implemented fluorescent nucleosides.[1]

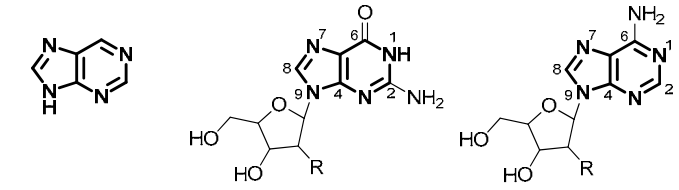

Figure 2.1: Purine, guanosine and adenosine and their photophysical properties.[80,81] R = H or OH.

2.2 Fluorescent purine analogs and purine mimics

2.2.1 Chromophore-conjugated purine analogs

Like other sites in DNA and RNA, purine residues can serve as attachement sites to fluorescent metal complexes and organic fluorophores (Figures 2.2 and 2.3). Flexible, non-conjugating linkers yield nucleobase analogs with photophysical characteristics that are very similar to those of the parent fluorophore attached. In contrast, electronic conjugation between the attached fluorophore and the purine core often leads to chromophores with unique photophysical properties (Table 2.1).

Many examples of chromophoric purine analogs consist of a pyrene unit attached to the nucleobase (Figure 2.2). The fluorescence of pyrene is solvatochromic (**P.1**)[82] and is usually quenched upon stacking with natural nucleobases. Numerous sensing applications have exploited these properties to detect structural molecular events. The guanosine analog **P.2** was used to detect DNA hybridization translated by a red-shift of the fluorophore emission maximum. In addition, this nucleobase analog acts as a photoinducable donor for charge transfer within duplex DNA and with peptides.[83,84] Base pair mismatches, neighboring residues and global DNA structure are all factors that influence the stacking interactions and fluorescence properties of the pyrene unit in nucleic acids. Exploiting this

[1] In the context of nucleic acids, the photophysical properties of most of the fluorescent nucleobase analogs being frequently strongly dependent on the sequence, hybridization state and neighboring base, the photophysical parameters provided in this context correspond to the ranges of values reported in the different contributions cited.

phenomenon, **P.3** and **P.4**[85,86] or **P.9**[87,88] where shown to have the capacity to detect base pair mismatches. **P.9** was also exploited for the detection of B → Z transition of DNA,[89] G-quadruplex formation[90] and even the discrimination of alternative G-quadruplex folds.[91] **P.7** was used to detect DNA hybridization. This fluorophore was prepared by post-synthetic modification of a *C*8 alkylamino-substituted 2'-deoxyguanosine with an active ester of pyrene carboxylic acid.[92]

The close proximity of two pyrene units can lead to exciton formation with red-shifted emission (ca. 480 nm) as compared to isolated pyrene (450 nm). Double-substitutions of nucleic acids with pyrene modified nucleobases were therefore used as readout for the geometrical distance between the probes. Using this strategy, nucleosides **P.4**,[86,93] **P.5**,[94] **P.8**,[95] and **P.9**[96-98] were used to discriminate duplex *versus* hairpin formation. **P.8** and **P.9** were also used in combination with 5-(1-ethenylpyrene)-cytidine and 5-(1-ethenylpyrene)-uridine for B → Z DNA transition studies.[95-97,99] *Saito* and co-workers developed a pyrene-based system involving ^{8Py}**G** (**P.6**), where the quenching upon base stacking and exciton emission are exploited for the distinction between single strand, duplex and G-quadruplex structures.[100] Conjugation of a pyrene substituted with electron withdrawing groups to position 8 of guanosine leads to push-pull type solvatochromic fluorophores, with red-shifted emission (62 nm) and fluorescence quenching in acetonitrile as compared to less polar solvents (**P.13 - P.17**).[101]

A few chromophoric purine analogs based on the dansyl chromophore were reported. The fluorescence of dansyl is highly sensitive to the hydration and polarity of its local environment. Introduced on the position 2 of deoxyguanosine (**P.10**), and the position 8 of deoxyguanosine (**P.11**) or deoxyadenosine (**P.12**), it responds to the local changes in groove environment. These characteristics were used to probe DNA hybridization (**P.11**, **P.12**),[102] duplex A → B and B → Z transitions (**P.10**),[103,104] and for the detection of single base pair mismatches (**P.11**, **P.12**).[102] Pyrene, fluorenyl or naphthalene, linked by a vinyl unit to the *C*8 position of guanosine (**P.18** – **P.20**) yields nucleobases that display reasonable quantum yield in the *trans* configuration. These compounds have shown to photoisomerize to the poorly fluorescent *cis* isomers upon irradiation with UV light.[105-107] Using these properties in the context of oligonucleotides, purines **P.19** and **P.20** were used to photoregulate duplex and G-quadruplex formation.[105,107]

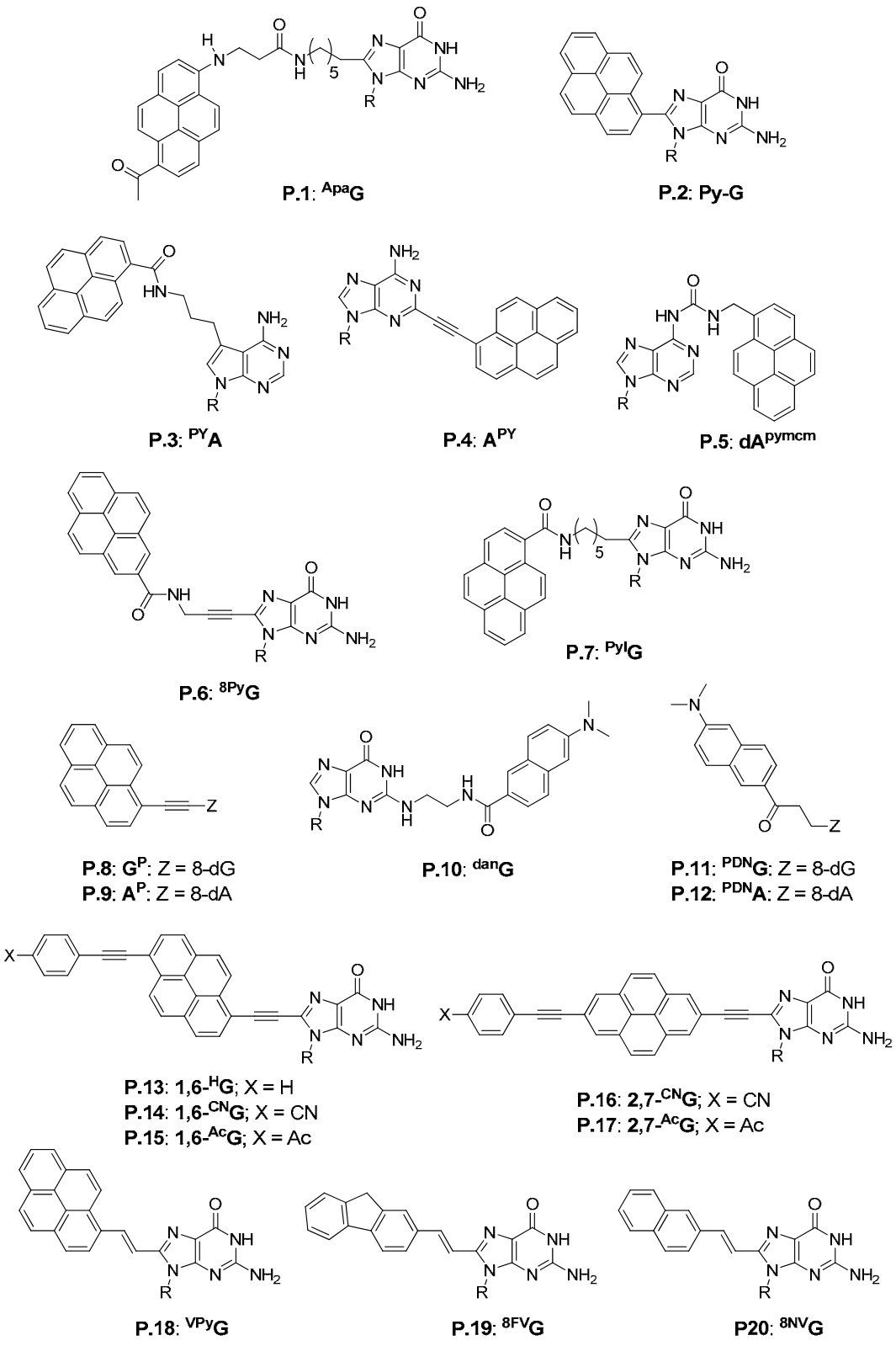

Figure 2.2: Chromophore-conjugated purine analogs (R = 2'-deoxyribose) (Part 1).

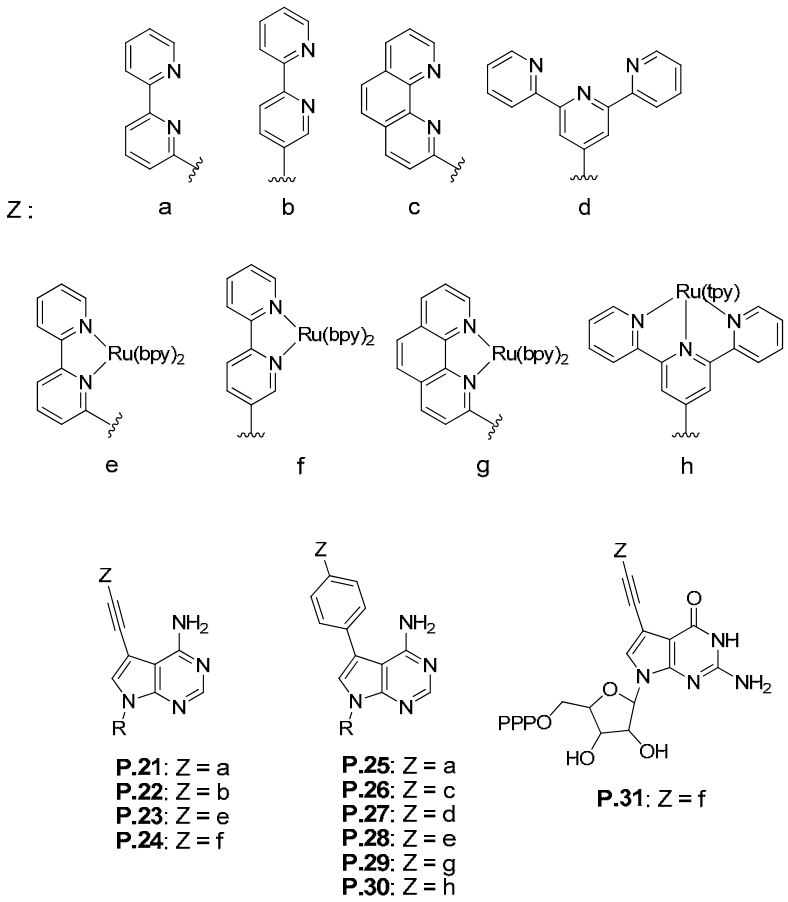

Figure 2.3: Chromophore-conjugated purine analogs (R = 2'-deoxyribose) (Part 2).

The fluorescence of 7-deazapurine analogs conjugated to bipyridine, phenanthroline, terpyridine, and the corresponding ruthenium-containing complexes were investigated by *Hocek* and co-workers.[108,109] Notably, the triphosphate **P.31** is incorporated into modified oligonucleotides by polymerases.[109] **P.31** was successfully used for luminescent single nucleotide polymorphism detection.[109] The specific properties and applications of these chromophoric nucleobase analogs are summarized in Table 2.2.

Very few fluorophores are characterized in the context of folded nucleic acids. In almost all cases, the incorporation of fluorophores into DNA/RNA causes fluorescent quenching by photo-induced electron transfer (Table 2.1).[110] The impact of these nucleobase analogs on the global structure and stability of modified nucleic acids is highly variable and depends on the shape, size, and hydrogen bonding capabilities of each probe.

Table 2.1: Spectroscopic properties of chromophore-conjugated purine analogs.

No.	Name	Cond.	λ_{abs} (nm)	λ_{ex} (nm)	Φ	REF
P.1	^{Apa}**G**	Water	460	573	0.27	[82]
P.2	**Py-G**	ssDNA	350	445	0.08-0.11	[83,84]
		dsDNA	370	455	0.25-0.34	[83,84]
P.3	^{PY}**A**	ssDNA	347-353	388-397	0.006-0.1	[85]
P.4	**A**^{PY}	DNA	380-405	450-480	0.11-0.88	[86,93]
P.5	**dA**^{pymcm}	DNA	350	400	n.d.	[94]
P.6	^{8Py}**G**	Methanol	342		0.10	[100]
		DNA	372	405-458	0.01-0.12	[100]
P.7	^{PyI}**G**	DNA	350	400-535	0.01-0.26	[92]
P.8	**G**^{P}	DNA	421	430	n.d.	[69,95,99]
P.9	**A**^{P}	MeOH	420	434	0.73	[87-91,96-98]
		DNA	420	451-480	n.d.	[87-91,96-98]
P.10	^{dan}**G**	DNA	325	443	n.d.	[103,104]
P.11	^{PGN}**G**	DNA	391-406	515-524	0.07-0.13	[102]
P.12	^{PGN}**A**	DNA	382-405	517-526	0.07-0.20	[102]
P.13	**1,6-**^{H}**G**	$CHCl_3$	413	482	0.41	[101]
P.14	**1,6-**^{CN}**G**	$CHCl_3$	420	493	0.26	[101]
P.15	**1,6-**^{Ac}**G**	$CHCl_3$	421	487	0.24	[101]
P.16	**2,7-**^{CN}**G**	$CHCl_3$	341	427	0.13	[101]
P.17	**2,7-**^{Ac}**G**	$CHCl_3$	341	426	0.08	[101]
P.18	^{VPy}**G**	Methanol	405	489	0.43	[106]
P.19	^{8NV}**G**	DNA	373	470	n.d	[105]
P.20	^{8FV}**G**	DNA	370	470	n.d.	[105,107]
P.21		$CHCl_3$	321,351	406	n.d.	[108]
P.22		$CHCl_3$	336, 368	427	n.d.	[108]
P.23		CH_3CN	448	639	0.0002	[108]
P.24		CH_3CN	384	665	0.03	[108]
P.25		$CHCl_3$	325, 340	395	n.d.	[108]
P.26		$CHCl_3$	322, 330	424	n.d.	[108]
P.27		$CHCl_3$	284, 343	425	n.d.	[108]
P.28		CH_3CN	450	667	0.0002	[108]
P.29		CH_3CN	448	648	0.0004	[108]
P.30		CH_3CN	485	633	0.0002	[108]
P.31		CH_3CN		635	0.01	[109]

Table 2.2: Characteristics and environment-sensing applications of chromophore-conjugated purine analogs.

No.	Name	Properties & Applications
P.1	^{Apa}**G**	Solvatochromic [82]
P.2	**Py-G**	Detection of DNA hybridization, single nucleotide polymorphism; photoinducable donor for charge transfer studies [83,84]
P.3	^{PY}**A**	Base discriminating fluorescence: C vsT detection [85]
P.4	**A**^{PY}	RNA hybridization assay [86,93]
P.5	**dA**^{pymcm}	DNA hybridization assay [94]
P.6	^{8Py}**G**	Distinction between single strand, duplex and G-quadruplex structures [100]
P.7	^{PyI}**G**	DNA hybridization assay [92]
P.8	**G**^{P}	Molecular beacon; Energy acceptor from 1-ethynylpyrene modified cytosine [95]; Detection of B → Z DNA transition [99]
P.9	**A**^{P}	Molecular beacon [97]; Detection of B → Z DNA transition [89], single nucleotide polymorphism [87,88,96], G-quadruplex folding [90,91]
P.10	^{dan}**G**	Probing groove polarity [103,104]
P.11	^{PGN}**G**	Detection of single nucleotide polymorphism [102]
P.12	^{PGN}**A**	Detection of single nucleotide polymorphism [102]
P.13	**1,6-**^{H}**G**	Solvatochromic, quenched in polar solvents [101]
P.14	**1,6-**^{CN}**G**	Solvatochromic, quenched in polar solvents [101]
P.15	**1,6-**^{Ac}**G**	Solvatochromic, quenched in polar solvents [101]
P.16	**2,7-**^{CN}**G**	Solvatochromic, quenched in polar solvents [101]
P.17	**2,7-**^{Ac}**G**	Solvatochromic, quenched in polar solvents [101]
P.18	^{VPy}**G**	Photoswitch (420 nm: E →Z, E:Z = 8:92; 365 nm: Z →E, E:Z = 82:18) [106]
P.19	^{8FV}**G**	Photoswitch (410 nm: E →Z, E:Z = 37:63; 290 nm: Z →E, E:Z = 87:13); Photoregulation of duplex hybridization [105]
P.20	^{8FV}**G**	Photoswitch (420 nm: E →Z, E:Z = 23:77; 310 nm: Z →E, E:Z = 77:23); Photoregulation of duplex hybridization [105] and G-quadruplex folding [107]
P.31		Detection by luminescence; Detection of single nucleotide polymorphism [109]

2.2.2 Pteridines

Pteridines are naturally occurring fluorescent purine mimics. The most optimized fluorophores from this family include **3-MI** (**P.32**), **6-MI** (**P.33**), **6-MAP** (**P.34**), and **DMAP** (**P.35**) (Figure 2.4). At the monomer level, these fluorophores display strong visible fluorescence (λ_{em} = ~430 nm; Φ = 0.39 – 0.88), but their emission is significantly

quenched upon incorporation into oligonucleotides (Φ = 0.004 – 0.29). This quenching effect is sequence dependent in the context of single stranded and duplex DNA, where purines are more efficient quenchers than pyrimidines.[75,111] Having a methyl group pointing to the *Watson & Crick* face of the nucleobase, **3-MI** and **DMAP** are most disruptive to duplex DNA, resulting in destabilizations corresponding to a base pair mismatch. Despite this, **3-MI** has found numerous applications in the context of nucleic acids.[50,112-115] **6-MAP** and **6-MI** induce much less perturbation and show some evidence of hydrogen bonding with cytosine and thymidine respectively.[50,74]

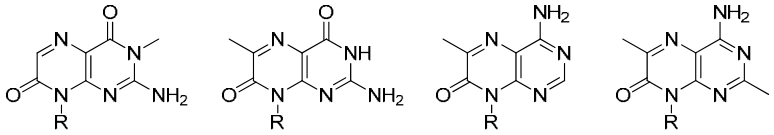

Figure 2.4: Examples of pteridines (R = 2'-deoxyribose or ribose).

Table 2.3: Spectroscopic properties of pteridine fluorophores.

No.	Name	Cond.	λ_{abs} (nm)	λ_{em} (nm)	Φ	REF
P.32	**3-MI**	MeOH	348	430	0.88	[50,51]
		ssDNA			0.005-0.29	[74,75]
		dsDNA			0.004-0.05	[74,75]
P.33	**6-MI**	MeOH	340	431	0.70	[50,51]
		ssDNA			0.03-0.29	[74]
		dsDNA			0.04-0.20	[74]
P.34	**6-MAP**	MeOH	320	430	0.39	[50,51]
		ssDNA			0.005-0.04	[111]
		dsDNA			0.005-0.01	[111]
P.35	**DMAP**	MeOH	310	430	0.48	[50,51]
		ssDNA			< 0.01-0.11	[111]

Because the fluorescence properties of the pteridine nucleosides strongly depend on their local environment and interactions with neighbouring bases, they efficiently report structural events occurring even at the nucleoside level by changes in fluorescence intensities. **3-MI** and **6-MI** were utilized in DNA-protein interaction studies, reporting changes in stacking interactions induced by the cleavage, unwinding or bending of the

DNA upon protein binding.[51,65,112,116] With similar underlying principles, alkyl transferase activity,[114] DNA/RNA polymerase interactions,[50] antibiotics binding,[113] and DNA structure,[117] can be reported using **6-MAP**.

Table 2.4: Characteristics and environment-sensing applications of pteridine-based purine mimics.

No.	Name	Properties & Applications
P.32	**3-MI**	Detection of DNA hybridization [50], DNA structures [50], alkyl transferase activity [114], DNA-protein interactions [112], DNA-RNA polymerase interactions [50], nucleoside cellular uptake [50], RNA-aminoglycoside interaction [113]; Single molecule detection [115]
P.33	**6-MI**	Detection of DNA-protein [116], DNA-RNA polymerase [50] and RNA-aminoglycoside interactions [113]
P.34	**6-MAP**	Detection of DNA structure [117]; Two-photon excitation [118]

In addition to fluorescent changes resulting from changes in stacking interactions, the fluorescence anisotropy of **3-MI** was used to detect protein binding.[112] **3-MI** has also been used in single molecule detection[115] and for the study of intracellular transport of oligonucleotides.[50] **6-MAP** has a reasonable two photon cross section and is therefore a potential two photon excitation probe.[118]

2.2.3 Isomorphic purine analogs

Subtle changes to the amino and carbonyl substitutents of the purine scaffold can lead to fluorescent isomorphic nucleobase analogs of guanosine and adenosine. Their small size and strong similarity to the native nucleosides provide a clear advantage to these nucleobases in terms of minimal impact on nucleic acids structures and folding. Selected examples of isomorphic purine analogs are shown in Figure 2.5 and their spectroscopic characteristics are summarized in Table 2.5.

2-Aminopurine (**2AP**, **P.36**) is a constitutional isomer of adenine (6-aminopurine) and is the most widely used fluorescent nucleoside analog. In contrary to adenosine which is not emissive ($\Phi = < 10^{-4}$ in water),[80] **2AP** has a high quantum efficiency ($\Phi = 0.68$ in water). **2AP** is highly sensitive to its environment and has red-shifted absorption band as compared to DNA.[119] Variations of **2AP** including the 7-deaza and 8-aza-7-deaza analogs display larger Stokes shifts but lower quantum efficiencies ($\Phi = 0.47$ and 0.53 respectively).[120] Interestingly, 2,6-diaminopurine (**DAP**, **P.37**) and formycin (**P.38**), two related emissive

adenosine analogs display significantly lower quantum efficiencies (Φ = 0.01 and 0.06 respectively).[119]

2AP can form base pairs with thymidine and uracil without significant perturbation to nucleic acids double helixes.[121] **2AP** can also form a wobble base pair with cytosine and is therefore considered as an adenine and guanine mimic.[122-124] The fluorescence of **2AP** is significantly quenched upon its incorporation into nucleic acids, due to base-stacking interactions. The fluorescence of **2AP** is sensitive to its local environment and to base pairing interactions. Numerous assays involving **2AP** as internal fluorescent probe have exploited these characteristics as readout for molecular events. **2AP** has been used in many different applications including: DNA hybridization assays,[121,125,126] DNA-protein interactions and enzymatic activity,[121,126,127] DNA and RNA folding,[128,129] G-quadruplex folding,[66] DNA RNA-polymerase interactions,[130-132] base flipping,[133] abasic site sensing,[134] base pairing interactions,[123,124,135-138] and RNA-aminoglycoside binding interactions.[139-142] **2AP** has also been used as fluorescent nucleoside molecular beacon together with pyrrolo-dC (Figure 1.6) for the detection of DNA hybridization.[143] In another application, **2AP** has been used to act as an energy acceptor for energy and electron transfer processes taking place in duplex DNA.[78,144-149]

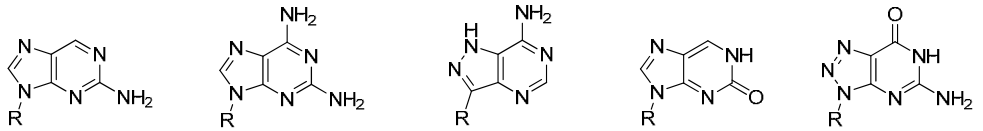

Figure 2.5: Examples of isomorphic nucleobases (R = 2'-deoxyribose or ribose).

The isomorphic purine analog 2'-deoxyisoinosine (**P.39**) is a fluorescent isomer of the naturally occurring inosine. However, its incorporation into DNA resulted in little base pairing selectivity and significant destabilized duplexes.[150]

8-Aza-2'-deoxyguanosine (**8-AzadG**, **P.40**) is a purine isomorph showing noticeable fluorescence at neutral pH (Φ = 0.01) and strong fluorescence in the anionic form under alkaline conditions (Φ = 0.55).[151-153] The presence of an electronegative nitrogen atom on position 8 decreases the pKa of the *N*1H proton by one unit as compared to 2'-deoxyguanosine (pKa = 8.3 and 9.3 respectively). The photophysical characteristics of **8-AzadG** are therefore strongly sensitive to pH. Upon incorporation into oligonucleotides, its fluorescence is significantly quenched, although this effect is smaller than what is

observed in the case of **2AP**.[152] **8-AzadG** was used as a reporter of purine ionization states in structured RNAs [154] and base pair mismatches. As a result of its perfect 2'-deoxyguanosine shape mimic, **8-AzadG** induces almost no destabilization of nucleic acids duplexes.[152,155] This nucleobase, however, is not compatible with G-tetrad formation.[155]

Table 2.5: Spectroscopic properties of isomorphic purines.

No.	Name	Cond.	λ_{abs} (nm)	λ_{em} (nm)	Φ	REF
P.36	**2AP**	Water	303	370	0.68	[119]
		ssDNA	310	370	0.01-0.03	[78,121,123-145,147-149]
		dsDNA	310	370	0.002-0.05	
P.37	**DAP**	Water	280	350	0.01	[119]
P.38	**Formycin**	Water	295	340	0.06	[119]
P.39	**Isoinosine**	Water	320	382	n.d.	[150]
		DNA	318	383	n.d.	[150]
P.40	**8-AzadG**	Buffer	256	347	0.01-0.55	[151,152,154]
		RNA	285	377	0.005-0.06	[151,152,154]

Table 2.6: Characteristics and applications of isomorphic purines.

No.	Name	Properties & Applications
P.36	**2AP**	Fluorescence sensitive to base-stacking interactions; Detection of DNA hybridization, enzymatic acitivity [121,126,127], DNA or RNA structure [128,129], DNA-protein interactions, G-quadruplex folding [66], DNA-RNA-polymerase interactions [130-132], base hybridization [124,125,133,134], base pair interactions [123,124,135-138], RNA-aminoglycoside interaction [139-142], energy and charge transfer in DNA [78,144-149]; Molecular beacons [143]
P.40	**8-AzadG**	pH-dependent fluorescence [154]; Study of purine ionization state in RNA structures [154]; Detection of mismatches [152] and single nucleotide polymorphism [151]

2.2.4 Fused purine analogs

The addition of fused aromatic rings onto purines results in extended-conjugation nucleobases that can be highly emissive (Figure 2.6, Table 2.7). 1,N^6-ethenoadenosine (**Etheno-A, P.41**) was first reported in the early 1970s as a fluorescent derivative of adenosine (Φ = 0.56 in aqueous solution) having a large *Stokes* shift (140 nm) and retaining strong fluorescence in a wide range of solvents.[156,157] **Etheno-A** is susceptible to degradation by acid or base and *Seela* and co-workers later reported that the corresponding 7-deaza derivative (1,N^6-etheno-7-deaza-2'-deoxyadenosine, **εc^7A_d**, **P.42**), is much more stable over a wide range of pH, and shows similar emission efficiency (Φ = 0.53) and *Stokes* shift (134 nm). In the context of DNA, **εc^7A_d** was used to monitor oligonucleotide denaturation. Interestingly, the excitation spectra of **εc^7A_d**-containing oligonucleotides show a maximum around 260 nm, suggesting the presence of DNA-to-**εc^7A_d** energy transfer. Unfortunately, the *Watson & Crick* face of **Etheno-A** and **εc^7A_d** is masked by the etheno group, preventing proper base pair formation with thymidine and strongly destabilizing duplex structures. However, as a "dangling-end" residue, it stabilizes the duplex by efficient base-stacking interactions.[158]

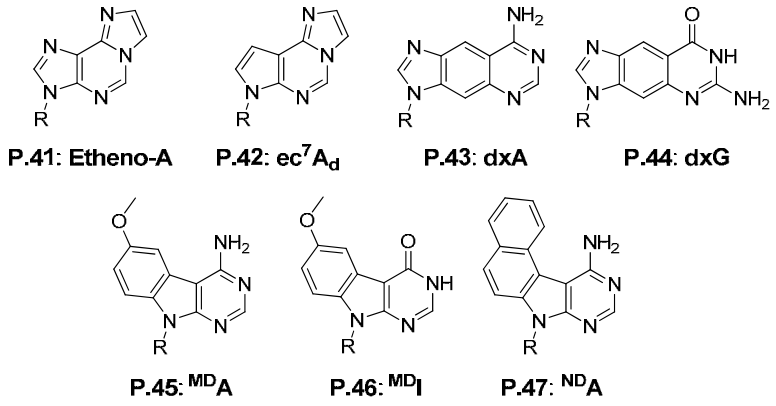

Figure 2.6: Examples of fused purine analogs (R = 2'-deoxyribose or ribose).

dxA (**P.43**) and **dxG** (**P.44**) are elongated adenosine and guanosine analogs containing a benzene ring inserted between the imidazole and the pyrimidine rings. This elongation results in fluorescence emissions in the blue-violet range (λ_{em} = 393 – 413 nm). The quantum yields of these nucleosides (Φ = 0.40 – 0.44 in methanol) is reduced upon incorporation into oligonucleotides but remains reasonably good (Φ = 0.02 – 0.08). Due to their larger size, significant destabilisation is observed in duplexes containing a single modification.[159] However, **dxA** or **dxG** substitution in all the base pair of a double helix

results in highly stable, sequence specific, size-expanded DNA helixes.[159] Recent evidence suggests that certain DNA polymerases can read the chemical information stored in these ring-expanded genetic codes and that sequences encoded by **dxA** are recognized by the replication machinery of *E. coli*.[160]

Table 2.7: Spectroscopic properties of fused purine analogs.

No.	Name	Cond.	λ_{abs} (nm)	λ_{em} (nm)	Φ	REF
P.41	**Etheno-A**	Buffer	275	415	0.56	[116,156,157]
P.42	εc^7A_d	Water	284	418	0.53	[158]
		DNA	260, 290	419	n.d.	[158]
P.43	**dxA**	MeOH	333	393	0.44	[159-163]
		DNA	333	393	0.02-0.04	[161]
P.44	**dxG**	MeOH	320	413	0.40	[159-162,164]
		DNA	320	390	0.06-0.08	[161]
P.45	^{MD}**I**	Buffer	315	442	0.12	[165]
		DNA	315	424	0.002-0.01	[165]
P.46	^{MD}**A**	Buffer	327	427	0.12	[165]
		DNA	327	424	0.001-0.08	[165]
P.47	ND**A**	DNA	352-354	383	0.005-0.03	[166]

Table 2.8: Characteristics and applications of fused purine analogs.

No.	Name	Properties & Applications
P.41	**Etheno-A**	Substitute for ATP in enzymatic studies [156,157]; Detection of DNA-protein binding interactions [116]
P.42	εc^7A_d	Energy acceptor for DNA; DNA hybridization assays [158]
P.43	**dxA**	Reporting of base pairing and stacking interactions [161]; Ring-expanded genetic code [159,160]
P.44	**dxG**	Reporting of base pairing and stacking interactions [161]; Ring-expanded genetic code [159,160]
P.45	^{MD}**I**	Base discriminating fluorescent probe [165]
P.46	^{MD}**A**	Base discriminating fluorescent probe[165]
P.47	ND**A**	Base discriminating fluorescent probe; FRET pair with fluorescein [166]

The addition of fused aromatic rings at positions 7 and 8 of 7-deaza purines can afford new fluorescent nucleobases. ^{MD}**I** (**P.45**) and ^{MD}**A** (**P.46**), isosine and adenosine mimics respectively, show reasonable fluorescence at the monomer level (Φ = 0.12) but are quenched in the context of oligonucleotides. ^{MD}**I** and ^{MD}**A** can be used as base discriminating fluorescent probes and show stronger fluorescence when paired with T and C respectively.[165] The naphthodeazaadenine derivative ND**A** (**P.47**), shows similar fluorescent behavior and was used as FRET-base-discriminating fluorescent nucleobase when used in conjugation with fluorescein.[166]

2.2.5 Substituted purine derivatives

Fluorescent nucleobases substituted with small, non-fluorescent moieties are classified as substituted purine derivatives. Given the large aromatic surface of the purine scaffold, small modifications elongating the conjugated π-system, such as introduction of vinyl or arylation, can be sufficient to yield emissive products. These purine derivatives generally show red-shifted emission maxima as compared to isomorphic nucleobase analogs, but can be less disruptive to DNA/RNA folding and stability as compared to the fused nucleobase analogs. Accordingly, our recent efforts to develop new emissive purine analogs are principally concentrated on this strategy.

Castellano and co-workers recently reported a series of "push-pull" purine fluorophores (**P.48** – **P.70,** Figure 2.7) having electron donating groups, such as amino, methylamino, dimethylamino or benzylether in position 2 and/or 6, complemented by electron accepting groups such as cyano, methyl ester or carboxyamide moieties in position 8. Nucleobases bearing these complementary groups ("push-pull") (**P.55** – **P.70**) have favorable photophysical characteristics compared to their acceptor-free analogs (**P.48** – **P.54**), including red-shifted absorption and emission maxima, enhanced quantum yields and strong solvatochromism (Table 2.9). This strategy provides a means for tunable purines across the blue-UV spectrum.[63] **P.64** was reported in the construction of a blue-violet electroluminescent device,[167] and "push-pull" fluorophores can find a board range of applications in biosensing and material science. None of these derivatives, however, contains an O^6 carbonyl and therefore they will not exhibit proper base pairing interactions with cytidine residues in the context of DNA/RNA duplexes.

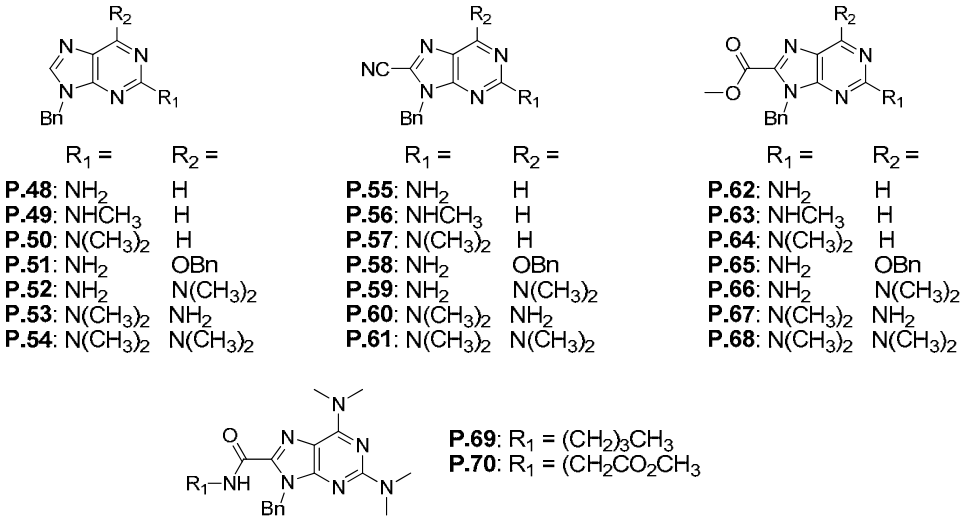

Figure 2.7: "Push-Pull" purine analogs developed by Castellano et al.[63]

Table 2.9: Spectroscopic properties of the purine analogs developed by *Castellano* et al. in dichloromethane.[63]

No.	λ_{abs} (nm)	λ_{em} (nm)	Φ	No.	λ_{abs} (nm)	λ_{em} (nm)	Φ
P.48	304	357	0.20	**P.60**	336	387	>0.95
P.49	317	386	0.25	**P.61**	348	388	0.20
P.50	330	393	0.76	**P.62**	328	379	0.42
P.51	281	360	0.03	**P.63**	345	403	0.65
P.52	286	351	0.01	**P.64**	362	433	0.81
P.53	299	360	0.12	**P.65**	315	371	>0.95
P.54	297	392	0.03	**P.66**	330	393	>0.95
P.55	326	371	0.20	**P.67**	338	409	>0.95
P.56	341	383	0.58	**P.68**	351	409	0.90
P.57	361	429	0.90	**P.69**	338	402	0.87
P.58	311	355	0.81	**P.70**	343	407	0.91
P.59	324	375	0.30				

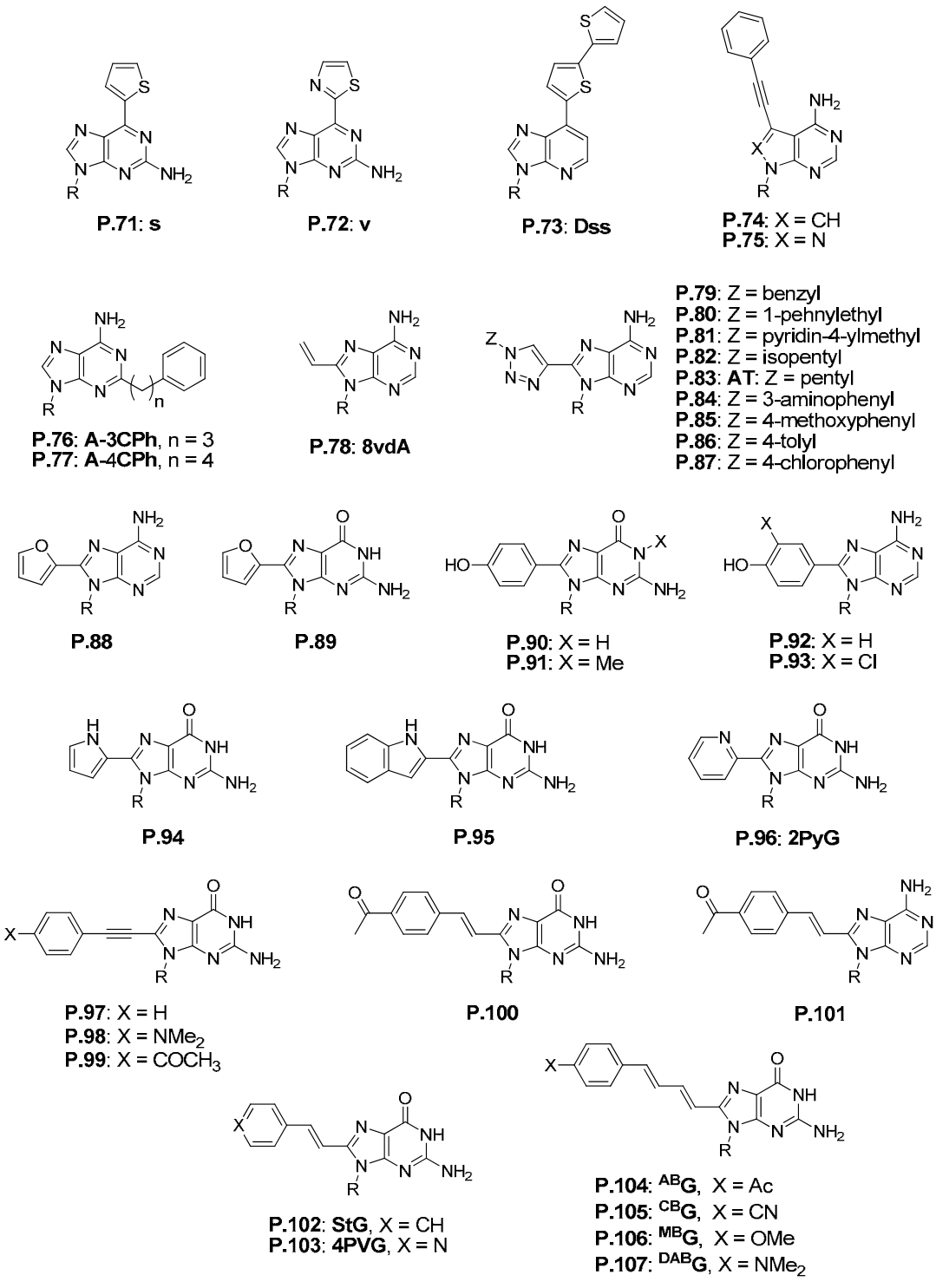

Figure 2.8: Examples of substituted purine derivatives (R = 2'-deoxyribose or ribose).

Table 2.10: Spectroscopic properties of substituted purine derivatives.

No.	Name	Cond.	λ_{abs} (nm)	λ_{em} (nm)	Φ	REF
P.71	**S**	Buffer	348	434	0.41	[168]
		DNA	352	440	0.07-0.20	[168]
P.72	**V**	Buffer	359	461	0.46	[168]
		DNA	363	465	0.02-0.17	[168]
P.73	**Dss**	EtOH	370	442	0.32	[169]
P.74		Water	297	412	0.02	[170]
P.75		Water	295	360	0.08	[170]
P.76	**A-3CPh**	Water	292	385	0.01	[171]
		RNA	292	399-422	0.17-0.32	[171]
P.77	**A-4CPh**	Water	278	396	0.007	[171]
		RNA	278	395-416	0.08-0.57	[171]
P.78	**8vdA**	Buffer	290	382	0.66	[172,173]
		DNA	290	382-389	0.005-0.04	[172,173]
P.79		THF	290	344	0.64	[174]
P.80		THF	289	342	0.63	[174]
P.81		THF	289	346	0.49	[174]
P.82		THF	289	343	0.62	[174]
P.83	$\mathbf{A^T}$	THF	289	342	0.62	[174]
		DNA	282	349-358	0.003-0.21	[175]
P.84		THF	296	402	0.38	[174]
P.85		THF	294	370	0.03	[174]
P.86		THF	294	368	0.05	[174]
P.87		THF	294	396	0.05	[174]
P.88		Water	304	374	0.69	[48]
P.89		Water	294	378	0.57	[48]
P.90		Buffer	278	390	0.47	[176]
P.91		Buffer	279	378	0.25	[176]
P.92		Buffer	282	391	0.56	[176]
P.93		Buffer	290	383	0.22	[176]
P.94		Buffer	292	379	0.10	[177]
P.95		Buffer	321	390	0.78	[177]

No.	Name	Cond.	λ_{abs} (nm)	λ_{em} (nm)	Φ	REF
P.96	**2PyG**	Water	300	415	0.02	[77,178,179]
		CH_3CN	316	395	0.71	[77,178,179]
		DNA	305-320	415	0.01-0.15	[77,178,179]
P.100		THF	370	499	0.49	[180]
P.101		THF	350	470	0.37	[180]
P.102	**StG**	Water	340	450	0.49	[64,179]
		DNA	360	450	0.13-0.45	[179]
P.103	**4PVG**	Water	355	490	0.16	[179]
		CH_3CN	355	490	0.57	[179]
		DNA	375	475	0.03-0.10	[179]
P.104	^{AB}**G**	CH_3CN	392	547	0.57	[181]
P.105	^{CB}**G**	CH_3CN	387	526	0.47	[181]
P.106	^{MB}**G**	CH_3CN	352	441	0.68	[181]
P.107	^{DAB}**G**	CH_3CN	349	443	0.75	[181]

The introduction of a thiophene or thiazole ring on position 6 of 2-aminopurine provides 2-amino-6-(2-thienyl)purine (**s**, **P.71**) and 2-amino-6-(2-thiazolyl)purine (**v**, **P.72**). These compounds exhibit significantly red-shifted absorption (λ_{abs} = 348 – 359 nm) and emission maxima (λ_{em} = 434 – 461 nm), and similar quantum efficiencies (Φ = 0.41 and 0.46 in aqueous solution) as compared to 2-aminopurine. These derivatives are reported to retain higher quantum yields (Φ = 0.02 – 0.20) than their unsubstituted analogs upon incorporation into nucleic acids, but they do not exhibit proper pairing with natural pyrimidines. In this context, the fluorescence of **P.71** and **P.72** is highly sensitive to local environment and stacking interactions with neighboring bases.[168] **P.71** and **P.72** can form stable, unnatural base pairs with 2-oxo-(1H)pyridine[182] which were exploited for site-specific incorporation into RNA for aptamer labeling.[182] **P.71** can also make a non-canonical base pair with pyrrole-2-carbaldehyde that was used to analyze the local structural conformation of functional RNA molecules.[183,184] The analog 7-(2,2'-bithien-5-yl)-imidazo[4,5-b]pyridine (**Dss, P.73**) has an intense fluorescence and it is reported to be a universal base for duplex formation, despite a large substituent that lacks proper hydrogen bonding capacity.[169] *Seela* and co-workers have investigated the effect of conjugating substituted alkynes to 7-deaza- and 8-aza-7-deaza-2'-deoxyadenosine. Whereas the parent compounds are non-fluorescent, extending the conjugated system with

phenyl ethynyl side chains on position 7 yields moderately emissive compounds (**P.74** and **P.75** respectively).[170]

Elongation of the π-conjugated system is a common strategy to provide fluorescent purines, but the introduction of non-conjugating phenylalkyl groups on the position 2 of adenosine can also yield compounds with remarkable photophysical properties. At the nucleoside/monomer level, 2-(3-phenylpropyl)adenosine (**A-3CPh**, **P.76**) and 2-(4-phenylbutyl)adenosine (**A-4CPh**, **P.77**) display low quantum yield (Φ = 0.01 and 0.007 respectively) as compared to the natural nucleobase. Remarkably, upon incorporation into RNA hairpins, the quantum yield of these analogs is significantly enhanced (Φ = 0.08 – 0.57). The origin of this effect remains unknown.[171]

While there are a modest number of fluorescent purines substituted at position 2, 6 or 7, the vast majority of the modifications is introduced at position 8 of the scaffold. Substitution of the position 8 of purines is an attractive avenue since it is not involved in hydrogen bonding in either *Watson & Crick* or *Hoogsteen*-type interactions. In comparison to the parent nucleobase, remarkable photophysical characteristics are observed upon substitution of adenosine with a vinyl group at the position 8. 8-vinyl-2'-deoxyadenosine (**8vdA**, **P.78**) shows a strong fluorescence (Φ = 0.66 in water) at 392 nm. This nucleobase was shown to be less disruptive and less significantly quenched than **2AP** upon incorporation into DNA.[173] Time-resolved fluorescence showed that **8vdA** can be used as a direct means to identify the opposite base.[172]

The introduction of a triazole ring on position 8 yields compounds (**P.79** – **P.87**) having slightly blue-shifted absorption and emission maxima as compared to **8vdA**. Changing the substitutent on the triazole ring tunes the emission wavelength without changing the absorption significantly. Substitution of the triazole ring with aliphatic moieties yield compounds that exhibit high quantum yields (Φ = 0.49 – 0.64). Aromatic moieties result in compounds with emission maxima red-shifted by 25 to 55 nm as compared to aliphatic analogs. With the notable exception of **P.84** (Φ = 0.38), these compounds are only moderately emissive (Φ = 0.03 – 0.05).[174] The related pentyl derivative **P.83** ($\mathbf{A^T}$) was recently incorporated into DNA. Remarkably, this fluorescent adenine analog shows only minor destabilization of duplexes and quantum yields ranging between 0.003 and 0.20; values that strongly depend on the neighboring base and hybridization state of the oligonucleotide.[175]

Arylation of the 8 position of purines with furan (**P.88** and **P.89**),[48] phenol derivatives (**P.90** – **P.93**), pyrrole (**P.94**), indole (**P.95**) or pyridine rings (**2PyG**, **P.96**) gives a series of fluorescent guanosine and adenosine analogs with red-shifted absorption (λ_{abs} = 278 – 321 nm) and emission (λ_{em} = 378 – 415 nm) as compared to guanosine. These compounds also exhibit a wide range of quantum efficiencies in water (Φ = 0.02 – 0.78). The emission intensities of the phenolic derivatives **P.91** – **P.93** are highly pH-sensitive.[176] The pyrrole and indole derivatives are reported to be fluorescent reporters of hydrogen bonding that are quenched upon H-bonding to dC, but enhanced upon *Hoogsteen* H-bonding to G.[177]

Table 2.11: Characteristics and environment-sensing applications of substituted purine derivatives.

No.	Name	Properties & Applications
P.71	**s**	RNA structure and dynamics [168,182-184]; RNA aptamer labeling [182]
P.72	**v**	RNA structure and dynamics [168,182]; RNA aptamer labeling [182]
P.73	**Dss**	Triphosphates enzymatically incorporated in DNA and RNA [169]
P.76	**A-3CPh**	High fluorescence in the context of DNA [171]
P.77	**A-4CPh**	High fluorescence in the context of DNA [171]
P.78	**8vdA**	Base discriminating fluorescent probe [172]
P.83	$\mathbf{A^T}$	Environmentally-sensitive fluorescence [175]
P.91		pH sensitive fluorescence [176]
P.92		pH sensitive fluorescence [176]
P.93		pH sensitive fluorescence [176]
P.94		Fluorescence sensitive to base pairing [177]
P.95		Fluorescence sensitive to base pairing [177]
P.96	**2PyG**	Solvatochromic; Energy acceptor from dG; Detection of energy transfer in DNA [77]; Localization of metal ions in DNA [185]
P.99		Base discriminating fluorescent probe [186]
P.100		Solvatochromic, quenched in polar solvents [180]
P.101		Solvatochromic, quenched in polar solvents [180]
P.102	**StG**	Strong fluorescence in the context of DNA; Energy acceptor from dG; Detection of energy transfer in DNA [179]; Photoswitch (370 nm: E →Z, E:Z = 6:94; 254 nm: Z →E, E:Z = 80:20) [64]
P.103	**4PVG**	Energy acceptor from dG; Detection of energy transfer in DNA [179]
P.104	$\mathbf{^{AB}G}$	Solvatochromic [181]
P.105	$\mathbf{^{CB}G}$	Solvatochromic [181]

Among the *C*8 arylated purine analogs reported, 8-(2-pyridyl)-2'-deoxyguanosine (**2PyG**, **P.96**) exhibits the highest emission wavelength (λ_{em} = 415 nm). Due to its "push-pull" character, this fluorophore exhibits strong solvatochromism. Due to excited-state proton transfer reactions with bulk solvent, its fluorescence is quenched in water (Φ = 0.02) but maintained in less acidic and non-polar solvents such as acetonitrile (Φ = 0.71), resulting in highly environmentally-sensitive quantum yields. Remarkably, upon incorporation into oligonucleotides, **2PyG** typically exhibits enhanced quantum yields (Φ = 0.01 – 0.15) as compared to the free nucleoside in water.[178] **2PyG** is minimally disruptive to duplex and G-quadruplex structures and has enabled the quantification of DNA-to-**2PyG** energy transfer taking place in G-quadruplexes. In addition, the (2-pyridyl)-imidazole moiety has the ability to bind divalent metals and provided the first means to selectively localize metal ions to arbitrary *N*7 sites in nucleic acids.[185]

Elongation of the conjugated π-system of a fluorophore is a straightforward strategy to red-shift excitation and emission maxima. Following this approach, conjugated linkers were introduced between purine and aryl groups at the 8-position. The addition of an acetylene bridge between guanosine and phenyl groups furnishes compounds with red-shifted emission maxima (λ_{em} = 475 nm) (**P.97** – **P.99**). Although little detail is reported about the photophysical characteristics of these compounds, their fluorescence intensity was shown to be strongly solvent-dependent. **P.99** was introduced in oligonucleotides and acts as a T-specific base-discriminating fluorophore.[186]

Acetyl-substituted 8-styryl deoxyguanosine and deoxyadenosine (**P.100** and **P.101**) show strong solvatochromism along with fluorescence quenching and red-shifted emission maxima ranging from 477 to 558 nm (1,4-dioxane → methanol). The corresponding 8-styryl-2'-deoxyguanosine (**StG**, **P.102**) shows little fluorescence environment sensitivity and retains strong fluorescence at 450 nm over a broad range of solvents (Φ = 0.49 and 0.74 in water and acetonitrile respectively). **StG** was shown to photoisomerize upon irradiation with UV light.[64] The presence of a nitrogen atom in the *para* position of the phenyl ring such as in 8-[2-(pyrid-4-yl)-ethenyl]-2'-deoxyguanosine (**4PVG, P.103**) yields a compound that undergoes little if any light-induced photoisomerization. These compounds also display environmentally-sensitive quantum yields (Φ = 0.16 and 0.57 in water and acetonitrile respectively) and red-shifted emission (λ_{em} = 490 nm). These two fluorophores exhibit little quenching upon incorporation into oligonucleotides (Φ = 0.13 – 0.45 and 0.03 – 0.10 for **StG** and **4PVG** respectively). In analogy to **2PyG**, **StG** and **4PVG** also act as energy acceptors from unmodified DNA bases, allowing the utilization of

energy transfer as readout of G-quadruplex formation. For **StG,** the resulting combination of energy transfer, high probe quantum yield, and high oligonucleotide molar extinction coefficient provides a highly sensitive and reliable readout of G-quadruplex formation even in sample solutions diluted below 1 nM.[179]

Further elaboration of this "conjugated π–system" strategy has recently been reported for 8-arylbutadienyl-2'-deoxyguanosines derivatives (**P.104** – **P.107**). The inclusion of electron donating groups, such as a methoxy (**^{MB}G**, **P.106**) or a dimethylamine (**^{DAB}G**, **P.107**), yields compounds with strong, environment insensitive fluorescence ($\Phi = 0.56 - 0.75$), but similar absorption and red-shifted emissions (λ_{abs} = 343 – 354 nm and λ_{em} = 429 – 443 nm) as compared to the styryl derivatives. Electron withdrawing groups such as acetyl (**^{AB}G**, **P.104**) or cyano group (**^{CB}G**, **P.105**) in constrast, yield to fluorophores with "push-pull" characteristics. This is accompanied by significantly red-shifted excitation and emission (λ_{abs} = 387 – 399 nm and λ_{em} = 486 – 547 nm respectively) as well as environmentally sensitive quantum yields (Φ = 0.02 – 0.59 and 0.32 – 0.75 for **^{AB}G** and **^{CB}G** respectively).[181]

2.3 Perspectives

The emissive purine analogs reviewed exhibit a broad range of photophysical and structural characteristics, and many of them have found utility in sensing applications. The availability of probes possessing complementary characteristics is highly desirable to fulfill the specific requirements of different types of assays. The typical readouts exploited are: (1) Fluorescence intensities: an increase in fluorescence resulting from the event under consideration is desirable. Conformational changes, nucleic acids cleavage, base pairing,… are usually detected by changes in fluorescence intensities. (2) Energy transfer: typically performed using FRET or exciton base pair to detect distance-dependent probe-to-probe energy transfer. Alternatively, DNA-to-probe energy transfer can provide a highly sensitive means to detect nucleic acids conformations. (3) Fluorescence microscopy: fluorophores displaying excitation and emission maxima similar or higher than 350 and 450 nm respectively can be suitable for imaging in cells or living systems using this technique.

Minimal structural impact, reasonable quantum yield in the context of nucleic acids and visible fluorescence for application to biological systems are conditions that have to be fulfilled in all three of these examples. Unfortunately, the same characteristics that normally generate favorable photophysical properties (enlargement of the conjugated

π-system or aromatic surface) are usually responsible for the perturbation of the modified nucleic acids structures. The design of new fluorescent base analogs therefore has to form a balance of these criteria.

Substituted purine analogs are an attractive alternative to tackle this problem. While the introduction of a small aromatic ring on the purine scaffold can afford highly emissive products, the modification can be minimally disruptive to the nucleic acids structures studied. Substitution of the position 8 of the purine scaffold can provide highly emissive nucleobase derivatives having the ability to mediate proper base pairing interactions along both *Watson & Crick* and *Hoogsteen* faces. Although the introduction of bulky groups to the position 8 of purines can shift the conformational equilibrium of the glycosidic bond from *anti* to *syn* (Chapter 3),[173,187-195] DNA folding can force 8-modified guanosines to adopt *anti* conformations with relatively small energetic penalties to DNA folding ($\Delta\Delta G < 1$ kcal / mol).[188,189,192]

For these reasons, 8-substituted-2'-deoxyguanosines are attractive probes for the detection of DNA folding in various structures, including G-quadruplexes. This dissertation will focus on the synthesis, photophysical characterization and implementation into oligonucleotides of 8-aryl- and 8-(2-arylethenyl)-2'-deoxyguanosine analogs. These fluorescent probes are not significantly quenched in the context of nucleic acids, are minimally disruptive to the DNA structures studied and can be used as probes for energy transfer taking place in nucleic acids.

CHAPTER 3

Synthesis, Photophysical Characterization and Conformational Analysis of 8-(Substituted)-2'-deoxyguanosines

A small family of 8-aryl- and 8-(2-arylethenyl)-2'-deoxyguanosine analogs was synthesized to evaluate their photophysical and conformational characteristics. A strategy involving the O^6 protection of guanosine was developed to inhibit palladium complexation during cross-coupling reactions. This approach provides broad access to palladium-catalyzed cross-coupling reactions for the synthesis of guanine derivatives containing vinyl, phenyl, pyridine, thiophene, furan and larger conjugated π-systems at the *C*8 position. The resulting 8-substituted-2'-deoxyguanosines exhibit quantum yields for fluorescence (Φ) ranging from 0.47 to 0.79 in acetonitrile. Among the nucleosides synthesized, derivatives containing pyridine groups exhibit environmentally-sensitive fluorescence properties (Φ = 0.001 – 0.72) due to excited-state proton transfer reactions involving bulk solvent. Among them, 8-(2-pyridyl)-2'-deoxyguanosine (**2PyG**) is a particularly interesting derivative retaining reasonable fluorescence in water (Φ = 0.02) and displaying strong solvatochromism. ^{1}H, ^{13}C and 2D-NOESY NMR was used to determine the glycosydic conformation of 8-substituted-2'-deoxyguanosines synthesized. All the 8-(aryl)-2'-deoxyguanosine derivatives showed a *syn* glycosidic preference. Interestingly, the presence of a vinyl bridge between the nucleobase and the aryl reverses this tendency to provide 8-substituted derivatives having an *anti* glycosidic bond preference similar to unmodified guanosine residues.

3.1 Introduction

Micro-environment sensitive fluorescent nucleoside analogs can act as internal probes for DNA folding. The development of new fluorescent guanine analogs that can be introduced directly into the G-quadruplex core will lead to new techniques for the detection of G-quadruplex formation *in vitro* and *in vivo*. For this purpose, the internal probe needs to fulfill different criteria, such as (1) environment-sensitive photophysical characteristics, (2) sufficient emission quantum efficiency in the context of nucleic acids, (3) emission at relatively long wavelengths (typically in the visible range) (4) minimal perturbation of the system. To fulfill these goals, modification of the position 8 of guanosine is an attractive avenue, because it is not directly involved in base pairing interactions in G-quadruplex or duplex structures (Figure 4.4 A & C), and has already shown to provide emissive compounds.[48,69,95,99,105-108,176,177,180] Carbon-carbon bond formation at the *C*8 position of guanosine is typically achieved *via* palladium-catalyzed cross-coupling reactions starting from 8-bromo guanosine derivatives. However, most of the reported methodology for these reactions focus on the coupling of phenyl derivatives and do not tackle the introduction of heterocyclic aromatic substituents.[62,64,196] A synthetic strategy involving the O^6 protection of guanosine was designed to prevent detrimental complexation of palladium to the nucleobase and allow broad access to palladium-catalyzed cross-coupling reactions for the synthesis of 8-substituted guanine derivatives. Using this approach, a collection of ten 8-aryl- and 8-(2-arylethenyl)-2'-deoxyguanosine analogs was successfully synthesized. The resulting nucleosides are emissive and display diverse photophysical characteristics. Derivatives containing a pyridine group exhibit environment sensitive fluorescent properties and are therefore good candidates for the detection of nucleic acids structural changes. Among them, 8-(2-pyridyl)-2'-deoxyguanosine (**2PyG**) presents strong solvatochromism and other interesting environment sensitive spectral properties.

The addition of bulky groups to the *C*8 position of guanosine can shift the natural *anti* conformational equilibrium of the glycosidic bond to *syn*.[173,187-195] Determination of the glycosidic preference of the synthesized nucleosides can provide insights to their ability to mimic natural guanosine residues in the context of nucleic acids. The glycosidic bond preferences of all nucleosides was characterized by ^{1}H, ^{13}C and 2D-NOESY NMR. These results indicate that a *syn* conformation is preferred for the 8-aryl-2'-deoxyguanosines, whereas a vinyl bridge between the aryl group and *C*8 of the nucleobase reverses this tendency.

3.2 Results and discussion

3.2.1 Synthesis of 8-(substituted)-2'-deoxyguanosines[2]

The synthesis of 8-aryl- and 8-(2-arylethenyl)-2'-deoxyguanosine involves the formation of a carbon-carbon bond at the *C*8 position of the nucleobase. This is commonly achieved using palladium-catalyzed cross-coupling chemistry. Previous work of *Western* et al. reports the synthesis of 8-aryl-2'-deoxyguanosines by a *Suzuki-Miyaura* coupling on unprotected 8-bromo-2'-deoxyguanosine in water using water-soluble palladium catalysts.[196] This straightforward approach can give the desired 8-substituted guanosine derivatives in two steps starting from 2'-deoxyguanosine. 8-Bromo-2'-deoxyguanosine (**2**) was therefore prepared by bromination of 2'-deoxyguanosine (**1**) with *N*-bromosuccinimide (NBS) in a 1:4 water:acetonitrile mixture in good yields. **2** was then utilized in *Suzuki-Miyaura* coupling with aryl boronic acids or boronic acid pinacol esters in a 1:2 acetonitrile:water mixture using palladium acetate / tris(4,6-dimethyl-3-sulfonato-phenyl)phosphine trisodium salt (TXPTS) as a water-soluble catalytic system (Scheme 3.1). However, in our hands, only 8-phenyl-2'-deoxyguanosine (**3, PhG**) (Table 3.1, entry 1) was obtained in reasonable yield (77%) under these conditions. Reactions involving other boronic acids or esters, such as 2-aminopyridine-5-boronic acid pinacol ester, 2-nitro-5-pyridineboronic acid pinacol ester and 4-pyridineboronic acid did not show any conversion (Table 3.1, entries 2-4). Attempts to achieve this reaction *via Stille* coupling on the deprotected 8-bromo-2'-deoxyguanosine with 2-pyridyl-tributylstannane with different catalysts were also unsuccessful even after protection of 3'-*O* and 5'-*O* with *tert*butyldimethylsilyl (TBDMS) or of the 3'-*O*, 5'-*O* and N^2 with isobutyryl (Table 3.1, entries 5-10).

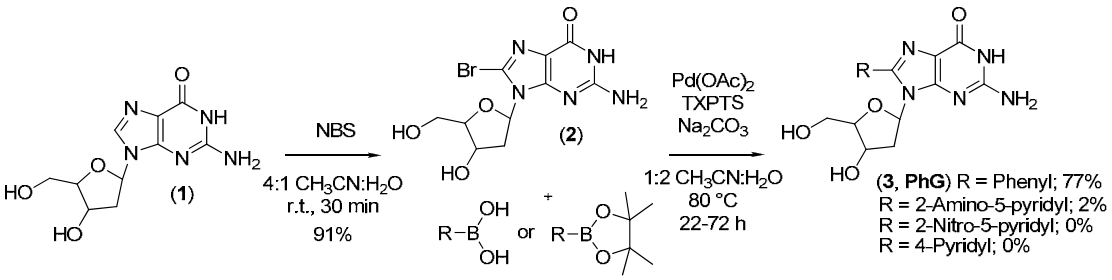

Scheme 3.1: Synthesis of 8-aryl-2'-deoxyguanosines *via Suzuki-Miyaura* coupling in aqueous conditions as reported by *Western* et al.[196]

[2] Detailed synthetic procedures and characterization of these compounds and intermediates are available in Chapter 8.

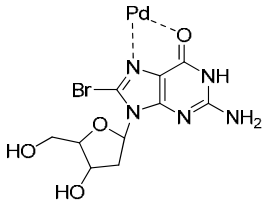

Figure 3.1: Proposed complexation mode of palladium with 8-bromo-2'-deoxyguanosine.

The complexation of the palladium catalyst by interaction through O^6 and $N7$ positions of the nucleobase was suggested to cause the poor reactivity of guanosine towards palladium-catalyzed cross-coupling reactions (Figure 3.1).[197] To inhibit the complexation of metals by guanosine derivatives, the O^6 position was protected as a benzyl ether. To achieve selective protection, the ribose 5'- and 3'-hydroxy groups were protected as *tert*butyldimethylsilyl ethers by reaction of 8-bromo-2'-deoxyguanosine (**2**) with *tert*-butyl(chloro)dimethylsilane and imidazole in DMF to give 8-bromo-3',5'-*O*-bis(*tert*-butyldimethylsilyl)-2'-deoxyguanosine (**4**)**.** The benzyl group was then introduced at O^6 by a modified *Mitsunobu* reaction involving benzyl alcohol, diisopropyl azodicarboxylate (DIAD) and triphenylphosphine in dioxane to give 8-bromo-3',5'-*O*-bis(*tert*-butyldimethylsilyl)-O^6-benzyl-2'-deoxyguanosine (**5**).

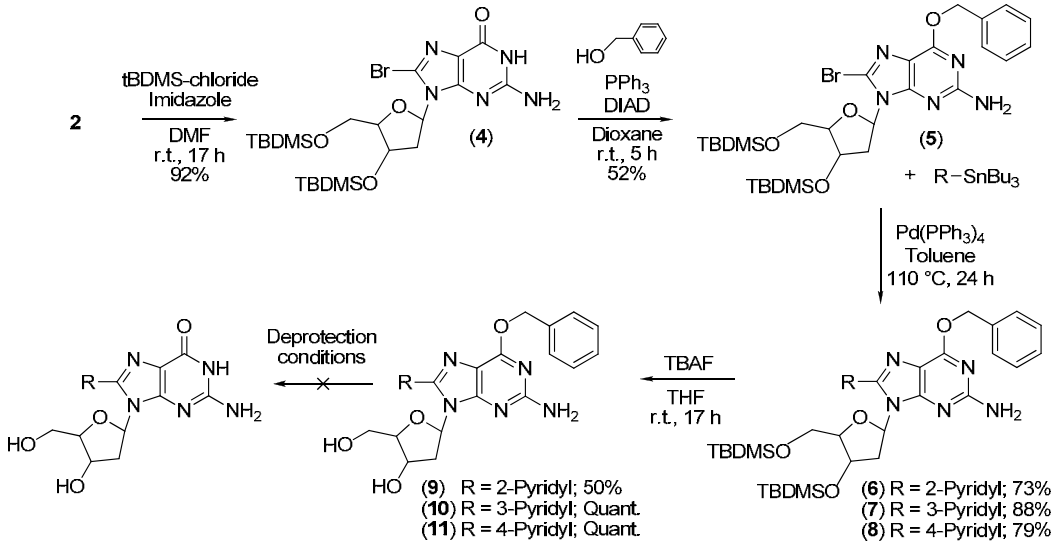

Scheme 3.2: Synthesis of 8-substituted-2'-deoxyguanosines involving O^6-benzyl protection.

Stille coupling reactions utilizing the protected guanosine derivative (**5**) were successful. This strategy provided straightforward coupling of **5** with 2-pyridyl-, 3-pyridyl- and 4-pyridyl-tributylstannane in 73%, 88% and 79% respectively to give compounds **6** – **8**

(Scheme 3.2, Table 3.1, entries 11-13). The *tert*butyldimethylsilyl groups of nucleosides **6** – **8** were then removed by treatment with tetrabutylammonium fluoride (TBAF) in THF in yields ranging from 50 – 100%. However, subsequent removal of the benzyl group from the O^6 position was unsuccessful. A number of reaction conditions, involving hydrogen gas, cyclohexene or cyclohexadiene as an hydrogen source and Pd/C or $Pd(OH)_2$ as catalysts did not show any conversion. Deprotection attempts involving boron trifluoride etherate in mercaptoethanol led to depurination.

To overcome these difficulties, benzyl was replaced by 2-trimethylsilyl-ethyl for the protection of the O^6-position of guanosine. Compound **4** was protected *via Mitsunobu* reaction involving trimethylsilylethanol, DIAD and triphenylphosphine in dioxane to give 8-bromo-3',5'-*O*-bis(*tert*-butyldimethylsilyl)-O^6-(trimethylsilylethyl)-2'-deoxyguanosine (**12**) in modest yield (50%). Attempts to optimize the reaction yield were unsuccessful, however, the unreacted starting material can be recovered after the reaction and recycled. Compound **12** was successfully involved in a wide variety of cross-coupling reactions including *Stille*, *Suzuki* and *Sonogashira* couplings. The reaction of **12** with 2-, 3-, 4-pyridyl-, 2-thiophene- and 2-furyltributylstannane with tetrakis(triphenylphosphine) palladium in toluene at 110 °C furnished compounds **13** – **17** in 37 – 89% yield (Scheme 3.3, Table 3.1, entries 14-18).

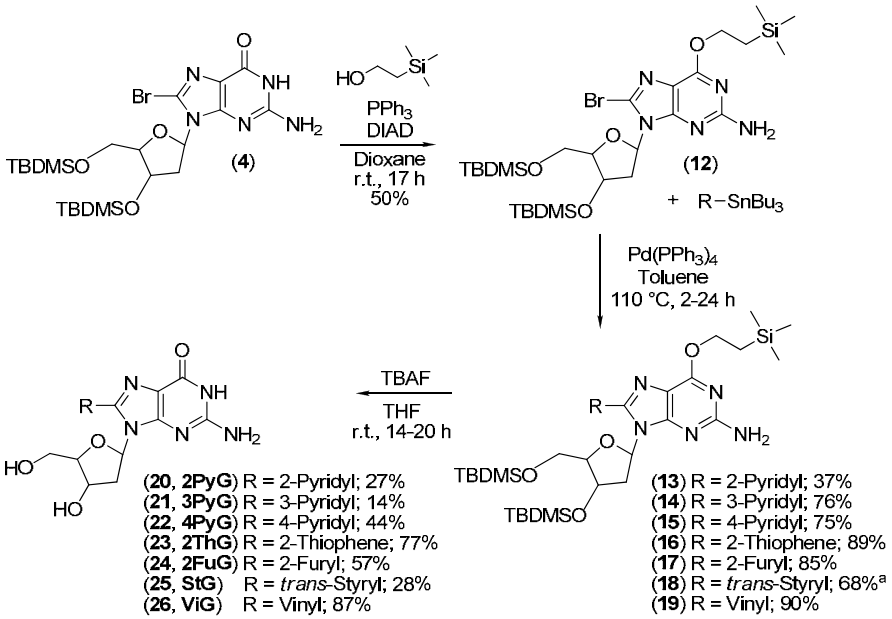

Scheme 3.3: Synthesis of 8-substituted-2'-deoxyguanosine involving O^6-trimethysilylethyl ether protection. [a] This compound was obtained under *Suzuki-Miyaura* coupling conditions with (*E*)-2-styreneboronic acid pinacol ester.

Table 3.1: Test reaction results for *Suzuki-Miyaura* and *Stille* cross couplings of 8-substituted-2'-deoxyguanosines.

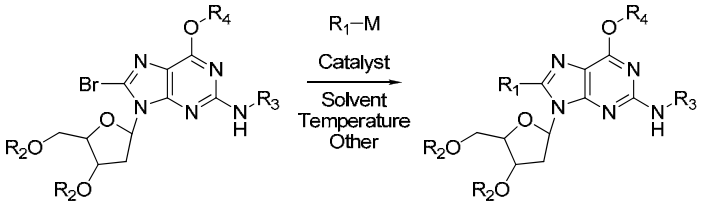

Entry	R_1-M	R_2	R_3	R_4	Catalyst	Solvent Temperature	Other	Result (Cpd No)
1	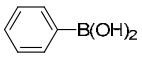	H	H	H	$Pd(OAc)_2$/ TXPTS	ACN/H_2O 80 ºC	Na_2CO_3	70%[a] **(3)**
2	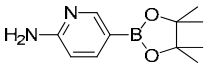	H	H	H	$Pd(OAc)_2$/ TXPTS	ACN/H_2O 80 ºC	Na_2CO_3	2%
3	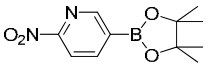	H	H	H	$Pd(OAc)_2$/ TXPTS	ACN/H_2O 80 ºC	Na_2CO_3	No reaction[b]
4	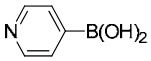	H	H	H	$Pd(OAc)_2$/ TXPTS	ACN/H_2O 80 ºC	Na_2CO_3	No reaction[b]
5	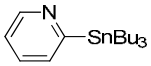	H	H	H	$Pd(PPh_3)_2Cl_2$	Dioxane 90 ºC	-	No reaction[b]
6	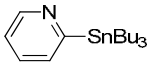	H	H	H	$Pd(PPh_3)_2Cl_2$	DME 90 ºC	-	No reaction[b]
7	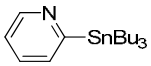	TBDMS	H	H	$Pd(PPh_3)_2Cl_2$	Dioxane 90 ºC	-	No reaction[b]
8	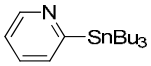	TBDMS	H	H	$Pd(PPh_3)_2Cl_2$	Toluene 110 ºC	-	No reaction[b]
9	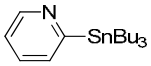	TBDMS	H	H	$Pd(PPh_3)_4$	Toluene 110 ºC	-	No reaction[b]
10	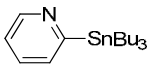	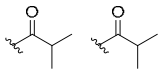	H		$Pd(PPh_3)_4$	Toluene 110 ºC	-	No reaction[b]
11	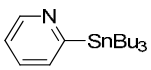	TBDMS	H	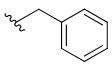	$Pd(PPh_3)_4$	Toluene 110 ºC	-	73%[a] **(6)**
12	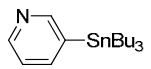	TBDMS	H	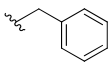	$Pd(PPh_3)_4$	Toluene 110 ºC	-	88%[a] **(7)**
13	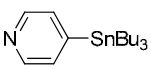	TBDMS	H	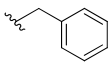	$Pd(PPh_3)_4$	Toluene 110 ºC	-	79%[a] **(8)**

Entry	R_1-M	R_2	R_3	R_4	Catalyst	Solvent Temperature	Other	Result (Cpd No)
14	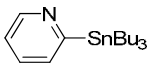	TBDMS	H	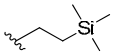	$Pd(PPh_3)_4$	Toluene 110 °C	-	37%[a] (**13**)
15	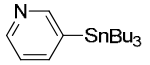	TBDMS	H	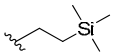	$Pd(PPh_3)_4$	Toluene 110 °C	-	76%[a] (**14**)
16	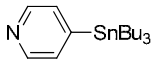	TBDMS	H	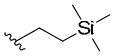	$Pd(PPh_3)_4$	Toluene 110 °C	-	75%[a] (**15**)
17	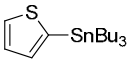	TBDMS	H	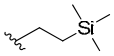	$Pd(PPh_3)_4$	Toluene 110 °C	-	89%[a] (**16**)
18	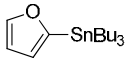	TBDMS	H	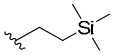	$Pd(PPh_3)_4$	Toluene 110 °C	-	85%[a] (**17**)
19	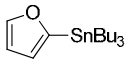	TBDMS	H	H	$Pd(PPh_3)_4$	Toluene 110 °C	-	No reaction[b]
20	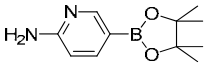	TBDMS	H	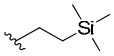	$Pd(PPh_3)_4$	DME/Toluene 80 °C	Na_2CO_3	Successful coupling[c]
21	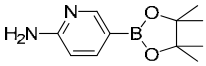	TBDMS	H	H	$Pd(PPh_3)_4$	DME/Toluene 80 °C	Na_2CO_3	No reaction[b]
22	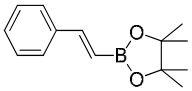	TBDMS	H	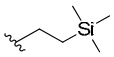	$Pd(PPh_3)_4$	DME/Toluene 80 °C	Na_2CO_3	68%[a] (**18**)
23	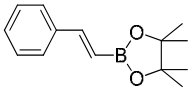	TBDMS	H	H	$Pd(PPh_3)_4$	DME/Toluene 80 °C	Na_2CO_3	Successful coupling[c]
24	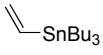	TBDMS	H	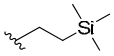	$Pd(PPh_3)_4$	Toluene 110 °C	-	90%[a] (**19**)
25	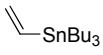	TBDMS	H	H	$Pd(PPh_3)_4$	Toluene 110 °C	-	Successful coupling[c]

[a] isolated yields; [b] no conversion observed by TLC; [c] test reactions performed on small scale, showing >80% conversion by TLC after 24 hours, the product was not isolated.

Under identical reaction conditions using 2-pyridyltributylstannane, no conversion is observed with compound **4**, lacking O^6-protection (Table 3.1, entries 9 and 14). The same observation was made for the 2-furyl-derivative (Table 3.1, entries 18 and 19) and for the 2-aminopyridine-5-boronic acid pinacol ester under *Suzuki-Miyaura* conditions (Table 3.1, entries 20 and 21). These control reactions demonstrate O^6-protection as a key strategy for the coupling 2'-deoxyguanosines with heteroaromatic moieties.

It should be noted that if the substituent introduced on position *C*8 does not contain heteroatoms, as in the case of 8-phenyl-2'-deoxyguanosine (**3**) and the *trans*-styryl

derivative (**23**), protection of O^6 is not necessary and coupling reactions are successful using the unprotected 8-bromo derivatives **2** and **4** (Table 3.1, entries 1, 22 and 23). For the vinyl substituent, *Stille* coupling was successful in the absence of O^6 protection, but this reaction did not reach completion. However, the presence of the O^6-trimethylsilyl ether significantly accelerated the reaction (9 hours *versus* 2 hours) and resulted in complete conversion (Table 3.1, entries 24 and 25). Following derivatization of the *C*8 position, the three silyl-ether protecting groups can be removed in a single deprotection step using TBAF in THF to give final 8-substituted-2'-deoxyguanosines **20** – **26** in 14 – 77% non-optimized yields (Scheme 3.3).

Guanosine analogs with elongated π-systems including the vinyl bridged derivative *trans*-8-(2-phenylethenyl)-2'-deoxyguanosine (**StG**), can have very favourable photophysical characteristics, but the commercial availability of pure *trans*-(2-arylethenyl)-boronic acids and stannane precursors is very limited. A small series of 8-vinyl bridged guanosine derivatives was therefore synthesized *via Heck* coupling starting from the fully protected 8-vinyl-2'-deoxyguanosine derivative **19**. 3- and 4-Bromopyridine were successfully coupled with excellent stereo- and regioselectivity, giving (*E*)-3',5'-*O*-bis(*tert*-butyldimethylsilyl)-8-[2-(pyrid-3-yl)-ethenyl]-O^6-(trimethylsilylethyl)-2'-deoxyguanosine (**27**) and (*E*)-3',5'-*O*-bis(*tert*-butyldimethylsilyl)-8-[2-(pyrid-4-yl)-ethenyl]-O^6-(trimethyl-silylethyl)-2'-deoxyguanosine (**28**) in 15 and 72% yield respectively. Palladium-catalyzed coupling of 2-pyridyl derivatives is frequently significantly more challenging than for other heteroaryl groups[198,199] and was unsuccessful in this case. In analogy to the synthetic path described before, the final compounds were obtained in one single deprotection step using TBAF in THF to give (*E*)-8-[2-(pyrid-3-yl)-ethenyl]-2'-deoxyguanosine (**29**, **3PVG**) and (*E*)-8-[2-(pyrid-4-yl)-ethenyl]-2'-deoxyguanosine (**30**, **4PVG**) in 22 and 15% unoptimized yields respectively. NMR and analytical HPLC confirmed the presence of the pure *trans*-isomers.

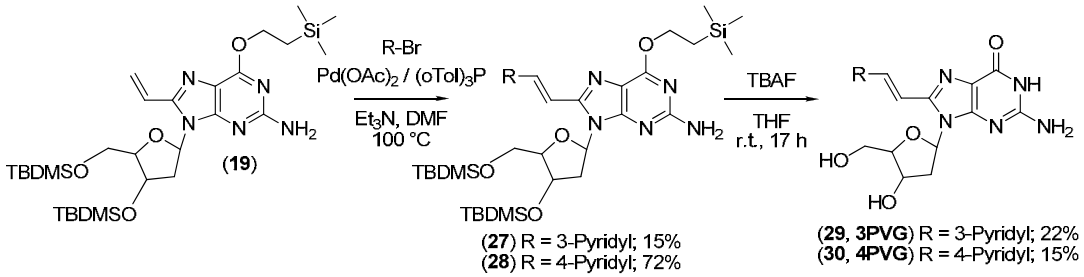

Scheme 3.4: Synthesis of elongated 8-(2-arylethenyl)-2'-deoxyguanosines *via Heck* coupling.

3.2.2 Photophysical characterization of 8-(substituted)-2'-deoxyguanosines

The photophysical properties of the synthesized 8-substituted nucleosides are summarized in Table 3.2. All reported derivatives exhibit relatively high molar extinction coefficients ($\varepsilon_{275\text{-}294nm}$ = 11'000 – 24'000 $cm^{-1}M^{-1}$) and red-shifted absorption maxima as compared to 2'-deoxyguanosine (ε_{260nm} = 13'500 $cm^{-1}M^{-1}$). Due to their larger conjugated π-systems, compounds **25**, **29** and **30** show more pronounced red-shifts than their aryl analogs. All reported nucleosides exhibit large *Stokes* shifts in water (90 – 156 nm), and compounds **3** (**PhG**), and **23** – **26** (**2ThG, 2FuG, StG, ViG**) display high quantum yields in both water and acetonitrile (Φ = 0.47 – 0.79). The pyridine derivatives **20** – **22** (**2PyG**, **3PyG**, **4PyG**) and **30** (**4PVG**) in contrast, exhibit much lower quantum yields in water (Φ = 0.001 – 0.16), but approach unity in acetonitrile (Φ = 0.57 – 0.72). To evaluate the origin of this effect, quantum yields were measured in D_2O and compared to the values in H_2O. Two-fold higher quantum yields for all three compounds in D_2O revealed a kinetic isotope effect that suggests proton transfer reactions with bulk solvent are responsible for rapid non-emissive decay of compounds **20** – **22** and **30** in H_2O (Table 3.2).[200] Compound **29** (**3PVG**) is the only pyridyl derivative that is not significantly quenched in water (Φ = 0.44) and exhibits only a modestly higher quantum yield in D_2O (Φ = 0.54). Nucleosides **3** and **23** – **26**, in contrast, exhibited much less environmental sensitivity, as their quantum yields are essentially unchanged in H_2O, D_2O, and acetonitrile (Table 3.2). These results suggest that the pyridyl nitrogens of **20** – **22** and **30** are the relevant sites of increased basicity and protonation upon photoexcitation. This conclusion is supported by orbital density plots of the planar **2PyG** chromophore that shows increased electron density on the pyridine ring upon going from HOMO → LUMO (Figure 3.2).

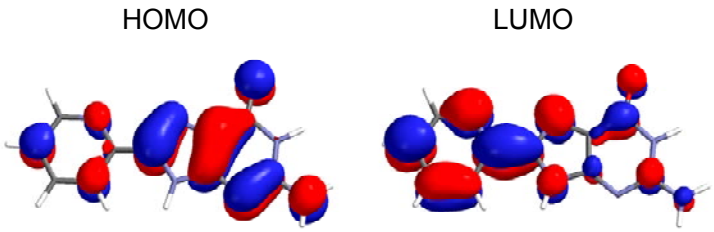

Figure 3.2: Orbital density plots calculated from DFT (pBP/DN**) optimized geometries of the isolated **2PyG** nucleobase. Geometries were optimized starting from a planar, *cis* conformation. Similar results were observed for *trans*.

Table 3.2: Primary fluorescent parameters determined for 8-substituted-2'-deoxyguanosines.

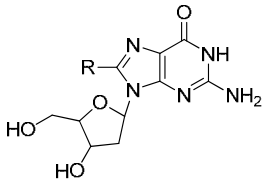

	Name	R	λ_{abs} (nm)	λ_{em} (nm)	ε^{a} (H_2O)	Φ^{b} (CH_3CN)	Φ^{b} (H_2O)	Φ^{b} (D_2O)	Φ (D_2O)/ Φ (H_2O)
1	**dG**	H–	260	330	13'500[c]	n.d.[d]	$<10^{-4}$ [e]	n.d.[d]	n.d.[d]
3	**PhG**	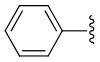	275	394	22'000	0.54	0.76	0.73	1.0
20	**2PyG**	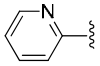	280/300	415	20'000[f]	0.71	0.02	0.04	2.1
21	**3PyG**	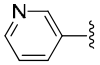	280	418	18'000	0.59	0.001	0.002	2.0
22	**4PyG**	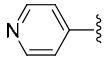	280/306	436	17'000[f]	0.72	0.005	0.011	2.1
23	**2ThG**		284	418	20'000	0.69	0.72	0.74	1.0
24	**2FuG**		294	384	24'000	0.66	0.47	0.46	1.0
26	**ViG**		280	390	11'000	0.49	0.79	0.84	1.1
25	**StG**	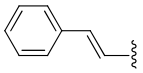	340	450	17'000	0.74	0.49	0.50	1.0
29	**3PVG**	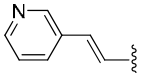	345	460	16'000	0.64	0.44	0.54	1.3
30	**4PVG**	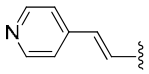	355	490	18'000	0.57	0.16	0.30	1.9

[a] errors (STP) associated with ε are approximatively ±25%; [b] errors associated with Φ are approximatively ±5% of the given values; [c] [12,80]; [d] n.d.: not determined; [e] [14]; [f] λ_{abs} = 280 nm.

3.2.3 Solvatochromism of 8-(2-pyridyl)-2'-deoxyguanosine

Solvatochromic base analogs can provide powerful tools for detecting changes in nucleic acids' micro-environments occurring at the nucleoside level. The absorbance and emission spectra of **2PyG** were therefore characterized in methanol, ethanol, DMSO, and 1,4-dioxane (Figure 3.3 A, Table 3.3). In less polar solvents the absorption maximum of **2PyG** is red-shifted and the emission maximum is blue-shifted as compared to aqueous samples. As a result, the Stokes' shifts of **2PyG** decrease from 115 nm to 64 nm going

from water to 1,4-dioxane (Figure 3.3 A, Table 3.3). This trend is consistent with solvent-mediated stabilization of a charge separated emissive state having a larger dipole moment than the ground state.[63,201] The Stokes' shifts measured in six solvents were therefore plotted against Reichardt's normalized solvent polarity parameter "E_T^N"– a polarity scale taking microenvironment solvent-solute interactions into account.[202,203] The resulting plot exhibits an excellent linear correlation ($R^2 = 0.98$) and large positive solvatochromic response slope of 4094 cm^{-1} (Figure 3.3 B). This slope is even larger than those reported for a related series of "push-pull" purines having electron-accepting groups at position *C*8.[63] Orbital density plots calculated from DFT optimized geometries are also consistent with the push-pull nature of the **2PyG** chromophore, where increased electron density on the pyridine ring and decreased electron density on the guanine moiety are observed upon going from HOMO → LUMO (Figure 3.2). Together these results confirm **2PyG**'s excellent potential for microenvironment sensing applications. The emission intensity of **2PyG** is also highly sensitive to solvent identity with a 30-fold increase from water to 1,4-dioxane. In this case, the quantum yield of **2PyG** is only modestly correlated to solvent polarity ($R^2 = 0.81$), but a better correlation ($R^2 = 0.89$) is observed for solvent acidity (SA, Figure 3.3 C).[204] These results are consistent with the trends observed for H_2O *versus* D_2O and further support excited state proton transfer as a dominant non-radiative decay pathway of **2PyG** in aqueous and organic solvents.

Table 3.3: **2PyG** fluorescence properties in different solvents, Reichardt's normalized solvent polarity parameter (E_T^N) and solvent acidity (SA) of the solvents.

Solvent	λ_{abs} (nm)	λ_{em} (nm)	Stokes shift (cm^{-1})	Quantum yield	E_T^N	SA
Water	305	415	8691	0.02	1.00	1.06
Methanol	310	415	7549	0.06	0.76	0.61
Ethanol	316	404	6893	0.34	0.65	0.40
DMSO	327	415	6485	0.70	0.44	0.07
Acetonitrile	316	395	6329	0.71	0.46	0.04
Dioxane	322	386	5149	0.73	0.16	0.00

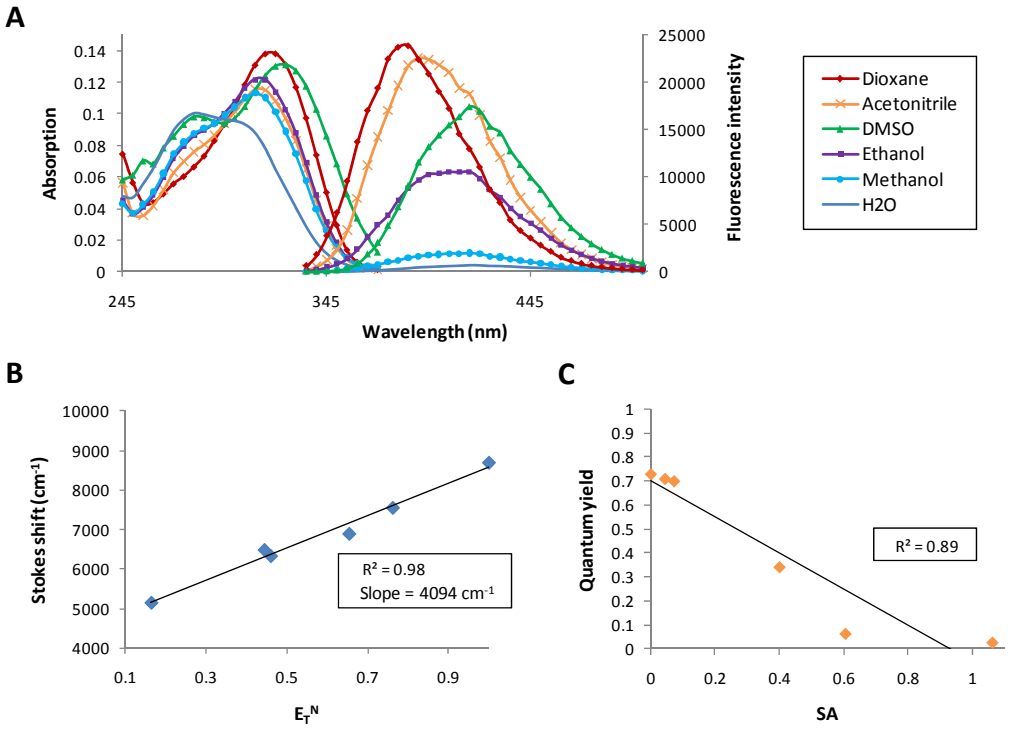

Figure 3.3: (A) Absorption and emission spectra of **2PyG** in 1,4-dioxane, acetonitrile, DMSO, ethanol, methanol and water (λ_{ex} = 300 nm). (B) *Stokes* shift of **2PyG** *versus Reichardt*'s normalized solvent polarity parameter, E_T^N [202] (λ_{ex} = 300 nm). (C) Quantum yield of **2PyG** *versus* solvent acidity SA [204] (λ_{ex} = 300 nm).

3.2.4 *Cis-trans* photoisomerizations

Derivatives of 8-vinyl guanosine, including 8-(2-phenylethenyl)-2'-deoxyguanosine (**25**), were recently reported to be *cis-trans* photoisomerizable switches capable of influencing DNA conformations.[64,105-107] **StG** photoisomerizes upon irradiation at 370 nm to reach a photostationary E:Z ratio of 6:94, while irradiation at 254 nm causes the reverse photoisomerization and reach a E:Z ratio of 80:20. According to HPLC and NMR analysis, we were able to reproduce these results with nucleoside **25** in our laboratory.[64] Replacing the phenyl ring of **25** with a pyridine group generates new fluorescent nucleoside derivatives trans-8-(3-pyridyl-vinyl)-2'-deoxyguanosine (**29**, **3PVG**) and trans-8-(4-pyridyl-vinyl)-2'-deoxyguanosine (**30**, **4PVG**) that exhibits little, if any photoswitching. Upon extensive irradiation of **3PVG** at 370 nm, a maximum of 18% of the Z form was observed in water at room temperature (E:Z = 82:18). Irradiation at 254 nm caused an almost complete reverse photoisomerization and reached a E:Z ratio of 98:2. In the case of **4PVG**, irradiation at 370 nm leads to a maximum of 24% isomerization, with an E:Z ratio of 76:24. The reversed process is also nearly complete, with a photostationary state reached

with a E:Z of 94:6 after irradiation at 254 nm. The poor switching abilities of these nucleosides will serve to simplify the interpretation of CD and fluorescence data collected using compound **4PVG** in the context of oligonucleotides (Chapter 6).

3.2.5 Conformational analysis

The addition of bulky groups to the position 8 of guanosine can shift the conformational equilibrium of the glycosidic bond from *anti* to *syn*.[173,187-195] The *anti* conformation of 8-phenol-2'-deoxyguanosine derivatives for examples, are less stable than the *syn* by ca. 6 kcal/mol.[195] Although DNA folding can force 8-modified guanosines to adopt *anti* conformations with relatively small energetic penalties to DNA folding ($\Delta\Delta G < 1$ kcal/mol),[188,189,192] the introduction of one nucleobase analog with *syn* preference can change the G-quadruplex topology adopted by a given sequence.[77] The glycosidic conformation of 8-substituted purine nucleosides can be evaluated using ^{1}H- and ^{13}C-NMR. A conformational change from *anti* to *syn* correlates with a downfield shift of H(2'), C(1'), C(3') and C(4') and an upfield shift of the C(2') signal.[190,191]

2'-Deoxyguanosine (**1**) and 8-bromo-2'-deoxyguanosine (**2**), are known to adopt *anti* and *syn* glycosidic conformations respectively, and can be used as references for interpretation of 1-D NMR data. According to this analysis, the guanosine derivatives substituted with an aryl group directly attached to *C*8, such as **PhG**, **2PyG, 3PyG**, **4PyG**, **2ThG** and **2FuG**, prefer a *syn* conformation (Table 3.4). In contrast, the compounds bearing only a vinyl substituent, such as in **ViG**, or a vinyl group bridging *C*8 and the aryl group, such as in **StG**, **3PVG** and **4PVG**, exhibit chemical shifts consistent with an *anti* conformational preference of the glycosidic bond (Table 3.4). These preferences were confirmed by 2D-ROESY experiments for **2PyG**, **StG** and **4PVG**. Strong cross peaks were observed between the phenyl/pyridyl rings and 5'-OH, H5', H3' and H2' of **StG** and **4PVG**, but were absent in the case of **2PyG** (Figures 3.4-3.6). These results confirm a *syn* conformational preference for **2PyG**, and *anti* preference for **StG** and **4PVG**. These conformational preferences might be important in the context of oligonucleotides, where **StG** and 4**PVG** are found to be generally less disruptive to DNA folding than **2PyG** (Chapter 6).

Table 3.4: Chemical shifts (ppm) of H(2'), C(2'), C(1'), C(3') and C(4') of the 8-substituted-2'-deoxyguanosines synthesized as compared to 2'-deoxyguanosine (**dG**) and 8-bromo-2'-deoxyguanosine (**8BrdG**). The values corresponding to mainly *anti* or *syn* glycosidic conformations are highlighted in blue or orange respectively.

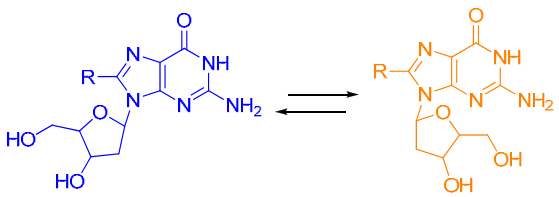

anti *syn*

Name	R	δH(2')	δC(2')	δC(1')	δC(3')	δC(4')
dG	H—	2.50	39.5	82.5	70.7	87.5
8BrdG	Br—	3.14	36.4	85.0	70.9	87.8
PhG		3.16	36.4	84.5	71.1	87.8
2PyG		3.12	37.7	85.2	71.4	87.9
3PyG		3.14	36.5	84.4	71.0	87.8
4PyG	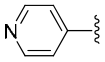	3.16	36.5	84.3	70.9	87.8
2FuG		3.16	36.9	84.4	71.1	87.8
2ThG		3.28	36.3	84.4	71.0	87.8
ViG		2.61	-	82.5	70.5	87.4
StG	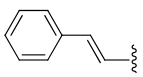	2.59	-	82.3	70.2	87.2
3PVG	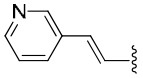	2.59	-	82.5	70.2	87.3
4PVG	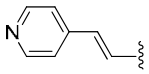	2.56	-	82.5	70.3	87.4

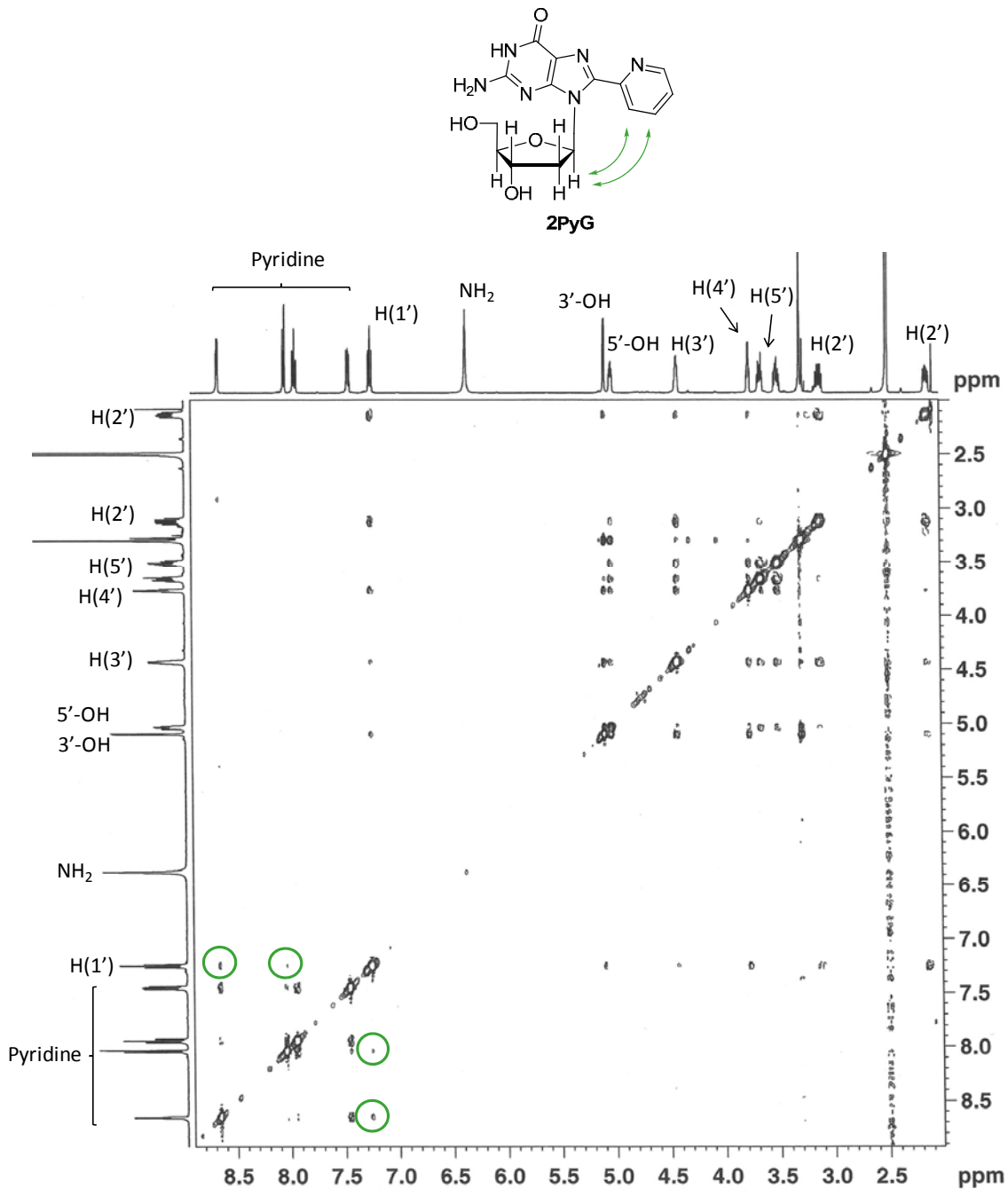

Figure 3.4: 2D-ROESY of **2PyG** in d_6-DMSO (mixing time = 250 ms).

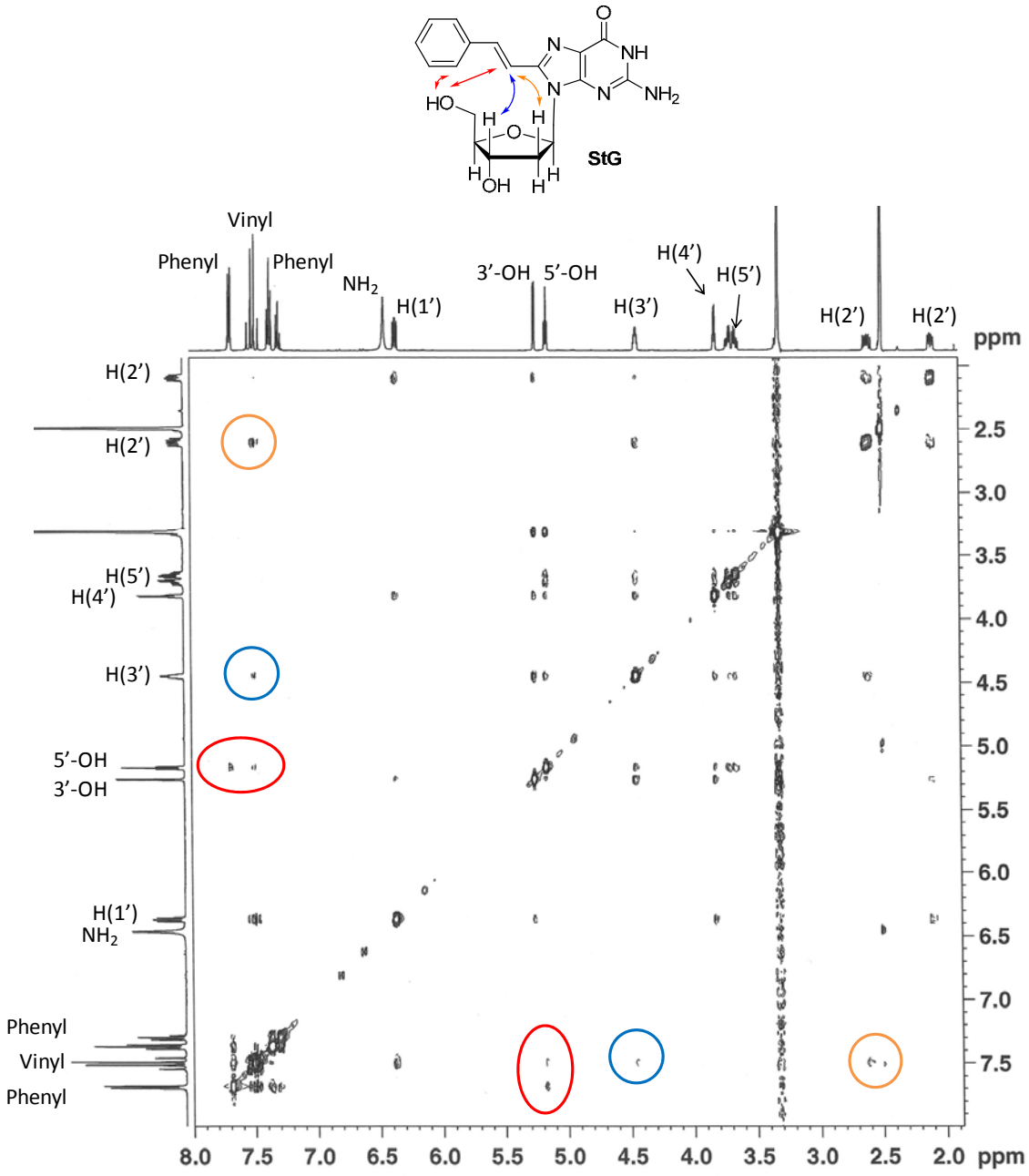

Figure 3.5: 2D-ROESY of **StG** in d_6-DMSO (mixing time = 250 ms).

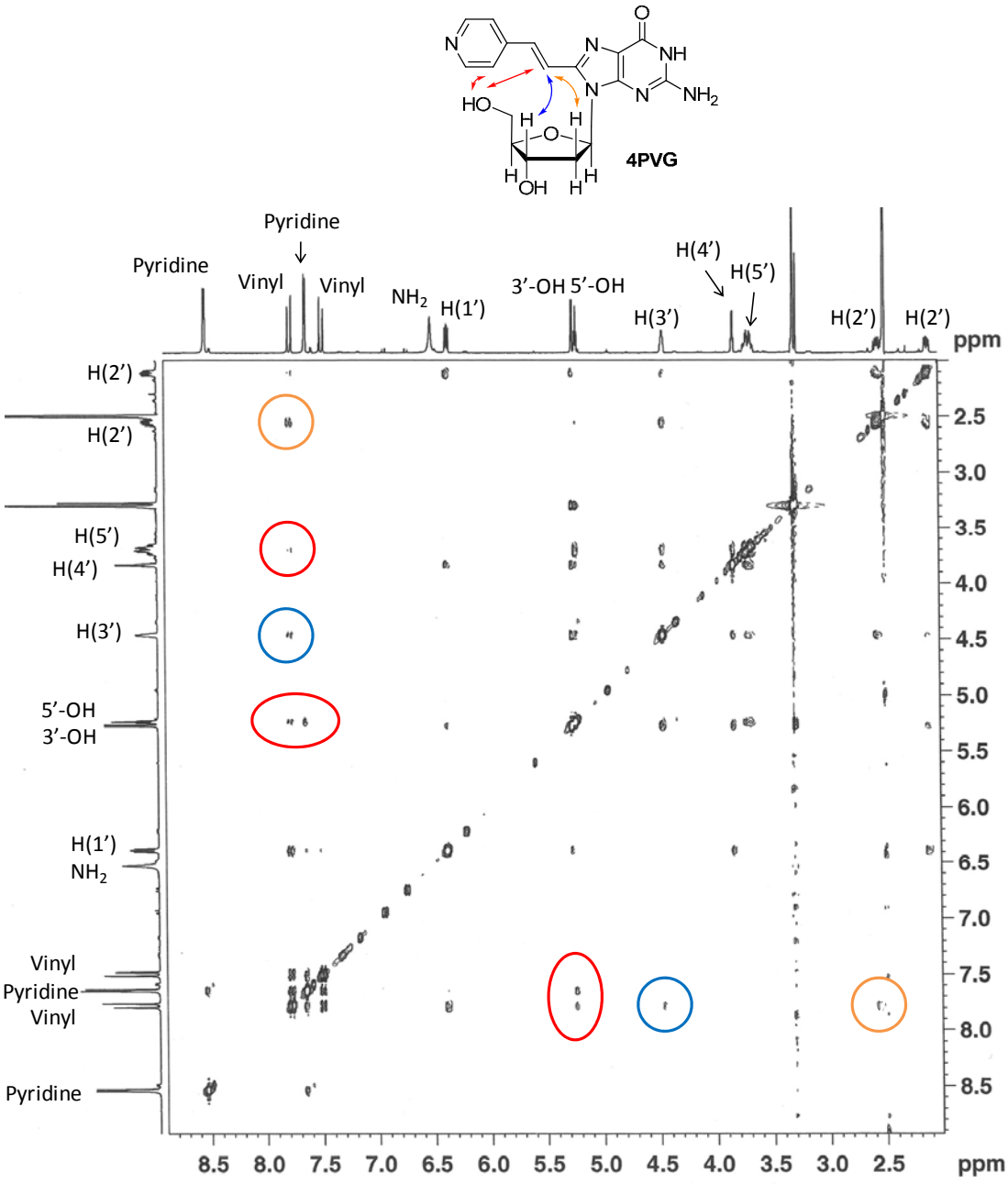

Figure 3.6: 2D-ROESY of **4PVG** in d_6-DMSO (mixing time = 250 ms).

3.3 Conclusions

Synthetic nucleoside analogs are potential tools for probing DNA structures and functions. Here, fluorescent 8-aryl- and 8-(2-arylethenyl)-2'-deoxyguanosines were synthesized. A new synthetic strategy involving the O^6 protection of 8-bromo-2'-deoxyguanosine was developed to inhibit catalyst complexation by the guanine core and provides a general route for the derivatization of *C*8 *via* palladium-catalyzed cross-coupling reactions. In water, the resulting nucleosides exhibit relatively high molar extinction coefficients ($\varepsilon_{275\text{-}294nm}$ = 11'000 – 24'000 $cm^{-1}M^{-1}$), quantum yields for fluorescence (Φ) ranging from 0.47 to 0.79 in acetonitrile and large *Stokes* shifts. 8-aryl-2'-deoxyguanosines display absorption maxima ranging from 275 to 306 nm and emission between 384 and 418 nm. The presence of a pyridine at position 8 leads to strongly fluorescent compounds in acetonitrile that are quenched in water. The origin of this quenching is attributed to proton transfer between photoexcited pyridyl nitrogens and bulk solvent. Consistent with this, the quantum yield of 8-(2-pyridyl)-2'-deoxyguanosine (**2PyG**) strongly correlated to solvent acidity (SA). In addition, **2PyG** shows a strong solvatochromic response with excellent correlation between *Stokes* shift and solvent polarity (E_T^N). Such environment-sensitive photophysical characteristics are powerful features for sensing applications in a wide range of biological events.

The elongated 8-(2-arylethenyl)-2'-deoxyguanosines display significantly red-shifted absoption (λ_{abs} = 340 – 355 nm) and emission (λ_{em} = 450 – 490 nm) maxima, which is desirable for applications to biological systems. However, derivatives of 8-(2-penylethenyl)-2'-deoxyguanosine were shown to photoisomerize into the non-fluorescent *cis* isomer upon irradiation with UV light.[64,105,107] This isomerization can potentially destabilize nucleic acids structures and complicate fluorescence and CD data interpretation. Here, two pyridine analogs, **3PVG** and **4PVG**, were synthesized and show very little or no photo-switching upon irradiation, and other favorable properties including high quantum yields. In addition, NMR analysis showed that the 8-aryl-2'-deoxyguanosines prefer to adopt a *syn* conformation in solution. 8-vinyl-2'-deoxyguanosine and 8-(2-arylethenyl)-2'-deoxyguanosine analogs, in contrast, retain the natural *anti* preference of the glycosidic bond. These parameters might be related to the potential impact of each probe on the global structure and stability of nucleic acids.

Taken together, these results suggest that 8-aryl- and 8-(2-arylethenyl)-2'-deoxyguanosines are interesting candidates as fluorescent internal probes for the detection of nucleic acids structural changes. The strongly solvatochromic **2PyG** as well as the elongated **StG** and **4PVG** will therefore be incorporated into DNA for photophysical and structural studies.

CHAPTER 4

8-(2-Pyridyl)-2'-deoxyguanosine "2PyG": Fluorescence Properties and Structural Impact in DNA[3]

Due to their environment-sensitive fluorescence quantum yields, base analogs like 2-aminopurine (**2AP**), 6-methylisoxanthopterin (**6-MI**) and 3-methylisoxanthopterin (**3-MI**) are widely used in nucleic acid folding and catalysis assays. Emissions from these guanine mimics are quenched by base-stacking interactions and collisions with purine residues. The development of new, minimally disruptive guanine mimics that remain highly emissive in folded nucleic acids and are capable of proper base stacking and base pairing interactions can provide sensitive means to differentiate DNA/RNA structures. Here a comparison of the structural impact and fluorescent properties in DNA of the most commonly used probe 2-aminopurine (**2AP**) to 8-(2-pyridyl)-2'-deoxyguanosine (**2PyG**) is reported. The photophysical properties of these purine derivatives are very different. *Stern-Volmer* plots using nucleoside monomers revealed upward curvature of F_o/F plots of **2AP** fluorescence *versus* guanosine monophosphate (GMP), while F_o/F plots of **2PyG** exhibited unusual downward curvature that ultimately resulted in a recovery of fluorescence at high GMP concentrations. Interestingly, these trends are retained in substituted oligonucleotides. **2PyG** is the first guanosine mimic that exhibits enhanced and not reduced fluorescence quantum yields upon its incorporation into folded nucleic acids, resulting in approximately 50-fold brighter fluorescence intensities than **2AP** in the context of duplex DNA.

[3] Parts of this chapter were published in: Dumas, A. and Luedtke, N. W. *ChemBioChem*, **2011**, *12*, 2044-2051.

4.1 Introduction

Fluorescence phenomena enable powerful and readily accessible technologies for characterizing biomolecules folding and enzymatic activities.[42] Due to their small size and predictable location, internal fluorescent probes offer some advantages over linker-attached chromophores, including the ability to highlight subtle structural changes with single nucleotide resolution.[48,51,59-71] Fluorescence-based assays involving fluorescent nucleobase analogs typically assess conformational changes and/or phosphodiester bond cleavage using probes that exhibit lower quantum yields when base-stacked with neighboring residues.[48,51,59-71] This approach is effective when large changes in base-stacking/solvation of the probe occur during the course of a reaction. Internal probes that are highly emissive in both base-stacked and solvated environments can provide an alternative and highly sensitive means to differentiate DNA/RNA structures with variable base-stacking configurations.

The sensitivity of this approach is normally limited by static and dynamic quenching of the fluorescent base analog by their close proximity and base-stacking interactions with purine residues. To date, there are only a small number of reported internal fluorescent probes that have similar or higher quantum yields in the context of proper *Watson & Crick* base pairs in folded nucleic acids. These include 1,3-diaza-2-oxophenothiazine,[72] 5-(fur-2-yl)-2'-deoxyuridine,[48] and certain 2-substituted-adenosine analogs.[73] None of these probes, however, are mimics of guanine residues.

2-Aminopurine (**2AP**) can form a wobble base pair with cytosine and is therefore considered a guanine mimic (Figure 4.4 D).[122,123] Due to its limited structural impact on many nucleic acid structures, **2AP** has become the most commonly used fluorescent base analog, but **2AP** is not very bright due to a low molar extinction coefficient ($\varepsilon_{305\ nm} = 5'600\ cm^{-1}M^{-1}$) and low quantum yield ($\Phi \approx 0.004$) when base-stacked with purine residues.[144] Other common guanine mimics such as 6-methylisoxanthopterin (**6-MI**) and 3-methylisoxanthopterin (**3-MI**) are also imperfect structural mimics of guanine that are generally disruptive to nucleic acids' structures and are quenched by stacking interactions and collisions with purine residues.[50,51,74,76]

Here, **2AP** and 8-(2-pyridyl)-2'-deoxyguanosine (**2PyG)** are compared for their structural impact and their ability to report DNA folding in G-quadruplex, and duplex DNA. At the nucleoside level, dramatic differences between these probes are observed in their susceptibility to fluorescence quenching by the addition of guanosine monophosphate

(GMP). Interestingly, the fluorescence quenching of the **2AP** nucleoside by GMP exhibits F_o/F plots with upward curvature, while F_o/F plots of **2PyG** fluorescence exhibit downward curvature at high GMP concentrations. These results are consistent with the changes in fluorescence upon incorporation of each probe into folded oligonucleotides, and suggest that high concentrations of GMP can, in some ways, mimic the local nucleobase environments of folded nucleic acids.

To the best of our knowledge, **2PyG** is the first example of a guanine mimic that exhibits a higher quantum yield following its incorporation into folded oligonucleotides ($\Phi = 0.03 - 0.15$) as compared to the free nucleoside in water ($\Phi = 0.02$).[77,178,179] **2PyG** has unperturbed *Watson & Crick* and *Hoogsteen* hydrogen bonding faces and it can be directly incorporated into the G-tetrads of natively-folded G-quadruplexes with relatively little impact on global structure or stability.[77,178,179]

4.2 Results and discussion

4.2.1 *Stern-Volmer* plots using 2PyG and 2AP monomers with GMP

To evaluate their susceptibilities to intermolecular quenching in solution, the fluorescence intensities of 100 μM solutions of **2AP** and **2PyG** were monitored upon titration of guanosine monophosphate disodium salt (GMP). *Stern-Volmer* plots illustrate the dramatically differing behaviors of these nucleosides in the presence of GMP (Figure 4.1). Compared to **2AP**, very little quenching of **2PyG** by GMP was observed (Figure 4.1 A). In both cases, non-linear effects were observed at GMP concentrations above 0.1 M, indicating the presence of at least two different processes taking place.

Points collected over a relatively low concentration range of GMP (0.01 – 0.1 M) were therefore used to calculate the initial F_0/F slopes of approximately 0.004 and 0.030 for **2PyG** and **2AP**, respectively. At GMP concentrations above 0.1 M, **2AP** exhibits an irregular upward curvature in F_0/F slope that possibly reflects the presence of static quenching processes.[122] **2PyG**, in contrast, exhibited a downward curvature (Figure 4.1 B) over this same concentration range. At GMP concentrations above 0.4 M, **2PyG** excitation spectra revealed a recovery of fluorescence intensity coinciding with a large red-shift of the excitation peak from 300 nm to 330 nm (Figure 4.1 C). These spectral features are not observed for **2AP** (Figure 4.1 D). A similar red-shift is observed for **2PyG** upon its incorporation into oligonucleotides, therefore suggesting the formation of **2PyG**-G

stacking interactions with GMP that has a protective effect on its fluorescence quantum yield. Solutions containing high concentrations of GMP can in some ways mimic the nucleosides micro-environment encountered in nucleic acids, suggesting that **2PyG** can benefit from protection from solvent in the context of DNA.

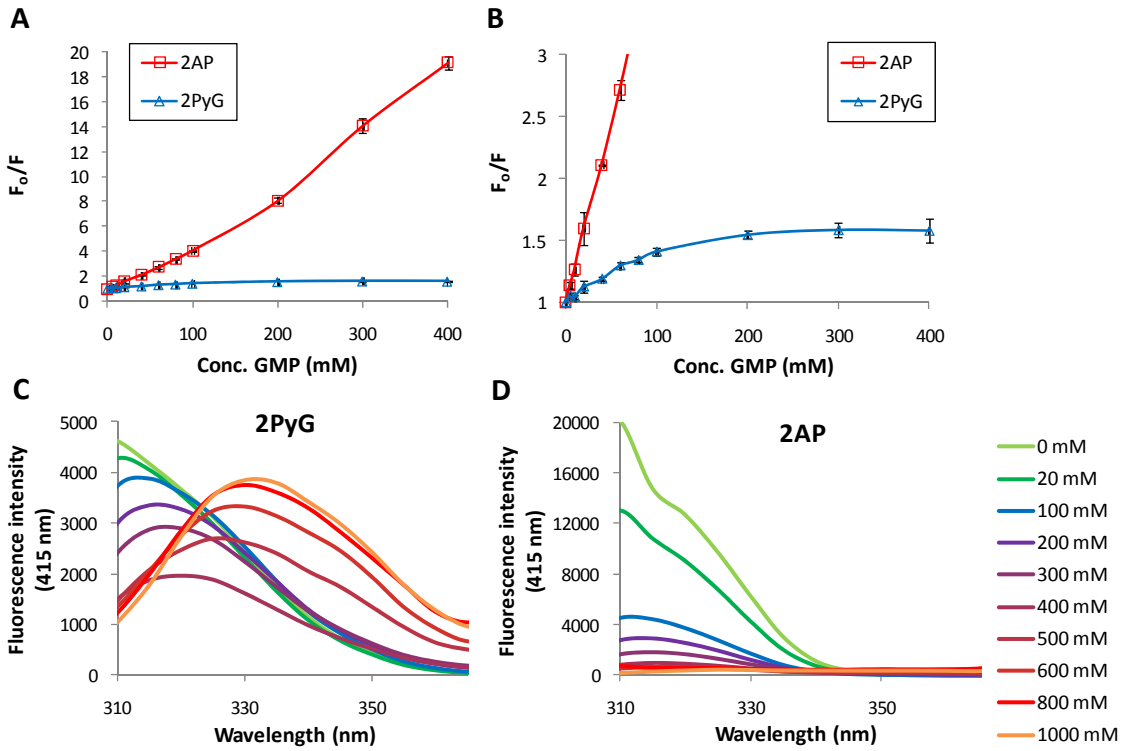

Figure 4.1: *Stern-Volmer* plots of **2PyG** and **2AP** upon addition of guanosine monophosphate disodium salt (GMP), where F_o = fluorescence intensity in the absence of quencher, and F = fluorescence intensity at the indicated concentration of quencher, full view (A) and zoom-in view (B). Excitation spectra of **2PyG** (C) and **2AP** (D) in the presence of different concentrations of GMP (λ_{em} = 415 nm). All samples contained 100 µM of **2AP** or **2PyG** in an aqueous 10 mM lithium cacodylate buffer (pH 7.4). Excitation spectra (C & D) were corrected for high absorbance (eq. 8.2, Chapter 8). Fluorescence intensities (A & B) were collected using λ_{ex} = 325 nm / λ_{em} = 370 nm for **2AP** and λ_{ex} = 325 nm / λ_{em} = 415 nm for **2PyG**.

4.2.2 Synthesis of 2PyG β-cyanoethyl phosphoramidite[4]

To study the photophysical characteristics of **2PyG** in the context of DNA, the corresponding 5'-protected and 3'-activated phosphoramidite was prepared. 8-(2-pyridyl)-2′-deoxyguanosine 5′-DMT-3′-phosphoramidite was synthesized from the commercially available 2'-deoxyguanosine in 8 steps in 11% overall yield. Starting from O^6, 5'-OH and

[4] Detailed synthetic procedures and characterization of these compounds and intermediates are available in Chapter 8.

3'-OH protected 8-(2-pyridyl) intermediate **13**, N^2 was protected with isobutyryl chloride to give compound **31**, followed by deprotection of the three sililated protecting groups with tetrabutylammonium fluoride (TBAF) (**32**). 5'-OH was then protected with dimethoxytrityl by reaction of the nucleotide with dimethoxytrityl chloride in pyridine to give compound **33**. The cyanoethyl phosphoramidite was introduced on the 3'-OH in a base catalyzed reaction with 2-cyanoethyl diisopropylchloro phosphoramidite to give the final $O^{3'}$-[(2-cyanoethoxy)(diisopropylamino)phosphino]-$O^{5'}$-dimethoxytrityl-N^2-isobutyryl-8-(2-pyridyl)-2'-deoxyguanosine (**34**) (Scheme 4.1). This building block was introduced into single sites of G-quadruplex-prone sequences using semi-automated DNA synthesis.

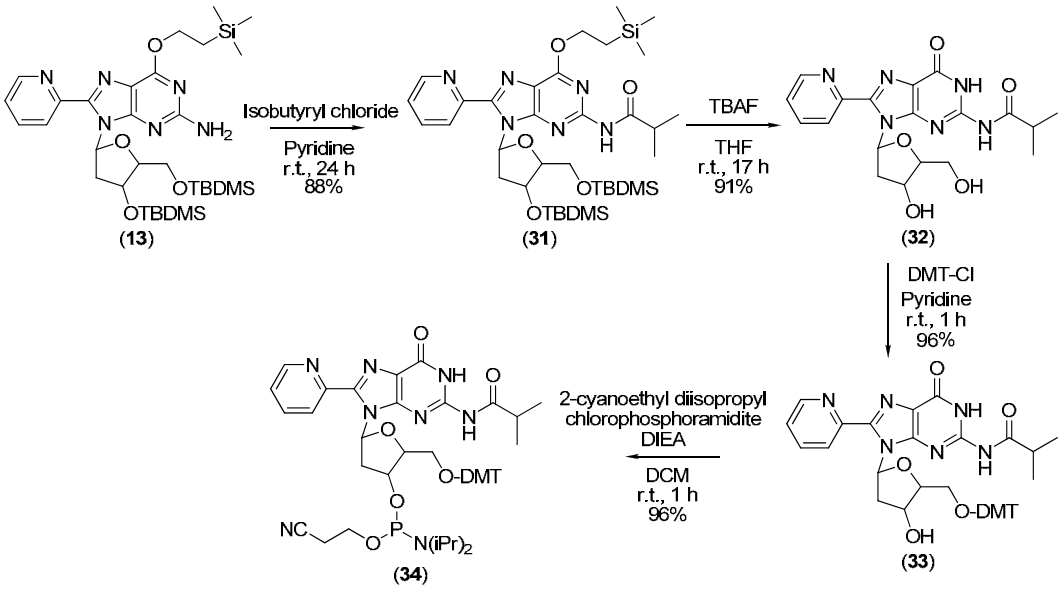

Scheme 4.1: Synthesis of the 8-(2-pyridyl)-2'-deoxyguanosine phosphoramidite derivative.

4.2.3 Sequences studied

To compare the abilities of **2AP** and **2PyG** to serve as guanine mimics in the context of folded G-tetrads, eight different oligonucleotides derived from four G-quadruplex-prone sequences were synthesized and characterized (Figure 4.2). G-quadruplex structures derived from NMR-resolved sequences were selected for site-specific modification at positions known to be directly involved in G-tetrad formation.[3,35,205-210]

Three sites in the human telomeric sequence hTelo (G9, G17, or G23) were selected for substitution with **2PyG**, **2AP**, or thymine "T" as a negative control (Figure 4.2). In K^+ solutions the wild type human telomeric repeat sequence [$G_3(T_2AG_3)_3$] can fold into several distinct G-quadruplex topologies in populations that are largely determined by the 5'- and

3'-flanking bases.[3,205-207] The sequence studied here [$TTG_3(T_2AG_3)_3A$], "hTelo", adopts a "(3+1) parallel-antiparallel hybrid" topology in the presence of K^+ to about 95% (Figure 4.3 A).[206] In Na^+-containing solutions this same sequence folds into an "anti-parallel" topology in solution (Figure 4.3 B).[207,208] Each structure in Na^+ or K^+ contains a characteristic mixture of *syn* and *anti* glycosidic conformations of the guanine residues involved in G-tetrad formation.[3]

hTeloG9: 5'-TTGGGTTA**X**GGTTAGGGTTAGGGA-3'

hTeloG17: 5'-TTGGGTTAGGGTTAGG**X**TTAGGGA-3'

hTeloG23: 5'-TTGGGTTAGGGTTAGGGTTAGG**X**A-3'

cKitG10: 5'-AGGGAGGGC**X**CTGGGAGGAGGG-3'

cKitG15: 5'-AGGGAGGGCGCTGG**X**AGGAGGG-3'

cMycG8: 5'-TGAGGGT**Y**GGTAGGGTGGGTAA-3'

T1: 5'-T**Y**GGT-3'

T2: 5'-TGG**Y**T-3'

Where **X** = G, 2PyG, 2AP or T

Y = G, 2PyG or T

Figure 4.2: Oligonucleotides sequences studied.

Two sequences derived from cKit(1), cKitG10 and cKitG15 were investigated (Figure 4.2). The 22-mer cKit(1) sequence $AG_3AG_3CGCTG_3AG_2AG_3$ is positioned between -87 and -109 nt upstream of the transcription start site of the human c-kit oncogene, encoding for a thyrosine kinase receptor, thereby regulating signal transduction cascades that control cell growth and proliferation.[211] Its secondary structure in the presence of K^+ is an atypical "parallel" G-quadruplex, where an isolated guanine G10 is involved in G-tetrad formation, but G20 of the last G-tract is excluded (Figure 4.3 C). All the guanines involved in G-tetrad formation adopt *anti* conformations.[35,209]

The cMyc promoter region counts a purine rich sequence, responsible for controlling the expression of the c-myc transcription factor, regulating cell growth, proliferation, differentiation and apoptosis.[212,213] Mutation of this sequence gives the cMyc-2345 sequence $TGAG_3TG_3TAG_3TG_3TA_2$, known to adopt a single propeller-type

parallel-stranded G-quadruplex structure in K^+ solution (Figure 4.3 D).[210] All the guanines involved in G-tetrad formation adopt *anti* conformations. Only one modified sequence derived from cMyc-2345, "cMycG8", was prepared (Figure 4.2).

Finally, two sequences derived from the 5-mer TGGGT, T1 and T2 (Figure 4.2), were investigated. This sequence is known to form tetramolecular G-quadruplexes in K^+ solutions,[214,215] with guanine glycosidic conformations influenced by the nucleosides preference.[216,217]

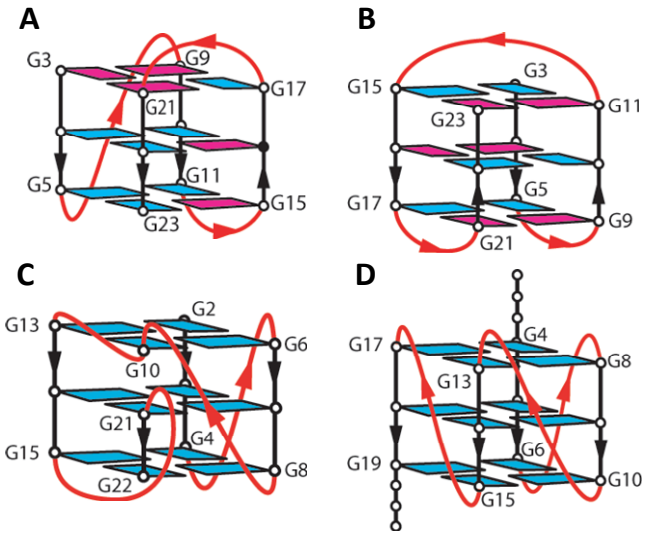

Figure 4.3: Schematic structure of the G-quadruplex constructs studied. Human telomeric sequence hTelo in K^+ [206] (A) and Na^+ [208] (B), cKit(1) in K^+ [35] (C) and c-myc-2345 in K^+ [210] (D). *Anti* guanines are shown in blue and *syn* guanines in magenta.

The global structure and stability of the **2PyG**-substituted oligonucleotides were analyzed by circular dichroism (CD) and temperature-dependent CD and compared to the wild-type sequences (**X** or **Y** = G, Figure 4.2) and to thymidine mismatches (T mutants) (**X** or **Y** = T, Figure 4.2) as positive and negative controls respectively. In addition, hTeloG9, hTeloG17, hTeloG23, cKitG10 and cKitG15 were substituted with **2AP** to compare the performance of this widely-used nucleotide analog to **2PyG**.

The folding of single-stranded oligonucleotides was controlled by variation of alkali metal salts in the buffer. G-quadruplex structures were prepared as single-stranded oligonucleotides in 100 mM of NaCl, KCl, RbCl or NH_4Cl-containing buffers or as tetramolecular G-quadruplexes in 100 mM KCl (TGGGT, T1 and T2 sequences). Duplex DNA samples were prepared in the presence of 100 mM NaCl and 1.1 equivalents of the

complementary strand.[38] Due to their small size and large desolvation energies, lithium ions are not normally compatible with G-tetrad formation.[218] Mainly unfolded single strands were prepared in 100 mM LiCl to maintain the same salt concentration as the other samples. CD data of these samples were consistent with mostly unfolded, G-stacked single-stranded DNA (Figure 4.5 C, Appendix A.1).

4.2.4 Probe impact on G-quadruplex structures and stability

Substitution of the position 8 of guanosine is an attractive avenue to new fluorescent derivatives because it is not directly involved in base pairing interactions in G-quadruplex or duplex structures (Figure 4.4 A & C). While the addition of bulky groups to the *C*8 position of guanosine can shift the conformational equilibrium of the glycosidic bond from *anti* to *syn*,[173,187-192] DNA folding can force 8-modified guanosines to adopt *anti* conformations with relatively small energetic penalties to DNA folding ($\Delta\Delta G < 1$ kcal/mol).[188,189,192] **2AP** in contrast retains an *anti* glycosidic conformation and can form a wobble base pair with cytosine. **2AP** is therefore considered as a guanine mimic (Figure 4.4 D).[122,123] Upon incorporation into the G-tetrads of folded G-quadruplex structures, **2AP** might serve as a guanine mimic, forming two N^2(H)-*N*7 and *N*7-N^2(H) hydrogen bonds with neighboring guanines as it is the case for natural guanine (Figure 4.4 B).

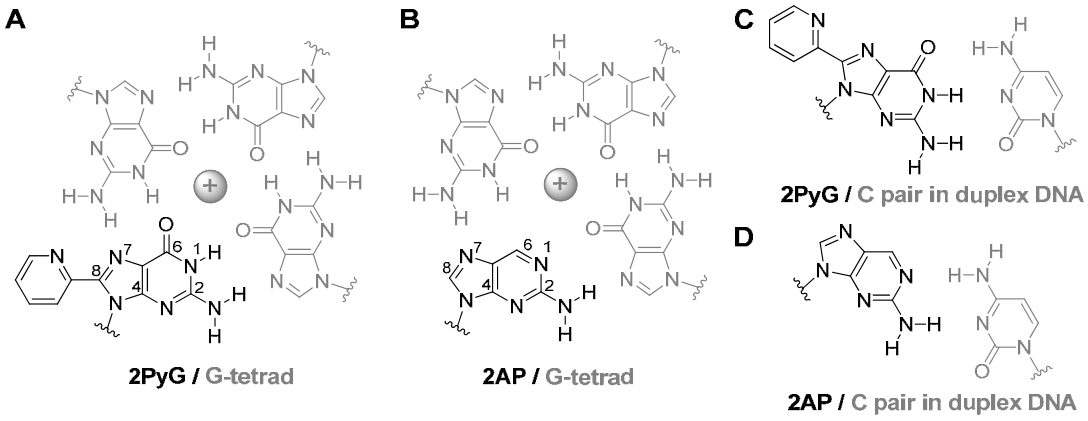

Figure 4.4: **2PyG** and **2AP** in an ion-containing G-tetrad (A & B) or in base pairs with cytidine (C & D).

Polymorphic G-quadruplex structures provide highly demanding model systems to evaluate internal fluorescent probes for their potential impact on the folding and stability of nucleic acids. To effectively mimic guanine residues in G-quadruplexes, both the *Watson & Crick*

and *Hoogsteen* hydrogen bonding faces must be maintained. Previous studies demonstrated that subtle changes to either face (e.g. 7-deazaguanine, 6-thioguanine, or inosine) are highly detrimental to intermolecular G-quadruplex folding kinetics and stabilities.[76]

While **2AP** can serve as an effective fluorescent probe when located in the loop regions of G-quadruplexes,[66,67,71,189] no previous studies have reported the ability of **2AP** to serve as a guanine mimic upon its direct incorporation into the G-tetrads of folded G-quadruplex structures (Figure 4.4 B). In terms of glycosidic bond conformations, **2AP** should exhibit the same *syn-anti* equilibrium as guanosine,[191] while **2PyG** prefers a *syn* glycosidic bond.[77,179] It was unclear *a priori* if the ability of **2PyG** to mediate proper base pairing interactions is more important than the *anti* glycosidic bond preference of **2AP** or *vice versa*.

To compare the abilities of **2AP** and **2PyG** to serve as guanine mimics in the context of folded G-tetrads, G-quadruplex sequences derived from hTelo and cKit(1) were site-specifically modified with **2PyG**, **2AP**, or thymine "T" as a negative control at positions known to be directly involved in G-tetrad formation.[3,35,205-209] The global structure and stability of each oligonucleotide was assessed using temperature-dependent circular dichroism (CD). In K^+-containing solutions, the unmodified hTelo sequence (hTelo(wt)) adopts a "(3 + 1) hybrid" structure that exhibits a CD spectrum with a positive peak at 288 nm, a shoulder at 270 nm, and a minimum at 242 nm.[206] This same characteristic CD spectrum is observed upon replacing G9 with **2PyG** (Figure 4.5 A), but results in a significant thermal stabilization of this structure (ΔT_m = +10 ^oC) due to *syn* conformational preferences shared by this position and **2PyG**.[77] This stabilization is therefore consistent with the integration of **2PyG** directly into the 5' terminal G-tetrad of this natively-folded G-quadruplex. The presence of **2PyG**-G base-stacking interactions is also suggested by a 30 nm red-shift in **2PyG**'s excitation maximum (λ_{ex} = 330 nm) upon its incorporation into hTeloG9 and all other oligonucleotides reported here (Chapter 5).[219]

In contrast to **2PyG**, replacing G9 with **2AP** or T resulted in very large changes to the global structure of hTelo according to CD (Figure 4.5 A). These changes were accompanied by dramatic losses in thermal stability (ΔT_m = -28 ^oC and -23 ^oC respectively) as compared to the unmodified oligonucleotide. Similar losses in stability were observed for **2AP** and T for all other positions in hTelo evaluated (Figure 4.5 A, B & D, Table 4.1). Surprisingly, **2AP** was even more disruptive to hTelo quadruplex stability (averaged ΔT_m = -28 ^oC) than T (averaged ΔT_m = -20 ^oC) for all three hTelo constructs evaluated in both sodium and potassium containing buffers (Table 4.1). We interpret the spectral

changes and loss of stability resulting from **2AP** and T incorporation as the formation of G-quadruplexes containing only two G-tetrads having a "head-to-head" heteropolar stacking orientation.[205,220-222] Additional evidence for the inability of **2AP** to support G-tetrad formation is apparent in the quantum yield values of **2AP** fluorescence that are similar in both G-quadruplex and single-stranded oligonucleotides, but much lower in duplex DNA (Section 4.2.6, Table 4.2). These results are in accordance with the observation that the carbonyl in position 6 of guanine is critical for mediating stable quadruplex assembly, as revealed by thermal melting of intermolecular G-quadruplex structures by *Mergny* and co-workers.[76]

While **2AP** and T incorporation consistently has detrimental effects on the global structures and stabilities of all G-quadruplexes evaluated, the impact of **2PyG** incorporation is highly context dependent. For example, the substitution of position G17 with **2PyG**, caused a significant change to the CD spectrum (Figure 4.5 B) consistent with the formation of a "parallel" G-quadruplex structure containing three G-tetrads each having a "head-to-tail" stacking orientations.[220-222] Only a small loss in thermal stability accompanying this conformational change was observed (ΔT_m = -4 ^oC). In the case of G23, **2PyG** caused hTelo to fold into an "antiparallel" type structure even in K^+ solutions (Figure 4.5 D). This structure, where G23 adopts a *syn* conformation, is normally only observed in Na^+-containing solutions.[207,208] hTeloG23 was therefore characterized in Na^+ buffer, where it exhibited approximately the same global structure and thermal stability as the wild-type sequence in Na^+ (ΔT_m = -2 ^oC, Figure 4.5 E).

In Na^+-containing solutions, hTelo adopts an "antiparallel" structure having a maximum at 294 nm, a minimum at 263 nm and a second maximum at 245 nm.[207] Interestingly, the substitution of G23 with **2PyG**, **2AP**, and T resulted in very similar CD spectra in Na^+ solutions (Figure 4.5 E), but the corresponding impacts on thermal stability were highly variable (ΔT_m = -2 ^oC, -20 ^oC, and -8 ^oC, respectively). These results suggest that the thermal stability, but not necessarily the CD spectra of these constructs is sensitive to the formation of 2 *versus* 3 stacked G-tetrads in the presence of both K^+ and Na^+ (Figure 4.5 D & E). In the case of G9 and G17 in Na^+-containing solutions, **2PyG** caused modest changes to the CD spectrum of hTelo (Appendix A.1), and had modest impacts on thermal stability (ΔT_m = +8 ^oC and -9 ^oC, respectively) as compared to the wild-type oligonucleotide. While significant, these changes were much smaller in magnitude than those observed for **2AP** and T-containing constructs ($\Delta T_m \approx$ -30 ^oC).

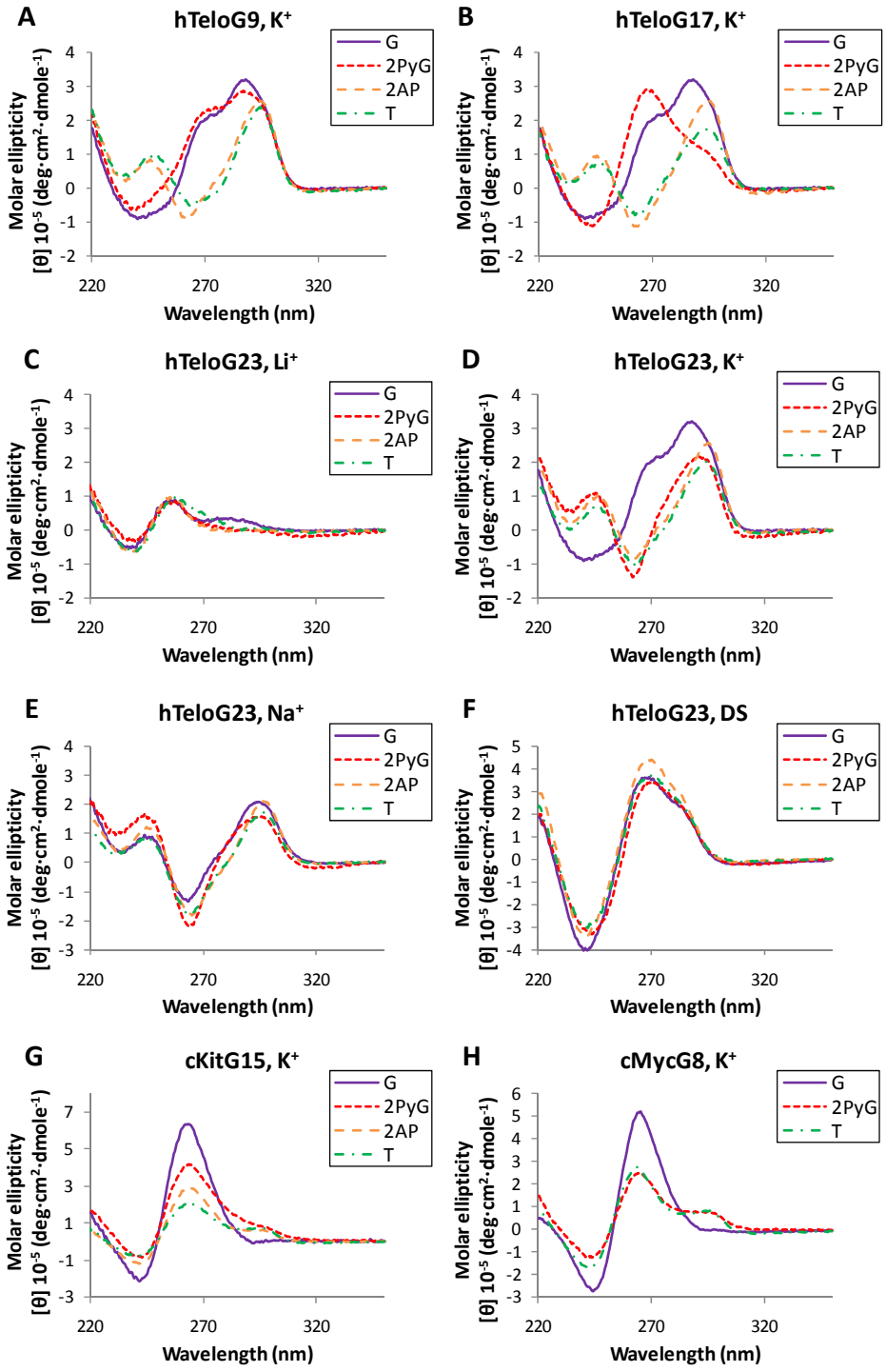

Figure 4.5: CD spectra of hTeloG9 (A), hTeloG17 (B), cKitG15 (G) and cMycG8 (H) in 100 mM KCl. CD spectra of hTeloG23 in 100 mM LiCl (C) 100 mM KCl (D) and 100 mM NaCl (E). Double-stranded hTeloG23 samples "DS" included 1.1 equivalents of the complementary strand and were prepared in 100 mM NaCl (F). All samples contained 2 µM of DNA in an aqueous 10 mM cacodylate buffer (pH 7.4). The CD spectra of all oligonucleotides in the conditions discussed are reported in Appendix A.1.

Table 4.1: Thermal denaturation melting temperatures (T_m) and deviation from wild-type oligonucleotides (+/-ΔT_m)[a] in potassium (K^+) and sodium (Na^+) buffers, and double-stranded DNA (DS) in Na^+.

Name	X	T_m in K^+ (ΔT_m)[a]	T_m in Na^+ (ΔT_m)[a]	T_m of DS (ΔT_m)[a]
hTelowt	G	67.7	53.5	66.0
hTeloG9	2PyG	77.5 (9.8)	61.8 (8.3)	61.2 (-4.8)
	2AP	40.0 (-27.7)	22.5 (-31.0)	61.5 (-4.5)
	T	44.6 (-23.1)	39.2 (-14.3)	57.8 (-8.2)
hTeloG17	2PyG	63.3 (-4.4)	44.1 (-9.4)	62.3 (-3.7)
	2AP	40.3 (-27.4)	22.0 (-31.5)	60.9 (-5.1)
	T	42.9 (-24.8)	25.3 (-28.2)	58.2 (-7.8)
hTeloG23	2PyG	59.3 (-8.4)	51.6 (-1.9)	66.2 (0.2)
	2AP	43.7 (-27)	33.3 (-20.2)	64.7 (-1.3)
	T	45.2 (-22.5)	45.1 (-8.4)	64.5 (-1.5)
cKitwt	G	64.3	n.d.[b]	74.4
cKitG10	2PyG	60.3 (-4.0)	n.d.[b]	68.1 (-6.3)
	2AP	58.0 (-6.3)	n.d.[b]	70.2 (-4.2)
	T	59.3 (-5.0)	n.d.[b]	65.2 (-9.2)
cKitG15	2PyG	62.4 (-1.9)	n.d.[b]	70.7 (-3.7)
	2AP	45.7 (-18.6)	n.d.[b]	70.5 (-3.9)
	T	36.5 (-27.8)	n.d.[b]	68.8 (-5.6)
cMycwt	G	86.7	n.d.[b]	n.d.[b]
cMycG8	2PyG	70.2 (-16.5)	n.d.[b]	n.d.[b]
	T	51.3/68.7	n.d.[b]	n.d.[b]
TGGGT	G	48.7	n.d.[b]	n.d.[b]
T1	2PyG	77.8 (+29.1)	n.d.[b]	n.d.[b]
T2	2PyG	29.4 (-19.3)	n.d.[b]	n.d.[b]

[a] ΔT_m = T_m (modified oligo) - T_m (wild-type).
[b] n.d. = not determined.

In Rb^+ and NH_4^+, hTelo showed the typical "(3 + 1) hybrid" structure type CD spectra seen in K^+-buffer, although the G-quadruplexes formed are relatively unstable (T_m = 45 °C and 44 °C for Rb^+ and NH_4^+ respectively) (Appendix A.1). When G9 is substituted by **2PyG**, similar CD spectra with bigger amplitude were observed (Appendix A.1). In analogy to the stabilization observed in K^+ when G9 is replaced by a nucleoside with *syn* glycosidic preference, the thermal stability of the structure was significantly increased upon substitution of G9 with **2PyG** (T_m = 57 °C for Rb^+ and NH_4^+).

While hTelo is a particularly "plastic" DNA sequence capable of adopting a wide variety of different G-quadruplex structures with similar energies,[3,205-208] CD data collected using the cKit(1) promoter sequence $AG_3AG_3CGCTG_3AG_2AG_3$ were much less variable. cKit(1) folds in a "parallel" G-quadruplex in K^+-containing solutions with a characteristic maximum at 263 nm and a minimum at 242 nm.[35,209] The substitution of G15 with **2PyG**, **2AP**, and T resulted in CD spectra having similar features but with variable amplitudes and a small shoulder around 290 nm (Figure 4.5 G). These data are consistent with the formation of cKit G-quadruplex structure(s) containing two or three stacked G-tetrads each having a "head-to-tail" homopolar stacking orientations.[220-222] **2PyG** exhibited only a minimal impact (ΔT_m = -2 °C) on the thermal stability of the cKit construct, despite the *anti* conformational preference at this position. In comparison, **2AP** and T imparted much more dramatic thermal destabilizations (ΔT_m = -19 °C and -28 °C, respectively) as compared to the wild-type construct (Table 4.1). The substitution of G10 with **2PyG**, **2AP**, and T resulted in CD spectra having similar features (Appendix A.1). However, in contrast to the other hTelo and cKit constructs studied in K^+ and Na^+ solution, **2AP** and T substitutions have only a minimal impact on the thermal stability of cKitG10 (ΔT_m = -6 °C and -5 °C respectively). These results suggest that upon mutation of G10, cKit can fold in an alternative structure of similar energy possibly excluding G10 of G-tetrad formation and engaging an alternative guanine residue normally forming a loop.

In K^+-containing solutions cMyc folds in a "parallel" G-quadruplex with a characteristic maximum at 263 nm and a minimum at 242 nm. Substitution of G8 with T results in spectra of decreased amplitude with a shoulder around 290 nm and a biphasic melting curve (T_m = 51 °C and 69 °C). **2PyG** results in the same spectral features (Figure 4.5 H) and important thermal destabilization (ΔT_m = -17 °C), suggesting the exclusion of **2PyG** from G-tetrad formation in this construct.

Short oligonucleotides containing G-tracks of three guanine residues or more can self-assemble in parallel tertameric G-quadruplexes. TGGGT shows a typical "parallel"

G-quadruplex CD spectrum with a characteristic maximum at 263 nm and a minimum at 242 nm. Upon substitution of the 5'- or 3'-end guanine by **2PyG** an additional peak is observed around 290 nm (Appendix A.1). We interpret these spectral changes as the formation of a reverse "head-to-head" heteropolar stacking orientation tetrad composed of four **2PyG** residues that adopt *syn* conformations.[216,217] The impact on the G-quadruplex stability is highly dependent on the site of substitution. Introduction of **2PyG** in the 5'-tetrad results in a strong stabilization (ΔT_m = +29 ^oC) of the quadruplex, whereas substitution of the 3'-tetrad leads to important destabilization (ΔT_m = -19 ^oC).

4.2.5 Probe impact on duplex structure and stability

To prepare duplexes, oligonucleotides were heated in the presence of Na^+ and 1.1 equivalents of complementary strand. In all cases, CD spectra consistent with B-form double-stranded DNAs having a maximum at 266 nm and a minimum at 238 nm were observed (Figure 4.5 F, Appendix A.1). As compared to the same oligonucleotides folded into G-quadruplexes, the substitution of a guanine by **2PyG**, **2AP**, or T has relatively little impact on the global structure or stability of duplex DNA. The absolute magnitudes of duplex destabilization were roughly proportional to the distance between site of substitution and the nearest end of each oligo (Table 4.1). This is consistent with "end breathing" effects of duplexes, because the base pairs near the termini are less stabilizing than those in the center of the oligonucleotide. **2PyG** generally caused less thermal destabilization of duplex DNA (ΔT_m = -3.5 ^oC on average) than **2AP** and T (ΔT_m = -4 $^\circ C$ and ΔT_m = -6 $^\circ C$, respectively). These data suggest that base stacking and pairing interactions can "force" a single **2PyG** residue to adopt an *anti* conformation with energetic penalties to global stability that are smaller than the energies associated with the formation of a single base pair.[223,224] Taken together, these results suggest that maintaining proper base pairing interactions can be more important than subtle changes in glycosidic bond conformational preferences for the stability of both G-quadruplex and duplex nucleic acids.

4.2.6 Quantum yields of 2PyG and 2AP in modified oligonucleotides

The fluorescence properties of **2AP** are highly dependent upon the folded state(s) of the DNA containing it. The quantum yield (Φ) of **2AP** is inversely proportional to the extent of base stacking interactions with neighboring residues.[122,144,145] Consistent with this, the quantum yield of the **2AP** nucleoside (Φ = 0.68) decreases by approximately 200-fold upon its incorporation into G-rich duplex DNA (Φ = 0.002 – 0.004) (Figure 4.6 B,

Table 4.2). Consistent with the observations made upon titration with GMP, **2PyG** is an exceptional fluorescent probe because it exhibits the same or even enhanced fluorescence emissions upon its incorporation into DNA (Figure 4.6 A, Table 4.2). This is true for all the constructs studied, except the short sequences T1 and T2, where four **2PyG** units are assembled in a G-tetrad where self-quenching might occur.

The quantum yield of the **2PyG** nucleoside changed little when incorporated into duplex DNA (average Φ = 0.03, Table 4.2). Somewhat higher quantum yields are observed for **2PyG** in unfolded, single-stranded DNAs in Li^+-solutions (average Φ = 0.05, Table 4.2). Even higher quantum yields are observed for **2PyG** in these same oligonucleotides when they are folded into single stranded G-quadruplex structures (average Φ = 0.08, Table 4.2). The modest quantum yields of **2PyG** are compensated by the relatively large molar extinction coefficient ($\varepsilon_{280nm} \approx 20'000\ cm^{-1}M^{-1}$). **2AP**, in comparison, is approximately 100-times less bright than **2PyG** due to its low molar extinction coefficient ($\varepsilon_{305nm} = 5'600\ cm^{-1}M^{-1}$) and low quantum yield ($\Phi \approx 0.003$) when it is base-stacked with guanine residues in the context of duplex DNA.

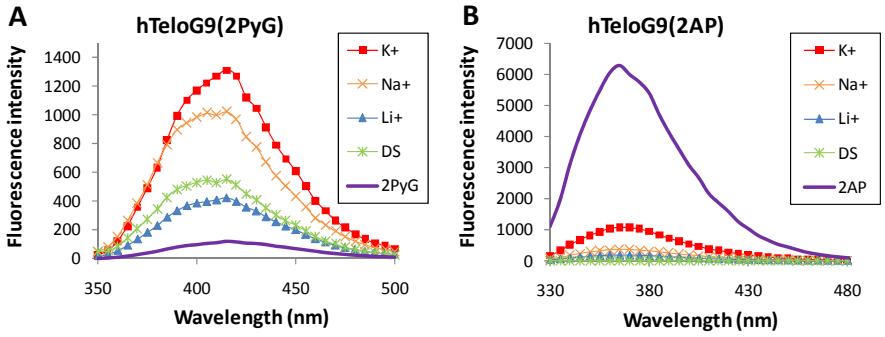

Figure 4.6: Fluorescence spectra of the free nucleosides **2PyG** and **2AP** compared to hTeloG9(2PyG) (A) and hTeloG9(2AP) (B) in 100 mM KCl (K^+), 100 mM NaCl (Na^+), 100 mM LiCl (Li^+) or 100 mM NaCl. Double-stranded DNA sample (DS) contained 100 mM NaCl and 1.1 equivalents of the complementary strand. (λ_{ex} = 330 nm for **2PyG**- and 310 nm for **2AP**-samples).

Table 4.2: Quantum yields (Φ) of modified oligonucleotides as unfolded single-strands (Li^+), G-quadruplex structures (K^+, Na^+, Rb^+, NH_4^+), or double-stranded DNA (DS).

Name	Cond.	2PyG Φ (330 nm)	2AP Φ (310 nm)
Monomer	Buffer	0.02	0.68
hTeloG9	Li^+	0.04	0.01
	K^+	0.09	0.07
	Na^+	0.08	0.03
	Rb^+	0.15	n.d.[a]
	NH_4^+	0.11	n.d.[a]
	DS	0.03	0.002
hTeloG17	Li^+	0.02	0.01
	K^+	0.02	0.04
	Na^+	0.03	0.03
	DS	0.01	0.002
hTeloG23	Li^+	0.05	0.02
	K^+	0.05	0.03
	Na^+	0.10	0.05
	DS	0.04	0.01
cKitG10	Li^+	0.05	0.05
	K^+	0.05	0.02
	DS	0.02	0.003
cKitG15	Li^+	0.12	0.03
	K^+	0.05	0.03
	DS	0.02	0.004
cMycG8	Li^+	0.03	n.d.[a]
	K^+	0.04	n.d.[a]
T1	Li^+	0.009	n.d.[a]
	K^+	0.04	n.d.[a]
T2	Li^+	0.005	n.d.[a]
	K^+	0.01	n.d.[a]

[a] n.d. = not determined.

4.3 Conclusions

FRET-based studies using conjugated "external" probes like fluorescein and rhodamine are frequently used in folding assays,[39-41] but data interpretations are typically limited to changes in probe-to-probe distances. The use of "internal" fluorescent probes can provide a direct readout of characteristic photophysical properties of nucleic acids structures containing them.

Surprisingly, F_o/F plots of **2AP** fluorescence *versus* guanosine monophoshate (GMP) revealed upward curvature, while F_o/F plots of **2PyG** exhibited downward curvature that ultimately resulted in a recovery of fluorescence at high GMP concentrations. This recovery coincided with a red-shift in **2PyG** excitation to the same maximal wavelength observed upon its incorporation into oligonucleotides (λ_{ex} = 330 nm). These results are consistent with the trends observed for **2PyG**- and **2AP**-containing oligonucleotides and suggest that solutions containing high concentrations of GMP can, in some ways, mimic the high local densities of nucleobases found in oligonucleotides.

8-(2-pyridyl)-2'-deoxyguanosine "**2PyG**" is a minimally disruptive fluorescent probe for both G-quadruplex and duplex DNA structures and exhibits modest quantum yields (Φ = 0.01 – 0.12) when it is base-stacked with guanosine. In contrast, **2AP** consistently exhibits very low quantum yields (Φ = 0.002 – 0.004) when incorporated into double-stranded DNA, and did not support the formation of stacked G-tetrads in intramolecular G-quadruplex structures. As a result, **2AP** is generally a poor probe for G-quadruplex folding.

Our comparison of **2AP** and **2PyG** has revealed fundamental differences between the photophysical properties of these probes. **2PyG** exhibits enhanced, not diminished quantum yields of fluorescence upon its incorporation into folded nucleic acids. As a result of its higher quantum yield, red-shifted emission, and 4-fold higher molar extinction coefficients, **2PyG** can be detected with more than 50-fold greater sensitivity than **2AP** in the context of duplex DNA.

CHAPTER 5

Cation-Mediated Energy Transfer in G-Quadruplexes[5]

8-(2-Pyridyl)-2′-deoxyguanosine, "**2PyG**", is a highly sensitive internal fluorescent probe of G-quadruplex folding and energy transfer. **2PyG** was minimally disruptive to G-quadruplex folding and exhibited intense fluorescence, even when it was base-stacked with other guanine residues. Here, **2PyG** is used to quantify energy transfer efficiencies from unmodified DNA nucleobases. Under excess-salt conditions, energy transfer efficiencies are highly structure selective, with η_t(duplex) < η_t(single-strand) < η_t(G-quadruplex), independently of the exact structural features and thermal stabilities of the G-quadruplexes or duplexes containing them. However, G-quadruplexes folded in 40% polyethylene glycol (PEG) under salt deficient conditions exhibited very little energy transfer. Experiments conducted using unmodified G-quadruplexes suggest that cation coordination at the O^6 position of guanine residues results in enhanced quantum yields of G-quadruplex nucleobases that, in turn, serve as efficient energy donors to **2PyG**. Given the growing interest in G-quadruplex-based devices and materials, these results will provide important design principles toward harnessing the potentially useful photophysical properties of G-quadruplex wires and other G-rich structures.

[5] Parts of this chapter were published in: Dumas, A. and Luedtke, N. W. *J. Am. Chem. Soc.*, **2010**, *132*, 18004-18007.

5.1 Introduction

G-quadruplexes are intriguing nanostructures possessing potential biological relevance[4,8,21,22,218,225-231] and interesting photophysical and material properties.[232-244] Energy and electron transfer reactions involving G-quadruplexes can mediate DNA damage and repair[239-241] and might facilitate the development of new molecular devices.[242-244] Previous studies have suggested that G-G base-stacking, hydrogen bonding, and/or restricted motions within G-quadruplexes can enhance the photo-excited lifetimes and energy transfer properties of guanine residues.[12-15] However, the poor quantum yield ($\Phi \approx 10^{-4}$), short-lived excited state ($\tau \approx 1$ ps), and spectral overlap of 2′-deoxyguanosine (**1**) with other nucleobases prevent the quantification of energy transfer efficiencies (η_t) within unmodified G-quadruplexes.[12-15]

Internal fluorescent probes serving as energy acceptors can provide powerful means to characterize energy transfer processes within DNA as well as readouts of local nucleobase arrangements.[78,144-146,245] In this approach, a fluorescent nucleobase analog serves as an emissive energy acceptor and the proximal ensemble of unmodified residues serves as an energy donor. The resulting energy transfer efficiencies can be interpreted in terms of the folded state(s) of nucleic acids.[77,145,179] Nucleobase analogs that remain highly emissive in the context of proper base pairing and stacking interactions are therefore an important prerequisite to our approach. In contrast to other nucleobase analogs such as **2AP**, **6-MI** or **3-MI** that are quenched 100-fold or more by close proximity and base-stacking interactions with purines, 8-(2-pyridyl)-2'-deoxyguanosine (**2PyG**) was shown to have similar or even enhanced fluorescence in the context of DNA and to be minimally disruptive to duplex and G-quadruplex structures.

Here, **2AP** and **2PyG** were evaluated for their ability to report folding and internal energy transfer reactions in the G-quadruplexes previously reported. Although it is significantly quenched upon stacking with other nucleobases, **2AP** was previously reported to be an energy acceptor in the context of duplex DNA,[145] but where neighboring guanines act as poor energy donors.[78] In the context of the G-quadruplex sequences studied, **2AP** indeed was found to be mostly insensitive to structure-specific trends in energy transfer, consistent with its probable exclusion from G-tetrad formation. In contrary, due to its environmental sensitivity and spectral overlap with 2′-deoxyguanosine, **2PyG** acts as an efficient "turn-on" fluorescent probe of G-quadruplex folding and energy transfer. Due to its bright fluorescence, **2PyG** can be used to accurately quantify energy transfer efficiencies (η_t) within G-quadruplexes single-stranded, and duplex DNA.

η_t is defined as the number of photons transferred from active nucleobase energy donors to the energy acceptor (**2PyG**), divided by the total number of photons absorbed by all nucleobases at 260 nm (eq. 5.1). Due to distance and geometry constraints, many of the nucleobases present in each DNA will be inactive donors, so the calculated efficiencies provide a lower limit for the transfer efficiencies of the active donors.

$$\eta_t = \frac{\text{\# of photons transferred from active donor to } \mathbf{2PyG}}{\text{total \# of photons absorbed by all nucleobases at 260 nm}} \qquad \text{(eq. 5.1)}$$

Interestingly, energy transfer efficiencies are highly sensitive to DNA folding as well as the presence of cations within the folded G-quadruplexes. Indeed, G-quadruplexes prepared under conditions of excess NaCl or KCl (100 mM) exhibit more efficient DNA-to-probe energy transfer reactions (η_t = 0.11 – 0.41) than the corresponding unfolded single strand (η_t = 0.05 – 0.11) or duplex DNAs (η_t = 0.01 – 0.07). However, almost no energy transfer (η_t = 0.02 – 0.07) is observed when the G-quadruplex is folded in 40% polyethylene glycol 200 (PEG) under salt-deficient conditions (10 mM lithium cacodylate). Similar experiments performed with unmodified DNA revealed that the G-quadruplex structure is necessary but not sufficient for promoting efficient intramolecular energy transfer. The binding of ions to the O^6 positions of guanine residues is also needed for the unusually efficient energy transfer reactions within G-quadruplex structures.

5.2 Results and discussion

5.2.1 Quantification of energy transfer in modified oligonucleotides

While slightly higher quantum yields of **2AP** and **2PyG** are generally observed in G-quadruplex *versus* single-stranded oligonucleotides (Chapter 4), these differences are not large enough to serve as reliable diagnostic of structure. The quantification of energy transfer efficiencies, in contrast, can provide an excellent readout of G-quadruplex formation. Consistent with the presence of **2PyG**-G base-stacking interactions, the excitation peak of the **2PyG** nucleoside monomer (λ_{ex} = 300 nm) was red-shifted by approximately 30 nm in the context of DNA.[219] This red-shift in **2PyG** excitation corresponds to the maximal excitation wavelength observed for the monomer at high GMP concentrations. Notably, the emission maximum of unmodified guanine residues is approximately 330 nm, indicating **2PyG** as a potential FRET energy acceptor.

Table 5.1: DNA-to-probe energy transfer efficiencies (η_t), and the ratio of fluorescence intensities obtained upon excitation at 260 nm and at 325 nm (F(260)/F(325)) for **2PyG**-modified oligonucleotides.

Name	Conditions	η_t	F(260)/ F(325)	Name	Conditions	η_t	F(260)/ F(325)
Monomer	Buffer	0	1.1	**Monomer**	Buffer	0	1.1
hTeloG9	Li^+	0.09	2.3	**cKitG10**	Li^+	0.05	1.4
	No salt	0.12	2.1		K^+	0.11	2.5
	K^+	0.24	4.0		DS	0.01	0.7
	Na^+	0.30	4.7		PEG	0.02	0.6
	Rb^+	0.41	4.2	**cKitG15**	Li^+	0.09	1.8
	NH_4^+	0.28	3.9		K^+	0.18	3.4
	DS	0.03	1.1		DS	0.07	1.3
	PEG	0.06	1.0	**T1**	Li^+	0.17	-[a]
	PEG & Na^+	0.29	4.3		K^+	0.34	-[a]
hTeloG17	Li^+	0.06	1.5	**T2**	Li^+	0.15	-[a]
	K^+	0.18	3.2		K^+	0.23	-[a]
	Na^+	0.31	4.1				
	DS	0.05	1.3				
hTeloG23	Li^+	0.11	1.8				
	K^+	0.19	3.0				
	Na^+	0.26	3.3				
	DS	0.06	1.4				

[a] F(260)/F(325) ratio used to evaluate energy transfer efficiencies within intramolecular G-quadruplexes is irrelevant in the case of tetramolecular G-quadruplexes, since the **2PyG**/G ratio is biased in these constructs.
cMycG8 was excluded from this study since CD data suggested that **2PyG** was excluded from G-tetrad formation in these constructs.

The excitation spectra of the oligonucleotides containing **2PyG** exhibit two maxima corresponding to direct excitation (λ_{ex} = 330 nm) and indirect excitation of the probe *via* unmodified nucleobases (λ_{ex} = 260 nm) (Figure 5.1 A & E). The ratio of these excitation peaks weighted by the absorbance properties of the DNA and quantum yields of each probe can be used to calculate energy transfer efficiencies (η_t).[6][145]

[6] Detailed procedure for the calculation of energy transfer efficiencies are presented in Section 8.5.5, Chapter 8.

Under cation-mediated folding conditions with Na^+, K^+, NH_4^+, and Rb^+, five diverse and well-defined single stranded G-quadruplex structures were prepared. Energy transfer efficiencies from unmodified bases to **2PyG** were 3- to 4-fold higher in G-quadruplexes (η_t = 0.11 – 0.41) as compared to the same oligonucleotides in duplex DNA (η_t = 0.01 - 0.07, Table 5.1). This was independent on the structure and the stability of the resulting G-quadruplex. Mostly unfolded single-stranded DNAs in Li^+ solutions gave intermediate values (η_t = 0.05 – 0.11). The combination of strong DNA molar absorptivity ($\varepsilon_{260nm} \approx 250{,}000\ cm^{-1}M^{-1}$) with efficient energy transfer reactions resulted in fluorescence enhancements of 10- to 30-fold for **2PyG**-containing G-quadruplexes upon excitation at 260 nm, as compared to the same oligonucleotides when single-stranded or folded into duplexes (Figure 5.1 B & D).

Intermolecular G-quadruplexes formed by T1 and T2 in K^+-solutions also exhibit efficient energy transfer reactions (η_t = 0.23 – 0.34). In Li^+, transfer is significantly more efficient for these short constructs (η_t = 0.15 – 0.17) than in longer oligonucleotides. This suggests that residual stacking of guanines-tracks containing the probe is responsible for the energy transfer efficiencies observed in these nucleotides in Li^+ solutions (Table 5.1).

While the calculation of energy transfer efficiencies requires numerous measurements and data processing, a simple comparison of fluorescence intensities resulting from DNA excitation *versus* selective probe excitation can provide a simple and highly sensitive readout of G-quadruplex formation. According to this approach, the intensity of probe fluorescence upon DNA excitation at 260 nm (F(260)) is divided by the fluorescence intensity upon selective probe excitation (F(325)). Consistent with the trends in energy transfer efficiencies (η_t), duplex DNA exhibited the lowest F(260)/F(325) ratios of 0.7 - 1.4, single-stranded DNA in Li^+ exhibited intermediate F(260)/F(X) ratios of 1.6 - 2.3, while G-quadruplex structures have the highest F(260)/F(X) ratios with 2.5 - 4.7 (Table 5.1).

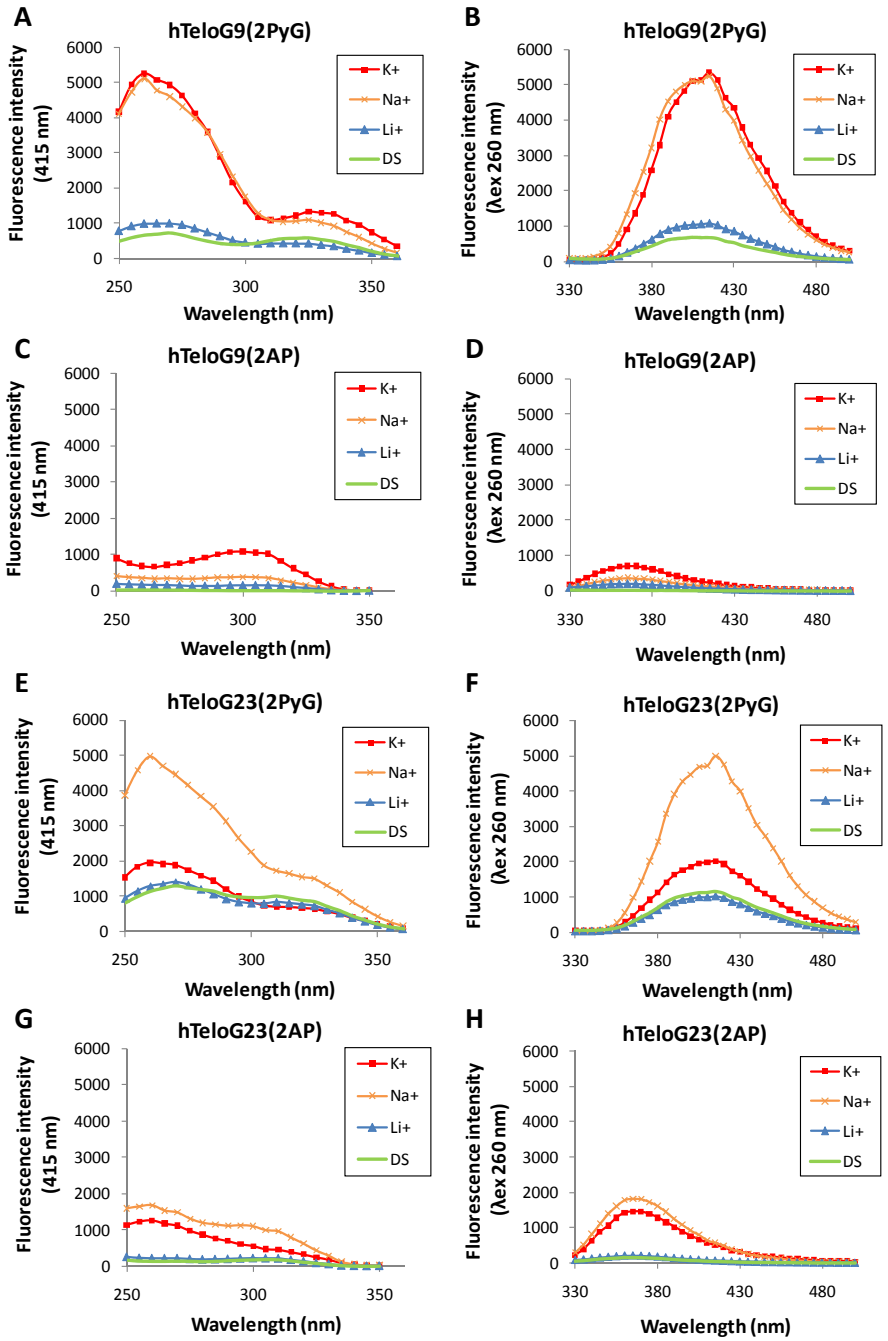

Figure 5.1: Excitation spectra of hTeloG9(2PyG) (A), hTeloG9(2AP) (C), hTeloG23(2PyG) (E), and hTeloG23(2AP) (G) in 100 mM KCl (K^+), 100 mM NaCl (Na^+), 100 mM LiCl (Li^+) or 100 mM NaCl Double-stranded DNA samples (DS) contained 100 mM NaCl and 1.1 equivalents of the complementary strand. Excitation spectra were collected using emission at 415 nm and 370 nm for **2PyG** and **2AP**, respectively. Emission spectra of hTeloG9(2PyG) (B), hTeloG9(2AP) (D), hTeloG23(2PyG) (F), and hTeloG23(2AP) (H) collected using λ_{ex} = 260 nm. All samples contained 2 μM of DNA in an aqueous 10 mM cacodylate buffer (pH 7.4).

Table 5.2: DNA-to-probe energy transfer efficiency (η_t) for **2AP**-modified oligonucleotides.

Name	Conditions	η_t	Name	Conditions	η_t
hTeloG9	Li^+	0.03	**cKitG10**	Li^+	0.01
	K^+	0.02		K^+	0.03
	Na^+	0.03		DS	0.02
	DS	0.03	**cKitG15**	Li^+	0.02
hTeloG17	Li^+	0.02		K^+	0.03
	K^+	0.05		DS	0.02
	Na^+	0.03			
	DS	0.03			
hTeloG23	Li^+	0.03			
	K^+	0.11			
	Na^+	0.08			
	DS	0.01			

While our thermal stability and quantum yield data suggest that **2AP** is not well incorporated into the G-tetrads of hTelo or cKit G-quadruplex structures, there is some suggestion of energy transfer in the case of hTeloG23 (Table 5.2, Figure 5.1 G). Higher energy transfer efficiencies in the hTeloG23 G-quadruplexes (η_t = 0.10 and 0.08 in potassium and sodium solutions, respectively) were observed as compared to the same, unfolded DNA in Li^+ (η_t = 0.03) and duplex DNA (η_t = 0.01). For all other oligonucleotides tested, however, **2AP** was insensitive to structure-specific trends in energy transfer efficiencies (η_t(duplex) = 0.01 – 0.03; η_t(single-strand) = 0.01 – 0.03; η_t(G quadruplex) = 0.02 – 0.05) (Table 5.2).

5.2.2 Energy transfer under salt deficient conditions

To dissect the multiple roles that metal ions might play in mediating both G-quadruplex folding and energy transfer, G-quadruplexes of hteloG9(2PyG) and cKitG10(2PyG) were prepared under salt-deficient conditions (10 mM lithium cacodylate) by molecular crowding/partial dehydration in 40% polyethylene glycol 200 (PEG).[246-249] Under these conditions, cations are absent or only weakly bound in the central cavities of each G-quadruplex.[246-249] For all DNAs evaluated, PEG-mediated folding resulted in G-quadruplex structures exhibiting cooperative and reversible folding, as well as highly

variable thermal stabilities. The structural integrity of the resulting G-quadruplexes was evaluated by CD. hTeloG9(2PyG) in PEG shows a CD trace very similar to what is normally observed in Na^+ solutions for this sequence. Addition of sodium salt to the solution results indeed in a similar CD spectrum with slightly increased intensity. Unsubstituted hTelo however, is misfolded in PEG where the CD spectrum shows a peak around 260 nm (data not shown). **2PyG**-substituted and wild-type cKit in contrast retain similar structural features compared to the G-quadruplexes folded by cation mediation. The single maximum around 260 nm shows however reduced intensity compared to the G-quadruplexes in excess-salt conditions (Figure 5.2 D). Unexpectedly, PEG mediated cKitG10(2PyG) G-quadruplex is stabilized in comparison to its K^+ folded form (T_m = 66 °C and 60 °C for PEG and K^+-folded cKitG10(2PyG) respectively). For hTeloG9(2PyG) however, the G-quadruplex folded in PEG is significantly less stable than the analogs stabilized by O^6 Na^+ coordination (T_m = 30 °C and 61 °C for PEG and Na^+-folded hTeloG9(2PyG) respectively). Introduction of Na^+ in addition to the PEG results however, in a particularly stable G-quadruplex (T_m = 72 °C for hTeloG9(2PyG) in PEG & Na^+).

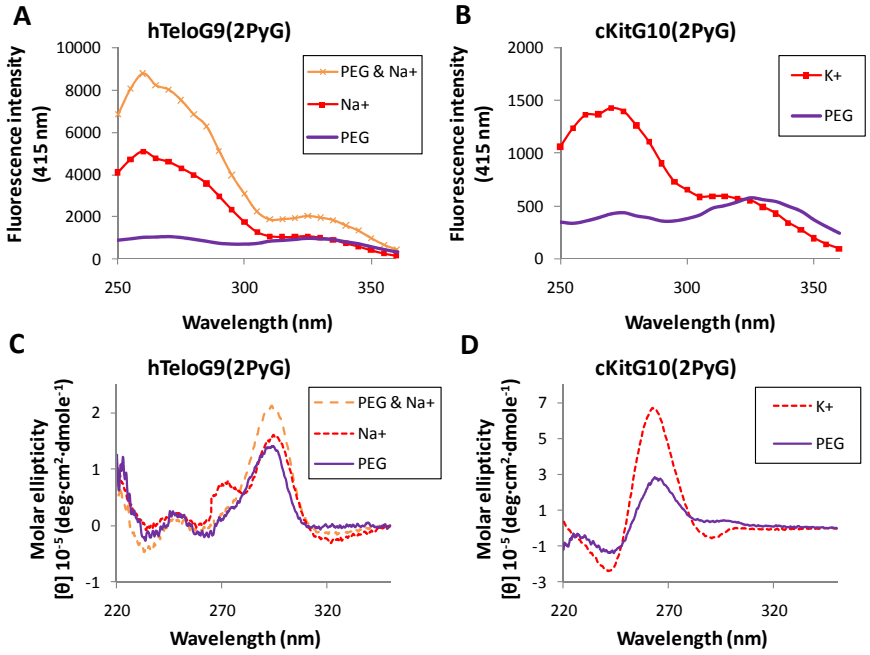

Figure 5.2: Excitation (A) and CD spectra (C) of hTeloG9(2PyG) folded in the presence of 40% PEG, 100 mM NaCl, or 40% PEG and NaCl. Excitation spectra (B) and CD spectra (D) of cKitG10(2PyG) folded in the presence of 40% PEG, or 100 mM KCl.

Interestingly, very little energy transfer was observed in the PEG-folded G-quadruplexes under salt-deficient conditions ($\eta_t \approx 0.02 - 0.07$, Figure 5.2 A & B, Table 5.1). Quadruplexes prepared in the presence of both PEG and 100 mM NaCl, in contrast, exhibited energy transfer efficiencies similar to that for the samples prepared in 110 mM Na^+ ($\eta_t \approx 0.30$, Figure 5.2 A, Table 5.1). Non-specific electrostatic stabilization of backbone phosphate repulsion is not responsible for the enhanced energy transfer, because PEG-folded G-quadruplexes prepared in 110 mM of tetrabutylammonium chloride exhibited approximately the same energy transfer efficiencies as the PEG-only samples. Taken together, these results suggest that the G-quadruplex structure by itself is not sufficient for promoting efficient energy transfer and that ions coordinated directly to the O^6-position of guanine residues play a critical role in mediating energy transfer reactions in G-quadruplex structures.

5.2.3 Fluorescence properties of unmodified oligonucleotides

Previous studies proposed that G-G base-stacking, hydrogen bonding, and/or restricted motions within G-quadruplex structures can enhance the photo-excited lifetimes and quantum yields of guanine residues.[12-15] To evaluate the impact of cation binding on the quantum yields of unmodified guanine residues, unmodified G-quadruplexes from hTelo(wt) in the presence of 40% PEG under salt-deficient conditions or in the presence of 40% PEG and 100 mM NaCl were prepared.

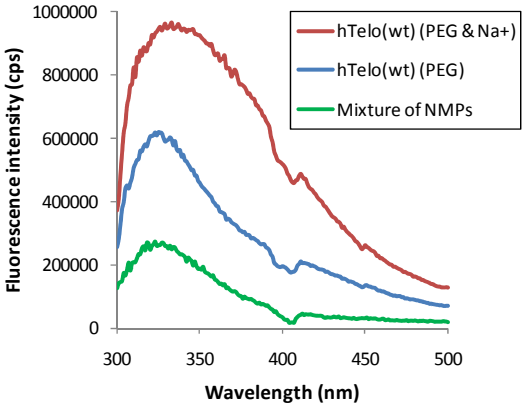

Figure 5.3: Emission spectra (λ_{ex} = 270 nm) of hTelo(wt) and a nucleotide monophosphate mixture in 40% PEG with or without salt.

While both samples were more fluorescent than a comparable mixture of nucleotide monophosphates, samples containing PEG and Na^+ exhibited a higher quantum yield and red-shifted emission as compared to the G-quadruplexes prepared in 40% PEG only (Figure 5.3). These results suggest that guanine-cation coordination is largely responsible for the enhanced photoexcited lifetimes and quantum yields reported for guanine residues in G-quadruplex structures.[12-15] The enhanced quantum yields of the unmodified guanine residues, in turn, facilitate the unusually efficient DNA-to-**2PyG** energy transfer reactions reported here.

5.3 Conclusions

The incorporation of a single pyridine unit into G-quadruplexes revealed efficient intramolecular energy transfer reactions in ion-containing G-quadruplex structures ($\eta_t = 0.11 - 0.41$). Given the growing interest in G-quadruplex-based devices and materials,[232-238,242-244] these results may provide important design principles toward harnessing the potentially useful photophysical properties of G-quadruplex wires and related structures.[12-15,242-244] **2PyG** has shown to provide a useful structure sensitive fluorescent probe for monitoring G-quadruplex folding. In contrast, the most commonly used internal probe, **2AP**, is a poor reporter of energy transfer in the context of G-quadruplexes.

2PyG was used in conjunction with PEG-promoted G-quadruplex folding to dissect the multiple roles metal ions play in mediating both G-quadruplex folding and energy transfer. Elucidating the exact mechanism of cation-mediated energy transfer will require additional studies, but our results suggest that the enhanced quantum yields of unmodified guanine residues upon O^6-ion coordination are responsible for the unusually efficient energy transfer reactions mediated by G-quadruplex structures. Interestingly, the O^6 carbonyl stretching frequencies of guanine residues are known to decrease upon NH_4^+-mediated quadruplex folding,[250] and the "trapped enol" mimic O^6,9-dimethylguanine is known to be highly fluorescent when protonated.[251] Taken together, these results suggest that the ion-coordinated guanine residues in G-quadruplexes may electronically resemble emissive enol forms of guanine more than the corresponding ion-free guanine residues.

To the best of our knowledge, direct O^6 to potassium coordination is a unique feature of G-quadruplex structures. The resulting impact on energy transfer therefore provides a highly specific readout of G-tetrad formation over single-stranded or duplex DNA with

η_t(duplex) < η_t(single-strand) < η_t(G-quadruplex). Together with advances in multi-photon fluorescence microscopy this phenomenon might provide an important imaging tool compatible with complex cellular environments.[252]

CHAPTER 6

Elongated 8-(Substituted)-2'-deoxyguanosine Mimics for Folding and Energy Transfer Studies[7]

8-substituted guanosines are an important new family of fluorescent base analogs that effectively mimic guanine residues even in highly demanding model systems such as polymorphic G-quadruplexes and duplex DNA. Here two 8-substituted-2'-deoxy-guanosines and their incorporation into the human telomeric repeat sequence are reported. These include 8-(2-phenylethenyl)-2'-deoxyguanosine (**StG**), and 8-[2-(pyrid-4-yl)-ethenyl]-2'-deoxyguanosine (**4PVG**). In contrast to previously reported fluorescent guanine analogs, the 8-substituted guanosines are not significantly quenched upon their incorporation into nucleic acids (Φ = 0.01 – 0.45). These highly emissive probes were used to quantify energy transfer efficiencies from unmodified DNA nucleobases to 8-substituted guanosines. As for **2PyG**, efficiencies are highly structure selective, with η_t(duplex) < η_t(single-strand) < η_t(G-quadruplex). These trends are independent of the exact structural features and thermal stabilities of the G-quadruplexes or duplexes containing them. The resulting combination of energy transfer, high probe quantum yield, and high oligonucleotide molar extinction coefficient provides a highly sensitive and reliable readout of G-quadruplex formation even in sample solutions diluted below 250 pM.

[7] Parts of this chapter were published in: Dumas, A. and Luedtke, N. W. *Nucleic Acids Res.*, **2011**, *39,* 6825-6834.

6.1 Introduction

Modification of the position 8 of guanosine is an attractive avenue to fluorescent derivatives because it is not directly involved in base pairing interactions within G-quadruplex or duplex structures (Figure 4.4 A & C). Derivatization of this position can generate fluorescent products,[48,62,63,77,253] with emission properties that are sensitive to DNA folding.(34) 8-(2-pyridyl)-2'-deoxyguanosine "**2PyG**" was reported as a "turn-on" fluorescence probe of G-quadruplex folding and energy transfer.[77] Upon its incorporation into G-tetrads, **2PyG** was minimally disruptive to intramolecular G-quadruplex folding where it exhibited higher quantum yields (Φ = 0.04 – 0.15) than the corresponding nucleoside in water (Φ = 0.02). Using **2PyG** efficient energy transfer reactions (η_t = 0.11 – 0.41) involving unmodified guanosines in G-quadruplex structures and depended on the presence and identities of cations coordinated to the O^6 positions of the guanine residues was discovered. It was unclear from these studies, however, if the reported intramolecular energy transfer reactions resulted from unusual intrinsic properties of G-quadruplexes, the unusual photophysical characteristics of **2PyG**, or some combination thereof. To help address this question, oligonucleotides containing 8-(2-phenylethenyl)-2'-deoxyguanosine (**StG**) and 8-[2-(pyrid-4-yl)-ethenyl]-2'-deoxyguanosine (**4PVG**) were synthesized and evaluated for their ability to report DNA folding and internal energy transfer reactions in G-quadruplex, single-stranded, and duplex structures derived from the human telomeric repeat and cKit(1) promoter sequence. As compared to **2PyG**, both of the vinyl-bridged derivatives **4PVG** and **StG** exhibit red-shifted excitation and emission maxima, lower potentials for perturbing DNA structure, and higher quantum yields (Φ = 0.03 – 0.44) in the context of folded DNA. For all three 8-substituted guanosines, DNA-to-probe energy transfer efficiencies were much higher in G-quadruplex structures (η_t = 0.12 – 0.30) than the same oligonucleotides folded into B-form duplexes (η_t = 0.02 – 0.06). The unusual photophysical properties of cation-containing G-quadruplexes are therefore responsible for the efficient energy transfer reactions within these structures.(34) These phenomena together provide a reliable and highly sensitive means for deciphering the folded state of the DNA (duplex *versus* quadruplex) even in highly diluted sample solutions of 250 pM or less.

6.2 Results and discussion

6.2.1 Synthesis of the β-cyanoethyl phosphoramidites[8]

The preparation of the **2PyG**-containing oligonucleotides used for this comparative study are reported in Chapter 4 and 8.[77] The phosphoramidites of 8-(2-phenylethenyl)- and 8-[2-(pyrid-4-yl)-ethenyl]-2'-deoxyguanosine were synthesized according to Scheme 6.1. The (E)-8-(2-arylethenyl)-3',5'-*O*-bis(*tert*-butyldimethylsilyl)-O^6-(trimethylsilylethyl)-2'-deoxyguanosine derivatives **18** and **28**, described in Chapter 3, were carried forward into phosphoramidite synthesis using standard methodologies (Scheme 6.1). First, N^2 was protected with isobutyryl chloride to give compound **35** and **39**, followed by deprotection of the three silyl protecting groups with tetrabutylammonium fluoride (TBAF) (**36** and **40**). Dimethoxytrityl groups were then added to the 5'-OH groups of the nucleosides by reaction of the nucleotide with dimethoxytrityl chloride in pyridine to give compounds **37** and **41**.

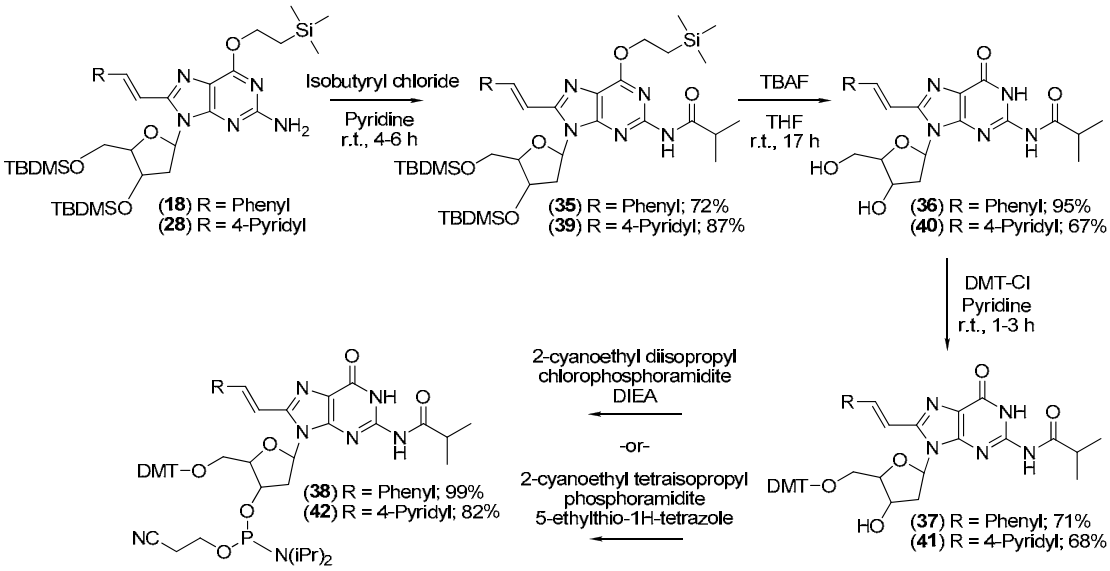

Scheme 6.1: Synthesis of the 8-(2-phenylethenyl)-2'-deoxyguanosine- and 8-[2-(pyrid-4-yl)-ethenyl]-2'-deoxyguanosine phosphoramidites.

[8] Detailed synthetic procedures and characterization of these compounds and intermediates are available in Chapter 8.

Slightly different procedures were needed for the introduction of the cyanoethyl phosphoramidite on the 3'-OH of each compound. The pyridyl derivative **41** was derivatized by a standard base-catalyzed reaction with 2-cyanoethyl diisopropylchloro phosphoramidite to give compound **42**. In the case of the phenyl derivative **37**, these reactions conditions were unsuccessful. The phosphoramidite **38** was therefore prepared from **37** with 2-cyanoethyl tetraisopropyl phosphordiamidite using 5-ethylthio-(1*H*)-tetrazole as a catalyst (Scheme 6.1).

Phosphoramidite building blocks were incorporated into the human telomeric sequence at position 9 (hTeloG9) or 23 (hTeloG23) and in the cKit sequence at position 10 (cKitG10) (Figure 6.1) *via* semi-automated DNA synthesis. Details regarding the oligonucleotide synthesis are presented in Chapter 8. The following sections present a systematic study of the **StG** and **4PVG**-substituted oligonucleotides compared to the wild-type sequences, **2PyG**-substituted oligonucleotides and T-mutants.

hTeloG9: 5'-TTGGGTTA**X**GGTTAGGGTTAGGGA-3'

hTeloG23: 5'-TTGGGTTAGGGTTAGGGTTAGG**X**A-3'

cKitG10: 5'-AGGGAGGGC**X**CTGGGAGGAGGG-3'

Where **X** = G, 2PyG, StG, 4PVG or T

Figure 6.1: Oligonucleotide sequences studied.

6.2.2 Global structures and thermal stabilities of oligonucleotides

Folding of single-stranded hTelo oligonucleotides was controlled by variation of alkali metal salts in the buffer. The global structures and stabilities of the resulting mixtures were assessed using temperature-dependent circular dichroism (CD) and are summarized in Figure 6.2 and Table 6.1. In Li^+-containing solutions, CD data were consistent with mostly unfolded, G-stacked single-stranded DNA (Figure 6.2 A). Under these conditions, similar results were obtained for all the constructs studied. In buffers containing 100 mM KCl, hTelo adopts a "(3 + 1) hybrid" structure that exhibits a positive CD peak at 288 nm with a shoulder at 270 nm and a minimum at 242 nm.[206] The same characteristic CD spectrum was observed when G9 was replaced with **2PyG**, **StG**, and **4PVG**, suggesting the presence of wild-type folds (Figure 6.2 B). In K^+ buffers, **2PyG** caused a larger thermal stabilization of the "(3 + 1) hybrid" structure ($\Delta T_m = +10\ ^oC$) as compared to **StG** and **4PVG** ($\Delta T_m = +5\ ^oC$ and $+8\ ^oC$, Table 6.2). In contrast, replacing G9 with T caused very large

changes to the global structure of hTelo in K^+ (Figure 6.2 B) that were accompanied by a dramatic decrease in thermal stability (ΔT_m = -23 °C, Table 6.1). We interpret these spectral changes and decreased stability as the loss of one G-tetrad and formation of a G-quadruplex containing only two G-tetrads with "head-to-head" heteropolar stacking orientation.[220] These results suggest that position G9 is sensitive to mutation, and that **2PyG**, **StG**, and **4PVG** are incorporated directly into the G-tetrads of natively folded hTelo in the presence of K^+.

The substitution of G23 with **2PyG** caused hTelo to fold into an "antiparallel" topology even in K^+ solutions (Figure 6.2 C). This structure, where G23 adopts a *syn* conformation, is normally only observed in Na^+-containing solutions.[207,208] hTeloG23(2PyG) was therefore characterized in Na^+ buffer, where it exhibited nearly the same global structure and thermal stability as the wild-type sequence in Na^+ (ΔT_m = -2 °C, Figure 6.2 D and Table 6.1). **StG** and **4PVG**, in contrast, did not force hTeloG23 to fold into an "antiparallel" structure in K^+ solutions, and, like the wild-type sequence, two maxima in the region between 270 and 305 nm, and a minimum at ~240 nm were observed (Figure 6.2 C). **StG** and **4PVG** were also compatible with the formation of the "antiparallel" hTelo structure in Na^+ solutions (Figure 6.2 D). In cKitG10, **2PyG, StG** and **4PVG** have a minor impact on the structure and stability in K^+ solutions, showing a decrease in the intensity of the maximum around 263 nm (ΔT_m = +5 °C to -3 °C). Interestingly, no shoulder is observed around 290 nm as it is the case for the thymidine mutant (Figure 6.2 E). Taken together, these results suggest that G-quadruplexes containing **StG** and **4PVG** exhibit folding behavior more similar to wild-type sequences than **2PyG**, especially in the case of hTelo. Globally speaking, 8-substituted-2'-deoxyguanosines are better tolerated by G-quadruplex and duplex than pyrimidine mismatches.

In contrast to the mutation-sensitive folding of G-quadruplexes, the substitution of the corresponding duplex DNAs with **2PyG**, **StG**, **4PVG** or T resulted in little impact on the global structure (Figure 6.2 F, Appendix A.2). In cKit, the substitution of G10 with an 8-substituted guanosine analog resulted in a decrease in signal intensity and moderate destabilization (ΔT_m = -3 °C to -7 °C) as compared to the thymidine mutant (ΔT_m = -9 °C). In hTelo, due to the close proximity of G23 to the end of the oligonucleotide, these modifications had little impact on thermal stability of the duplex (Table 6.1). Duplexes containing modifications at the central G9 position, in contrast, exhibited thermal stabilities that were highly sensitive to mutations. T incorporation at G9 caused an important destabilization (ΔT_m = -8 °C) as compared to the wild-type hTelo duplex (Table 6.1). The

8-substituted guanosines caused much less loss in thermal stability than T, with ΔT_m = -5 °C, -3 °C, and -1 °C for **2PyG**, **StG**, and **4PVG**, respectively (Table 6.1). Consistent with our results from hTelo G-quadruplexes, these data suggest that duplex oligonucleotides containing **StG** and **4PVG** exhibit duplex folding equilibria more similar to wild-type hTelo than either **2PyG** or T mutations.

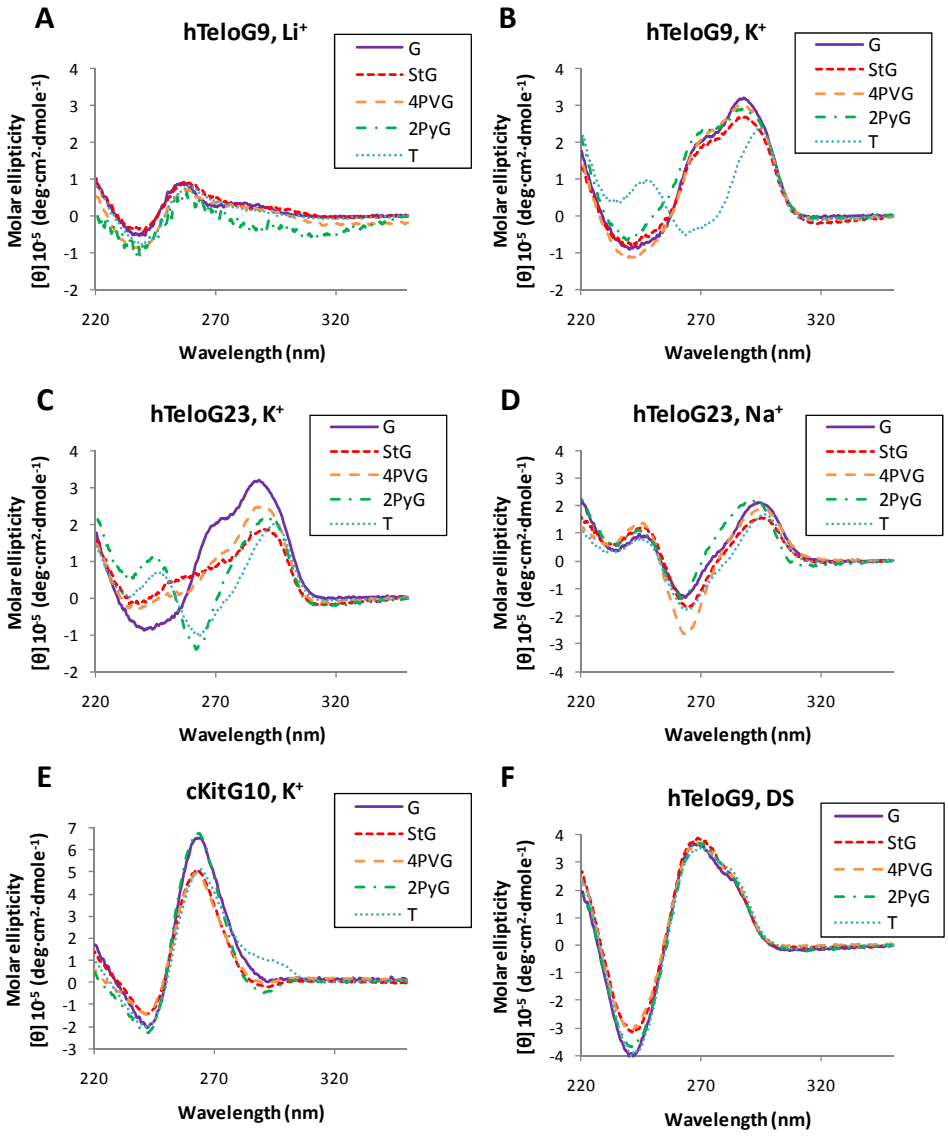

Figure 6.2: CD spectra of single-stranded hTeloG9, hTeloG23 and cKitG10 derivatives in 100 mM LiCl (A), 100 mM KCl (B, C & E) or 100 mM NaCl (D). Double-stranded hTeloG9 samples "DS" included 1.1 equivalents of the complementary strand and were prepared in 100 mM NaCl (F). All samples contained 2 μM of DNA in an aqueous 10 mM cacodylate buffer (pH 7.4).

Table 6.1: Thermal denaturation melting temperatures (T_m) of single-stranded oligonucleotides in K^+ or Na^+, and duplex samples (DS) in Na^+ as determined by temperature-dependent CD.

Name	X	T_m in K^+ (ΔT_m)[a]	T_m in Na^+ (ΔT_m)[a]	T_m of DS (ΔT_m)[a]
hTelowt	**G**	67.7	53.5	66.0
hTeloG9	**StG**	73.1 (5.4)	60.6 (7.1)	63.0 (-3.0)
	4PVG	75.9 (8.2)	61.1 (7.6)	64.6 (-1.4)
	2PyG	77.5 (9.8)	61.8 (8.3)	61.2 (-4.8)
	T	44.6 (-23)	39.2 (-14)	57.8 (-8.2)
hTeloG23	**StG**	59.5 (-8.2)	52.7 (-0.8)	66.5 (0.5)
	4PVG	61.5 (-6.2)	47.5 (-6.0)	66.9 (0.9)
	2PyG	59.3 (-8.4)	51.6 (-1.9)	66.2 (0.2)
	T	45.2 (-23)	45.1 (-8.4)	64.5 (-1.5)
cKitwt	**G**	64.3	n.d.[b]	74.4
cKitG10	**StG**	69.1 (4.8)	n.d.[b]	67.4 (-7.0)
	4PVG	61.2 (-3.1)	n.d.[b]	71.8 (-2.6)
	2PyG	62.4 (-1.9)	n.d.[b]	68.1 (-6.3)
	T	59.3 (-5.0)	n.d.[b]	65.2 (-9.2)

[a] $\Delta T_m = T_m$ (modified oligo) - T_m (wild-type).
[b] n.d. = not determined.

6.2.3 Quantum yields of 8-substituted guanosines in modified oligonucleotides

The vast majority of fluorescent guanosine analogs, such as 2-aminopurine (**2AP**), 6-methylisoxanthopterin (**6-MI**) and 3-methylisoxanthopterin (**3-MI**) are quenched by close proximity and collisions with unmodified purine residues.[225,254] These result in large (10 to 300-fold) decreases in quantum yield upon their incorporation into duplex DNA.[50,74,144] 8-substituted guanosines, in contrast, exhibit relatively little, if any quenching upon their incorporation into G-quadruplex, single-stranded, or duplex DNA. The quantum yield of **2PyG** in water (Φ = 0.02) increases to Φ = 0.03 – 0.05 upon its incorporation into single-stranded or duplex hTelo DNA, and it increases to Φ = 0.05 - 0.15 when the same oligonucleotides were folded into G-quadruplex structures.[77] In the case of **4PVG** (Φ = 0.16 in water), somewhat lower quantum yields were obtained upon its incorporation into single-stranded and quadruplex structures (Φ = 0.03 – 0.10) and still

lower quantum yields were observed in the context of duplex DNA (Φ = 0.02 – 0.06). Upon its incorporation into DNA, **StG** exhibited quantum yields that were much higher than both **2PyG** and **4PVG** (Table 6.2). The values measured for the hTelo single-strand and G-quadruplex samples containing **StG** (Φ = 0.33 – 0.45) were higher than the values obtained for duplex DNA (Φ = 0.20 – 0.32). This trend was reversed in the case of cKit, where the duplex was more strongly fluorescent (Φ = 0.30) than the other samples (Φ = 0.13 – 0.16). The quantum yields of **StG** are approximately 10- to 100-fold higher than all previously reported fluorescent guanine mimics in the context of well-folded nucleic acids with strong base-stacking interactions.[50,74,144,225,254] Taken together, these results suggest that water mediated quenching of **2PyG** and **4PVG** involves proton transfer between photoexcited pyridyl nitrogens and bulk solvent. According to molecular modeling of known structures,[206,208] the pyridyl nitrogen of **2PyG** should be partially protected from bulk solvent upon its incorporation into positions G9 and G23 of hTelo and G10 of cKit. This may explain the higher quantum yields of **2PyG** in the context of G-quadruplex folded DNA (Section 4.2.6). The same modeling studies suggest that the pyridyl nitrogen of **4PVG** will remain fully solvated in both quadruplex and duplex DNA. No enhancement in the quantum yield of **4PVG** was therefore predicted upon its incorporation into DNA.

6.2.4 Quantification of energy transfer in modified oligonucleotides

The excitation spectra of the oligonucleotides containing 8-substituted guanosines exhibit two maxima corresponding to direct excitation (λ_{ex} = 330 – 400 nm) and indirect excitation *via* unmodified nucleobases (λ_{ex} = 260 nm) (Figure 6.3). The ratio of these excitation peaks weighted by the absorbance properties of the DNA and quantum yields of the probe can be used to calculate energy transfer efficiencies (η_t).[77,78,145]

Energy transfer efficiencies from unmodified bases to **2PyG**, **StG**, and **4PVG** were approximately 2- to 20-fold higher in G-quadruplexes (η_t = 0.07 – 0.36) as compared to the same oligonucleotides in duplex DNA (η_t = 0.01 – 0.06). Single-stranded samples in Li^+ exhibited intermediate efficiencies (Table 6.2). In cKitG10, the three probes showed significantly lower energy transfer efficiencies than in the other sequences studied, independently of the structure adopted. Unmodified guanine residues probably serve as the main energy donors due to their proximity, spectral overlap and abundance. In single-strands and duplex DNA, the absence of neighboring guanine for position 10 can explain the small values observed. In the context of G-quadruplex, the low energy transfer

efficiencies support the possible presence of an alternative DNA fold that excludes 8-modified G10 residues from G-tetrad formation.

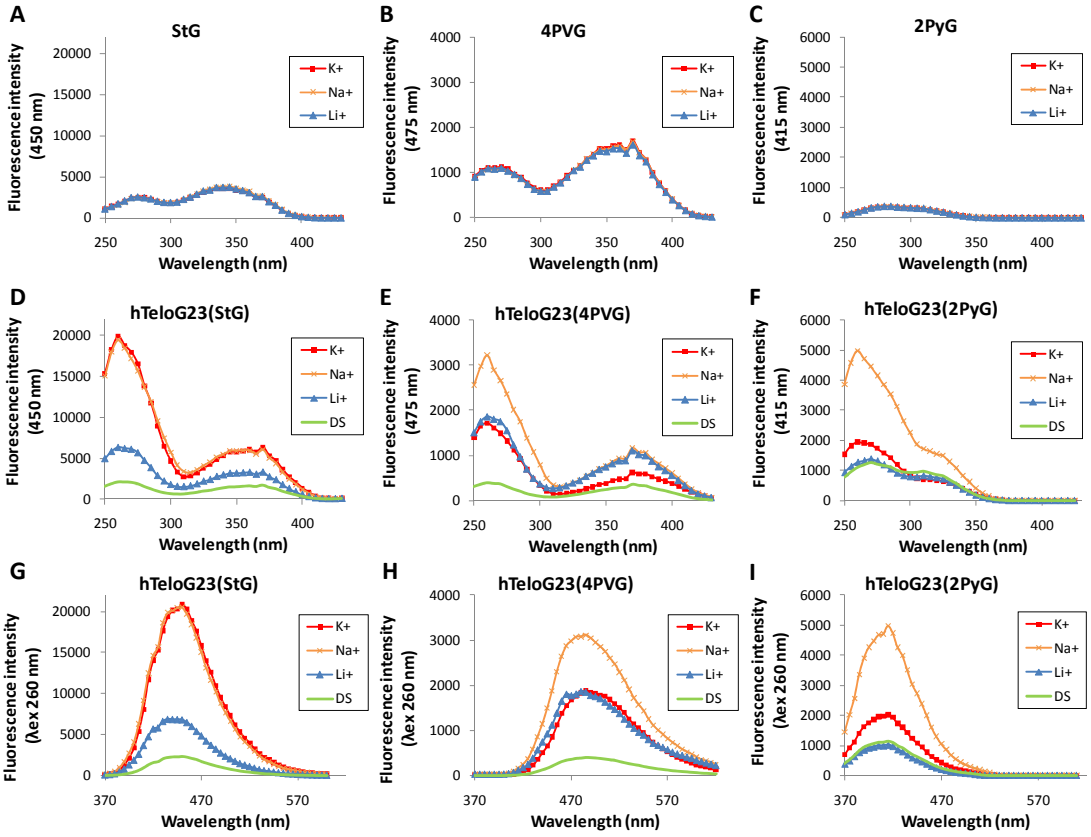

Figure 6.3: Excitation spectra of 2 μM of **StG** (A), **4PVG** (B) or **2PyG** (C) in the presence of 100 mM KCl (K^+), 100 mM NaCl (Na^+) or 100 mM LiCl (Li^+). Excitation spectra of hTeloG23(StG) (D), hTeloG23(4PVG) (E) and hTeloG23(2PyG) (F) collected using emission at 450 nm, 475 nm and 415 nm, respectively. Emission spectra of hTeloG23(StG) (G), hTeloG23(4PVG) (H) and hTeloG23(2PyG) (I) collected using excitation at 260 nm. Double-stranded samples "DS" included 1.1 equivalents of the complementary strand and were prepared in 100 mM NaCl. All samples contained 2 μM of DNA or 8-substituted-2'-deoxyguanosine nucleoside in an aqueous 10 mM cacodylate buffer (pH 7.4).

Ratiometric analysis of the fluorescence intensities resulting from DNA excitation *versus* selective probe excitation can provide a simple and highly sensitive readout of G-quadruplex formation. According to this approach, the intensity of probe fluorescence upon DNA excitation at 260 nm (F(260)) is divided by the fluorescence intensity upon selective probe excitation (F(X)), where X = 325 nm for **2PyG**, 360 nm for **StG**, and 375 nm for **4PVG**. Consistent with the trends in energy transfer efficiencies (η_t) and with **2PyG**, duplex DNA exhibited the lowest F(260)/F(X) ratios of 0.7 – 1.4, single-stranded DNA in Li^+ exhibited intermediate F(260)/F(X) ratios of 1.6 – 2.3, while G-quadruplex

structures have the highest F(260)/F(X) ratios with 2.5 – 4.7. These values were similar for all three 8-substituted guanosines, and were independent of the exact structural features and thermal stabilities of the G-quadruplexes or duplexes containing them (Table 6.2).

Table 6.2: Quantum yield (Φ), DNA-to-probe energy transfer efficiency (η_t), and the ratio of fluorescence intensities obtained upon excitation at 260 nm (F(260)) and at 360 nm (F(360)) for **StG**, 375 nm (F(375)) for **4PVG**, and 325 nm (F(325)) for **2PyG**.

		StG			4PVG			2PyG		
Name	**Cond.**	**Φ**	**η_t**	**F(260)/ F(360)**	**Φ**	**η_t**	**F(260)/ F(375)**	**Φ**	**η_t**	**F(260)/ F(325)**
hTeloG9	Li^+	0.45	0.06	2.0	0.05	0.17	2.0	0.04	0.09	2.3
	K^+	0.44	0.21	3.5	0.04	0.28	3.3	0.09	0.24	4.0
	Na^+	0.37	0.18	3.9	0.03	0.36	3.7	0.08	0.30	4.7
	DS	0.32	0.02	0.9	0.03	0.04	1.0	0.03	0.03	1.1
hTeloG23	Li^+	0.35	0.03	1.9	0.07	0.16	1.8	0.05	0.11	1.8
	K^+	0.33	0.12	3.3	0.04	0.24	2.9	0.05	0.19	3.0
	Na^+	0.37	0.12	3.3	0.06	0.31	3.0	0.10	0.26	3.3
	DS	0.20	0.02	1.3	0.02	0.05	1.2	0.04	0.06	1.4
cKitG10	Li^+	0.13	0.04	1.7	0.10	0.12	1.6	0.03	0.05	1.6
	K^+	0.16	0.07	2.9	0.07	0.17	2.5	0.04	0.12	2.6
	DS	0.30	0.01	0.7	0.06	0.03	0.8	0.03	0.01	0.7

To evaluate the sensitivity of this F(260)/F(X) analysis, serial 2-fold dilutions of hTeloG9 duplex and G-quadruplex DNA containing **StG** were performed (Figure 6.4 B & C). High sample absorption at the excitation wavelength can attenuate the excitation beam, causing reduced fluorescence intensities, as revealed by the non-linearity between concentration and fluorescence signal when the DNA sample is excited at 260 nm (Figure 6.4 A). To overcome this problem, the DNA samples raw fluorescence signals are multiplied by the correction factor "CF" (eq. 8.2, Chapter 8) (Figure 6.4 B & C). Upon direct excitation of the probe at 360 nm, where the sample has a low optical density (OD < 0.01), attenuation of the excitation beam is minimal and no correction is required. After correction for high sample absorbance, the ratios in F(260)/F(X) were concentration independent (quadruplex ~ 4, and duplex ~ 1) (Figure 6.4 D) and could be readily measured with a standard fluorimeter and sample holder (1 cm path length) using 250 pM solutions of **StG**-labeled

DNA. This approach therefore provides a simple and highly sensitive fluorescence readout of G-quadruplex folding that is compatible with extremely diluted sample mixtures.

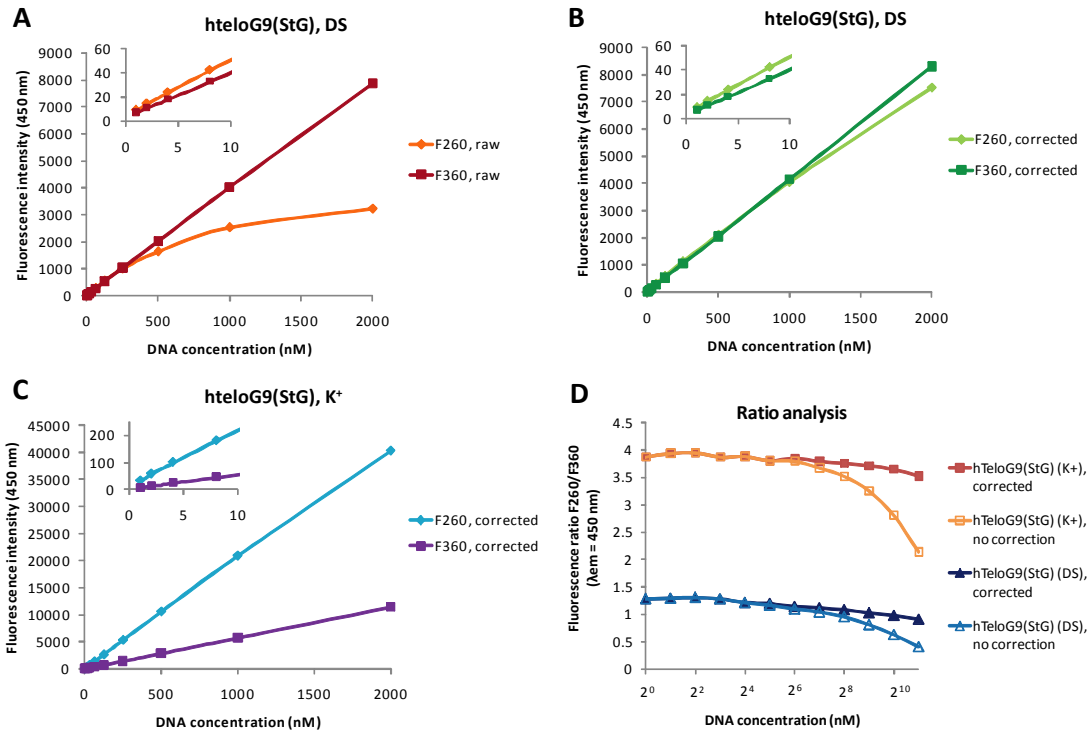

Figure 6.4: Sensitivity analysis and effect of absorbance correction factor CF. Raw (A) and corrected (B) fluorescence emission intensities at 450 nm upon excitation hTeloG9(StG) double-stranded DNA "DS" at 260 nm (F260) or selective excitation of the probe at 360 nm (F360). Corrected values were obtained by the multiplication of the raw intensities by the correction factor "CF" (eq. 8.2, Chapter 8) accounting for the attenuation of the excitation beam and reduction of the fluorescence intensities resulting from absorption of the sample at each wavelength of excitation. (C) CF-corrected fluorescence emission intensities at 450 nm upon excitation at 260 nm (F260) or 360 nm (F360) of hTeloG9(StG) G-quadruplex DNA in the presence of 100 mM KCl "K^+". (D) Ratios of raw and CF-corrected ratios of F(260)/F(360) for duplex "DS" and G-quadruplex "K^+" hTeloG9(StG) DNA at variable DNA concentrations. Data were collected in a 1 cm fluorescence cuvette starting from 2 μM solutions of DNA by performing sequential 2-fold dilutions. Double-stranded samples "DS" included 1.1 equivalents of the complementary strand and were prepared in 100 mM NaCl. All samples were prepared in aqueous 10 mM cacodylate buffer (pH 7.4).

6.3 Conclusions

Fluorescence phenomena enable powerful and readily accessible technologies for probing biomolecule folding and activity.[42] Fluorescence-based assays involving fluorescent nucleobase analogs typically assess conformational changes using probes that exhibit lower quantum yields when base-stacked with neighboring residues.[51,65-68] Probes that

remain highly emissive when involved in base-stacking interactions will increase the sensitivity of nucleic acid folding studies, and may provide a means to differentiate DNA/RNA folds where alternative base-stacking interactions are present (ex. duplex *versus* quadruplex). Here we demonstrate how highly emissive probes that mimic guanine residues can be used to differentiate DNA secondary structures by estimating energy transfer efficiencies between unmodified nucleobases and 8-substituted guanines. To the best of our knowledge, this represents a new paradigm in detecting conformational changes in nucleic acids. While FRET-based studies using large "external" probes are frequently reported,[40] interpretations of the resulting data are limited to changes in probe-to-probe distances, whereas the use of an "internal" fluorescent base analog can provide a direct readout of the characteristic photophysical properties of secondary structures of nucleic acids containing them. Notably, this can be accomplished by introducing a very small modification (e.g. a single styrene or pyridine group) into the oligonucleotide at a strategic location to provide a highly sensitive and minimally perturbing fluorescent readout of structure.

Polymorphic G-quadruplex structures derived from the human telomeric repeat (hTelo) provide demanding model systems to evaluate internal fluorescent probes for their potential impact on DNA folding and stability. To effectively mimic guanosine in G-quadruplexes, both the *Watson & Crick* and *Hoogsteen* hydrogen bonding faces must be maintained. Previous studies have demonstrated that subtle changes to either face (e.g. 7-deazaguanine, 6-thioguanine, or inosine) result in large losses in G-quadruplex folding kinetics and stability.[76] Indeed, single base mutations (G → T) in hTelo DNA resulted in large losses to intramolecular G-quadruplex thermal stabilities ranging from 8 – 24 ^{o}C, while duplexes containing the same mutations lost only 2 – 8 ^{o}C of thermal stability. 8-susbtituted guanosines exhibited context-dependent effects on DNA folding and stability, but were generally well-tolerated in both G-quadruplex and duplex oligonucleotides.

2PyG was the first reported example of a fluorescent guanine mimic that exhibits the same or higher quantum yield when base-stacked with neighboring purine residues.[77] As a nucleobase analog, however, **2PyG** suffers from some limitations including a *syn* glycosidic conformational preference, a relatively low quantum yield in water (Φ = 0.02 - 0.15), and an excitation maximum in the UV. Here we report related derivatives 8-(2-phenylethenyl)-2'-deoxyguanosine (**StG**) and 8-[2-(pyrid-4-yl)-ethenyl]-2'-deoxyguanosine (**4PVG**) that exhibit a preference for an *anti* glycosidic conformation. As compared to **2PyG**, both of these vinyl-bridged derivatives exhibit red-shifted excitation

and emission maxima, lower perturbations of DNA structure/stability, and higher quantum yields. To the best of our knowledge, **StG** displays the highest quantum yield of all reported purine base analogs in the context of folded nucleic acids ($\Phi = 0.20 – 0.45$). The quantum yield of **StG** is not as environmentally sensitive as **2PyG** and **4PVG**, but it can still report DNA folding due to its ability to serve as an emissive energy acceptor for unmodified nucleobase donors.

Previous studies have suggested that the enhanced quantum yields of unmodified guanine residues upon O^6 ion coordination are responsible for the unusually efficient energy transfer reactions mediated by G-quadruplex structures.[77] It was not clear from these results, however, if efficient energy transfer resulted from the intrinsic properties of G-quadruplexes, the unusual photophysical characteristics of **2PyG**, or some combination thereof. Here we report a similar range of transfer efficiencies for all three 8-substitued guanosines evaluated in G-quadruplexes ($\eta_t = 0.12 – 0.31$), suggesting that efficient energy transfer results from the intrinsic properties of G-quadruplex structures, not the probes. In all cases, the energy transfer efficiencies were structure dependent, with $\eta_t(\text{duplex}) < \eta_t(\text{single strand}) < \eta_t(\text{G-quadruplex})$. In the case of G-quadruplex structures, the combination of efficient energy transfer, high probe quantum yields, and high molar extinction coefficient of the oligonucleotide ($\varepsilon_{260nm} \approx 250'000\ cm^{-1}M^{-1}$) result in very bright fluorescence emissions that allow for the detection of G-quadruplex conformations at oligonucleotide concentrations of 250 pM or lower using a standard fluorimeter and sample holder. Even in such dilute solutions, a simple comparison of emission intensities resulting from selective probe excitation *versus* excitation of the DNA provides a highly convenient, sensitive, and reliable means to characterize the folded states of oligonucleotides. The trends from these ratiometric analyses matched those from detailed analyses of energy transfer efficiencies. In both cases, the trends were independent of the exact structural features of the G-quadruplex or 8-substituted guanosine probe used. Given the simplicity and sensitivity of this approach, we expect that it will be compatible with conformational analyses using fluorescence microscopy and single molecule spectroscopy.

CHAPTER 7

Site-specific Control of *N*7-Metal Coordination in DNA Using 8-(2-Pyridyl)-2'-deoxyguanosine

8-Substituted-2'-deoxyguanosines are "push-pull" fluorophores that can exhibit environmentally-sensitive quantum yields (Φ = 0.001 – 0.72) due to excited-state proton transfer reactions with bulk solvent. Changes in nucleoside fluorescence were used to characterize metal binding affinity and specificity of 8-substituted-2'-deoxyguanosines. One derivative, 8-(2-pyridyl)-2'-deoxyguanosine (**2PyG**), exhibits selective binding of Cu(II), Ni(II), Cd(II), and Zn(II) *via* a bidentate effect provided by the *N*7 atom of guanine and 2-pyridine group. Upon incorporation into DNA, 2-pyridine-modified guanine residues selectively bind to Cu(II) and Ni(II) with equilibrium dissociation constants (K_d) ranging from 25 to 850 nM; affinities that depend on the folded state of the oligonucleotide (duplex > G-quadruplex) as well as the identity of the metal ion (Cu > Ni >> Cd). These binding affinities are approximately 10- to 1'000-fold higher than unmodified metal binding sites in DNA, thereby providing site-specific control of metal localization in alternatively folded nucleic acids. Temperature-dependent circular dichroism studies reveal metal-dependent stabilization of duplexes, but destabilization of G-quadruplex structures upon adding stoichiometric Cu(II) to **2PyG**-modified oligonucleotides. These results demonstrate how the addition of a single pyridine group to the *C*8-position of guanine provides a powerful new tool for studying the effects of *N*7 metallation on the structure, stability, and electronic properties of nucleic acids.

7.1 Introduction

Metal ions mediate the folding and function of biological nucleic acids,[255-259] and can provide stable junctions in synthetic supramolecular assemblies.[260-266] The most important metal ion binding sites in B-form duplexes include the *N*3 and *N*7 positions of purine residues and the phosphodiester backbone.[267-269] The binding of Pt(II) to proximal guanine residues *via* *N*7 coordination is thought to be responsible for the anti-tumor activity of cisplatin,[270,271] but cisplatin treatment of genomic DNA results in a heterogeneous mixture of monoadducts, intra- and inter-strand cross-links.[272,273] Likewise, Cu(II), Ni(II), Cd(II) and Pb(II) all have multiple DNA binding sites with variable affinities that complicate the interpretation of binding data.[274-281] Despite the critical role played by the *N*7 positions of purine residues in mediating these metal binding interactions, there are no previously reported methods for directing metal ions to specific *N*7 sites in nucleic acids.

The site-specific incorporation of kinetically inert metal complexes into oligonucleotides is a key design feature of studies aimed at characterizing energy and electron-transfer processes in DNA. In this approach, electroactive and/or luminescent metal complexes are introduced into DNA *via* intercalating agents,[282-284] covalent end-labels,[285-289] or C5-modified pyrimidine residues.[290-293] Metallo-nucleobase derivatives of purines are much less studied, with only a few reported examples of ferrocene, Ru(II) and Os(II) complexes of *C*7- and *C*8-modifed purines.[294-296]

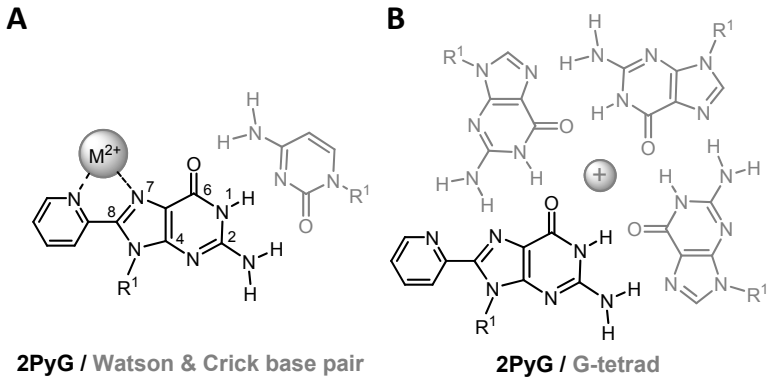

Figure 7.1: **(**A) *Watson & Crick* base pair between a **2PyG** metal complex (black) + cytidine (gray). (B) **2PyG** (black) incorporated in a G-tetrad (gray).

Due to biaryl-related fluorescence phenomena,[48] arylation of the 8-position of purines can provide highly emissive nucleobase derivatives[48,62,63,77,105,173,179,181,253]

having the ability to mediate proper base pairing interactions along both *Watson & Crick* and *Hoogsteen* faces.[77,178,179] Given the close proximity to *N*7, it was speculated that the addition of 2-substituted heterocyclic groups to the *C*8 position of purine residues would furnish bidentate metal ligands capable of directing metal ions to specific *N7* sites within folded DNA or RNA. While *N*7 positions are well solvated and available for metal binding in duplex DNA,[256,258,270,271] certain structures like G-quadruplexes and triplexes utilize *N*7 hydrogen bonding interactions for stabilization (Figure 7.1). Previous studies have demonstrated that G-tetrad formation in quadruplexes can compete with Pt(II) binding at *N*7,[297-299] but these reactions are under kinetic control and result in complex product mixtures. We were therefore interested in developing *C*8-modifed purines for the site-specific control of metal binding interactions in applications including the study of reversible *N*7 metallation on the structure and stability of nucleic acids. This approach has the added benefit that changes in nucleotide fluorescence can be used as a direct readout of metal binding.

7.2 Results and discussion

7.2.1 Nucleoside-metal binding interactions

O^6/*N*7 complexation is an important mode of guanine-Pd(II) binding,[197,300] but these atoms do not provide a suitable bite angle for Cu(II), Ni(II) or Zn(II).[268,301,302] The presence of heterocycles fused to the *C*8 position of purine residues can provide an alternative bidentate metal binding site that is suitable for first row transition metals. As an initial assessment of metal binding activities, the absorbance and fluorescence emission spectra of 50 μM solutions of 8-substituted-2'-deoxyguanosines were measured in the presence of 10 mM of Cu(II), Ni(II), Cd(II), Pd(II), Hg(II), or Zn(II). Quantum yields were measured in the presence (Φ_m) *versus* absence (Φ) of each metal ion and compared as Φ_m/Φ ratios (Table 7.1). Palladium (II) has a measurable quenching effect on all the nucleosides tested (Φ_m/Φ = 0 – 0.56). These results are consistent with problematic Pd(II)-catalyzed cross-coupling reactions that are often encountered in the absence of O^6 protection.[197,300,303] All other metals evaluated exhibited little or no effect on the emission intensities of **PhG**, **4PyG**, **2FuG**, and **2ThG** under these conditions.

Table 7.1: Ratios of quantum yield values expressed as (Φ_m/ Φ) of the nucleoside in the presence (Φ_m) *versus* absence (Φ) of various metal ions.

Name	R	No metal	Cu(II)	Ni(II)	Cd(II)	Pd(II)	Hg(II)	Zn(II)
PhG		1	0.7	0.9	0.9	0.4	0.7	0.9
2PyG		1	0.0	0.0	12	0.0	0.9	13
4PyG	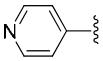	1	0.6	0.9	1.8	0.6	1.0	1.2
2ThG		1	0.7	0.9	1.0	0.6	0.8	1.0
2FuG		1	0.7	1.0	1.1	0.5	0.9	1.0

3PyG was excluded from this study because its exceptionally low fluorescence prevents the calculation of accurate quantum yield ratios.

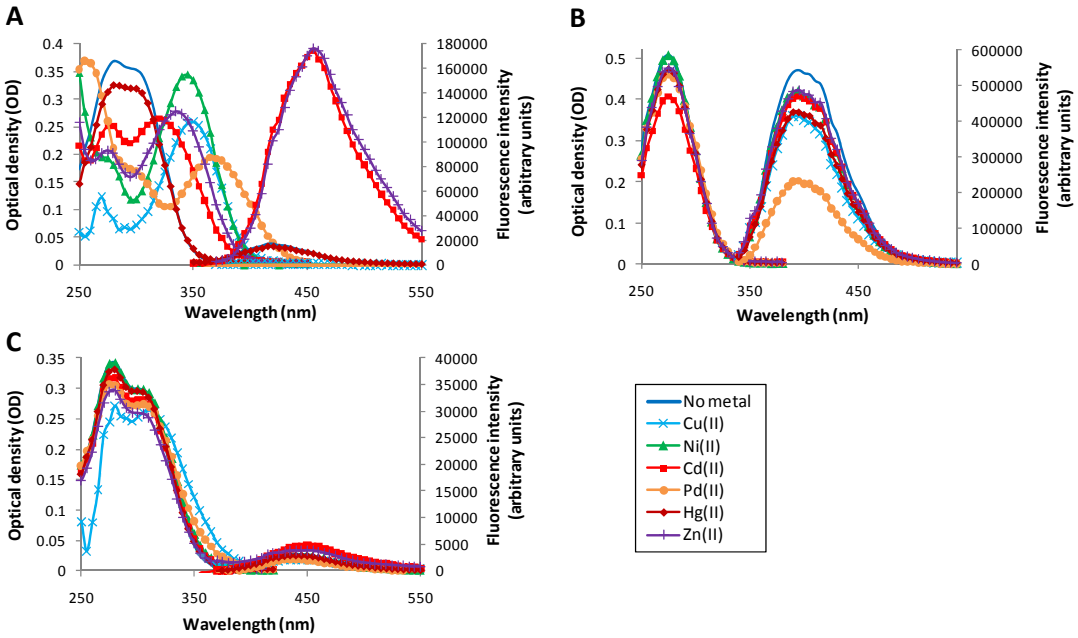

Figure 7.2: Absorption and emission spectra of **2PyG** (A), **PhG** (B) and **4PyG** (C) in the presence of different metals. (10 mM M^{2+}; 0.05 mM nucleoside; λ_{ex} 320 nm; 50 mM Tris, pH 7.4).

Upon addition of 10 mM of Cu(II), Ni(II), Cd(II), Pd(II), or Zn(II) the double absorbance maximum of **2PyG** (280/300 nm) is red-shifted to 325 – 375 nm, consistent with an enhancement of the "push-pull" character of the **2PyG** fluorophore upon metal ion binding (Figure 7.2 A). In contrast, the **2PyG** isosteres, **PhG** and **4PyG**, exhibit only small changes in their absorbance and emission spectra upon addition of these metals (Figure 7.2 B & C). Taken together, these results demonstrate the critical importance of the bidentate 2-(2-pyridyl)-imidazole moiety of the **2PyG** nucleoside for its metal binding properties.[304-308]

Upon saturation with Cd(II) or Zn(II) the fluorescence intensity of **2PyG** increases approximately 38-fold in buffered water (pH 7.4), resulting in quantum yields (Φ) ≈ 0.49 (Figure 7.3 A). These enhancements probably result from forced co-planarity of the pyridine/guanine moieties and/or "protection" of the **2PyG** pyridyl nitrogen from solvent-mediated quenching. In contrast, almost complete quenching of **2PyG** fluorescence occurs upon saturation with Cu(II), Ni(II), and Pd(II) (Φ ≈ 0.001) (Figure 7.3 B). Changes in **2PyG** fluorescence intensity were plotted against metal ion concentration to determine equilibrium dissociation constants (Figure 7.3). Given the relatively low **2PyG** concentrations used in these titrations (0.025 mM), the following K_d values were calculated with the assumption of 1:1 binding stoichiometry: Cu(II) = 0.26 mM; Ni(II) = 0.075 mM; Zn(II) = 4.8 mM; Cd(II) = 8.8 mM; Pd(II) = 0.15 mM.

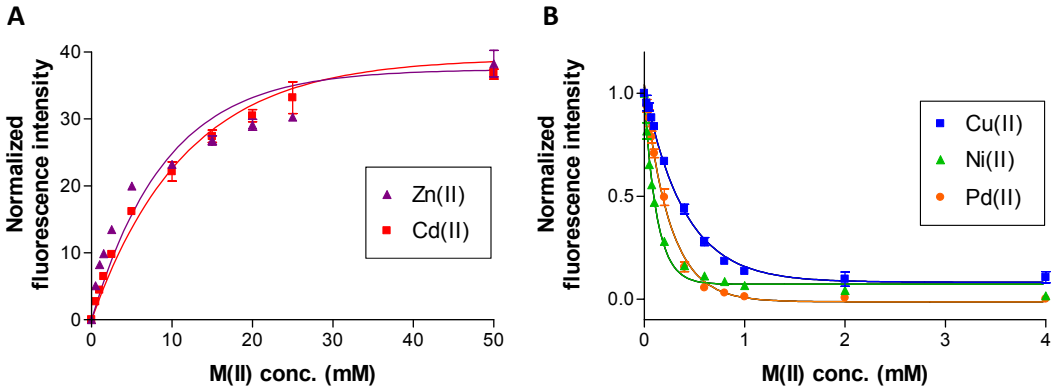

Figure 7.3: (A) Normalized fluorescence intensity of **2PyG** upon titration with $ZnCl_2$ or $CdCl_2$ (λ_{ex} = 320 nm and λ_{em} = 455 nm), (B) Normalized fluorescence intensity of **2PyG** upon titration with $CuCl_2$, $NiCl_2$ or $Pd(CH_3CN)_2Cl_2$ (λ_{ex} = 320 nm and λ_{em} = 415 nm). Final **2PyG** concentrations were 25 µM in an aqueous buffer containing 50 mM Tris-HCl (pH 7.4).

7.2.2 2PyG DNA-metal binding interactions

2PyG was inserted at positions G10 or G15 in the cKit(1) sequence: AGGGAGGGC**X**CTGG**X**AGGAGGG (X = **2PyG** or G) to furnish cKitG10(2PyG) and cKitG15(2PyG), respectively (Section 4.2.3, Chapter 4). This sequence adopts a single G-quadruplex conformation in potassium-containing solutions that has been implicated in the regulation of transcriptional control.[31,35,38,209] Positions G10 and G15 were selected for substitution with **2PyG** because both positions are directly involved in G-tetrad formation,[35,38,209] but have highly variable primary sequence contexts (underlined). G10 is flanked by pyrimidines, whereas G15 is flanked by other purine residues that might contribute to metal binding (underlined). Previous studies using temperature-dependent CD have demonstrated that the incorporation of **2PyG** at these positions has relatively little impact on the global conformation or stability of the resulting G-quadruplex and duplex structures.[77,178] To control the folding of these oligonucleotides *in vitro*, G-quadruplex structures were prepared from single-stranded DNA in 100 mM KCl, while B-form duplex-folded samples were prepared in 100 mM NaCl containing 1.1 equivalents of the C-rich complementary strand.[35,38,209] Following DNA folding by heating and slow cooling, transition metal ions were added and allowed to fully equilibrate at room temperature prior to the quantification of **2PyG** fluorescence. Consistent with the trends observed for the **2PyG** nucleoside monomer (Figure 7.3), the addition of Ni(II) and Cu(II) caused reversible **2PyG** fluorescence quenching, while Cd(II) binding caused fluorescence enhancement of **2PyG**-containing oligonucleotides (Figure 7.4).[9] Metal titrations conducted using relatively high concentrations (2 μM) of **2PyG**-modified oligonucleotides revealed 1:1 stoichiometric binding of Cu(II) (Figure 7.5). These results strongly suggest that **2PyG** is the primary Cu(II) binding site in pre-folded G-quadruplex and duplex structures. Titrations conducted at relatively low oligonucleotide concentrations (0.2 μM, Figure 7.4) were used to estimate metal binding affinities with the assumption of 1:1 binding stoichiometry for all interactions. Upon its incorporation into duplex DNA, **2PyG** binds to Cu(II) and Ni(II) ions with equilibrium dissociation constants (K_d) $\leq$ 25 – 850 nM. These affinities are approximately 10- to 1'000-fold higher than unmodified metal binding sites in duplex DNA ($K_d \approx$ 0.5 – 90 μM),[274,275,279,281] and are approximately 1'000- to 10'000-fold higher than the **2PyG** nucleoside monomer ($K_d \approx$ 75 – 260 μM) (Table 7.2). These results demonstrate additive contributions by both the pyridine and DNA that result in high metal binding affinities of **2PyG**-modified oligonucleotides,

[9] The addition of 2 equivalents of EDTA reverses the changes in fluorescence to values of the metal-free oligonucleotides.

and suggest that the DNA itself, not the 2-pyridine group, provides most of the energetic driving force for metal binding. Metal binding affinities were therefore predicted to be highly sensitive to the folded state of the **2PyG**-modified oligonucleotides.

Consistent with the competition between *N*7 metal binding and hydrogen bonding interactions in G-tetrads but not in *Watson & Crick* base pairs (Figure 7.1), Cu(II), Ni(II), and Cd(II) all exhibit lower affinities to G-quadruplex folded oligonucleotides ($K_d \approx 270$ nM – 2.6 mM) than the corresponding **2PyG**-modified duplex DNAs ($K_d \leq 25$ nM – 87 µM) (Table 7.2). The ratios of G-quadruplex *versus* duplex affinity depend on the identity of the metal ion and its affinity to the **2PyG** nucleoside monomer. Cd(II) is most sensitive to DNA folding with (K_d(quadruplex) / K_d(duplex)) ≈ 4 – 30, followed by Cu(II) (K_d(quadruplex) / K_d(duplex)) ≥ 3 – 11, and lastly Ni(II) (K_d(quadruplex) / K_d(duplex)) ≈ 1.4 – 17. The sensitivity of each metal ion to DNA folding (Cd(II) > Cu(II) > Ni(II)) is negatively correlated to the **2PyG** nucleoside binding affinities (Cd(II) < Cu(II) < Ni(II)) (Figure 7.4 and Table 7.2). Metal binding interactions that are driven by **2PyG** are therefore less sensitive to the folded state of the DNA. This effect is more pronounced for cKitG15(2PyG) than for cKitG10(2PyG).

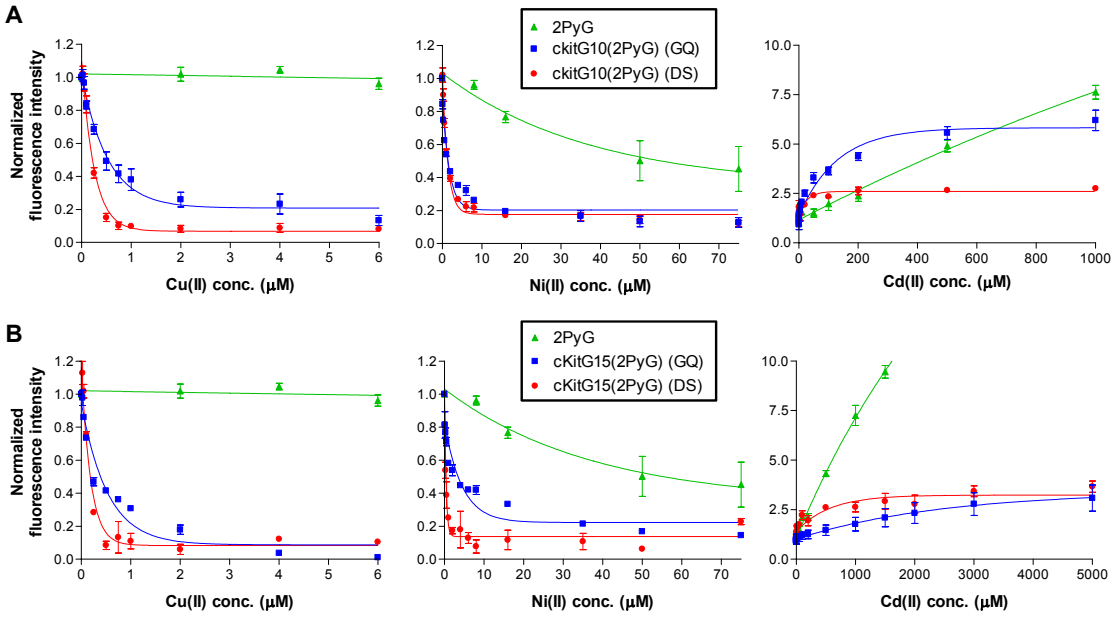

Figure 7.4: Normalized fluorescence intensities of cKitG10(2PyG) (A) and cKitG15(2PyG) (B) in the presence of $CuCl_2$, $NiCl_2$ or $CdCl_2$. All samples contained 0.2 µM of pre-folded DNA in an aqueous 10 mM cacodylate buffer (pH 7.4). G-quadruplex samples were prepared in 100 mM KCl. Duplex samples included 1.1 equivalents of the complementary strand and were prepared in 100 mM NaCl. Fluorescence intensities were normalized to metal-free samples. For Cu(II) and Ni(II) titrations λ_{ex} = 310 nm and λ_{em} = 415 nm. For Cd(II) titrations λ_{ex} = 320 nm and λ_{em} = 470 nm.

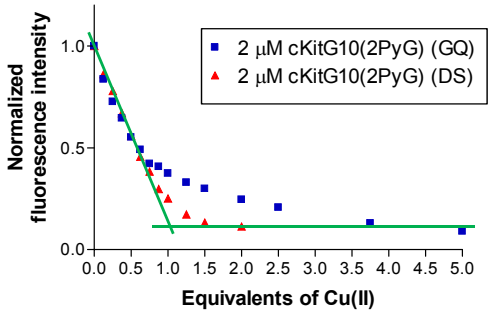

Figure 7.5: Normalized fluorescence intensities of 2 μM solutions of cKitG10(2PyG) upon titration with $CuCl_2$. All samples were prepared in an aqueous 10 mM cacodylate buffer (pH 7.4). G-quadruplex samples "GQ" also contained 100 mM KCl, while double-stranded DNA samples "DS" included 1.1 equivalents of the complementary strand and were prepared in 100 mM NaCl. DNA were folded overnight prior to the addition of Cu(II).

Table 7.2: K_d values for Cu(II), Ni(II) and Cd(II) binding the **2PyG** nucleoside, or **2PyG** in the context of duplex or G-quadruplex DNA (200 nM).

Metal	2PyG nucleoside	cKitG10 Duplex	cKitG10 Quadruplex	cKitG15 Duplex	cKitG15 Quadruplex	Unmodified Duplex DNA
Ni(II)	**75 μM** +/- 2 μM	**0.85 μM** +/- 0.04 μM	**1.2 μM** +/- 0.2 μM	**0.18 μM** +/- 0.04 μM	**3.0 μM** +/- 0.3 μM	**5 - 20 μM**[b]
Cu(II)	**260 μM** +/- 35 μM	**76 nM** +/- 6 nM	**270 nM** +/- 120 nM	**≤ 25 nM**[a]	**270 nM** +/- 110 nM	**6 μM**[c] **41 μM**[d] **91 μM**[e]
Cd(II)	**8.8 mM** +/- 0.7 mM	**18 μM** +/- 12 μM	**69 μM** +/- 15 μM	**87 μM** +/- 41 μM	**2.6 mM** +/- 1.4 mM	**7 μM**[e] **25 μM**[f]

Reported values are means +/- standard errors of three or more independent measurements. [a] Limit value given due to high affinity 1:1 stoichiometric binding. [b] Values taken from Kasprzak *et al*. in 5 mM ammonium acetate.[275] [c] Values taken from Gelagutashvili in 3 mM NaCl.[281] [d] Value taken from Sagripanti *et al.* in water.[279] [e] Value taken from Sayenko *et al.* in 250 mM NaCl.[276] [f] Value taken from Waalkes *et al.* in 2 mM Tris-HCl.[274]

Differences in metal ion affinities for G-quadruplex *versus* duplex DNA systematically depend on the DNA construct used. For Ni(II), Cu(II), and Cd(II), cKitG15(2PyG) gives (K_d(quadruplex) / K_d(duplex)) ≥ 11 – 30, while cKitG10(2PyG) gives small ratios ≈ 1.4 - 4. These results suggest that a greater binding energy is associated with the incorporation of G15 into the cKit quadruplex G-tetrad as compared to G10. Thermal denaturation experiments using the thymidine mutants cKitG15(T) and cKitG10(T) confirm a larger thermodynamic impact of mutating G15 → T15 (ΔT_m ≈ - 24 °C) than G10 → T10 (ΔT_m ≈ -8 °C) on the global stability of the cKit G-quadruplex (Table 7.3). The

incorporation of **2PyG** at these same sites, in contrast, leads to very little loss in thermal stability ($\Delta T_m \approx$ -2 °C to -4 °C). Together with the consistent differences in metal binding affinities of **2PyG**-modifed duplex *versus* quadruplex DNA, these results prove that **2PyG** is directly incorporated into the G-tetrads of cKit G-quadruplexes.

To explore the potential impact of site-specific metal binding on the global structure and stability of **2PyG**-modified DNA, temperature-dependent CD measurements were conducted in the presence of stoichiometric metal ions. Cu(II) was selected because it binds to **2PyG**-modified duplex and quadruplex structures over a concentration range where little non-specific binding of unmodified DNA or the **2PyG** nucleoside occurs (Figure 7.4, Table 7.2). 1 μM solutions of pre-folded DNA were therefore mixed with 1 μM $CuCl_2$ and incubated for 2 hours at room temperature before CD spectra were collected. According to fluorescence titrations under these same conditions, greater than 60 – 90% of the DNA in each sample is bound by Cu(II), but only small changes in the global structures of cKitG10(2PyG) were observed by CD (Figure 7.6). While the same characteristic CD spectra are present, small losses in amplitude are observed for the G-quadruplex-folded cKitG10(2PyG) upon addition of Cu(II) (Figure 7.6 A & B). In contrast, the unmodified "wt" construct and **2PyG**-modified duplexes remained essentially unchanged.

Table 7.3: Melting temperatures (T_m) of G-quadruplex and duplex-folded cKit constructs the presence or absence of 1 μM copper in an aqueous 10 mM cacodylate buffer (pH 7.4).

Oligonucleotide	+/- 1 μM Cu(II)	T_m G-Quadruplex	T_m Duplex
cKit(wt)	-	64	74
cKit(wt)	+	64	74
cKitG10(T)	-	56	65
cKitG15(T)	-	40	68
cKitG10(2PyG)	-	60	68
cKitG10(2PyG)	+	57	70
cKitG15(2PyG)	-	62	71
cKitG15(2PyG)	+	60	73

To evaluate the thermodynamic impact of site-specific metal binding on DNA stability, melting temperatures (T_m) were calculated from the changes in ellipticity as a function of

temperature. Consistent with competition between G-tetrad formation and *N*7-metal binding, the addition of stoichiometric Cu(II) caused thermal destabilization of **2PyG**-modified G-quadruplex-folded samples ($\Delta T_m \approx -3$ °C), while the corresponding duplexes were stabilized by Cu(II) ($\Delta T_m \approx +2$ °C) (Table 7.3). The increased thermal stability of duplex samples can be explained by the increased acidity of the (*N*1)H site of guanosine upon Cu(II) that results in enhanced G-C base-pairing stabilities.(322-324) Oligonucleotides lacking **2PyG**, cKit(wt), in contrast, showed no change in T_m upon addition of Cu(II) ($\Delta T_m = 0$ °C) for both G-quadruplex and duplex samples (Table 7.3). These results are consistent with the relative differences in Cu(II) binding affinities for **2PyG**-modified G-quadruplex, duplex, and unmodified DNAs (Table 7.2). Taken together, these results prove the involvement of site-specific *N*7 metal coordination in alternatively-folded **2PyG**-modified oligonucleotides.

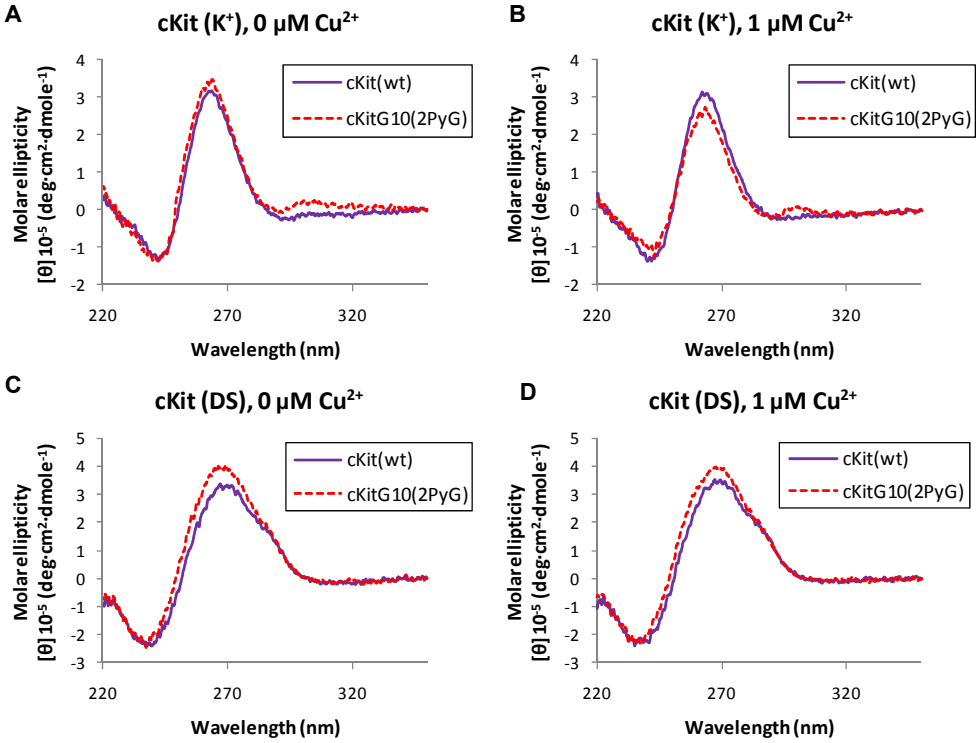

Figure 7.6: (A & B) CD spectra of G-quadruplex-folded "K^+" cKit(wt) and cKitG10(2PyG) in absence (A) or presence (B) of 1 µM $CuCl_2$. (C & B) CD spectra of duplex "DS" cKit(wt) and cKitG10(2PyG) in absence (C) or presence (D) of 1 µM $CuCl_2$. All samples contained 1 µM of DNA in an aqueous 10 mM cacodylate buffer (pH 7.4). G-quadruplex samples "K^+" were prepared in 100 mM KCl. Double-stranded samples "DS" included 1.1 equivalents of the complementary strand and were prepared in 100 mM NaCl. All samples were heated for 5 minutes at 95 ºC and then slowly cooled down to room temperature overnight. Samples containing $CuCl_2$ (1 µM), used pre-folded DNA that was incubated with Cu(II) for two hours at room temperature prior to scanning.

7.3 Conclusions

Metal centers play a critical role in mediating the catalytic activities of natural ribozymes[255-258] and synthetic DNA-based catalysts,[263,265] but complex mixtures of products are normally observed when transition metals are added to unmodified nucleic acids.[272-281,297-299] This can greatly complicate data analysis. The site-specific control of metal coordination will provide new opportunities for studying thermodynamics of metal-DNA interactions[274-281] as well as metal-dependent energy/charge transfer processes.[283-293] Previous studies to address this specific aim have reported large metal complexes conjugated to nucleic acids[284-293] or fully synthetic ligands in place of natural nucleobases.[309-315] To the best of our knowledge, **2PyG** provides the first means to site-specifically direct metal ions to *N*7 positions of purine residues in near-native nucleic acids. *N*7 is the most important *N*-heterocyclic metal binding site in duplex DNA[267-269] where it exhibits high solvent accessibility and high affinity for transition metals.[270-281] *N*7-metal binding can have a profound functional impact on the structure, electronics, and charge transfer properties of nucleic acids. By adding a single *ortho*-substituted pyridine to the position 8 of guanine, a bidentate, fluorescent metal ligand is created that can be used to direct metal ions to arbitrary sites in alternatively folded nucleic acids including G-quadruplex and duplex DNA. This enables thermodynamic analyses of site-specific *N*7 metal ion binding interactions that have hitherto been impossible to conduct.

As a proof of principle, we have used **2PyG** to evaluate the thermodynamic competition between *N*7 hydrogen bonding and metal ion binding at guanine residues involved in the G-tetrads of G-quadruplex structures *versus* the *Watson & Crick* base pairs of B-form duplexes. These studies have revealed highly specific binding interactions with Cu(II) and Ni(II) that result from additive effects from the DNA and 2-pyridyl group. Consistent with the involvement of *N7* metal binding, Cu(II), Ni(II), and Cd(II) all exhibit higher affinities for **2PyG**-containing duplexes as compared to corresponding quadruplex structures. Interestingly, the binding selectivity of each metal ion for duplex *versus* G-quadruplex DNA (Ni (II) < Cu(II) < Cd(II)) is inversely proportional to the **2PyG** nucleoside binding affinities (Ni (II) > Cu(II) > Cd(II)). Temperature-dependent CD measurements confirm site-selective metal binding in the presence of stoichiometric Cu(II) that results in a thermal stabilization of **2PyG** modified duplex DNAs, a thermal destabilization of the corresponding G-quadruplexes, and no impact on the corresponding unmodified DNAs. To the best of our knowledge, this is the first study to evaluate the competition between *N*7

hydrogen bonding and metal ion binding in G-tetrads using reversible metal binding interactions. All previous competition studies have been conducted under the kinetic control of *N*7-Pt(II) binding or *N*7-methylation.[297-299] In contrast to the labor-intensive analytical methods needed to assess sites of *N*7-platination and methylation, changes in **2PyG** fluorescence provide a highly convenient and direct readout of metal binding interactions at defined sites. The unusual fluorescence properties of **2PyG** also provide a photophysical handle for studies aimed at characterizing electron and energy transfer studies in nucleic acids.[77] **2PyG** and other 8-substituted purines therefore provide powerful new tools for characterizing the impact of *N*7 metallation on the structure and electronic properties of nucleic acids, and will provide new building blocks for the construction of metallo-DNA materials and catalysts.

CHAPTER 8

Experimental Procedures

8.1 General methods

Unless otherwise stated, starting materials were obtained in the highest commercial grades and used without further purification. All non-aqueous reactions were conducted under argon using anhydrous solvents. ^{1}H-NMR spectra were measured with a *Bruker AV-400* (400 MHz) or *Bruker AV-300* (300 MHz), residual solvent peaks were used as internal standards: DMSO (quint, δ_H = 2.49 ppm), $CHCl_3$ (s, δ_H = 7.28 ppm), MeOH (s, δ_H = 3.31 ppm). ^{13}C-NMR spectra were measured with a *Bruker AV-400* (100 MHz) or *Bruker AV-300* (75 MHz); δ rel. to DMSO (δ 40.5 ppm), $CHCl_3$ (δ 77.16 ppm), MeOH (δ 49.0 ppm). 2D-ROESY spectra were measured on a *Bruker AV-500* (500 MHz). ESI mass spectra were performed on a *Bruker ESQUIRE-LC* quadrupole ion trap instrument, equipped with a combined *Hewlett-Packard* Atmospheric Pressure Ion (API) source. High-resolution electrospray mass spectra were recorded on a Bruker maXis QTOF-MS instrument. MALDI-MS analyses were performed on time-of-flight mass spectrometer, model Autoflex with a 337 nm nitrogen laser. Absorbance and emission spectra of nucleosides and modified oligonucleotides were collected using a Molecular Devices Spectra Max M5 instrument. Emission spectra of natural DNA sequences were recorded on an Edinburgh FLS920 spectrophotometer, using 450W Xenon lamp. Circular dichroism measurements were performed on a JASCO J-715 spectrometer.

8.2 Synthetic methods

8.2.1 8-bromo-2'-deoxyguanosine (2)

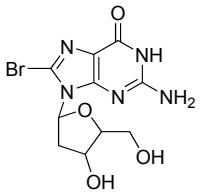
(**2**)

To a suspension of 2'-deoxyguanosine (**1**, 4 g, 14 mmoles) in acetonitrile (160 mL) and H_2O (40 mL), *N*-bromosuccinimide (NBS, 4 g, 22 mmoles) was added in 5 portions over 15 minutes. The reaction mixture was stirred at room temperature for 30 minutes. The solvents were then evaporated *in vacuo* with a rotary evaporator at room temperature. Remaining traces of water were removed by lyophilization. The residue was taken in acetone (80 mL), sonicated and stirred at room temperature for 2.5 hours. The mixture was then filtered and washed 10 times with acetone (20 mL). The resulting solid was collected and dried under high *vacuum* to yield 4.42 g (91%) of a slightly orange solid. **^{1}H-NMR** (300 MHz, d_6-DMSO) δ 10.79 (s, 1H), 6.48 (s, 2H), 6.17 (dd, J_1 = 6.9 Hz, J_2 = 6.9 Hz, 1H), 5.22 (br s, 1H), 5.03 (br s, 1H), 4.41 (t, J = 2.9 Hz, 1H), 3.82 (dd, J_1 = 8.0 Hz, J_2 = 5.3 Hz, 1H), 3.64 (dd, J_1 = 11.6 Hz, J_2 = 5.3 Hz, 1H), 3.51 (dd, J_1 = 11.6 Hz, J_2 = 5.3 Hz, 1H), 3.17 (dt, J_1 = 13.2 Hz, J_2 = 6.9 Hz, 1H), 2.15-2.10 (m, 1H). **^{13}C-NMR** (75 MHz, d_6-DMSO) δ 155.3, 153.2, 151.9, 120.4, 117.4, 87.8, 85.0, 70.9, 61.9, 36.4. **ESI MS** (*m*/*z*): $[M+Na]^+$ calcd for $C_{10}H_{12}BrN_5O_4$, 345.0; found 345.1.

8.2.2 8-phenyl-2'-deoxyguanosine (3)

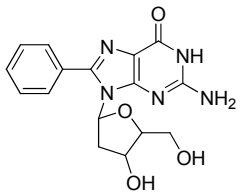
(**3**)

Palladium acetate (2.2 mg, 0.01 mmoles), tri(4,6-dimethyl-3-sulfonatophenyl)phosphine trisodium salt (TXPTS) (15.7 mg, 0.03 mmoles), sodium carbonate (80 mg, 0.75 mmoles), compound **2** (128.6 mg, 0.37 mmoles) and phenylboronic acid (54.7 mg, 0.45 mmoles) were placed in a round-bottomed flask purged with nitrogen. Degassed 2:1 water:acetonitrile mixture (3.5 mL) was added and the reaction was stirred at 80 ^{o}C for 20 hours. The reaction mixture was then allowed to cool down, diluted with water (ca. 20 mL) and the pH was adjusted to 6 - 7 by the addition of 10% aqueous HCl. The mixture was heated in order to dissolve precipitated solids and then cooled down to 0 ^{o}C on an ice bath for 1 hour. The precipitate formed was filtered, washed twice with water (ca. 5 mL) and lyophilized to yield 100 mg (77%) of an off-grey solid. **^{1}H-NMR** (400 MHz, d_6-DMSO) δ 10.74 (br s, 1H), 7.64 (d, J = 4.6 Hz, 2H), 7.53-7.51 (m, 3H), 6.38 (s, 2H), 6.07 (dd, J_1 = 7.4 Hz, J_2 = 6.9 Hz, 1H), 5.11 (d, J = 3.8 Hz, 1H), 4.96 (t, J = 5.3 Hz, 1H), 4.32 (d, J = 2.7 Hz, 1H), 3.81-3.75 (m, 1H), 3.65-3.62 (m, 1H), 3.55-3.51 (m,

1H), 3.15 (quint, J = 6.6 Hz, 1H), 2.03-1.99 (m, 1H). **^{13}C-NMR** (100 MHz, d_6-DMSO) δ 156.6, 152.9, 151.9, 147.0, 130.2, 129.3, 129.0, 128.5, 117.1, 87.8, 84.5, 71.1, 62.0, 36.4. **HR-ESI MS** (*m*/*z*): $[M+Na]^+$ calcd for $C_{16}H_{17}N_5O_4$, 366.1173; found 366.1175. **UV-Vis** (H_2O) λ_{max} (nm) and ε ($cm^{-1}M^{-1}$): 275 (2.2 x 10^4).

8.2.3 8-bromo-3',5'-*O*-bis(*tert*-butyldimethylsilyl)-2'-deoxyguanosine (4)

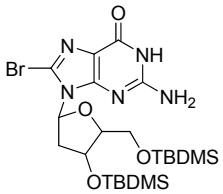
(**4**)

Compound **2** (6 g, 17.4 mmoles) and imidazole (7.2 g, 105.8 mmoles) were suspended in DMF (60 mL) and *tert*-butyl(chloro)dimethylsilane (7.2 g, 48.0 mmoles) was added. The reaction mixture was stirred at room temperature for 17 hours, after which the solvents were removed *in vacuo*. A saturated $NaHCO_3$ solution was added to the resulting solid and the mixture was extensively sonicated. The yellowish precipitate obtained was collected by filtration, washed twice with water and three times with ethanol. The residue was then dried *in vacuo* to yield 9.19 g (92%) of a slightly yellow solid. **^{1}H-NMR** (400 MHz, d_6-DMSO) δ 10.91 (br s, 1H), 6.44 (s, 2H), 6.14 (dd, J_1 = 7.0 Hz, J_2 = 7.0 Hz, 1H), 4.59 (t, J = 2.6 Hz, 1H), 3.76-3.74 (m, 2H), 3.64 (dd, J_1 = 13.1 Hz, J_2 = 5.9 Hz, 1H), 3.41-3.24 (m, 1H), 2.14 (ddd, J_1 = 12.9 Hz, J_2 = 6.7 Hz, J_3 = 3.4 Hz, 1H), 0.89 (s, 9H), 0.82 (s, 9H), 0.10 (s, 6H), -0.01 (s, 3H), -0.02 (s, 3H). **^{13}C-NMR** (100 MHz, d_6-DMSO) δ 156.8, 154.5, 153.1, 121.5, 118.4, 88.1, 85.7, 73.4, 63.8, 37.0, 26.7, 26.6, 18.9, 18.7, -3.7, -4.5. **ESI MS** (*m*/*z*): $[M+Na]^+$ calcd for $C_{22}H_{40}BrN_5O_4Si_2$, 596.2; found 596.2.

8.2.4 O^6-(benzyl)-8-bromo-3',5'-*O*-bis(*tert*-butyldimethylsilyl)-2'-deoxyguanosine (5)

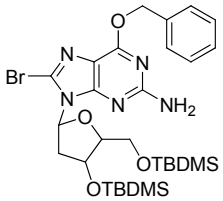
(**5**)

To a suspension of **4** (662 mg, 1.15 mmoles) and triphenylphosphine (454.1 mg, 1.72 mmoles) in dioxane (13.3 mL) were added benzyl alcohol (182.0 uL, 1.68 mmoles) and diisopropyl azodicarboxylate (DIAD) (271 uL, 1.34 mmoles). The reaction mixture was stirred for 7 hours at room temperature. The solvents and other volatiles were removed *in vacuo*. The product was purified by column chromatography on silica gel (Hex:AcOEt 95:5 to 90:10) to yield 400 mg (52%) of a yellowish oil. **^{1}H-NMR** (400 MHz, d_6-DMSO) δ 7.50-7.47 (m, 2H), 7.42-7.31 (m, 3H), 6.45 (br s, 2H), 6.18 (dd, J_1 = 6.8 Hz, J_2 = 6.9 Hz, 1H), 5.50 (d, J = 12.2 Hz, 1H), 5.46 (d, J = 12.2 Hz, 1H), 4.69-4.65 (m, 1H), 3.80-3.74 (m, 2H), 3.65-3.60 (m, 1H), 3.52 (quint, J = 6.7 Hz, 1H), 2.19 (ddd, J_1 = 13.2 Hz,

J_2 = 7.0 Hz, J_3 = 4.0 Hz, 1H), 0.90 (s, 9H), 0.80 (s, 9H), 0.13 (s, 6H), -0.04 (s, 3H), -0.06 (s, 3H). **ESI MS** (*m*/*z*): $[M+H]^+$ calcd for $C_{29}H_{46}BrN_5O_4Si_2$, 664.2; found 664.4.

8.2.5 O^6-(benzyl)-3',5'-*O*-bis(*tert*-butyldimethylsilyl)-8-(2-pyridyl)-2'-deoxyguanosine (6)

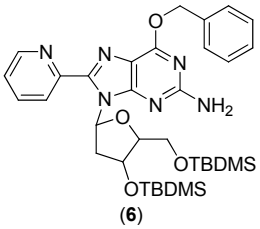

(**6**)

5 (270 mg, 0.41 mmoles) and 2-tributylstannyl pyridine (441.6 mg, 1.2 mmoles) were dissolved in dry toluene (20 mL) in a dry round-bottomed flask previously purged with nitrogen. The mixture was bubbled with argon for 30 minutes and then tetrakis(triphenylphosphine) palladium (57.2 mg, 0.05 mmoles) was added all at once. The resulting solution was heated at 110 °C under argon for 24 hours. The solvents and other volatiles were then evaporated *in vacuo* and the residue was purified by column chromatography (Hex:AcOEt 85:15) to yield 197 mg (73%) of a yellowish oil. **^{1}H-NMR** (400 MHz, d_6-DMSO) δ 8.69 (dd, J_1 = 4.0 Hz, J_2 = 0.8 Hz, 1H), 8.63 (dd, J_1 = 4.8 Hz, J_2 = 0.8 Hz, 1H), 8.39 (dd, J_1 = 8.0 Hz, J_2 = 0.8 Hz, 1H), 8.08 (dd, J_1 = 8.0 Hz, J_2 = 0.8 Hz, 1H), 7.95 (t, J = 7.7 Hz, 2H), 7.53-7.34 (m, 4H), 6.46 (br s, 2H), 5.53 (s, 2H), 4.63 (t, J = 2.8 Hz, 1H), 3.78 (dd, J_1 = 12.0 Hz, J_2 = 8.3 Hz,1H), 3.72-3.69 (m, 1H), 3.63 (dd, J_1 = 12.0 Hz, J_2 = 7.8 Hz, 1H), 3.53 (quint, J = 6.6 Hz, 1H), 2.15 (ddd, J_1 = 13.2 Hz, J_2 = 7.0 Hz, J_3 = 4.0 Hz, 1H), 0.90 (s, 9H), 0.82 (s, 9H), 0.12 (d, J = 3.3 Hz, 6H), 0.01 (s, 3H), -0.03 (s, 3H). **ESI MS** (*m*/*z*): $[M+Na]^+$ calcd for $C_{34}H_{50}N_6O_4Si_2$, 686.2; found 686.3.

8.2.6 O^6-(benzyl)-3',5'-*O*-bis(*tert*-butyldimethylsilyl)-8-(3-pyridyl)-2'-deoxyguanosine (7)

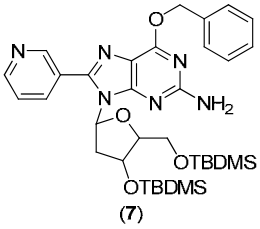

(**7**)

5 (200 mg, 0.30 mmoles) and 3-tributylstannyl pyridine (310.8 mg, 0.84 mmoles) were dissolved in dry toluene (14 mL) in a dry round-bottomed flask previously purged with nitrogen. The mixture was bubbled with argon for 1 hour and then tetrakis-(triphenylphosphine) palladium (40.2 mg, 0.04 mmoles) was added all at once. The resulting mixture was heated at 110 °C under argon for 24 hours. The solvents and other volatiles were then evaporated *in vacuo* and the residue was purified by column chromatography (Hex:AcOEt 65:35) to yield 175 mg (88%) of a yellowish oil. **^{1}H-NMR** (400 MHz, d_6-DMSO) δ 8.87 (s, 1H), 8.71 (s, 1H), 8.10 (d, J = 4.7 Hz, 1H), 7.57-7.34 (m, 6H), 6.43 (br s, 2H), 6.09 (dd, J_1 = 7.8 Hz, J_2 = 6.8 Hz, 1H), 5.52 (s, 2H), 4.61 (s, 1H), 3.77-3.63 (m, 3H), 3.47-3.45 (m, 1H), 2.17-2.11 (m, 1H), 0.85 (s, 9H), 0.81

(s, 9H), 0.08 (s, 6H), -0.01 (s, 3H), -0.03 (s, 3H). **ESI MS** (*m*/*z*): $[M+Na]^+$ calcd for $C_{34}H_{50}N_6O_4Si_2$, 686.2; found 686.5.

8.2.7 O^6-(benzyl)-3',5'-*O*-bis(*tert*-butyldimethylsilyl)-8-(4-pyridyl)-2'-deoxyguanosine (8)

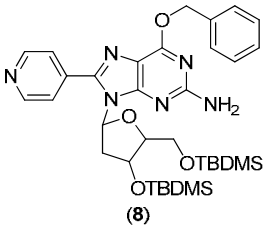

(8)

5 (200 mg, 0.30 mmoles) and 4-tributylstannyl pyridine (310.8 mg, 0.84 mmoles) were dissolved in dry toluene (14 mL) in a dry round-bottomed flask previously purged with nitrogen. The mixture was bubbled with argon for 1 hour and then tetrakis-(triphenylphosphine) palladium (40.2 mg, 0.04 mmoles) was added all at once. The resulting mixture was heated at 110 °C under argon for 24 hours. The solvents and other volatiles were then evaporated *in vacuo* and the residue was purified by column chromatography (Hex:AcOEt 80:20) to yield 159 mg (79%) of a yellowish oil. **^{1}H-NMR** (400 MHz, d_6-DMSO) δ 8.73 (s, 2H), 7.71 (s, 2H), 7.50-7.35 (m, 5H), 6.47 (br s, 2H), 6.16 (t, J = 9.2 Hz, 1H), 5.53 (s, 2H), 4.69-4.65 (m, 1H), 3.79-3.68 (m, 3H), 3.51-3.46 (m, 1H), 2.17-2.15 (m, 1H), 0.86 (d, J = 2.5 Hz, 9H), 0.81 (d, J = 2.5 Hz, 9H), 0.09 (d, J = 4.9 Hz, 6H), -0.01 (s, 3H), -0.02 (s, 3H). **ESI MS** (*m*/*z*): $[M+Na]^+$ calcd for $C_{34}H_{50}N_6O_4Si_2$, 686.2; found 685.5.

8.2.8 O^6-(benzyl)-8-(2-pyridyl)-2'-deoxyguanosine (9)

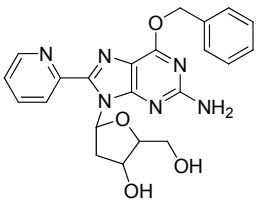

(9)

Compound **6** (200 mg, 0.30 mmoles) was dissolved in anhydrous tetrahydrofuran (7.5 mL) and tetrabutylammonium fluoride trihydrate (234.4 mg, 0.74 mmoles) was added. The reaction was stirred at room temperature for 1 hour. The solvents and other volatiles were then evaporated *in vacuo,* and the crude was purified by column chromatography (DCM:MeOH 95:5 to 90:10) to yield 66 mg (50%) of a yellowish oil. **^{1}H-NMR** (400 MHz, d_6-DMSO) δ 8.69 (dd, J_1 = 4.5 Hz, J_2 = 0.8 Hz, 1H), 8.09 (d, J = 7.8 Hz, 1H), 7.95 (dt, J_1 = 7.8 Hz, J_2 = 0.8 Hz, 1H), 7.54-7.48 (m, 3H), 7.43-7.34 (m, 3H), 7.26 (dd, J_1 = 6.8 Hz, J_2 = 7.9 Hz, 1H), 6.47 (br s, 2H), 5.53 (s, 2H), 5.29 (dd, J_1 = 7.6 Hz, J_2 = 4.2 Hz, 1H), 5.15 (d, J = 4.2 Hz, 1H), 4.49-4.45 (m, 1H), 3.83-3.79 (m, 1H), 3.72-3.67 (m, 1H), 3.56-3.49 (m, 1H), 3.23-3.16 (m, 1H), 2.16 (ddd, J_1 = 13.0 Hz, J_2 = 6.7 Hz, J_3 = 2.5 Hz, 1H). **ESI MS** (*m*/*z*): $[M+Na]^+$ calcd for $C_{22}H_{22}N_6O_4$, 457.2; found 457.0

8.2.9 O^6-(benzyl)-8-(3-pyridyl)-2'-deoxyguanosine (10)

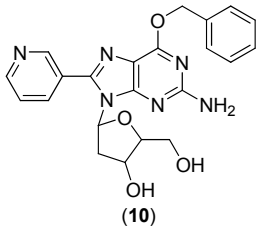
(**10**)

Compound **7** (200 mg, 0.30 mmoles) was dissolved in anhydrous tetrahydrofuran (7.5 mL) and tetrabutylammonium fluoride trihydrate (234.4 mg, 0.74 mmoles) was added. The reaction was stirred at room temperature for 1.5 hours. The solvents and other volatiles were then evaporated *in vacuo,* and the crude was purified by column chromatography (DCM:MeOH 93:7 to 90:10) to yield 96 mg (quant.) of a yellowish solid. **^{1}H-NMR** (400 MHz, d_6-DMSO) δ 8.87 (s, 1H), 8.73 (dd, J_1 = 5.2 Hz, J_2 = 1.7 Hz, 1H), 8.11 (dd, J_1 = 7.9 Hz, J_2 = 1.7 Hz, 1H), 7.58 (dd, J_1 = 7.9 Hz, J_2 = 5.2 Hz, 1H), 7.51 (d, J = 6.8 Hz, 2H), 7.42-7.35 (m, 3H), 6.53 (br s, 2H), 6.08 (dd, J_1 = 6.8 Hz, J_2 = 6.9 Hz, 1H), 5.52 (s, 2H), 5.17 (d, J = 4.4 Hz, 1H), 5.01 (t, J = 5.5 Hz, 1H), 4.40-4.36 (m, 1H), 3.84-3.80 (m, 1H), 3.67-3.62 (m, 1H), 3.55-3.49 (m, 1H), 3.18-3.16 (m, 1H), 2.09 (ddd, J_1 = 13.0 Hz, J_2 = 6.4 Hz, J_3 = 4.1 Hz, 1H). **ESI MS** (*m*/*z*): $[M+Na]^+$ calcd for $C_{22}H_{22}N_6O_4$, 457.2; found 457.1.

8.2.10 O^6-(benzyl)-8-(4-pyridyl)-2'-deoxyguanosine (11)

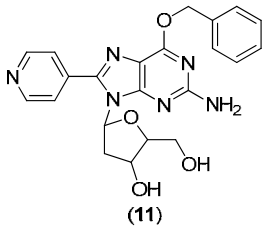
(**11**)

Compound **8** (200 mg, 0.30 mmoles) was dissolved in anhydrous tetrahydrofuran (7.5 mL) and tetrabutyl-ammonium fluoride trihydrate (234.4 mg, 0.74 mmoles) was added. The reaction was stirred at room temperature for 1 hour. The solvents and other volatiles were then evaporated *in vacuo,* and the crude was purified by column chromatography (DCM:MeOH 93:7 to 90:10) to yield 92 mg (quant.) of a yellowish solid. **^{1}H-NMR** (400 MHz, d_6-DMSO) δ 8.75 (d, J = 1.9 Hz, 2H), 7.72 (d, J = 1.9 Hz, 2H), 7.51 (d, J = 6.9 Hz, 2H), 7.40-7.34 (m, 3H), 6.59 (br s, 2H), 6.14 (dd, J_1 = 6.4 Hz, J_2 = 6.5 Hz, 1H), 5.52 (s, 2H), 5.18 (d, J = 2.6 Hz, 1H), 5.00 (t, J = 5.9 Hz, 1H), 4.40-4.38 (m, 1H), 3.84-3.80 (m, 1H), 3.69-3.62 (m, 1H), 3.55-3.49 (m, 1H), 3.17-3.14 (m, 1H), 2.07 (ddd, J_1 = 13.2 Hz, J_2 = 6.5 Hz, J_3 = 2.7 Hz, 1H). **ESI MS** (*m*/*z*): $[M+Na]^+$ calcd for $C_{22}H_{22}N_6O_4$, 457.2; found 457.1.

8.2.11 8-bromo-3',5'-*O*-bis(*tert*-butyldimethylsilyl)-O^6-(trimethylsilylethyl)-2'-deoxyguanosine (12)

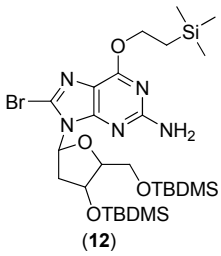

(**12**)

Compound **4** (1 g, 1.74 mmoles), triphenylphosphine (685 mg, 2.60 mmoles) and 2-(trimethylsilyl)-ethanol (308.3 mg, 371.87 uL, 2.80 mmoles) were mixed in anhydrous dioxane (20 mL). The mixture was stirred at room temperature for 10 minutes and then cooled down on ice. Diisopropyl azodicarboxylate (DIAD) (0.5 mL, 2.50 mmoles) was added slowly and the reaction was then stirred at room temperature for 17 hours. The solvents and other volatiles were removed *in vacuo*. The crude product was purified by silica gel column chromatography (Hex:AcOEt 93:7) to yield 588 mg (50%) of a colorless oil. **^{1}H-NMR** (400 MHz, $CDCl_3$) δ 6.29 (dd, J_1 = 6.8 Hz, J_2 = 6.8 Hz, 1H), 4.80 (dt, J_1 = 6.0 Hz, J_2 = 3.9 Hz, 1H), 4.72 (br s, 2H), 4.57-4.53 (m, 2H), 3.96-3.86 (m, 2H), 3.71 (dd, J_1 = 10.6 Hz, J_2 = 4.6 Hz, 1H), 3.60-3.56 (m, 1H), 2.17 (ddd, J_1 = 10.6 Hz, J_2 = 6.8 Hz, J_3 = 3.9 Hz, 1H), 1.25-1.20 (m, 2H), 0.96 (s, 9H), 0.87 (s, 9H), 0.16 (s, 6H), 0.10 (s, 9H), 0.04 (s, 3H), -0.01 (s, 3H). **^{13}C-NMR** (100 MHz, $CDCl_3$) δ 160.3, 158.6, 154.2, 125.6, 116.6, 87.4, 85.7, 72.4, 65.0, 62.7, 36.4, 18.3, 18.0, 17.5, -1.4, -4.6, -4.7, -5.4, -5.5. **ESI MS** (*m*/*z*): $[M+Na]^+$ calcd for $C_{27}H_{52}BrN_5O_4Si_3$, 696.3; found 696.4.

8.2.12 3',5'-*O*-bis(*tert*-butyldimethylsilyl)-8-(2-pyridyl)-O^6-(trimethylsilylethyl)-2'-deoxyguanosine (13)

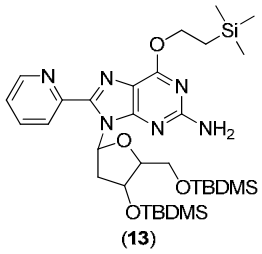

(**13**)

Compound **12** (119 mg, 0.17 mmoles) and 2-tributylstannyl pyridine (182.3 mg, 0.49 mmoles) were dissolved in dry toluene (8 mL) in a dry round-bottom flask previously purged with nitrogen. The mixture was bubbled with argon for 30 minutes and then tetrakis(triphenylphosphine) palladium (23.6 mg, 0.02 mmoles) was added all at once. The resulting mixture was heated at 110 ^oC under argon for 24 hours. The solvents and other volatiles were evaporated *in vacuo* and the residue was purified by silica gel column chromatography (Hex:AcOEt 90:10) to yield 42 mg (37%) of a yellowish oil. **^{1}H-NMR** (400 MHz, $CDCl_3$) δ 8.62 (ddd, J_1 = 4.8 Hz, J_2 = 1.8 Hz, J_3 = 0.9 Hz, 1H), 8.06 (dt, J_1 = 7.9 Hz, J_2 = 0.9 Hz, 1H), 7.96 (td, J_1 = 7.8 Hz, J_2 = 1.8 Hz, 1H), 7.46 (dd, J_1 = 7.0 Hz, J_2 = 7.0 Hz, 1H), 7.29 (ddd, J_1 = 7.6 Hz, J_2 = 4.8 Hz, J_3 = 1.1 Hz, 1H), 4.78-4.75 (m, 3H), 4.53 (dd, J_1 = 9.1 Hz, J_2 = 7.4 Hz, 2H), 3.98 (dd, J_1 = 10.1 Hz, J_2 = 7.6 Hz, 1H), 3.94-3.90 (m, 1H), 3.75 (dd, J_1 =

10.1 Hz, J_2 = 4.8 Hz, 1H), 3.52 (ddd, J_1 = 13.2 Hz, J_2 = 7.4 Hz, J_3 = 5.9 Hz, 1H), 2.26 (ddd, J_1 = 13.2 Hz, J_2 = 7.0 Hz, J_3 = 3.6 Hz, 1H), 1.26 (ddd, J_1 = 9.1 Hz, J_2 = 7.4 Hz, J_3 = 1.0 Hz, 2H), 0.93 (s, 9H), 0.89 (s, 9H), 0.14 (s, 3H), 0.13 (s, 3H), 0.09 (s, 9H), 0.04 (s, 3H), 0.03 (s, 3H). **^{13}C-NMR** (100 MHz, $CDCl_3$) δ 162.1, 159.2, 150.8, 149.0, 148.3, 137.2, 129.5, 128.7, 125.8, 125.6, 124.1, 116.9, 88.0, 86.2, 73.8, 65.3, 63.9, 37.4, 26.5, 26.3, 22.0, 18.9, 18.5, 18.2, -0.91, -4.1, -4.2, -4.7, -4.8. **HR-ESI MS** (*m*/*z*): $[M+H]^+$ calcd for $C_{32}H_{56}N_6O_4Si_3$, 673.3747; found 673.3746.

8.2.13 3',5'-*O*-bis(*tert*-butyldimethylsilyl)-8-(3-pyridyl)-O^6-(trimethylsilylethyl)-2'-deoxyguanosine (14)

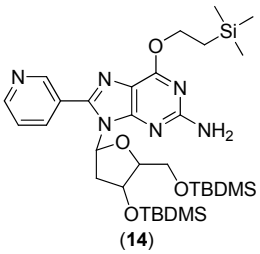

(**14**)

Compound **12** (200 mg, 0.29 mmoles) and 3-tributylstannyl pyridine (306.3 mg, 0.83 mmoles) were dissolved in dry toluene (13.5 mL) in a dry round-bottomed flask previously purged with nitrogen. The mixture was bubbled with argon for 1.5 hours and then tetrakis(triphenylphosphine) palladium (39.7 mg, 0.03 mmoles) was added all at once. The resulting mixture was heated at 110 ^{o}C under argon for 14 hours. The solvents and other volatiles were evaporated *in vacuo* and the residue was purified by column chromatography (Hex:AcOEt 75:25) to yield 152 mg (76%) of a yellowish oil. **^{1}H-NMR** (400 MHz, $CDCl_3$) δ 9.09 (dd, J_1 = 2.2 Hz, J_2 = 0.7 Hz, 1H), 8.72 (dd, J_1 = 4.8 Hz, J_2 = 1.7 Hz, 1H), 8.18 (ddd, J_1 = 7.9 Hz, J_2 = 2.2 Hz, J_3 = 1.7 Hz, 1H), 7.41 (ddd, J_1 = 7.9 Hz, J_2 = 4.8 Hz, J_3 = 0.7 Hz, 1H), 6.08 (dd, J_1 = 6.8 Hz, J_2 = 6.9 Hz, 1H), 4.84-4.81 (m, 1H), 4.77 (s, 2H), 4.64-4.55 (m, 2H), 3.95-3.89 (m, 2H), 3.75 (dd, J_1 = 13.2 Hz, J_2 = 7.6 Hz, 1H), 3.66 (quint, J = 6.6 Hz, 1H), 2.07 (ddd, J_1 = 13.2 Hz, J_2 = 7.0 Hz, J_3 = 4.1 Hz, 1H), 1.26 (t, J = 8.4 Hz, 2H), 0.90 (s, 9H), 0.88 (s, 9H), 0.13 (s, 3H), 0.11 (s, 3H), 0.09 (s, 9H), 0.05 (s, 3H), 0.01 (s, 3H). **^{13}C-NMR** (100 MHz, $CDCl_3$) δ 162.1, 159.2, 155.3, 151.0, 150.9, 148.4, 137.4, 127.1, 123.4, 117.0, 87.9, 85.18, 73.15, 65.4, 63.5, 37.1, 26.4, 26.3, 18.8, 18.4, 18.3, -1.0, -4.1, -4.2, -4.8, -4.9. **HR-ESI MS** (*m*/*z*): $[M+Na]^+$ calcd for $C_{32}H_{56}N_6O_4Si_3$, 695.3563; found 695.3556.

8.2.14 3',5'-*O*-bis(*tert*-butyldimethylsilyl)-8-(4-pyridyl)-O^6-(trimethylsilylethyl)-2'-deoxyguanosine (15)

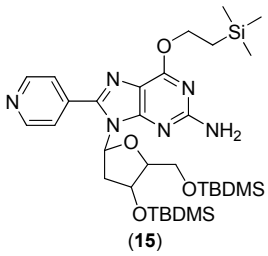

(**15**)

Compound **12** (200 mg, 0.29 mmoles) and 4-tributylstannyl pyridine (306.3 mg, 0.83 mmoles) were dissolved in dry toluene (13.5 mL) in a dry round-bottomed flask previously purged with nitrogen. The mixture was bubbled with argon for 1.5 hours and then tetrakis(triphenylphosphine) palladium (39.7 mg, 0.03 mmoles) was added all at once. The resulting mixture was heated at 110 ^{o}C under argon for 14 hours. The solvents and other volatiles were evaporated *in vacuo* and the residue was purified by column chromatography (Hex:AcOEt 75:25) to yield 150 mg (75%) of a yellowish oil. **^{1}H-NMR** (400 MHz, $CDCl_3$) δ 8.75 (dd, J_1 = 4.5 Hz, J_2 = 1.6 Hz, 2H), 7.81 (dd, J_1 = 4.5 Hz, J_2 = 1.6 Hz, 2H), 6.15 (dd, J_1 = 6.8 Hz, J_2 = 6.9 Hz, 1H), 4.85-4.83 (m, 1H), 4.80 (s, 2H), 4.64-4.59 (m, 2H), 3.98-3.92 (m, 2H), 3.77 (dd, J_1 = 13.3 Hz, J_2 = 7.9 Hz, 1H), 3.67 (quint, J = 6.6 Hz, 1H), 2.06 (ddd, J_1 = 13.3 Hz, J_2 = 7.0 Hz, J_3 = 4.0 Hz, 1H), 1.28-1.24 (m, 2H), 0.90 (s, 9H), 0.89 (s, 9H), 0.14 (s, 3H), 0.12 (s, 3H), 0.10 (s, 9H), 0.06 (s, 3H), 0.02 (s, 3H). **^{13}C-NMR** (100 MHz, $CDCl_3$) δ 161.7, 158.9, 154.8, 150.1, 148.0, 137.7, 123.6, 87.4, 84.7, 72.6, 65.0, 62.9, 36.3, 25.9, 25.8, 18.4, 18.0, 17.7, -1.42, -4.6, -4.7, -5.3, -5.4. **HR-ESI MS** (*m*/*z*): $[M+Na]^+$ calcd for $C_{32}H_{56}N_6O_4Si_3$, 695.3563; found 695.3563.

8.2.15 3',5'-*O*-bis(*tert*-butyldimethylsilyl)-8-(2-thiophene)-O^6-(trimethylsilylethyl)-2'-deoxyguanosine (16)

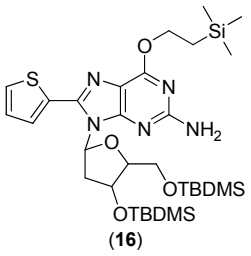

(**16**)

Compound **12** (200 mg, 0.30 mmoles) and 2-tributylstannyl thiophene (310 mg, 0.83 mmoles) were dissolved in dry toluene (13.5 mL) in a dry round-bottomed flask previously purged with nitrogen. The mixture was bubbled with argon for 30 minutes and then tetrakis(triphenylphosphine) palladium (39 mg, 0.03 mmoles) was added all at once. The resulting mixture was heated at 110 ^{o}C under argon for 17 hours. The solvents and other volatiles were evaporated *in vacuo* and the residue was purified by column chromatography (Hex:AcOEt 90:10) to yield 178 mg (89%) of a yellowish oil. **^{1}H-NMR** (400 MHz, $CDCl_3$) δ 7.66 (d, J = 3.9 Hz, 1H), 7.48 (d, J = 4.7 Hz, 1H), 7.15 (dd, J_1 = 4.7 Hz, J_2 = 3.9 Hz, 1H), 6.34 (dd, J_1 = 6.7 Hz, J_2 = 6.6 Hz, 1H), 4.90-4.86 (m, 1H), 4.73 (s, 2H), 4.63-4.58 (m, 2H), 3.98-3.90 (m, 2H), 3.77-3.69 (m, 2H), 2.12 (ddd, J_1 = 12.4 Hz, J_2 = 7.1 Hz, J_3 = 4.4 Hz, 1H), 1.29-1.24 (m, 2H), 0.93 (s, 9H),

0.87 (s, 9H), 0.16 (s, 3H), 0.15 (s, 3H), 0.11 (s, 9H), 0.03 (s, 3H), -0.01 (s, 3H). **^{13}C-NMR** (100 MHz, $CDCl_3$) δ 161.7, 159.0, 155.2, 145.7, 132.4, 129.6, 128.9, 128.1, 116.7, 87.8, 85.2, 73.1, 65.4, 63.4, 36.9, 28.7, 27.3, 26.4, 26.3, 26.2, 18.9, 18.5, 18.2, 17.8, 14.1, -0.9, -4.1, -4.2, -4.8, -4.9. **HR-ESI MS** (*m*/*z*): $[M+Na]^+$ calcd for $C_{31}H_{55}N_5O_4SSi_3$, 700.3175; found 700.3170.

8.2.16 3',5'-*O*-bis(*tert*-butyldimethylsilyl)-8-(2-furan)-*O*^{6}-(trimethylsilylethyl)-2'-deoxyguanosine (17)

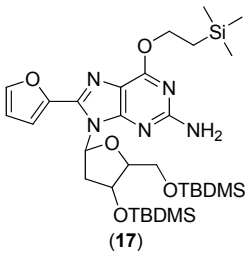

(**17**)

Compound **12** (200 mg, 0.30 mmoles) and 2-tributylstannyl furan (306 mg, 0.83 mmoles) were dissolved in dry toluene (13.5 mL) in a dry round-bottomed flask previously purged with nitrogen. The mixture was bubbled with argon for 30 minutes and then tetrakis(triphenylphosphine) palladium (39.7 mg, 0.03 mmoles) was added all at once. The resulting mixture was heated at 110 ^{o}C under argon for 17 hours. The solvents and other volatiles were evaporated *in vacuo* and the residue was purified by column chromatography (Hex:AcOEt 90:10) to yield 168 mg (85%) of a yellowish oil. **^{1}H-NMR** (400 MHz, $CDCl_3$) δ 7.58 (d, J = 0.8 Hz, 1H), 7.13 (d, J = 4.4 Hz, 1H), 6.59-6.54 (m, 2H), 4.84-4.80 (m, 1H), 4.73 (s, 2H), 4.61-4.56 (m, 2H), 3.98-3.89 (m, 2H), 3.73 (dd, J_1 = 12.9 Hz, J_2 = 4.5 Hz, 1H), 3.64 (quint, J = 6.8 Hz, 1H), 2.16 (ddd, J_1 = 12.9 Hz, J_2 = 6.8 Hz, J_3 = 4.0 Hz, 1H), 1.28-1.23 (m, 2H), 0.94 (s, 9H), 0.87 (s, 9H), 0.15 (s, 3H), 0.14 (s, 3H), 0.10 (s, 9H), 0.03 (s, 3H), -0.01 (s, 3H). **^{13}C-NMR** (100 MHz, $CDCl_3$) δ 161.9, 159.1, 154.8, 145.2, 144.4, 142.1, 117.0, 113.5, 112.2, 87.9, 85.4, 73.3, 65.3, 63.5, 37.2, 28.7, 27.3, 26.4, 26.3, 18.9, 18.5, 18.2, 17.8, 14.1, -0.9, -4.1, -4.2, -4.8, -4.9. **HR-ESI MS** (*m*/*z*): $[M+Na]^+$ calcd for $C_{31}H_{55}N_5O_5Si_3$, 684.3403; found 684.3396.

8.2.17 (*E*)-3',5'-*O*-bis(*tert*-butyldimethylsilyl)-8-(2-phenylethenyl)-*O*^{6}-(trimethylsilylethyl)-2'-deoxyguanosine (18)

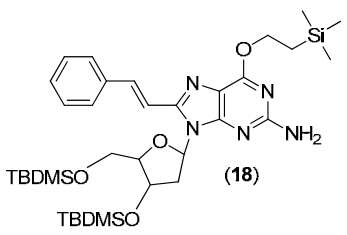

(**18**)

Compound **12** (800 mg, 1.19 mmoles) and (*E*)-2-styreneboronic acid pinacol ester (411 mg, 1.79 mmoles) were dissolved in DME (18.4 mL) and toluene (7.2 mL) in a round-bottom flask purged with nitrogen. The mixture was stirred and bubbled with argon for 30 minutes. Tetrakis(triphenylphosphine) palladium (164.1 mg,

0.14 mmoles) was then added, followed by a solution of sodium carbonate 3 M in water (1.2 mL) previously bubbled with argon. The reaction was stirred in the dark at 80 °C under argon for 20 hours. The solvents were removed *in vacuo*. The crude was taken in dichloromethane and washed successively with a saturated solution of Na_2CO_3 and brine. The layers were separated and the organic layer was dried over Na_2SO_4. The solvents were removed *in vacuo* and the compound was purified by silica gel column chromatography (Hex:AcOEt 90:10) to yield 569 mg (68%) of a yellow solid. **^{1}H-NMR** (400 MHz, $CDCl_3$) δ 7.90 (d, J = 15.9 Hz, 1H), 7.59-7.56 (m, 2H), 7.40-7.31 (m, 3H), 7.14 (d, J = 15.9 Hz, 1H), 6.38 (dd, J_1 = 6.8 Hz, J_2 = 6.8 Hz, 1H), 4.77 (dt, J_1 = 6.1 Hz, J_2 = 3.9 Hz, 1H), 4.73 (br s, 2H), 4.64-4.59 (m, 2H), 3.97 (ddd, J_1 = 8.6 Hz, J_2 = 6.2 Hz, J_3 = 4.8 Hz, 1H), 3.87 (dd, J_1 = 10.8 Hz, J_2 = 6.3 Hz, 1H), 3.77 (dd, J_1 = 10.8 Hz, J_2 = 4.8 Hz, 1H), 3.45 (ddd, J_1 = 13.2 Hz, J_2 = 6.7 Hz, J_3 = 6.6 Hz, 1H), 2.21 (ddd, J_1 = 13.2 Hz, J_2 = 6.7 Hz, J_3 = 4.0 Hz, 1H), 1.29-1.26 (m, 2H), 0.96 (s, 9H), 0.87 (s, 9H), 0.17 (s, 3H), 0.16 (s, 3H), 0.12 (s, 9H), 0.04 (s, 3H), 0.02 (s, 3H). **^{13}C-NMR** (100 MHz, $CDCl_3$) δ 161.4, 159.0, 155.0, 148.7, 137.0, 136.8, 129.3, 127.8, 114.7, 87.6, 84.0, 72.9, 65.3, 63.5, 38.2, 30.2, 26.4, 26.3, 18.9, 18.6, 18.3, 0.5, -0.9, -4.1, -4.2, -4.8, -4.9. **ESI MS** (*m*/*z*): $[M+Na]^+$ calcd for $C_{35}H_{59}N_5O_4Si_3$, 720.4; found 720.5.

8.2.18 3',5'-*O*-bis(*tert*-butyldimethylsilyl)-8-ethenyl-*O*^{6}-(trimethylsilylethyl)-2'-deoxyguanosine (19)

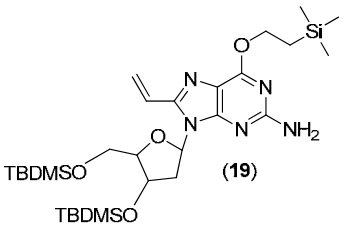

(19)

Compound **12** (1.2 g, 1.78 mmoles) and tributyl-(vinyl)tin (1.87 g, 1.72 mL, 5.89 mmoles) were dissolved in dry toluene (100 mL) in a dry round-bottom flask previously purged with nitrogen. The mixture was degassed by three freeze-pump-thaw cycles. After the last cycle, tetrakis-(triphenyl-phosphine) palladium (207.8 mg, 0.18 mmoles) was added as the mixture was still frozen, and the flask was purged with nitrogen. The resulting solution was stirred at 100 °C under argon for 1 hour. The solvent was removed *in vacuo* and the residue was purified by silica gel column chromatography (Hex:AcOEt 90:10) to yield 1000 mg (90%) of a yellowish solid. **^{1}H-NMR** (400 MHz, $CDCl_3$) δ 6.93 (dd, J_1 = 17.2 Hz, J_2 = 11.1 Hz, 1H), 6.49 (dd, J_1 = 17.2 Hz, J_2 = 1.6 Hz, 1H), 6.34 (dd, J_1 = 7.1 Hz, J_2 = 7.1 Hz, 1H), 5.56 (dd, J_1 = 11.1 Hz, J_2 = 1.6 Hz, 1H), 4.73-4.70 (m, 3H), 4.62-4.57 (m, 2H), 3.91-3.89 (m, 2H), 3.78-3.72 (m, 1H), 3.20 (ddd, J_1 = 13.2 Hz, J_2 = 6.8 Hz, J_3 = 6.4 Hz, 1H), 2.17 (ddd, J_1 = 13.2 Hz, J_2 = 6.6 Hz, J_3 = 3.5 Hz, 1H), 2.29-2.24 (m, 2H), 0.94 (s, 9H), 0.90 (s, 9H), 0.14 (s, 6H), 0.10 (s, 9H), 0.06 (s, 3H), 0.03 (s, 3H). **^{13}C-NMR** (100 MHz, $CDCl_3$) δ 161.1,

158.7, 154.4, 147.7, 124.3, 122.2, 115.6, 87.1, 83.1, 71.8, 64.8, 62.5, 38.6, 25.9, 25.8, 18.4, 18.0, 17.7, -1.4, -4.6, -4.7, -5.4, -5.5. **ESI MS** (*m*/*z*): $[M+H]^+$ calcd for $C_{29}H_{55}N_5O_4Si_3$, 622.4; found 622.4.

8.2.19 8-(2-pyridyl)-2'-deoxyguanosine (20)

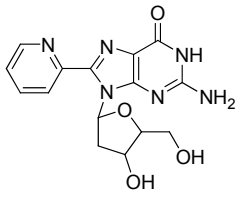
(**20**)

Compound **13** (43 mg, 0.06 mmoles) was dissolved in anhydrous tetrahydrofuran (4.3 mL) and tetrabutylammonium fluoride trihydrate (91.6 mg, 0.29 mmoles) was added. The reaction was stirred at room temperature for 14 hours. The solvents and other volatiles were evaporated *in vacuo* and the crude product was purified by silica gel column chromatography (DCM:MeOH 85:15). The solid residue was washed in a glass tube by addition of a solvent, sonication, centrifugation and removal of the supernatant with a glass pipette. This operation was performed four times using hexane (ca. 1 mL) and twice with methanol (ca. 400 uL). The residue was then dried to yield 6 mg (27%) of a white solid. **^{1}H-NMR** (400 MHz, d_6-DMSO) δ 10.80 (s, 1H), 8.66 (dd, J_1 = 2.5 Hz, J_2 = 0.9 Hz, 1H), 8.05 (dd, J_1 = 8.0 Hz, J_2 = 0.9 Hz, 1H), 7.95 (dt, J_1 = 7.8 Hz, J_2 = 1.6 Hz, 1H), 7.46 (ddd, J_1 = 7.8 Hz, J_2 = 4.9 Hz, J_3 = 0.9 Hz, 1H), 7.26 (dd, J_1 = 6.9 Hz, J_2 = 6.9 Hz, 1H), 6.38 (s, 2H), 5.11 (d, J = 4.2 Hz, 1H), 5.04 (t, J = 4.9 Hz, 1H), 4.44 (d, J = 2.7 Hz, 1H), 3.77 (d, J = 3.4 Hz, 1H), 3.69-3.64 (m, 1H), 3.54-3.48 (m, 1H), 3.15-3.08 (m, 1H), 2.16-2.11 (m, 1H). **^{13}C-NMR** (100 MHz, d_6-DMSO) δ 156.6, 153.1, 152.4, 149.8, 148.5, 144.2, 137.3, 124.0, 123.7, 117.5, 87.9, 85.2, 71.4, 62.4, 37.7. **HR-ESI MS** (*m*/*z*): $[M+Na]^+$ calcd for $C_{15}H_{16}N_6O_4$, 367.1125; found 367.1124. **UV-Vis** (H_2O) λ_{max} (nm) and ε ($cm^{-1}M^{-1}$): 280 (2.0×10^4), and 300 (1.9×10^4).

8.2.20 8-(3-pyridyl)-2'-deoxyguanosine (21)

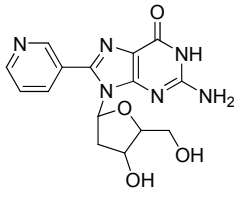
(**21**)

Compound **14** (198 mg, 0.29 mmoles) was dissolved in anhydrous tetrahydrofuran (21.5 mL) and tetrabutylammonium fluoride trihydrate (457.9 mg, 1.45 mmoles) was added. The reaction was stirred at room temperature for 14 hours. The solvents and other volatiles were then evaporated *in vacuo* and the crude was purified by column chromatography (DCM:MeOH 85:15). The solid residue was then washed in a glass tube by addition of a solvent, sonication, centrifugation and removal of the supernatant with a glass pipette. This operation was performed four times with water (ca. 500 uL) and four times with methanol (ca. 500 uL). The residue was then dried to yield

16 mg (14%) of a yellowish solid. **^{1}H-NMR** (400 MHz, d_6-DMSO) δ 10.79 (br s, 1H), 8.85 (dd, J_1 = 2.2 Hz, J_2 = 0.8 Hz, 1H), 8.72 (dd, J_1 = 4.8 Hz, J_2 = 1.7 Hz, 1H), 8.09 (ddd, J_1 = 8.1 Hz, J_2 = 2.2 Hz, J_3 = 1.7 Hz, 1H), 7.59 (ddd, J_1 = 8.1 Hz, J_2 = 4.8 Hz, J_3 = 0.8 Hz, 1H), 6.47 (s, 2H), 6.06 (dd, J_1 = 7.9 Hz, J_2 = 6.6 Hz, 1H), 5.17 (d, J = 4.4 Hz, 1H), 4.93 (t, J = 6.1 Hz, 1H), 4.33-4.31 (m, 1H), 3.83-3.79 (m, 1H), 3.65-3.60 (m, 1H), 3.56-3.52 (m, 1H), 3.16 (ddd, J_1 = 13.8 Hz, J_2 = 7.8 Hz, J_3 = 6.4 Hz, 1H), 2.07 (ddd, J_1 = 13.8 Hz, J_2 = 6.6 Hz, J_3 = 2.9 Hz, 1H). **^{13}C-NMR** (100 MHz, d_6-DMSO) δ 156.5, 153.1, 152.1, 150.0, 149.3, 144.3, 136.5, 123.5, 117.4, 87.8, 84.4, 71.0, 61.9, 36.5. **HR-ESI MS** (*m*/*z*): $[M+Na]^+$ calcd for $C_{15}H_{16}N_6O_4$, 367.1125; found 367.1124. **UV-Vis** (H_2O) λ_{max} (nm) and ε ($cm^{-1}M^{-1}$): 280 (1.8×10^4).

8.2.21 8-(4-pyridyl)-2'-deoxyguanosine (22)

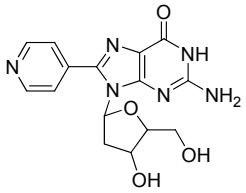
(**22**)

Compound **15** (145 mg, 0.21 mmoles) was dissolved in anhydrous tetrahydrofuran (14.2 mL) and tetrabutylammonium fluoride trihydrate (301.8 mg, 0.95 mmoles) was added. The reaction was stirred at room temperature for 14 hours. The solvents and other volatiles were then evaporated *in vacuo* and the crude was purified by column chromatography (DCM:MeOH 85:15). The solid residue was then washed in a glass tube by addition of a solvent, sonication, centrifugation and removal of the supernatant with a glass pipette. This operation was performed four times with hexane (ca. 500 uL) and four times with water (ca. 500 uL). The residue was then lyophilized to yield 33 mg (44%) of a yellowish solid. **^{1}H-NMR** (400 MHz, d_6-DMSO) δ 10.83 (br s, 1H), 8.73 (d, J = 6.1 Hz, 2H), 7.68 (d, J = 6.1 Hz, 2H), 6.51 (s, 2H), 6.11 (dd, J_1 = 7.6 Hz, J_2 = 7.1 Hz, 1H), 5.15 (d, J = 4.5 Hz, 1H), 4.92 (t, J = 5.8 Hz, 1H), 4.36 (dd, J_1 = 7.0 Hz, J_2 = 3.8 Hz, 1H), 3.82-3.79 (m, 1H), 3.67-3.63 (m, 1H), 3.57-3.51 (m, 1H), 3.16 (quint, J = 6.3 Hz, 1H), 2.07 (ddd, J_1 = 13.2 Hz, J_2 = 6.8 Hz, J_3 = 3.0 Hz, 1H). **^{13}C-NMR** (100 MHz, d_6-DMSO) δ 156.6, 153.4, 152.4, 149.9, 144.5, 137.5, 123.0, 117.5, 87.8, 84.3, 70.9, 61.8, 36.5. **HR-ESI MS** (*m*/*z*): $[M+Na]^+$ calcd for $C_{15}H_{16}N_6O_4$, 367.1125; found 367.1127. **UV-Vis** (H_2O) λ_{max} (nm) and ε ($cm^{-1}M^{-1}$): 280 (1.7×10^4), and 306 (1.6×10^4).

8.2.22 8-(2-thiophene)-2'-deoxyguanosine (23)

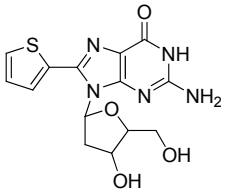
(**23**)

Compound **16** (162 mg, 0.24 mmoles) was dissolved in anhydrous tetrahydrofuran (15.7 mL) and tetrabutylammonium fluoride trihydrate (335 mg, 1.06 mmoles) was added. The reaction was stirred at room temperature for 17 hours. The solvents and other volatiles were then evaporated *in vacuo* and the crude was purified by column chromatography (DCM:MeOH 85:15). The solid residue was then washed in a glass tube by addition of a solvent, sonication, centrifugation and removal of the supernatant with a glass pipette. This operation was performed twice with DCM (ca. 400 uL), twice with acetic acid in water, pH 4 (ca. 500 uL) and twice with water (ca. 500 uL). The whole washing process was repeated a second time. The residue was then dried to yield 64 mg (77%) of a white solid. **^{1}H-NMR** (400 MHz, d_6-DMSO) δ 10.66 (s, 1H), 7.64 (dd, J_1 = 5.1 Hz, J_2 = 1.0 Hz, 1H), 7.38 (dd, J_1 = 3.5 Hz, J_2 = 1.0 Hz, 1H), 7.11 (dd, J_1 = 5.1 Hz, J_2 = 3.5 Hz, 1H), 6.34 (s, 2H), 6.16 (dd, J_1 = 7.6 Hz, J_2 = 7.0 Hz, 1H), 5.04 (d, J = 4.5 Hz, 1H), 4.83 (t, J = 5.9 Hz, 1H), 4.28 (dt, J_1 = 9.8 Hz, J_2 = 3.3 Hz, 1H), 3.73-3.70 (m, 1H), 3.57-3.51 (m, 1H), 3.45-3.39 (m, 1H), 3.25-3.17 (m, 1H), 2.02-1.97 (m, 1H). **^{13}C-NMR** (100 MHz, d_6-DMSO) δ 156.3, 152.9, 152.0, 141.2, 131.8, 128.5, 128.0, 127.8, 117.1, 87.8, 84.4, 71.0, 61.9, 36.2. **HR-ESI MS** (*m*/*z*): $[M+Na]^+$ calcd for $C_{14}H_{15}N_5O_4S$, 372.0737; found 372.0737. **UV-Vis** (H_2O) λ_{max} (nm) and ε ($cm^{-1}M^{-1}$): 284 (2.0 x 10^4).

8.2.23 8-(2-furan)-2'-deoxyguanosine (24)

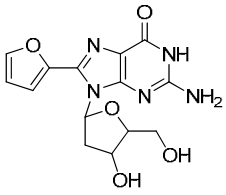
(**24**)

Compound **17** (157 mg, 0.24 mmoles) was dissolved in anhydrous tetrahydrofuran (15.6 mL) and tetrabutylammonium fluoride trihydrate (332 mg, 1.05 mmoles) was added. The reaction was stirred at room temperature for 17 hours. The solvents and other volatiles were then evaporated *in vacuo* and the crude was purified by column chromatography (DCM:MeOH 91:9 to 88:12). The solid residue was then washed in a glass tube by addition of a solvent, sonication, centrifugation and removal of the supernatant with a glass pipette. This operation was performed twice with hexane (ca. 400 uL), twice with acetic acid in water, pH 4 (ca. 400 uL) and twice with water (ca. 400 uL). The residue was then dried to yield 45 mg (57%) of a yellowish solid. **^{1}H-NMR** (400 MHz, d_6-DMSO) δ 10.80 (s, 1H), 7.90 (d, J = 1.8 Hz, 1H), 6.95 (d, J = 3.4 Hz, 1H), 6.68 (dd, J_1 = 3.4 Hz, J_2 = 1.8 Hz, 1H), 6.45 (s, 2H), 6.35 (dd, J_1 = 7.4 Hz, J_2 = 7.2 Hz, 1H), 5.08 (br s, 1H), 4.84 (br s, 1H), 4.32-4.25 (m, 1H), 3.70-3.69 (m, 1H), 3.51 (dd, J_1 = 11.5 Hz, J_2 = 5.3

Hz, 1H), 3.39 (dd, J_1 = 11.5 Hz, J_2 = 5.3 Hz, 1H), 3.07 (ddd, J_1 = 14.4 Hz, J_2 = 7.9 Hz, J_3 = 6.6 Hz, 1H), 2.01-1.97 (m, 1H). **^{13}C-NMR** (100 MHz, d_6-DMSO) δ 156.4, 153.1, 151.6, 144.3, 144.0, 137.8, 117.3, 112.0, 111.7, 87.8, 84.4, 71.1, 62.1, 36.9. **HR-ESI MS** (*m*/*z*): $[M+Na]^+$ calcd for $C_{14}H_{15}N_5O_5$, 356.0965; found 356.0966. **UV-Vis** (H_2O) λ_{max} (nm) and ε ($cm^{-1}M^{-1}$): 294 (2.4 x 10^4).

8.2.24 (*E*)-8-(2-phenylethenyl)-2'-deoxyguanosine (25)

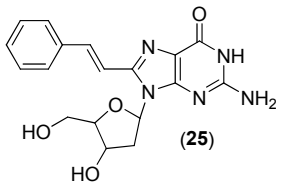

(**25**)

Compound **18** (81 mg, 0.12 mmoles) was dissolved in anhydrous tetrahydrofuran (7.8 mL) and tetrabutylammonium fluoride trihydrate (166.1 mg, 0.53 mmoles) was added. The reaction was stirred at room temperature in the dark for 14 hours. The solvents and other volatiles were evaporated *in vacuo*. The residue was precipitated in THF, centrifuged and the supernatant was removed. The crude was then washed in a glass tube by addition of a solvent, sonication, centrifugation and removal of the supernatant with a glass pipette. This operation was performed three times with hexane (ca. 300 uL), three times with a solution of 0.5% acetic acid in water (ca. 400 uL) and twice with pure water (ca. 300 uL). The residue was then dried to yield 12 mg (28%) of a white solid. **^{1}H-NMR** (400 MHz, d_6-DMSO) δ 10.65 (br s, 1H), 7.69 (d, *J* = 6.0 Hz, 2H), 7.54 (d, *J* = 12.7 Hz, 1H), 7.49 (d, *J* = 12.7 Hz, 1H), 7.40-7.36 (m, 2H), 7.32-7.29 (m, 1H), 6.48 (br s, 2H), 6.38 (dd, J_1 = 7.0 Hz, J_2 = 5.0 Hz, 1H), 5.27 (d, *J* = 3.3 Hz, 1H), 5.18 (t, *J* = 4.3 Hz, 1H), 4.47-4.44 (m, 1H), 3.83 (dd, J_1 = 5.6 Hz, J_2 = 2.8 Hz, 1H), 3.72 (ddd, J_1 = 13.4 Hz, J_2 = 3.9 Hz, J_3 = 3.1 Hz, 1H), 3.66 (ddd, J_1 = 9.4 Hz, J_2 = 4.4 Hz, J_3 = 3.3 Hz, 1H), 2.59 (ddd, J_1 = 12.5 Hz, J_2 = 6.9 Hz, J_3 = 5.6 Hz, 1H), 2.11 (ddd, J_1 = 10.5 Hz, J_2 = 4.9 Hz, J_3 = 1.8 Hz, 1H). **^{13}C-NMR** (100 MHz, d_6-DMSO) δ 156.3, 153.2, 151.6, 144.2, 136.2, 132.9, 128.6, 128.3, 127.1, 116.4, 115.8, 87.2, 82.3, 70.2, 61.2. **HR-ESI MS** (*m*/*z*): $[M+Na]^+$ calcd for $C_{18}H_{19}N_5O_4$, 392.1329; found 392.1329. **UV-Vis** (H_2O) λ_{max} (nm) and ε ($cm^{-1}M^{-1}$): 340 (1.7 x 10^4).

8.2.25 8-ethenyl- 2'-deoxyguanosine (26)

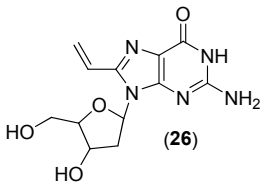

(**26**)

Compound **19** (170 mg, 0.27 mmoles) was dissolved in anhydrous tetrahydrofuran (17.6 mL) and tetrabutylammonium fluoride trihydrate (391 mg, 1.24 mmoles) was added. The reaction was stirred at room temperature in the dark for 20 hours. The solvents and other volatiles were evaporated *in vacuo* and the crude product was filtered on silica

gel (DCM:MeOH 85:15 to 80:20). The resulting yellowish solid was washed in a glass tube by addition of a solvent, sonication, centrifugation and removal of the supernatant with a glass pipette. This operation was performed with hexane (ca. 800 uL) and twice using hexane (ca. 400 uL). The residue was then dried to yield 70 mg (87%) of a yellowish solid. **^{1}H-NMR** (400 MHz, d_6-DMSO) δ 10.64 (br s, 1H), 6.99 (dd, J_1 = 17.0 Hz, J_2 = 11.0 Hz, 1H), 6.43 (br s, 2H), 6.24 (dd, J_1 = 8.8 Hz, J_2 = 6.1 Hz, 1H), 6.08 (dd, J_1 = 17.0 Hz, J_2 = 2.1 Hz, 1H), 5.38 (dd, J_1 = 11.0 Hz, J_2 = 2.1 Hz, 1H), 5.22 (d, J = 4.0 Hz, 1H), 4.96 (t, J = 5.2 Hz, 1H), 4.35 (d, J = 3.1 Hz, 1H), 3.77 (dd, J_1 = 7.5 Hz, J_2 = 4.3 Hz, 1H), 3.63-3.51 (m, 2H), 2.61 (ddd, J_1 = 15.4 Hz, J_2 = 8.8 Hz, J_3 = 6.6 Hz, 1H), 2.04 (ddd, J_1 = 13.0 Hz, J_2 = 6.1 Hz, J_3 = 2.3 Hz, 1H). **^{13}C-NMR** (100 MHz, d_6-DMSO) δ 153.4, 143.9, 125.1, 119.1, 116.2, 87.4, 82.5, 70.5, 61.5. **ESI MS** (*m*/*z*): $[M+H]^+$ calcd for $C_{12}H_{15}N_5O_4$, 294.1; found 294.1 **UV-Vis** (H_2O) λ_{max} (nm) and ε ($cm^{-1}M^{-1}$): 280 (1.1 x 10^4).

8.2.26 (*E*)-3',5'-*O*-bis(*tert*-butyldimethylsilyl)-8-[2-(pyrid-3-yl)-ethenyl]-O^6-(trimethylsilylethyl)-2'-deoxyguanosine (27)

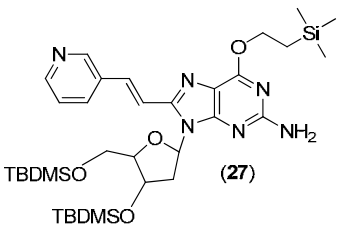

(**27**)

Palladium acetate (4.6 mg, 0.02 mmoles), triphenylphosphine (13.4 mg, 0.05 mmoles) and triethylamine (24.7 mg, 34.1 uL, 0.25 mmoles) were dissolved in dry DMF (2 mL) in a dry round-bottom flask previously purged with nitrogen. The mixture was degassed by three freeze-pump-thaw cycles. The solution was stirred at 60 °C for 2 minutes. The solution was then added to a mixture containing compound **19** (127 mg, 0.21 mmoles), 3-bromopyridine (65 mg, 40.2 uL, 0.41 mmoles) in DMF (1.5 mL) previously degassed by three freeze-pump-thaw cycles. The resulting mixture was stirred in the dark at 100 °C under argon for 24 hours. The solvent was removed *in vacuo* and the residue was purified by silica gel column chromatography (Hex:AcOEt 91:9 to 50:50) to yield 22 mg (15%) of a yellow fluorescent oil. **^{1}H-NMR** (400 MHz, $CDCl_3$) δ 8.78 (d, J = 1.5 Hz, 1H), 8.55 (dd, J_1 = 4.7 Hz, J_2 = 1.5 Hz, 1H), 7.87 (d, J = 15.9 Hz, 1H), 7.88-7.84 (m, 1H), 7.32 (dd, J_1 = 7.8 Hz, J_2 = 4.7 Hz, 1H), 7.23 (d, J = 15.9 Hz, 1H), 6.35 (dd, J_1 = 6.7 Hz, J_2 = 6.6 Hz, 1H), 4.79-4.75 (m, 3H), 4.63-4.59 (m, 2H), 3.97 (dt, J_1 = 8.6 Hz, J_2 = 4.8 Hz, 1H), 3.85 (dd, J_1 = 10.9 Hz, J_2 = 6.0 Hz, 1H), 3.74 (dd, J_1 = 10.9 Hz, J_2 = 4.8 Hz, 1H), 3.51 (quint, J = 6.7 Hz, 1H), 2.23 (ddd, J_1 = 13.2 Hz, J_2 = 6.8 Hz, J_3 = 4.1 Hz, 1H), 1.31-1.26 (m, 2H), 0.96 (s, 9H), 0.84 (s, 9H), 0.17 (s, 6H), 0.11 (s, 9H), 0.02 (s, 3H), -0.02 (s, 3H). **^{13}C-NMR** (100 MHz, $CDCl_3$) δ 161.1, 158.7, 154.4, 149.5, 149.1, 147.5, 133.4, 132.5, 132.1, 123.6, 116.3, 116.2, 87.2, 83.7, 72.3, 64.9, 62.9, 37.6, 28.0, 26.8, 25.9, 25.8, 18.4, 18.1, 17.8, 17.5, 13.6,

-1.4, -4.6, -4.7, -5.4, -5.5. **ESI MS** (*m*/*z*): $[M+H]^+$ calcd for $C_{34}H_{58}N_6O_4Si_3$, 699.4; found 699.5.

8.2.27 (*E*)-3',5'-*O*-bis(*tert*-butyldimethylsilyl)-8-[2-(pyrid-4-yl)-ethenyl]-O^6-(trimethylsilylethyl)-2'-deoxyguanosine (28)

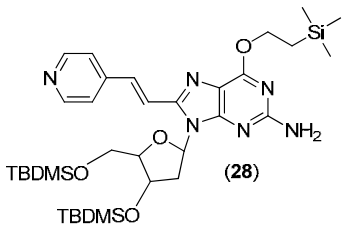

(**28**)

Palladium acetate (23.4 mg, 0.11 mmoles), tri(o-tolyl)-phosphine (66.3 mg, 0.22 mmoles) and triethylamine (136.4 mg, 188 uL, 1.36 mmoles) were dissolved in dry DMF (13 mL) in a dry round-bottom flask previously purged with nitrogen. The mixture was degassed by three freeze-pump-thaw cycles. The solution was stirred at 60 °C for 10 minutes. The solution was then added to a mixture containing compound **19** (650 mg, 1.05 mmoles), 4-bromopyridine hydrochloride (416 mg, 2.14 mmoles) in triethylamine (3.8 mL) and DMF (6 mL) previously degassed by three freeze-pump-thaw cycles. The resulting mixture was stirred in the dark at 100 °C under argon for 20 hours. The solvent was removed *in vacuo* and the residue was purified by silica gel column chromatography (Hex:AcOEt 85:15 to 60:40) to yield 526 mg (72%) of a yellow fluorescent oil. **^{1}H-NMR** (400 MHz, $CDCl_3$) δ 8.62 (d, J = 6.2 Hz, 2H), 7.81 (d, J = 15.9 Hz, 1H), 7.41 (d, J = 6.2 Hz, 2H), 7.36 (d, J = 15.9 Hz, 1H), 6.36 (dd, J_1 = 6.8 Hz, J_2 = 6.8 Hz, 1H), 4.78-4.75 (m, 3H), 4.64-4.59 (m, 2H), 3.97 (ddd, J_1 = 8.6 Hz, J_2 = 5.9 Hz, J_3 = 4.6 Hz, 1H), 3.86 (dd, J_1 = 10.9 Hz, J_2 = 6.1 Hz, 1H), 3.76 (dd, J_1 = 10.9 Hz, J_2 = 4.7 Hz, 1H), 3.46 (ddd, J_1 = 13.2 Hz, J_2 = 6.7 Hz, J_3 = 6.6 Hz, 1H), 2.25 (ddd, J_1 = 13.2 Hz, J_2 = 6.8 Hz, J_3 = 4.3 Hz, 1H), 1.31-1.26 (m, 2H), 0.96 (s, 9H), 0.85 (s, 9H), 0.18 (s, 3H), 0.17 (s, 3H), 0.11 (s, 9H), 0.03 (s, 3H), -0.02 (s, 3H). **^{13}C-NMR** (100 MHz, $CDCl_3$) δ 161.4, 159.0, 154.6, 150.6, 147.1, 143.7, 133.4, 121.5, 118.9, 116.5, 87.4, 83.9, 72.5, 65.1, 63.0, 38.0, 26.1, 26.0, 18.6, 18.3, 18.0, -1.2, -4.3, -4.4, -5.1, -5.2. **ESI MS** (*m*/*z*): $[M+Na]^+$ calcd for $C_{34}H_{58}N_6O_4Si_3$, 720.4; found 720.5.

8.2.28 (*E*)-8-[2-(pyrid-3-yl)-ethenyl]-2'-deoxyguanosine (29)

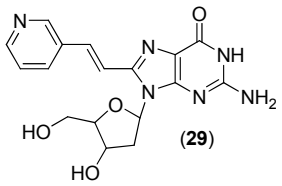

(**29**)

Compound **27** (22 mg, 0.03 mmoles) was dissolved in anhydrous tetrahydrofuran (2 mL) and tetrabutylammonium fluoride trihydrate (44.4 mg, 0.14 mmoles) was added. The reaction was stirred at room temperature in the dark for 20 hours. The solvents and other volatiles were evaporated *in vacuo* and the crude product was precipitated in tetrahydrofuran. The supernatant was removed and the resulting yellowish solid was washed in a glass tube by addition of a solvent, sonication, centrifugation and removal of

the supernatant with a glass pipette. This operation was performed twice with hexane (ca. 250 uL) and twice using water (ca. 250 uL). The residue was then dried to yield 2.5 mg (22%) of a yellow solid. **^{1}H-NMR** (400 MHz, d_6-DMSO) δ 10.74 (br s, 1H), 8.84 (d, J = 2.0 Hz, 1H), 8.48 (dd, J_1 = 4.7 Hz, J_2 = 1.5 Hz, 1H), 8.15 (dt, J_1 = 8.0 Hz, J_2 = 2.0 Hz, 1H), 7.65 (d, J = 15.9 Hz, 1H), 7.56 (d, J = 15.9 Hz, 1H), 7.39 (dd, J_1 = 8.0 Hz, J_2 = 4.7 Hz, 1H), 6.52 (br s, 2H), 6.39 (dd, J_1 = 8.8 Hz, J_2 = 6.2 Hz, 1H), 5.27-5.23 (m, 2H), 4.46 (d, J = 3.4 Hz, 1H), 3.84 (dd, J_1 = 6.6 Hz, J_2 = 3.3 Hz, 1H), 3.75-3.63 (m, 2H), 2.59 (ddd, J_1 = 15.6 Hz, J_2 = 8.7 Hz, J_3 = 6.8 Hz, 1H), 2.10 (ddd, J_1 = 13.0 Hz, J_2 = 6.0 Hz, J_3 = 2.2 Hz, 1H). **^{13}C-NMR** (100 MHz, d_6-DMSO) δ 156.7, 153.6, 151.7, 148.9, 143.8,133.3, 132.0, 129.2, 123.7, 117.9, 116.7, 87.3, 82.5, 70.2, 61.2. **HR-ESI MS** (m/z): [M+Na]+ calcd for $C_{17}H_{18}N_6O_4$, 393.1282; found 393.1282. **UV-Vis** (H_2O) λ_{max} (nm) and ε ($cm^{-1}M^{-1}$): 345 (1.6 x 10^4).

8.2.29 (*E*)-8-[2-(pyrid-4-yl)-ethenyl]-2'-deoxyguanosine (30)

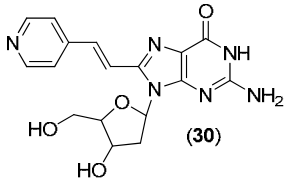

(**30**)

Compound **28** (30 mg, 0.04 mmoles) was dissolved in anhydrous tetrahydrofuran (2.6 mL) and tetrabutylammonium fluoride trihydrate (91.6 mg, 0.29 mmoles) was added. The reaction was stirred at room temperature in the dark for 20 hours. The solvents and other volatiles were evaporated *in vacuo* and the crude product was filtered on silica gel (DCM:MeOH 90:10 to 85:15). The product was then treated with 1.5 mL of 33% aqueous ammonium hydroxide at 55 °C for 17 hours in a 1.7 mL screw-top cap tube. The volatiles were removed and the resulting yellow solid was washed in a glass tube by addition of a solvent, sonication, centrifugation and removal of the supernatant with a glass pipette. This operation was performed twice with water (ca. 200 uL) and three times using hexane (ca. 300 uL). The residue was then dried to yield 2.2 mg (15%) of a yellow solid. **^{1}H-NMR** (400 MHz, d_6-DMSO) δ 10.98 (br s, 1H), 8.53 (d, J = 6.1 Hz, 2H), 7.77 (d, J = 15.9 Hz, 1H), 7.64 (d, J = 6.1 Hz, 2H), 7.49 (d, J = 15.9 Hz, 1H), 6.62 (br s, 2H), 6.39 (dd, J_1 = 8.9 Hz, J_2 = 6.0 Hz, 1H), 5.33 (br s, 1H), 5.28 (br s, 1H), 4.47-4.45 (m, 1H), 3.84 (dd, J_1 = 6.5 Hz, J_2 = 3.3 Hz, 1H), 3.74-3.65 (m, 2H), 2.56 (ddd, J_1 = 15.7 Hz, J_2 = 9.0 Hz, J_3 = 6.8 Hz, 1H), 2.10 (ddd, J_1 = 13.1 Hz, J_2 = 6.1 Hz, J_3 = 2.3 Hz, 1H). **^{13}C-NMR** (100 MHz, d_6-DMSO) δ 154.9, 151.9, 150.0, 143.4, 143.1, 129.8, 121.3, 120.5, 117.0, 87.4, 82.5, 75.2, 70.2, 61.2. **HR-ESI MS** (*m/z*): $[M+H]^+$ calcd for $C_{17}H_{18}N_6O_4$, 371.1462; found 371.1457. **UV-Vis** (H_2O) λ_{max} (nm) and ε ($cm^{-1}M^{-1}$): 355 (1.8 x 10^4).

8.2.30 3',5'-*O*-bis(*tert*-butyldimethylsilyl)-N^2-isobutyryl-8-(2-pyridyl)-O^6-(trimethylsilylethyl)-2'-deoxyguanosine (31)

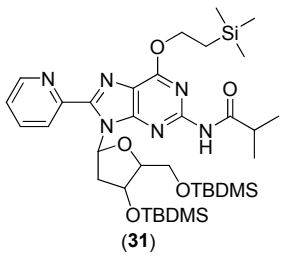

(**31**)

In a flask, compound **13** (600 mg, 0.89 mmoles) was twice coevaporated with dry pyridine and then dissolved in dry pyridine (5.2 mL). Isobutyryl chloride (193 mg, 190.3 uL, 3.05 mmoles) was added dropwise and the yellow solution was stirred at room temperature. After 24 hours, methanol (3 mL) was added to the mixture and the reaction was stirred for 10 minutes. The solvents were then removed *in vacuo* followed by coevaporation with toluene. The residue was then partitioned into water/DCM and the layers were separated. The aqueous layer was extracted twice with DCM and the combined organic layers were washed with water and dried over Na_2SO_4. The solvents were removed *in vacuo* and the compound was purified by silica gel column chromatography (Hex:AcOEt 90:10) to yield 583 mg (88%) of a yellowish solid. **^{1}H-NMR** (400 MHz, $CDCl_3$) δ 8.67 (ddd, J_1 = 4.8 Hz, J_2 = 1.8 Hz, J_3 = 0.9 Hz, 1H), 8.27 (dt, J_1 = 7.9 Hz, J_2 = 0.9 Hz, 1H), 7.83 (dt, J_1 = 7.9 Hz, J_2 = 1.8 Hz, 1H), 7.70 (br s, 1H), 7.51 (dd, J_1 = 7.0 Hz, J_2 = 7.0 Hz, 1H), 7.37 (ddd, J_1 = 7.6 Hz, J_2 = 4.8 Hz, J_3 = 1.2 Hz, 1H), 4.87 (quint, J = 2.9 Hz, 1H), 4.88-4.65 (m, 2H), 4.00-3.91 (m, 2H), 3.79 (dd, J_1 = 9.7 Hz, J_2 = 4.9 Hz, 1H), 3.54 (ddd, J_1 = 13.0 Hz, J_2 = 7.0 Hz, J_3 = 6.2 Hz, 1H), 3.19 (br s, 1H), 2.33 (ddd, J_1 = 13.0 Hz, J_2 = 6.6 Hz, J_3 = 3.4 Hz, 1H), 1.33-1.27 (m, 8H), 0.95 (s, 9H), 0.88 (s, 9H), 0.17 (s, 3H), 0.16 (s, 3H), 0.13 (s, 9H), 0.04 (s, 6H). **^{13}C-NMR** (100 MHz, $CDCl_3$) δ 161.6, 154.8, 151.9, 150.4, 150.3, 149.1, 137.3, 125.9, 124.6, 119.2, 88.4, 86.3, 73.5, 66.2, 64.2, 37.9, 26.5, 26.3, 20.0, 19.8, 18.9, 18.4, 18.1, 0.49, -0.9, -4.1, -4.2, -4.7, -4.8. **HR-ESI MS** (*m*/*z*): $[M+H]^+$ calcd for $C_{36}H_{62}N_6O_5Si_3$, 743.4162; found 743.4162.

8.2.31 N^2-isobutyryl-8-(2-pyridyl)-2'-deoxyguanosine (32)

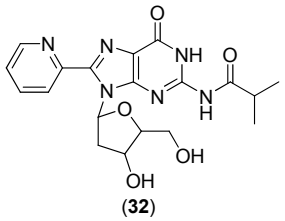

(**32**)

Compound **31** (180 mg, 0.24 mmoles) was dissolved in anhydrous tetrahydrofuran (16.2 mL) and tetrabutylammonium fluoride trihydrate (347 mg, 1.10 mmoles) was added. The reaction was stirred at room temperature for 17 hours. The solvents and other volatiles were then evaporated *in vacuo* and the crude was purified by silica gel column chromatography (DCM:MeOH 93:7) to yield 91 mg (91%) of a white solid. **^{1}H-NMR** (400 MHz, d_6-DMSO) δ 12.24 (br s, 1H), 11.37 (br s, 1H), 8.69 (d, J = 4.1 Hz, 1H), 8.08 (d, J = 8.0 Hz, 1H), 7.98 (dt, J_1 = 7.5 Hz, J_2 = 1.8

Hz, 1H), 7.50 (ddd, J_1 = 7.5 Hz, J_2 = 4.9 Hz, J_3 = 1.2 Hz, 1H), 7.24 (dd, J_1 = 7.2 Hz, J_2 = 7.2 Hz, 1H), 4.97 (d, J = 4.7 Hz, 1H), 4.50-4.42 (m, 2H), 3.74-3.71 (m, 1H), 3.65-3.60 (m, 1H), 3.51-3.45 (m, 1H), 3.28 (dt, J_1 = 13.2 Hz, J_2 = 6.1 Hz, 1H), 2.84 (sept, J = 6.8 Hz, 1H), 2.19 (ddd, J_1 = 13.2 Hz, J_2 = 7.0 Hz, J_3 = 3.6 Hz, 1H), 1.16 (d, J = 6.8 Hz, 6H). **^{13}C-NMR** (100 MHz, d_6-DMSO) δ 180.7, 155.2, 150.6, 149.9, 149.2, 147.9, 147.1, 138.0, 125.1, 124.8, 121.3, 88.1, 85.2, 71.5, 62.5 37.6, 35.2, 19.4, 19.3, 0.6. **HR-ESI MS** (*m*/*z*): $[M+Na]^+$ calcd for $C_{19}H_{22}N_6O_5$, 437.1544; found 437.1541.

8.2.32 *O*$^{5'}$-dimethoxytrityl-*N*^{2}-isobutyryl-8-(2-pyridyl)-2'-deoxyguanosine (33)

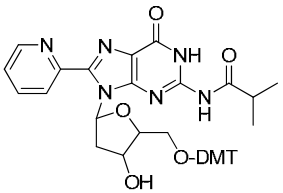

(33)

Compound **32** (81 mg, 0.20 mmoles) was twice coevaporated with pyridine and dissolved in dry pyridine (4.8 mL). 4,4'-dimethoxytrityl chloride (146 mg, 0.43 mmoles) was slowly added and the reaction was stirred at room temperature for 40 minutes. The reaction was stopped by adding an aqueous solution of saturated $NaHCO_3$. After addition of DCM, the two layers were separated and the aqueous layer was extracted three times with DCM. The combined organic layers were dried over Na_2SO_4 and the solvent was removed *in vacuo*. The residue was purified by silica gel column chromatography (DCM:MeOH:Et_3N 95:5:0.5) and concentrated *in vacuo* to yield 137 mg (96%) of a white solid. **^{1}H-NMR** (400 MHz, d_4-MeOH) δ 8.57 (ddd, J_1 = 4.9 Hz, J_2 = 1.7 Hz, J_3 = 0.9 Hz, 1H), 8.05 (dt, J_1 = 8.0 Hz, J_2 = 1.0 Hz, 1H), 7.85 (dt, J_1 = 7.8 Hz, J_2 = 1.8 Hz, 1H), 7.49 (ddd, J_1 = 7.6 Hz, J_2 = 4.9 Hz, J_3 = 1.2 Hz, 1H), 7.39 (dd, J_1 = 7.6 Hz, J_2 = 6.1 Hz, 1H), 7.36-7.33 (m, 2H), 7.23 (dt, J_1 = 8.9 Hz, J_2 = 2.0 Hz, 4H), 7.14-7.12 (m, 3H), 6.71 (dt, J_1 = 8.9 Hz, J_2 = 2.0 Hz, 2H), 6.65 (dt, J_1 = 8.9 Hz, J_2 = 2.0 Hz, 2H), 4.67 (dt, J_1 = 7.4 Hz, J_2 = 3.1 Hz, 1H), 4.11-4.06 (m, 1H), 3.76 (s, 3H), 3.75 (s, 3H), 3.59-3.45 (m, 3H), 3.16 (dd, J_1 = 10.0 Hz, J_2 = 2.6 Hz, 1H), 2.63 (sept, J = 6.8 Hz, 1H), 2.40 (ddd, J_1 = 13.6 Hz, J_2 = 7.4 Hz, J_3 = 4.4 Hz, 1H), 1.20 (d, J = 6.8 Hz, 6H). **^{13}C-NMR** (100 MHz, d_4-MeOH) δ 180.2, 158.6, 158.5, 156.2, 150.4, 149.1, 148.7, 148.3, 147.4, 145.1, 137.3, 136.0, 135.8, 130.0, 129.7, 128.0, 127.0, 126.3, 124.9, 124.4, 120.8, 112.4, 112.3, 87.0, 85.9, 85.7, 71.8, 64.9, 54.3, 54.2, 46.0, 37.5, 35.5, 18.2, 17.9, 8.8, 6.2, -1.4. **HR-ESI MS** (*m*/*z*): $[M+Na]^+$ calcd for $C_{40}H_{40}N_6O_7$, 739.2851; found 739.2846.

8.2.33 $O^{3'}$-[(2-cyanoethoxy)(diisopropylamino)phosphino]-$O^{5'}$-dimethoxytrityl-N^2-isobutyryl-8-(2-pyridyl)-2'-deoxyguanosine (34)

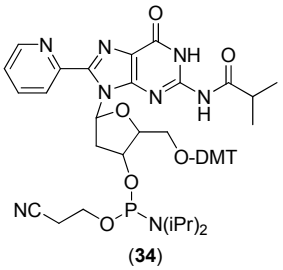

(**34**)

Compound **33** (65 mg, 0.09 mmoles) was added to a dry flask and dissolved into dry DCM (0.5 mL). Diisopropylethylamine (66 mg, 87.2 uL, 0.51 mmoles) was added, followed by 2-cyanoethyl *N,N*-diisopropyl-chlorophosphoramidite (36.1 mg, 34.1 uL, 0.15 mmoles). After 1 hour, the reaction mixture was directly filtered over a short silica gel column using a rapid flow rate (DCM:MeOH:Et_3N 97.5:3.5:1). After concentrating *in vacuo*, the resulting oil was dissolved in AcOEt and precipitated with hexane. The solvent was removed and the compound dried to yield 80 mg (96%) of a white solid. **^{1}H-NMR** (400 MHz, $CDCl_3$) δ 8.63 (ddd, J_1 = 4.9 Hz, J_2 = 1.8 Hz, J_3 = 0.9 Hz, 1H), 8.10 (dt, J_1 = 7.9 Hz, J_2 = 1.0 Hz, 1H), 7.92 (dt, J_1 = 7.8 Hz, J_2 = 1.8 Hz, 1H), 7.43 (ddd, J_1 = 7.6 Hz, J_2 = 4.9 Hz, J_3 = 1.2 Hz, 1H), 7.32 (dd, J_1 = 7.6 Hz, J_2 = 6.2 Hz, 1H), 7.29-7.26 (m, 2H), 7.16 (dt, J_1 = 9.9 Hz, J_2 = 3.0 Hz, 4H), 7.07-7.04 (m, 3H), 6.64 (dt, J_1 = 6.9 Hz, J_2 = 2.2 Hz, 2H), 6.58 (dt, J_1 = 6.8 Hz, J_2 = 2.2 Hz, 2H), 4.58 (dt, J_1 = 7.4 Hz, J_2 = 3.0 Hz, 1H), 4.00 (ddd, J_1 = 7.8 Hz, J_2 = 4.4 Hz, J_3 = 2.5 Hz, 1H), 3.69 (s, 3H), 3.68 (s, 3H), 3.51-3.39 (m, 2H), 3.29-3.24 (m, 13H), 3.09 (dd, J_1 = 9.9 Hz, J_2 = 2.6 Hz, 1H), 2.65 (q, J = 7.2 Hz, 1H), 2.54 (quint, J = 6.8 Hz, 1H), 2.32 (ddd, J_1 = 13.7 Hz, J_2 = 7.7 Hz, J_3 = 4.5 Hz, 1H), 1.13 (d, J = 6.8 Hz, 3H), 1.11 (d, J = 6.8 Hz, 3H), 1.05 (t, J = 7.2 Hz, 1H). **^{13}C-NMR** (100 MHz, $CDCl_3$) δ 180.2, 158.6, 158.5, 156.2, 150.4, 149.1, 148.7, 148.3, 147.4, 145.1, 137.3, 136.0, 135.8, 130.0, 129.7, 128.0, 127.1, 126.3, 124.9, 124.4, 120.8, 112.4, 112.3, 87.0, 85.9, 85.7, 71.8, 64.9, 54.3, 54.2, 46.0, 37.5, 35.5, 18.2, 17.9, 8.8, 6.2, -1.4. **^{31}P-NMR** (162 MHz, $CDCl_3$) δ 148.7, 147.9. **ESI MS** (*m/z*): $[M+Na]^+$ calcd for $C_{49}H_{57}N_8O_8P$, 939.4; found 939.6.

8.2.34 (*E*)-3',5'-*O*-bis(*tert*-butyldimethylsilyl)-N^2-isobutyryl-8-(2-phenylethenyl)-O^6-(trimethylsilylethyl)-2'-deoxyguanosine (35)

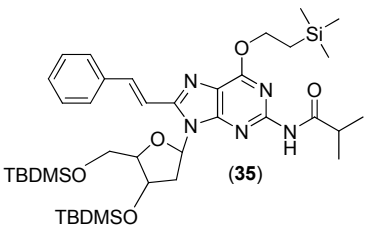

(**35**)

In a flask, compound **18** (452 mg, 0.65 mmoles) was twice coevaporated with dry pyridine and then dissolved in dry pyridine (3.8 mL). Isobutyryl chloride (162 mg, 159.5 uL, 2.56 mmoles) was added dropwise and the yellow solution was stirred at room temperature in the dark. After 6 hours, the reaction mixture was diluted with dichloromethane and the mixture was poured in brine. The organic layer was washed twice with brine, and the resulting

aqueous layers were then extracted with dichloromethane. The combined organic layers were dried over Na_2SO_4. The solvents were removed *in vacuo* and the compound was purified by silica gel column chromatography (Hex:AcOEt 90:10) to yield 358 mg (72%) of a yellowish solid. **^{1}H-NMR** (400 MHz, $CDCl_3$) δ 7.98 (d, J = 15.9 Hz, 1H), 7.60-7.58 (m, 2H), 7.43-7.35 (m, 3H), 7.20 (d, J = 15.9 Hz, 1H), 6.46 (dd, J_1 = 7.0 Hz, J_2 = 7.0 Hz, 1H), 4.78 (ddd, J_1 = 6.3 Hz, J_2 = 3.3 Hz, J_3 = 3.0 Hz, 1H), 4.69-4.64 (m, 2H), 4.03-3.99 (m, 1H), 3.86 (dd, J_1 = 10.8 Hz, J_2 = 6.4 Hz, 1H), 3.80 (dd, J_1 = 10.8 Hz, J_2 = 5.2 Hz, 1H), 3.45 (ddd, J_1 = 13.3 Hz, J_2 = 6.7 Hz, J_3 = 6.6 Hz, 1H), 3.34 (br s, 1H), 2.26 (ddd, J_1 = 13.3 Hz, J_2 = 6.4 Hz, J_3 = 3.4 Hz, 1H), 1.34-1.32 (m, 2H), 1.30 (d, J = 6.8 Hz, 6H), 0.96 (s, 9H), 0.86 (s, 9H), 0.18 (s, 3H), 0.16 (s, 3H), 0.13 (s, 9H), 0.04 (s, 3H), 0.01 (s, 3H). **^{13}C-NMR** (100 MHz, $CDCl_3$) δ 160.9, 154.1, 151.5, 150.9, 138.5, 136.4, 130.4, 129.7, 129.4, 127.9, 126.1, 120.7, 120.6, 118.9, 114.2, 88.2, 84.4, 73.0, 66.1, 63.7, 38.5, 35.5, 26.4, 26.3, 19.9, 19.8, 18.9, 18.5, 18.2, 0.5, -0.9, -4.1, -4.2, -4.9. **ESI MS** (*m*/*z*): $[M+H]^+$ calcd for $C_{39}H_{65}N_5O_5Si_3$, 767.4; found 767.6.

8.2.35 (*E*)-N^2-isobutyryl-8-(2-phenylethenyl)-2'-deoxyguanosine (36)

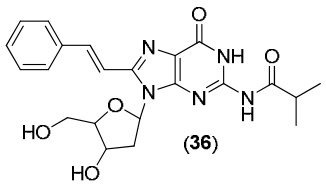

(**36**)

Compound **35** (638 mg, 0.83 mmoles) was dissolved in anhydrous tetrahydrofuran (55 mL) and tetrabutylammonium fluoride trihydrate (1.19 g, 3.78 mmoles) was added. The reaction was stirred in the dark at room temperature for 17 hours. The solvents and other volatiles were then evaporated *in vacuo*. The crude was precipitated with methanol, the mixture was centrifuged and the supernatant removed. The solid residue was washed in a glass tube by addition of a solvent, sonication, centrifugation and removal of the supernatant with a glass pipette. This operation was performed twice with methanol (ca. 300 uL), once with water (ca. 400 uL) and twice with hexane (ca. 1 mL). The residue was dried to yield 345 mg (95%) of a yellowish solid. **^{1}H-NMR** (400 MHz, d_6-DMSO) δ 12.10 (br s, 1H), 11.61 (br s, 1H), 7.74-7.72 (m, 2H), 7.66 (d, J = 15.9 Hz, 1H), 7.59 (d, J = 15.9 Hz, 1H), 7.41-7.32 (m, 3H), 6.46 (dd, J_1 = 8.8 Hz, J_2 = 6.1 Hz, 1H), 5.30 (d, J = 4.0 Hz, 1H), 5.17 (t, J = 5.1 Hz, 1H), 4.50-4.47 (m, 1H), 3.85 (dd, J_1 = 7.0 Hz, J_2 = 3.7 Hz, 1H), 3.72 (dd, J_1 = 11.9 Hz, J_2 = 3.5 Hz, 1H), 3.66 (dd, J_1 = 11.9 Hz, J_2 = 3.7 Hz, 1H), 2.74 (sept, J = 6.8 Hz, 1H), 2.64 (ddd, J_1 = 13.1 Hz, J_2 = 6.6 Hz, J_3 = 2.4 Hz, 1H), 2.13 (ddd, J_1 = 13.1 Hz, J_2 = 5.9 Hz, J_3 = 2.1 Hz, 1H), 1.11 (d, J = 6.8 Hz, 6H). **^{13}C-NMR** (100 MHz, d_6-DMSO) δ 180.4, 154.8, 149.4, 146.5, 136.0, 134.6, 128.8, 128.7, 127.5, 119.8, 115.6, 87.4, 82.7, 70.2, 61.2, 35.0, 23.0, 19.2, 19.0, 13.5. **HR-ESI MS** (*m*/*z*): $[M+Na]^+$ calcd for $C_{22}H_{25}N_5O_5$, 462.1748; found 462.1747.

8.2.36 (*E*)-*O*$^{5'}$-dimethoxytrityl-*N*^{2}-isobutyryl-8-(2-phenylethenyl)-2'-deoxyguanosine (37)

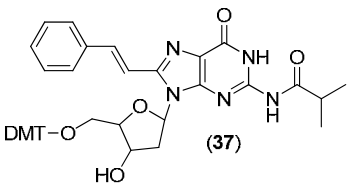

Compound **36** (50 mg, 0.11 mmoles) was twice coevaporated with dry pyridine and dissolved in dry pyridine (2.7 mL). 4,4'-dimethoxytrityl chloride (84.6 mg, 0.25 mmoles) was slowly added and the reaction was stirred in the dark at room temperature for 3 hours. The reaction was stopped by adding an aqueous solution of saturated $NaHCO_3$. After addition of dichloromethane, the two layers were separated and the aqueous layer was extracted three times with dichloromethane. The combined organic layers were dried over Na_2SO_4 and the solvent was removed *in vacuo*. The residue was purified by silica gel column chromatography (DCM:MeOH:Et_3N 98:2:0.5) and concentrated *in vacuo* to yield 60 mg (71%) of a white solid. **^{1}H-NMR** (400 MHz, d_4-MeOH) δ 7.75 (d, J = 16.0 Hz, 1H), 7.56-7.53 (m, 2H), 7.33-7.26 (m, 6H), 7.17 (dd, J_1 = 9.0 Hz, J_2 = 2.0 Hz, 4H), 7.13-7.08 (m, 3H), 6.66 (dd, J_1 = 11.0 Hz, J_2 = 9.0 Hz, 4H), 6.53 (dd, J_1 = 7.1 Hz, J_2 = 5.5 Hz, 1H), 4.71-4.68 (m, 1H), 4.13-4.09 (m, 1H), 3.67 (s, 3H), 3.66 (s, 3H), 3.47 (ddd, J_1 = 7.2 Hz, J_2 = 6.5 Hz, J_3 = 5.6 Hz, 1H), 3.35 (dd, J_1 = 10.2 Hz, J_2 = 6.4 Hz, 1H), 3.26 (dd, J_1 = 10.2 Hz, J_2 = 3.3 Hz, 1H), 2.97 (dd, J_1 = 13.8 Hz, J_2 = 7.3 Hz, 1H), 2.69 (sept, J = 6.8 Hz, 1H), 2.39 (ddd, J_1 = 13.8 Hz, J_2 = 7.3 Hz, J_3 = 5.3 Hz, 1H), 1.22 (d, J = 6.8 Hz, 3H), 1.21 (d, J = 6.8 Hz, 3H). **^{13}C-NMR** (100 MHz, d_4-MeOH) δ 181.8, 160.2, 160.1, 157.3, 150.7, 150.4, 148.6, 146.5, 138.3, 137.4, 137.3, 131.4, 131.3, 130.4, 130.1, 129.5, 128.7, 128.6, 127.9, 121.9, 115.1, 114.0, 87.9, 87.4, 85.9, 72.7, 65.3, 55.8, 55.7, 39.0, 37.1, 19.7, 19.5. **HR-ESI MS** (*m*/*z*): $[M+Na]^+$ calcd for $C_{43}H_{43}N_5O_7$, 764.3055; found 764.3050.

8.2.37 (*E*)-*O*$^{3'}$-[(2-cyanoethoxy)(diisopropylamino)phosphino]-*O*$^{5'}$-dimethoxytrityl-*N*^{2}-isobutyryl-8-(2-phenylethenyl)-2'-deoxyguanosine (38)

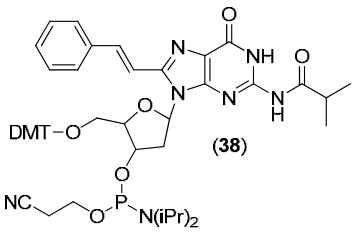

Dry dichloromethane (0.5 mL) was added to compound **37** (32 mg, 0.04 mmoles) in a dry flask purged with argon. 2-cyanoethyl tetraisopropyl-phosphordiamidite (15.5 mg, 16.3 uL, 0.05 mmoles) and a solution of 5-ethylthio-(1*H*)-tetrazole 0.25 M in dry dichloromethane (7.7 mg, 0.06 mmoles in 240 uL dry dichloromethane) was added. The reaction mixture was stirred in the dark at ambient temperature for 20 minutes. The reaction mixture was evaporated to dryness *in vacuo*, and dry acetonitrile (0.5 mL) was added. The mixture was sonicated and filtered through a disposable Nylon filter to remove the resulting precipitate. The filtrate

was evaporated to dryness *in vacuo*. The resulting product (31 mg) was directly used for DNA synthesis without further purification. **^{31}P-NMR** (162 MHz, $CDCl_3$) δ 149.2, 149.0.

8.2.38 (*E*)-3',5'-*O*-bis(*tert*-butyldimethylsilyl)-N^2-isobutyryl-8-[2-(pyrid-4-yl)-ethenyl]-O^6-(trimethylsilylethyl)-2'-deoxyguanosine (39)

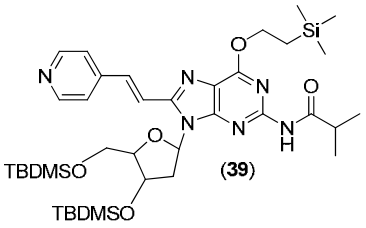

In a flask, compound **28** (454 mg, 0.65 mmoles) was twice coevaporated with dry pyridine and then dissolved in dry pyridine (5.8 mL). Isobutyryl chloride (162 mg, 159.5 uL, 2.56 mmoles) was added dropwise and the yellow solution was stirred at room temperature in the dark. After 4 hours, the reaction mixture was diluted with dichloromethane and the mixture was poured in brine. The organic layer was washed with brine. The layers were separated and the organic layers was dried over Na_2SO_4. The solvents were removed *in vacuo* and the compound was purified by silica gel column chromatography (Hex:AcOEt 70:30) to yield 435 mg (87%) of a yellow oil. **^{1}H-NMR** (400 MHz, $CDCl_3$) δ 8.63 (d, J = 6.1 Hz, 2H), 7.87 (d, J = 15.9 Hz, 1H), 7.42 (d, J = 6.1 Hz, 2H), 7.41 (d, J = 15.9 Hz, 1H), 6.44 (dd, J_1 = 6.8 Hz, J_2 = 6.8 Hz, 1H), 4.78 (ddd, J_1 = 6.4 Hz, J_2 = 3.4 Hz, J_3 = 3.0 Hz, 1H), 4.67-4.63 (m, 2H), 4.01 (dd, J_1 = 8.6 Hz, J_2 = 5.3 Hz, 1H), 3.85 (dd, J_1 = 10.8 Hz, J_2 = 6.1 Hz, 1H), 3.78 (dd, J_1 = 10.8 Hz, J_2 = 5.3 Hz, 1H), 3.46 (ddd, J_1 = 13.3 Hz, J_2 = 6.9 Hz, J_3 = 6.5 Hz, 1H), 3.28 (br s, 1H), 2.29 (ddd, J_1 = 13.3 Hz, J_2 = 6.4 Hz, J_3 = 3.5 Hz, 1H), 1.32-1.27 (m, 8H), 0.95 (s, 9H), 0.83 (s, 9H), 0.17 (s, 3H), 0.16 (s, 3H), 0.11 (s, 9H), 0.01 (s, 3H), -0.02 (s, 3H). **^{13}C-NMR** (100 MHz, $CDCl_3$) δ 160.9, 153.6, 151.6, 150.4, 149.3, 143.4, 134.9, 121.6, 118.8, 118.6, 88.0, 84.3, 72.6, 66.0, 63.3, 38.3, 26.1, 26.0, 25.9, 19.5, 19.4, 19.3, 18.6, 18.2, 17.9, -1.3, -4.4, -4.5, -5.2. **ESI MS** (*m*/*z*): $[M+Na]^+$ calcd for $C_{38}H_{64}N_6O_5Si_3$, 791.4; found 791.6.

8.2.39 (*E*)-N^2-isobutyryl-8-[2-(pyrid-4-yl)-ethenyl]-2'-deoxyguanosine (40)

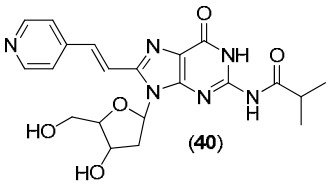

Compound **39** (430 mg, 0.23 mmoles) was dissolved in anhydrous tetrahydrofuran (37 mL) and tetrabutylammonium fluoride trihydrate (800 mg, 2.54 mmoles) was added. The reaction was stirred in the dark at room temperature for 17 hours. The solvents and other volatiles were then evaporated *in vacuo*. The crude product was precipitated with methanol, the mixture was centrifuged and the supernatant removed. The solid residue was washed in a glass tube by addition of a solvent, sonication, centrifugation and removal of the supernatant with a glass pipette. This operation was

performed twice with methanol (ca. 300 uL), once with water (ca. 400 uL) and twice with hexane (ca. 1 mL). The residue was dried to yield 166 mg (67%) of a yellowish solid. **^{1}H-NMR** (400 MHz, d_6-DMSO) δ 8.56 (d, J = 6.1 Hz, 2H), 7.88 (d, J = 15.9 Hz, 1H), 7.68 (d, J = 6.1 Hz, 2H), 7.63 (d, J = 15.9 Hz, 1H), 6.47 (dd, J_1 = 9.1 Hz, J_2 = 5.8 Hz, 1H), 5.32 (br s, 1H), 5.28 (br s, 1H), 4.50-4.48 (m, 1H), 3.87 (dd, J_1 = 6.5 Hz, J_2 = 3.4 Hz, 1H), 3.72-3.70 (m, 2H), 2.75 (sept, J = 6.8 Hz, 1H), 2.58 (ddd, J_1 = 15.8 Hz, J_2 = 9.0 Hz, J_3 = 6.4 Hz, 1H), 2.15 (ddd, J_1 = 13.0 Hz, J_2 = 5.8 Hz, J_3 = 2.2 Hz, 1H), 1.11 (d, J = 6.8 Hz, 6H). **^{13}C-NMR** (100 MHz, d_6-DMSO) δ 180.3, 154.7, 150.1, 149.5, 145.5, 143.0, 131.8, 121.5, 120.1, 87.5, 82.8, 70.1, 61.1, 34.9, 23.0, 18.9, 13.5. **HR-ESI MS** (m/z): $[M+H]^+$ calcd for $C_{21}H_{24}N_6O_5$, 441.1881; found 441.1883.

8.2.40 (*E*)-*O*$^{5'}$-dimethoxytrityl-*N*^{2}-isobutyryl-8-[2-(pyrid-4-yl)-ethenyl]-2'-deoxyguanosine (41)

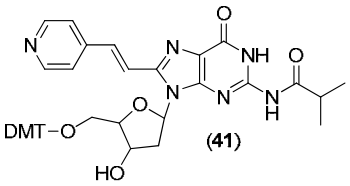

(41)

Compound **40** (49 mg, 0.11 mmoles) was twice coevaporated with pyridine and dissolved in dry pyridine (2.7 mL). 4,4'-dimethoxytrityl chloride (83 mg, 0.25 mmoles) was slowly added and the reaction was stirred in the dark at room temperature for 1 hour. The reaction was stopped by adding an aqueous solution of saturated $NaHCO_3$. After addition of dichloromethane, the two layers were separated and the aqueous layer was extracted three times with dichloromethane. The combined organic layers were dried over Na_2SO_4 and the solvent was removed *in vacuo*. The residue was purified by silica gel column chromatography (DCM:MeOH:Et_3N 96:4:0.5) and concentrated *in vacuo* to yield 56 mg (68%) of a yellow solid. **^{1}H-NMR** (400 MHz, d_4-MeOH) δ 8.48 (d, J = 6.2 Hz, 2H), 7.75 (d, J = 15.9 Hz, 1H), 7.63 (d, J = 15.9 Hz, 1H), 7.57 (d, J = 6.2 Hz, 2H), 7.32 (dd, J_1 = 8.0 Hz, J_2 = 2.1 Hz, 2H), 7.20 (d, J = 8.9 Hz, 4H), 7.18-7.12 (m, 3H), 6.72 (d, J = 8.9 Hz, 2H), 6.68 (d, J = 8.9 Hz, 2H), 6.62 (dd, J_1 = 6.1 Hz, J_2 = 6.1 Hz, 1H), 4.73 (dt, J_1 = 6.8 Hz, J_2 = 5.1 Hz, 1H), 4.18-4.14 (m, 1H), 3.73 (s, 3H), 3.72 (s, 3H), 3.48 (ddd, J_1 = 13.3 Hz, J_2 = 6.8 Hz, J_3 = 6.5 Hz, 1H), 3.38 (dd, J_1 = 10.2 Hz, J_2 = 6.5 Hz, 1H), 3.30 (dd, J_1 = 10.2 Hz, J_2 = 3.2 Hz, 1H), 2.73 (sept, J = 6.8 Hz, 1H), 2.44 (ddd, J_1 = 13.3 Hz, J_2 = 6.8 Hz, J_3 = 4.8 Hz, 1H), 1.26 (d, J = 6.8 Hz, 3H), 1.25 (d, J = 6.8 Hz, 3H). **^{13}C-NMR** (100 MHz, d_4-MeOH) δ 181.8, 160.1, 160.0, 157.2, 150.8, 150.7, 150.2, 149.0, 148.9, 146.4, 145.6, 138.5, 137.2, 137.1, 134.2, 131.4, 131.2, 129.4, 128.7, 127.9, 125.7, 123.2, 122.3, 120.6, 114.0, 113.9, 88.0, 87.4, 86.0, 72.7, 65.4, 55.8, 55.7, 39.3, 37.0, 19.7, 19.5, 9.4. **HR-ESI MS** (m/z): $[M+H]^+$ calcd for $C_{42}H_{42}N_6O_7$, 743.3188; found 743.3179.

8.2.41 (*E*)-$O^{3'}$-[(2-cyanoethoxy)(diisopropylamino)phosphino]-$O^{5'}$-dimethoxytrityl-N^2-isobutyryl-8-[2-(pyrid-4-yl)-ethenyl]-2'-deoxyguanosine (42)

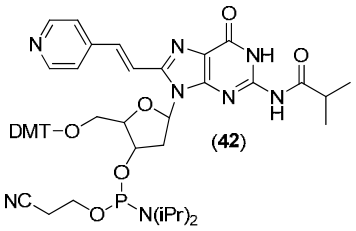

Compound **41** (50 mg, 0.07 mmoles) was added to a dry flask and dissolved into dry dichloromethane (0.4 mL). Diisopropylethylamine (48.4 mg, 64.2 uL, 0.37 mmoles) was added, followed by 2-cyanoethyl *N,N*-diisopropyl-chlorophosphoramidite (27 mg, 25.4 uL, 0.11 mmoles). The reaction was stirred in the dark at room temperature. After 1.5 hour, the reaction mixture was directly filtered over a short silica gel plug using a rapid flow rate (DCM:MeOH:Et_3N 95:5:0.5). After concentrating *in vacuo*, the resulting oil was dissolved in ethyl acetate and precipitated with hexane. The solvent was removed and the compound dried to yield 52 mg (82 %) of a yellow solid. **^{31}P-NMR** (162 MHz, $CDCl_3$) δ 149.4, 148.8. **HR-ESI MS** (*m*/*z*): $[M+H]^+$ calcd for $C_{51}H_{59}N_8O_8P$, 943.4266; found 943.4247.

8.3 Oligonucleotides synthesis

The wild-type sequences and T mutants were obtained from Sigma-Aldrich as HPLC purified products. The sequences containing **2AP** were obtained from IDT (Integrated DNA Technologies, Coralville, USA) HPLC purified. **2PyG-**, **StG-** and **4PVG**-modified oligonucleotides were synthesized on a 1 μmol scale using a Millipore Expedite 8909 DNA synthesizer according to the standard Trityl-off procedure, except that 5% dichloroacetic acid in CH_2Cl_2 was used for Trityl deprotection. Manual coupling reactions were used for the site-specific introduction of **2PyG, StG** and **4PVG** into oligonucleotides. The phosphoramidites (0.02 mmoles) were dissolved into 200 μL of 0.25 M 5-ethylthio-(1*H*)-tetrazole in dry acetonitrile and added to DNA columns *via* syringe for 10 minutes. The column was then returned to the automated synthesizer for the standard oxidation and capping steps. Upon completion of the sequence, the oligonucleotide was cleaved from the solid support and deprotected by treatment with 1.5 mL of 33% aqueous ammonium hydroxide at 55 °C for 17 hours in a 1.7 mL screw-top cap tube. The resulting products were lyophilized, and HPLC-purified with a C-18 reverse-phase column (YMCbasic B-22-10P 150 x 10 mm) using a *Varian Pro Star* HPLC system. Gradient conditions were typically 5 – 20% acetonitrile over 25 minutes at 3 mL/min in 0.1 M triethylammonium acetate (pH 7.0). Peaks were collected and lyophilized to dryness. Oligonucleotide stock solutions were prepared in pure water and quantified using the following molar extinction coefficients that were assumed to be equal for the wild-type and modified sequences at

260 nm: ε(hTelo) = 244’300 $cm^{-1}M^{-1}$; ε(cKit) = 226’700 $cm^{-1}M^{-1}$; ε(cMyc) = 228’700 $cm^{-1}M^{-1}$; ε(TGGGT) = 47’700 $cm^{-1}M^{-1}$; **MALDI-TOF MS** hTeloG9(2PyG) (*m*/*z*) calcd, 7651.4; found 7650.5; hTeloG17(2PyG) (*m*/*z*) calcd, 7651.4; found 7650.4; hTeloG23(2PyG) (*m*/*z*) calcd, 7651.4; found 7649.5; cKitG10(2PyG) (*m*/*z*) calcd, 7088.4; found 7089.2; cKitG15(2PyG) (*m*/*z*) calcd, 7088.4; found 7086.3; cMycG8(2PyG) (*m*/*z*) calcd, 7068.4; found 7059.9; T1: T(2PyG)GGT (*m*/*z*) calcd, 1611.0; found 1602.8; T2: TGG(2PyG)T (*m*/*z*) calcd, 1611.0; found 1603.5; hTeloG9(StG) (*m*/*z*) calcd, 7676.4; found 7684.5; hTeloG23(StG) (*m*/*z*) calcd, 7676.4; found 7678.4; cKitG10(StG) (*m*/*z*) calcd, 7114.4; found 7113.5; hTeloG9(4PVG) (*m*/*z*) calcd, 7677.4; found 7680.4; hTeloG23(4PVG) (*m*/*z*) calcd, 7677.4; found 7677.8; cKitG10(4PVG) (*m*/*z*) calcd, 7115.4; found 7113.9;.

8.4 DNA folding and buffer conditions

The folding of single-stranded oligonucleotides was controlled by variation of alkali metal salts in the buffer. Due to their small size and large desolvation energies, lithium ions are not normally compatible with G-tetrad formation. The same is true for large bulky cations such as tris(hydroxymethyl)-aminomethane (Tris) or tetrabutylammonium salts. For hTelo, cKit and cMyc-oligonucleotides, unfolded samples were prepared in the presence of 100 mM LiCl or 100 mM Tris. Duplex DNA samples were prepared in the presence of 100 mM NaCl and 1.1 equivalents of the complementary strand. Single-stranded G-quadruplex structures were prepared in 100 mM of NaCl, KCl, RbCl or NH_4Cl containing buffers or 40% PEG 200-containing solution. Buffers were prepared as 10 mM cacodylic acid solutions containing the indicated salt, and the pH was adjusted to 7.4 by neutralization with KOH (potassium cacodylate), NaOH (sodium cacodylate), LiOH (lithium cacodylate) or Tris (“no salt”). The buffers had the following composition: (K^+): 10 mM potassium cacodylate buffer, 100 mM KCl; (Na^+): 10 mM sodium cacodylate buffer, 100 mM NaCl; (Li^+): 10 mM lithium cacodylate buffer, 100 mM LiCl; (Rb^+): 10 mM lithium cacodylate buffer, 110 mM RbCl; (NH_4^+): 10 mM lithium cacodylate buffer, 110 mM NH_4Cl; (No salt): 10 mM Tris cacodylate buffer; (PEG): 10 mM lithium cacodylate buffer, 40% (w/v) PEG 200; (PEG & Na^+): 10 mM sodium cacodylate buffer, 100 mM NaCl, 40% (w/v) PEG 200. Oligonucleotide stock solutions prepared in water were diluted into the desired buffer to the final concentration, heated for 5 minutes at 95 °C, and slowly cooled to room temperature overnight before use.

The rate of association of tetramolecular G-quadruplexes is highly dependent on oligonucleotide concentration, temperature, and ionic strength among others.[316] To accelerate the association of TGGGT, T1 and T2, those samples were prepared to a oligonucleotide concentration of 100 μM in 10 mM cacodylate buffer containing 500 mM KCl or LiCl. The samples were heated for 5 minutes at 95 °C and slowly cooled to room temperature overnight and finally incubated for 4 days at 4 °C. The samples were diluted 5-fold with buffer before use, to reach a final strand concentration of 20 μM in 100 mM KCl or LiCl for circular dichroism and photophysical measurements. Under these conditions, in K^+-containing solutions, over 90% of the strands should be associated in G-quadruplex.[316]

8.5 Absorption and fluorescence measurements

8.5.1 Photophysical characterization of 8-substituted-2'-deoxyguanosines

For all experiments, fluorescent nucleosides were stored and used as 10 mM DMSO-stock solutions and stored at -20 °C. For all values reported, final DMSO concentrations after dilution were always less than 0.1%. Absorbance and emission spectra were collected using a Molecular Devices Spectra Max M5 spectrophotometer and measured in a quartz cuvette (1 cm). Molar extinction coefficient measurements were conducted in 96-well plates in H_2O containing 1X PBS buffer (pH 7.0). Quantum yield measurements, were performed in a quartz cuvette (1 cm). Optical densities were adjusted to 0.1 ± 0.01 at the indicated λ_{ex} of each nucleoside and corresponding standard. 2-aminopyridine in 0.1 N H_2SO_4 (Φ = 0.6) was used as the standard for **2PyG, 3PyG, 4PyG, ThG, FuG, ViG** (λ_{ex} = 300 nm), and 2-aminopurine (λ_{ex} = 305 nm). Quinine sulfate in 0.1 M H_2SO_4 (Φ = 0.56) was used as a reference for **StG, 3PVG** (λ_{ex} = 340 nm) and **4PVG** (λ_{ex} = 355 nm). Quantum yields were calculated as described, according to:[201]

$$\Phi = \Phi_R \frac{F}{F_R} \frac{A_R}{A} \frac{n^2}{n_R^2} \qquad \text{(eq. 8.1)}$$

where Φ_R is the quantum yield of the reference, F and F_R are the integrated emission intensities of the probe and the reference respectively. A and A_R are the optical densities of the probe and the reference respectively. n and n_R are the refractive indexes of the solvent in which the measurement was performed for the probe and the reference respectively ($n_{(H2O)}$ = 1.333; $n_{(MeCN)}$ = 1.344; $n_{(MeOH)}$ = 1.328; $n_{(Dioxane)}$ = 1.422; $n_{(DMSO)}$ = 1.479; $n_{(EtOH)}$ =

1.364). Reported quantum yields are reproducible within a standard deviation of approximately 10%.

8.5.2 GMP titrations

GMP titrations were performed in 96-well plates in 10 mM lithium cacodylate buffer (pH 7.4). 10 mM stock solutions of **2PyG** and **2AP** in DMSO were used to reach a final nucleoside concentration of 100 μM. A 1 M stock solution of guanosine 5'-monophosphate disodium salt hydrate ≥ 99% (Sigma-Aldrich) (GMP) prepared in 10 mM lithium cacodylate buffer (pH 7.4) was used for the titrations. *Stern-Volmer* plots were obtained by plotting F_0/F as a function of the concentration, where F_0 and F are the fluorescence intensities of the nucleosides in the absence and presence of GMP respectively. Excitation was performed at 325 nm for both nucleosides and emission was recorded at 415 and 370 nm for **2PyG** and **2AP** respectively. Average of three measurements was reported. *Stern-Volmer* plot for **2PyG** is accurate in the 0 – 400 mM GMP range only due to the significant red-shift of the excitation peak observed above these concentrations. Excitation spectra were measured by recording the fluorescence at 415 nm for both nucleosides. The raw fluorescence intensities $F_{raw}(\lambda_{ex})$ were corrected with the correction factor CF (eq. 8.2). At high GMP concentrations the absorbance around 260 nm was out of the linear range of the detector. Therefore, correction of the fluorescence signal with CF (eq. 8.2) was not possible for excitation wavelengths below 310 nm.

8.5.3 Photophysical characterization of modified oligonucleotides

Quantum yields of each probe in the context of oligonucleotides were determined as described above except that the corresponding nucleosides in water were used as references. The following wavelengths of excitation were used: 310 nm for **2AP-**, 330 nm for **2PyG-**, 360 nm for **StG-**, and 375 nm for **4PVG-**modified oligonucleotides. The excitation spectra of each probe in the context of DNA were collected using the following wavelengths of emission: 370 nm for **2AP**, 415 nm for **2PyG**, 450 nm for **StG**, and 475 nm for **4PVG**. All fluorescence spectra were measured using 2 μM solutions of pre-folded DNA for hTelo, cKit, cMyc-derived oligonucleotides, and 20 μM solutions for TGGGT, T1 and T2. This allowed for direct comparisons of CD and fluorescence spectra. The relatively high absorbance of DNA samples at 260 nm (~ 0.4 AU) caused a significant attenuation of the excitation beam that reduced the fluorescence intensities from each probe. This was evidenced by non-linear relationships between raw fluorescence intensities $F_{raw}(\lambda_{ex})$ and DNA concentrations above 50 nM when samples were photoexcited at

260 nm (Figure 6.4). $F_{raw}(\lambda_{ex})$ values at each excitation wavelength λ_{ex} were therefore corrected by multiplication with the following correction factor (CF) to obtain corrected $F(\lambda_{ex})$ values. Where $A(\lambda_{ex})$ is the absorbance of the sample at each wavelength of excitation.

$$CF = \frac{2.303 * A(\lambda_{ex})}{1 - 10^{-A(\lambda_{ex})}} \qquad \text{(eq. 8.2)}$$

To check the validity of this approach, serial dilutions of **StG**-containing duplex and G-quadruplex DNAs were analyzed for fluorescence intensity as a function of sample concentration (Figure 6.4). When the samples were excited at 260 nm, linear relationships were observed only after the application of the CF in eq. 8.2 (Figure 6.4 A & B). At DNA concentrations of 50 nM and below, the fluorescence intensities and F(260)/F(X) ratios for the CF-corrected and uncorrected fluorescence measurements converged to the same values due to the low absorbance of the samples. These results validate the use of eq. 8.2. It should be emphasized that this CF is not needed for dilute DNA samples (< 50 nM) having minimal optical densities (OD $\leq$ 0.01) at 260 nm. All reported energy transfer efficiencies, excitation and emission spectra (λ_{ex} = 260 nm) were corrected using CF.

8.5.4 Emission spectra of unmodified oligonucleotides

Emission spectra of unmodified hTelo (Figure 5.3) were recorded on an Edinburgh FLS920 spectrophotometer, using 450W Xenon lamp excitation, 3 nm excitation and 3 nm emission slit widths. Measurements were performed in a 1x1 cm fluorescence cuvette. 4 µM DNA samples were prepared as mentioned before in PEG or PEG & Na^+ buffers. The non-interacting nucleotides sample was prepared in 10 mM lithium cacodylate buffer, containing 40% (w/v) PEG 200 as follows: 16 µM 2'-deoxyadenosine-5'-monophosphate, 32 µM thymidine-5'-monophosphate disodium salt hydrate, 48 µM 2'-deoxyguanosine-5'-monophosphate sodium salt hydrate.

8.5.5 Energy transfer efficiencies calculations

Energy transfer efficiencies were calculated according to the method reported by Xu and Nordlund.[145] The transfer efficiency at any given excitation wavelength (λ_{ex}) is defined as $\eta_t(\lambda_{ex})$ as shown in equation 8.3.

$$\eta_t(\lambda_{ex}) = \frac{A_a(\lambda_{ex})}{A_d(\lambda_{ex})} \left(\frac{F(\lambda_{ex})}{F_a(\lambda_{ex})} - 1 \right) \qquad \text{(eq. 8.3)}$$

Where $A_a(\lambda_{ex})$ is the contribution of the acceptor (fluorescent probe) to the absorbance at wavelength λ_{ex}, $A_d(\lambda_{ex})$ is the contribution of the donor residues (unmodified DNA bases) to the absorbance at wavelength λ_{ex}. $F(\lambda_{ex})$ is the fluorescence intensity of the modified oligonucleotide upon excitation at wavelength λ_{ex} and $F_a(\lambda_{ex})$ is the contribution of the acceptor (only) to the fluorescence intensity obtained upon excitation at wavelength λ_{ex}. Unless stated otherwise, λ_{ex} was set to 260 nm and fluorescence intensities were measured at 370 nm for **2AP**, 415 nm for **2PyG**, 450 nm for **StG** and 475 nm for **4PVG**. The absorbance $A_a(\lambda_{ex})$ and fluorescence $F_{a,raw}(\lambda_{ex})$ of the acceptor were obtained by measuring the absorption and emission spectra of nucleoside monomer solutions of the same concentration as the probes in DNA oligonucleotides. The actual contribution of the acceptor to the fluorescence intensity of the probe-modified oligonucleotide, $F_a(\lambda_{ex})$, was calculated by multiplication of the measured fluorescence $F_{a,raw}(\lambda_{ex})$ by the factor: Φ(probe monomer) / Φ(probe in the oligo) to account for the differences in quantum yields of probes in each DNA as compared to the monomer. Quantum yields (Φ) were measured by direct excitation of the probes (λ_{ex} = 310 nm for **2AP-**, 330 nm for **2PyG-**, 360 nm for **StG-**, and 375 nm for **4PVG-**modified oligonucleotides) as described above. For fully aqueous solutions, the $A_a(\lambda_{ex})$ and $F_{a,raw}(\lambda_{ex})$ were measured in solutions of the probes in water (Φ(**2AP** monomer) = 0.68; Φ(**2PyG** monomer) = 0.023; Φ(**StG** monomer) = 0.49; Φ(**4PVG** monomer) = 0.16). For PEG containing solutions, those values were determined on **2PyG** solutions in 10 mM lithium cacodylate with 40% (w/v) PEG 200 (Φ(**2PyG** monomer) = 0.25). The absorbance of donor $A_d(\lambda_{ex})$ at wavelength λ_{ex} was calculated by subtracting the absorbance of the probe at λ_{ex} ($A_a(\lambda_{ex})$) from the absorbance of the modified DNA oligonucleotides at λ_{ex} ($A(\lambda_{ex})$). The measured fluorescence intensities $F_{raw}(\lambda_{ex})$ at each excitation wavelength λ_{ex} were corrected by the correction factor (CF) (eq. 8.2) to get the corrected $F(\lambda_{ex})$ values. All measurements were performed with 2 μM (hTelo, cKit, cMyc) or 20 μM (TGGGT, T1, T2) solutions of pre-folded oligonucleotides prepared as described above.

8.6 Circular dichroism (CD)

8.6.1 CD spectra

CD spectra were collected on a Jasco model J-715 spectropolarimeter equipped with a Julabo FS 18 temperature control system and a 1 cm path length thermo-controlled CD quartz cell. Spectra were collected at 25 ^{o}C between 220 and 400 nm with 0.1 nm steps,

2 nm band width, and scanning rate of 50 nm/min. Solutions of 2 μM (hTelo, cKit, cMyc) or 20 μM (TGGGT, T1, T2) of pre-folded oligonucleotides (same sample as used for fluorescence and energy transfer measurements) were measured at 25 °C. Three scans were averaged for each reported spectrum. For the metal containing samples, 1 μM $CuCl_2$ was added to 1 μM solutions of pre-folded DNA and incubated for 2 hours at room temperature prior to collecting spectra.

8.6.2 Thermal denaturation studies

CD melting experiments were carried out on a Jasco model J-715 spectropolarimeter equipped with a Julabo FS 18 temperature control system and a 1 cm path length thermo-controlled CD quartz cell. 2 μM (hTelo, cKit or cMyc derivatives) or 20 μM (TGGGT analogs) solutions of pre-folded DNA were equilibrated for 15 minutes at 10 °C and slowly ramped to 95 °C at a rate of 30 °C/h. Under these conditions, some of the PEG containing samples exhibited multiphasic thermal denaturation curves. To overcome the slow kinetics of PEG-mediated folding, unfolded oligonucleotides solutions were added to the thermo-controlled CD quartz cell preheated to 95 °C. After 1 minutes of incubation, the temperature was slowly decreased to 10 °C at a rate of 10 °C/h, followed by 1 hour of incubation at 10 °C. The melting temperature was then determined by increase of the temperature up to 95 °C at a rate of 10 °C/h. The slow temperature gradients used for the PEG containing samples significantly improved the quality of the melting temperature data, giving monophasic melting curves, but did not change the fluorescence properties of the PEG-folded samples. The ellipticity of each sample was monitored at 290 nm for the hTelo derived G-quadruplexes and 260 nm for the cKit, cMyc, TGGGT-derived G-quadruplexes and the corresponding duplexes. Reverse temperature scans showed no hysteresis for the unimolecular G-quadruplexes and the corresponding duplexes. Denaturation of the TGGGT-derived tetramolecular G-quadruplex was indeed irreversible.[316] After baseline and pre-melting corrections, T_m values were determined using non-linear regression. T_m values were reproducible within ± 1.0 ˚C of the reported values. For the metal containing samples, 1 μM $CuCl_2$ was added to 1 μM solutions of pre-folded DNA and incubated were equilibrated for 2 hours at room temperature, and 15 minutes at 10 °C, then slowly ramped to 95 °C at a rate of 30 °C/h. The ellipticity of each sample was monitored at 260 nm. T_m values were determined using non-linear regression of the raw data. T_m values were reproducible within ± 1.0 ˚C of the reported values.

8.7 Metal binding studies

8.7.1 Nucleoside metal binding studies

Absorption and fluorescence measurements conducted in the presence of metals were performed using 50 μM nucleoside solutions in 96-wells Greiner Star plate containing 50 mM Tris (pH 7.4) and measured with a Molecular Devices Spectra Max M5 spectrophotometer. After the addition of metal ions to a final concentration of 10 mM the plates were sealed and incubated for 3 hours prior to measuring fluorescence. The following metal salts were used: $CuCl_2$, $NiCl_2$, $PdCl_2(CH_3CN)_2$, $Hg(OAc)_2$, $ZnCl_2$ and $CdCl_2$. Fluorescence emission spectra were normalized for optical density at the excitation wavelength of 320 nm. Metal titrations to determine **2PyG** K_d values were performed under the same conditions except that the final **2PyG** concentration was 25 μM.

8.7.2 Metal ion – 2PyG-DNA titrations

Titrations were performed in Corning 384-well black plates. 2 μM solutions of DNA were folded in buffer as described above, diluted to a final DNA concentration of 200 nM in an aqueous buffer of 10 mM potassium cacodylate / 100 mM KCl (G-quadruplex samples) or 10 mM sodium cacodylate / 100 mM NaCl (duplex samples), (pH 7.4) and mixed with metal ions. While rapid equilibrium was typically observed after only 10 – 20 minutes, all metal-containing samples were incubated for 3 hours prior to quantification of fluorescence with excitation at 310 – 320 nm.

For high DNA concentrations copper titrations, 2 μM solutions of DNA was pre-folded in buffer as described above. The samples was then transferred to a 1 cm path length fluorescence quartz cuvette. Small quantities of $CuCl_2$ were then sequencially added. The mixtures were equilibrated for 20 minutes at room temperature prior to quantification of fluorescence. Excitation and emission wavelengths were λ_{ex} = 325 nm and λ_{em} = 415 nm, respectively.

APPENDIXES

Appendix A.1. Circular dichroism spectra, comparison of the impact of **2PyG** and **2AP** on the global DNA structures (Chapter 4).

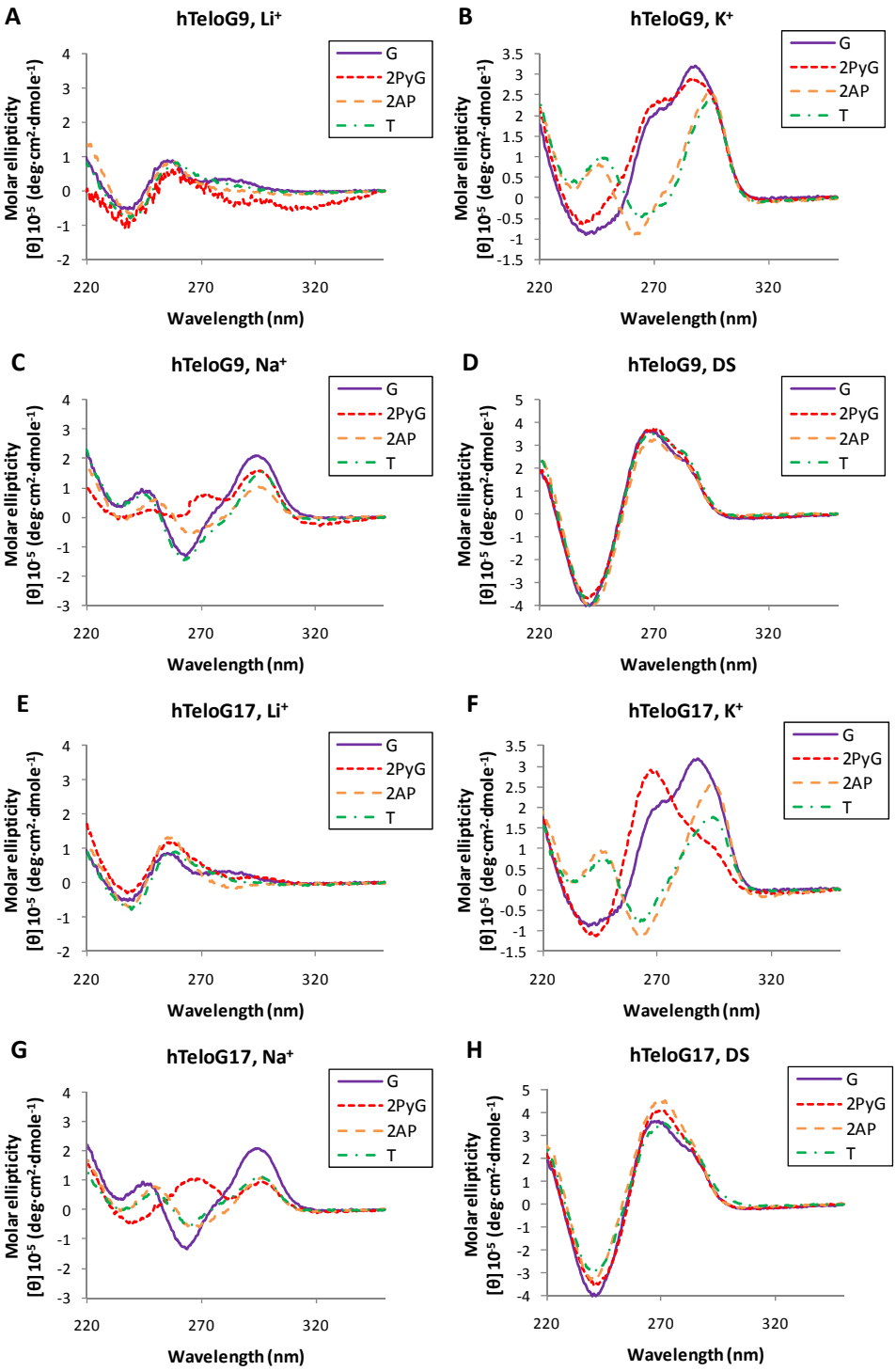

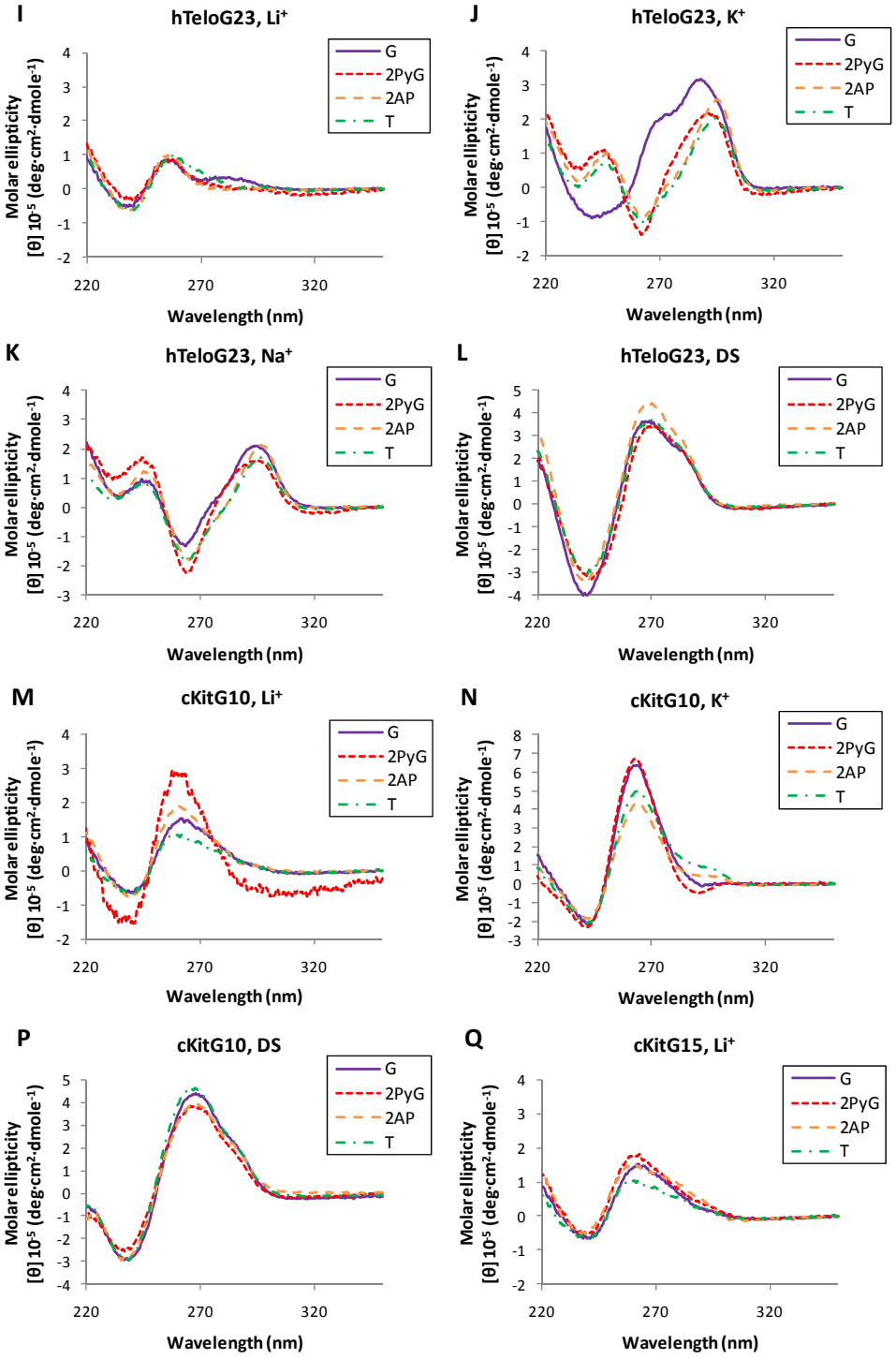
I
hTeloG23, Li+
J
hTeloG23, K+
K
hTeloG23, Na+
L
hTeloG23, DS
M
cKitG10, Li+
N
cKitG10, K+
P
cKitG10, DS
Q
cKitG15, Li+
G
2PyG
2AP
T
Molar ellipticity
[θ] 10-5 (deg·cm2·dmole-1)
Wavelength (nm)
220
270
320

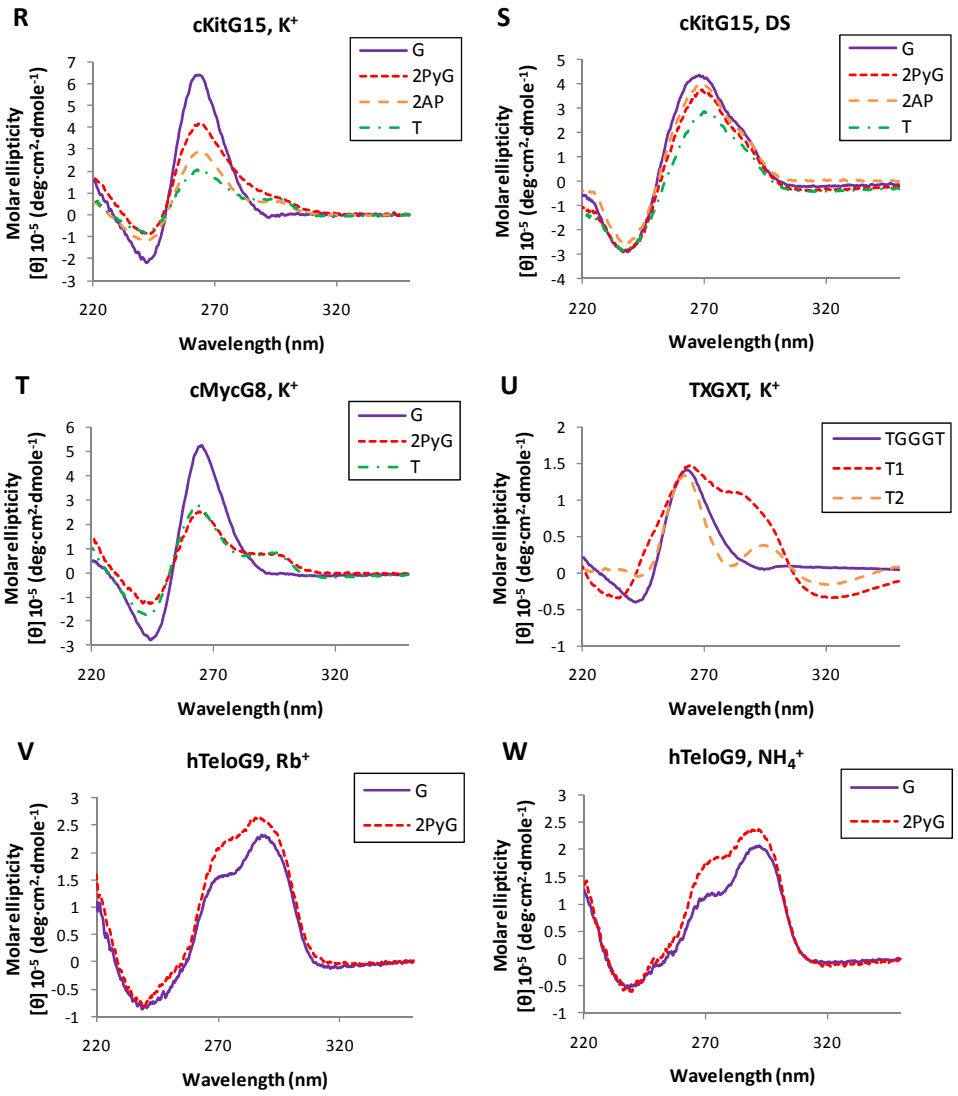

Figure A.1: CD spectra of hTeloG9 (A-D), hTeloG17 (E-H), hTeloG23 (I-L), cKitG10 (M-P), cKitG15 (Q-S), substituted with G, **2PyG**, **2AP** or T in 100 mM LiCl (Li^+), 100 mM KCl (K^+), 100 mM NaCl (Na^+) or including 1.1 equivalents of the complementary strand in 100 mM NaCl (DS). CD spectra of cMycG8 (T) substituted with G, **2PyG** or T in 100 mM KCl, TXGXT derivatives TGGGT, T1 and T2 in 100 mM KCl (U). CD spectra of hTeloG9 substituted with G or **2PyG**, in 110 mM RbCl (Rb^+) (V) or 110 mM NH_4Cl (NH_4^+) (W). All single-stranded G-quadruplexes contained 2 µM of DNA in an aqueous 10 mM cacodylate buffer (pH 7.4), TGGGT, T1 and T2 samples contained 20 µM of the oligonucleotide in an aqueous 10 mM cacodylate buffer (pH 7.4).

Appendix A.2. Circular dichroism spectra, comparison of the impact of **2PyG**, **StG** and **4PVG** on the global DNA structures (Chapter 6).

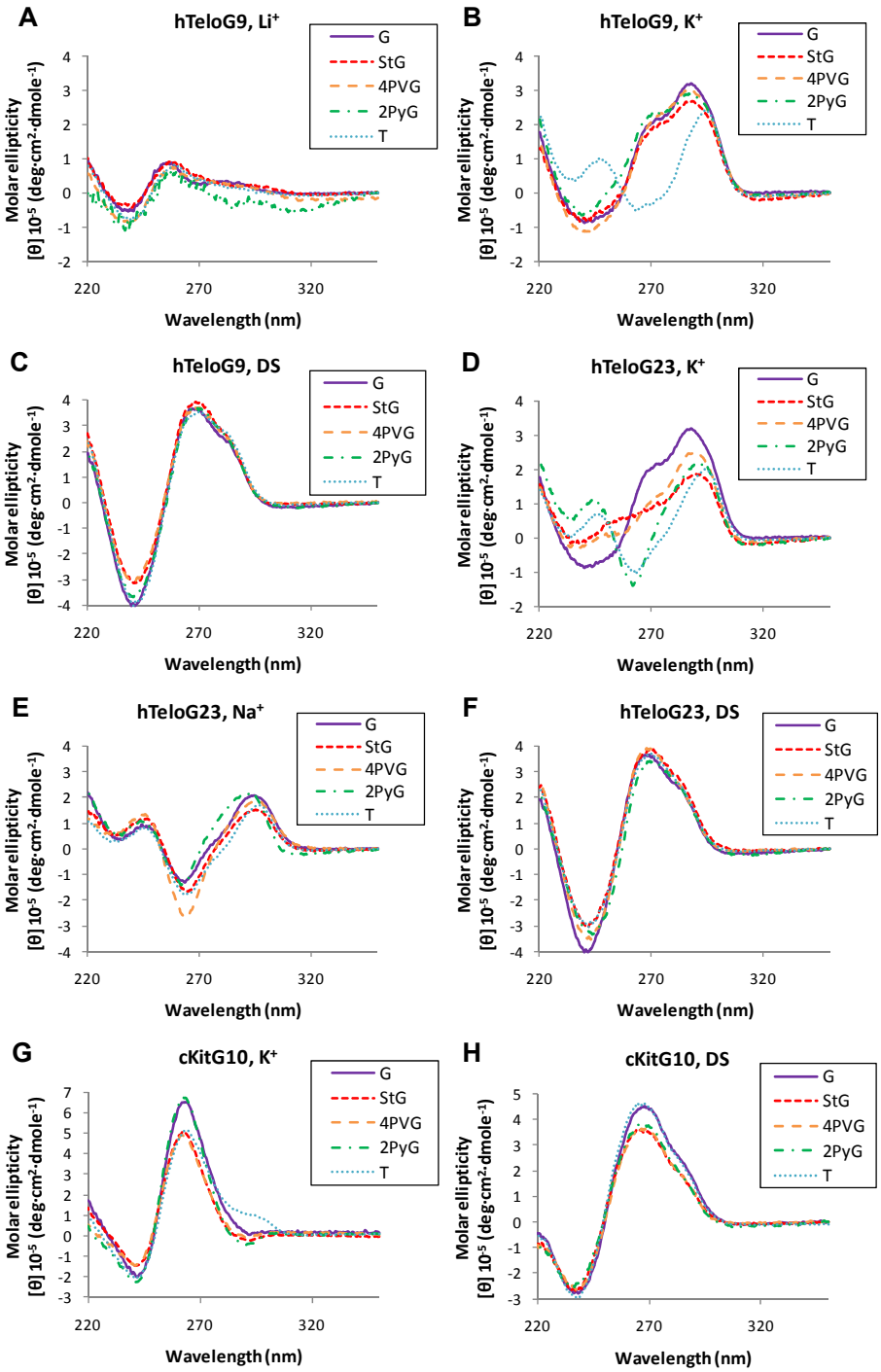

Figure A.2: CD spectra of hTeloG9 (A-C), hTeloG23 (D-F), cKitG10 (G-H) substituted with G, **StG**, **4PVG**, **2PyG** or T in 100 mM KCl (K^+), 100 mM NaCl (Na^+) or including 1.1 equivalents of the complementary strand in 100 mM NaCl (DS). All samples contained 2 μM of DNA in an aqueous 10 mM cacodylate buffer (pH 7.4).

Appendix A.3. Fluorescence of **2PyG** and **2AP** in the context of DNA, emission spectra (Chapter 4).

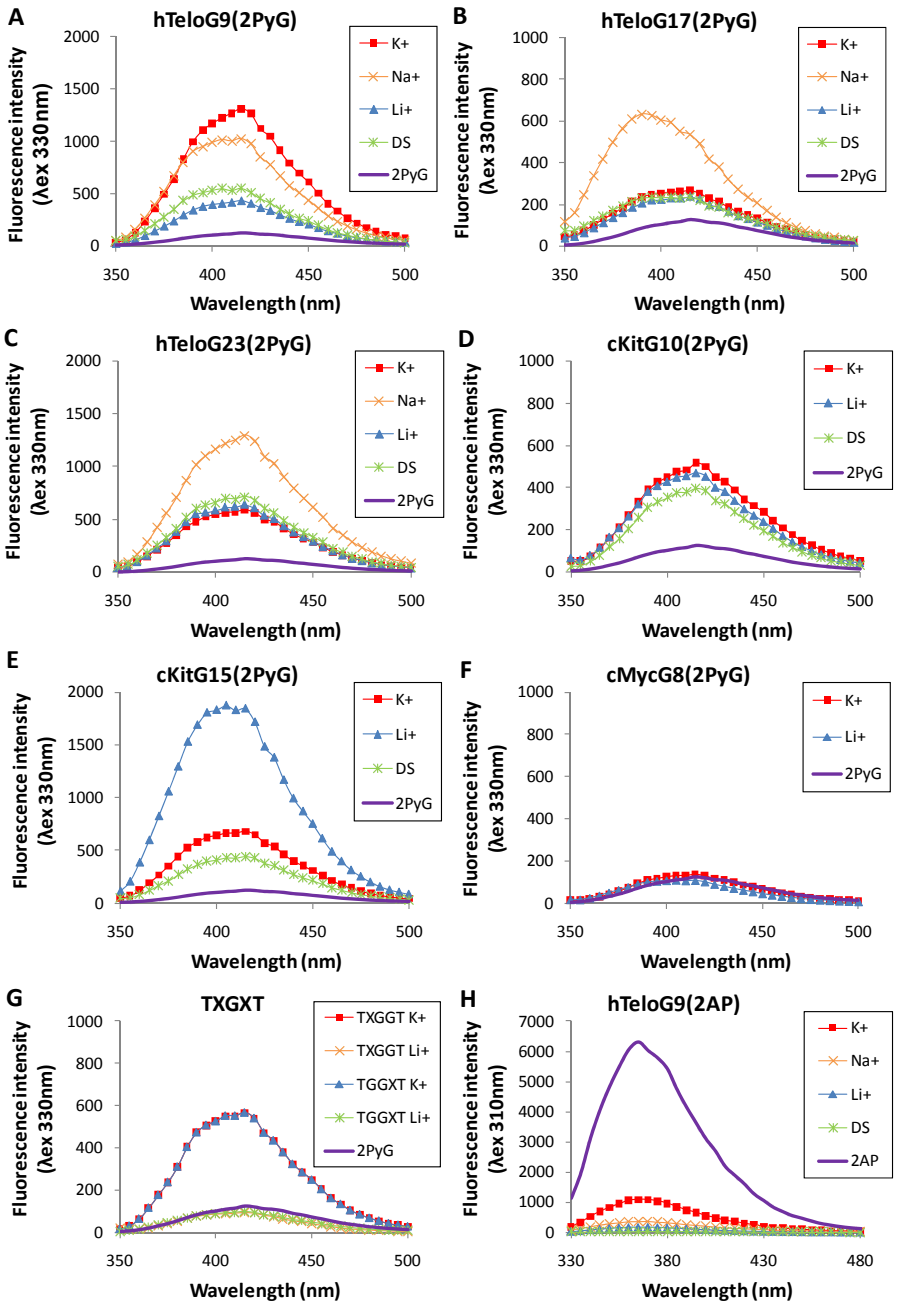

Figure A.3: Fluorescence spectra of the free nucleosides **2PyG** or **2AP** compared to hTeloG9(2PyG) (A), hTeloG17(2PyG) (B), hTeloG23(2PyG) (C), cKitG10(2PyG) (D), cKitG15(2PyG) (E), cMycG8(2PyG) (F), TXGXT (G) and hTeloG9(2AP) (H) in 100 mM KCl (K^+), 100 mM NaCl (Na^+), 100 mM LiCl (Li^+) or 100 mM NaCl including 1.1 equivalents of the complementary strand (DS). (λ_{ex} = 330 nm for **2PyG** and 310 nm for **2AP** and related oligonucleotides).

Appendix A.4. Fluorescence of **2PyG** and **2AP** in the context of DNA, excitation and emission spectra (Chapter 5).

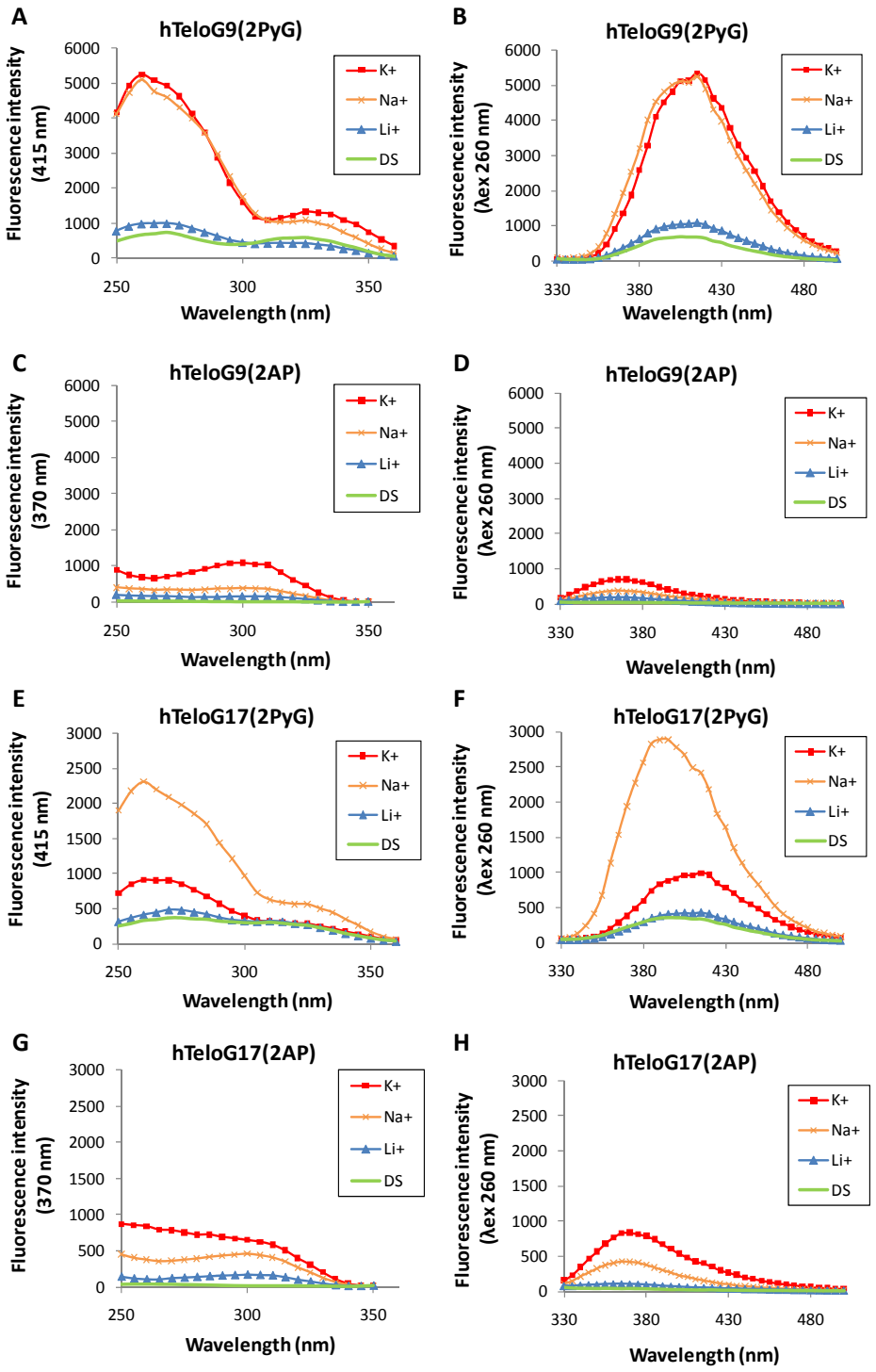

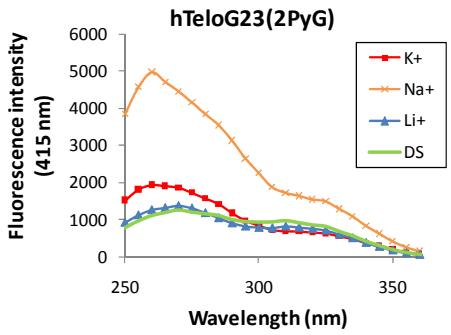
hTeloG23(2PyG)
Fluorescence intensity (415 nm)
Wavelength (nm)
K+
Na+
Li+
DS

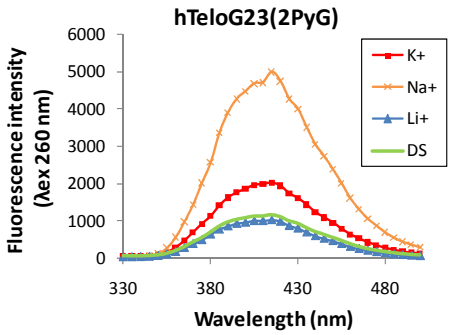
hTeloG23(2PyG)
Fluorescence intensity (λex 260 nm)
Wavelength (nm)
K+
Na+
Li+
DS

K

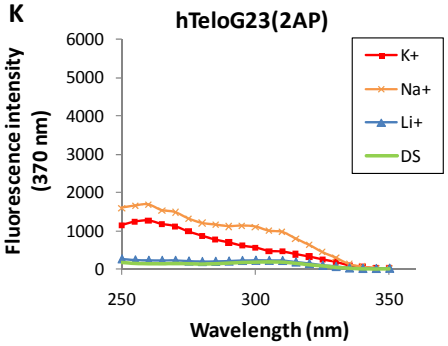
hTeloG23(2AP)
Fluorescence intensity (370 nm)
Wavelength (nm)
K+
Na+
Li+
DS

L

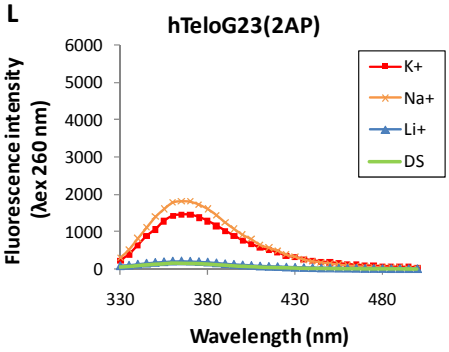
hTeloG23(2AP)
Fluorescence intensity (λex 260 nm)
Wavelength (nm)
K+
Na+
Li+
DS

M

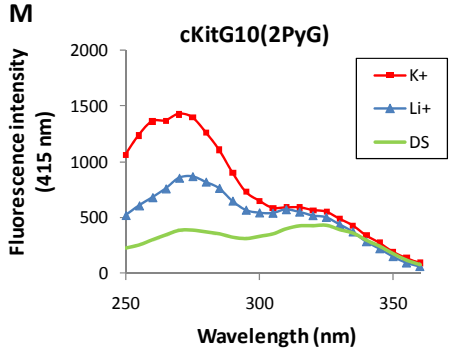
cKitG10(2PyG)
Fluorescence intensity (415 nm)
Wavelength (nm)
K+
Li+
DS

N

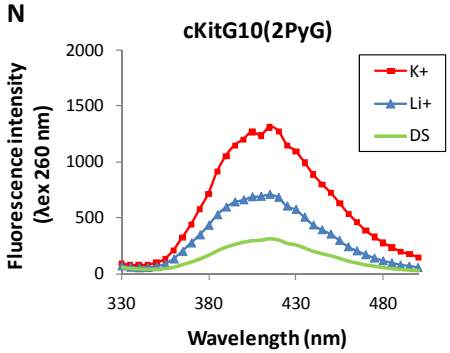
cKitG10(2PyG)
Fluorescence intensity (λex 260 nm)
Wavelength (nm)
K+
Li+
DS

O

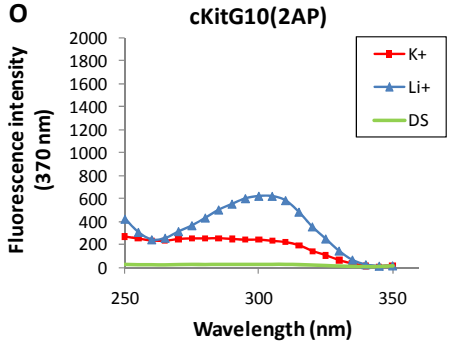
cKitG10(2AP)
Fluorescence intensity (370 nm)
Wavelength (nm)
K+
Li+
DS

P

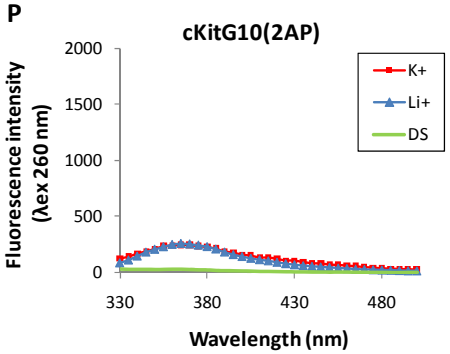
cKitG10(2AP)
Fluorescence intensity (λex 260 nm)
Wavelength (nm)
K+
Li+
DS

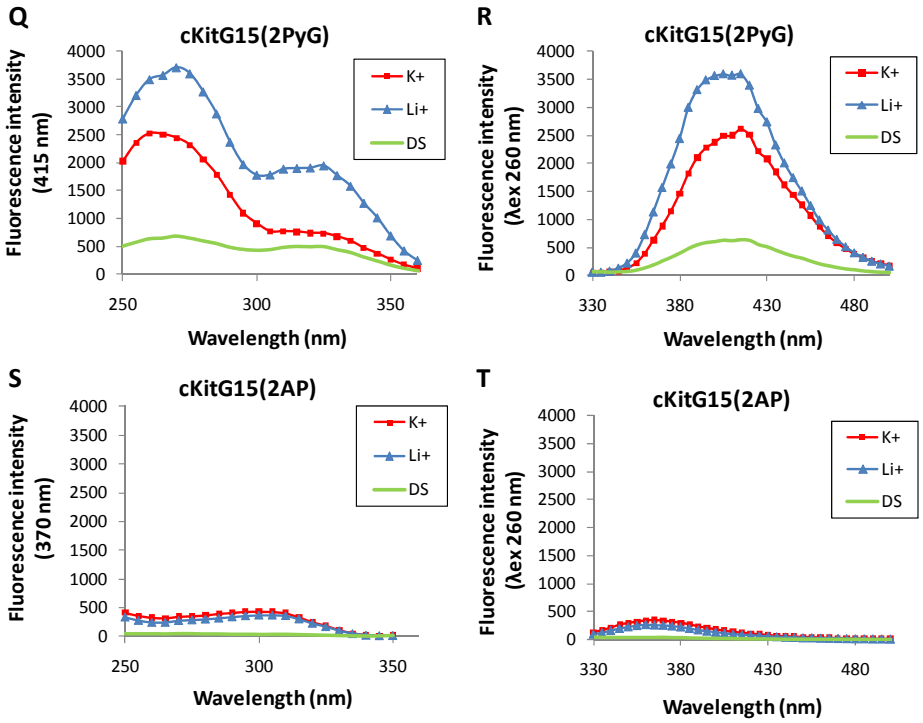

Figure A.4: Excitation spectra of hTeloG9(2PyG) (A), hTeloG9(2AP) (C), hTeloG17(2PyG) (E), hTeloG17(2AP) (G), hTeloG23(2PyG) (I), hTeloG23(2AP) (K), cKitG10(2PyG) (M), cKitG10(2AP) (O), cKitG15(2PyG) (Q), cKitG15(2AP) (S) in 100 mM KCl (K^+), 100 mM NaCl (Na^+), 100 mM LiCl (Li^+) or 100 mM NaCl double-stranded DNA sample (DS) containing 100 mM NaCl and 1.1 equivalents of the complementary strand. λ_{em} = 415 nm and 370 nm for **2PyG** and **2AP**-derived oligonucleotides respectively. Emission spectra of hTeloG9(2PyG) (B), hTeloG9(2AP) (D), hTeloG17(2PyG) (F), hTeloG17(2AP) (H), hTeloG23(2PyG) (J), hTeloG23(2AP) (L), cKitG10(2PyG) (N), cKitG10(2AP) (P), cKitG15(2PyG) (R), cKitG15(2AP) (T) collected using λ_{ex} = 260 nm in 100 mM KCl (K^+), 100 mM NaCl (Na^+), 100 mM LiCl (Li^+) or 100 mM NaCl double-stranded DNA sample (DS) containing 100 mM NaCl and 1.1 equivalents of the complementary strand. All samples contained 2 µM of DNA in an aqueous 10 mM cacodylate buffer (pH 7.4). Excitation spectra were collected using emission at 415 nm and 370 nm for **2PyG** and **2AP**, respectively.

Appendix A.5. Fluorescence of **2PyG**, **StG** and **4PVG** in the context of DNA, excitation and emission spectra (Chapter 6).

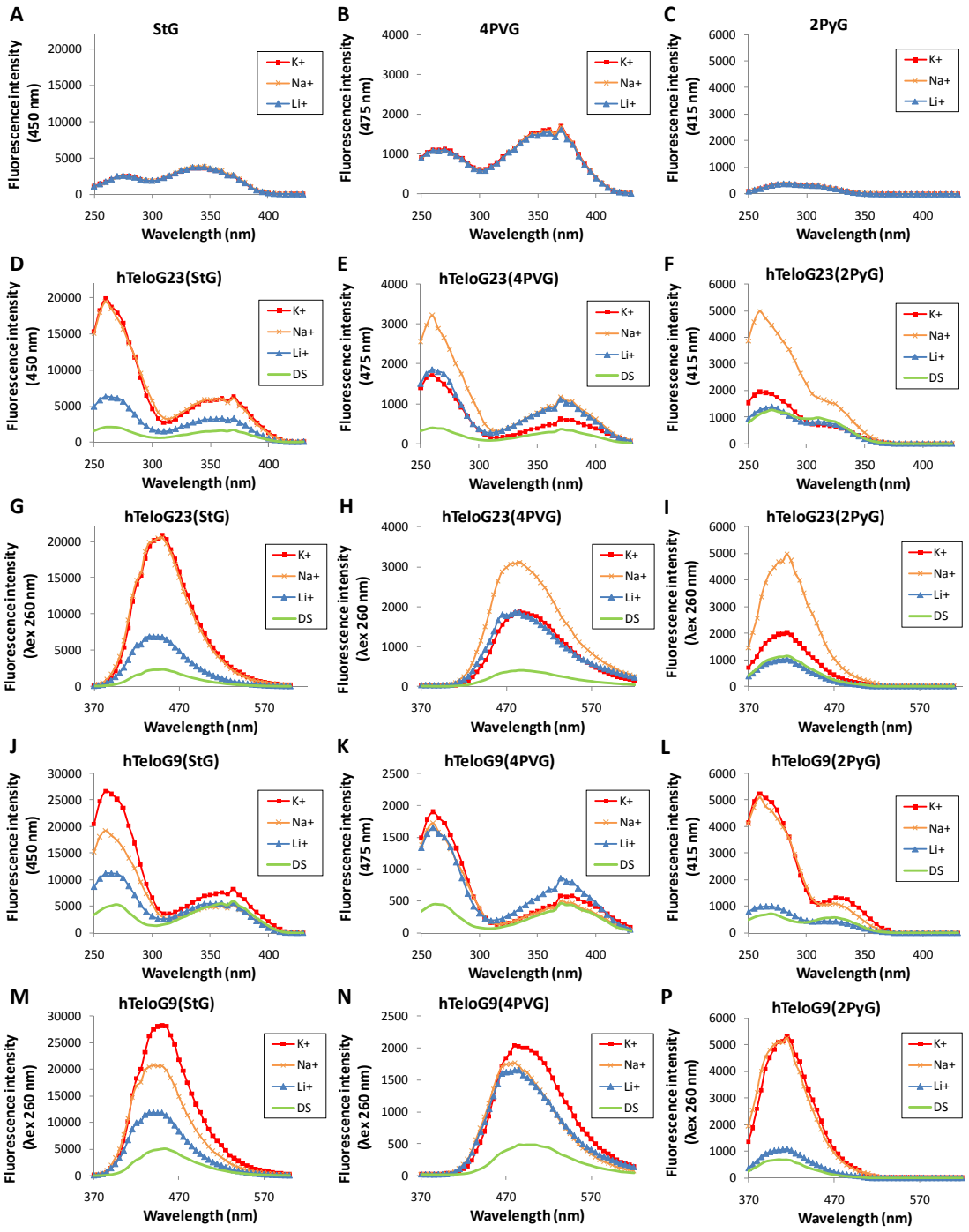

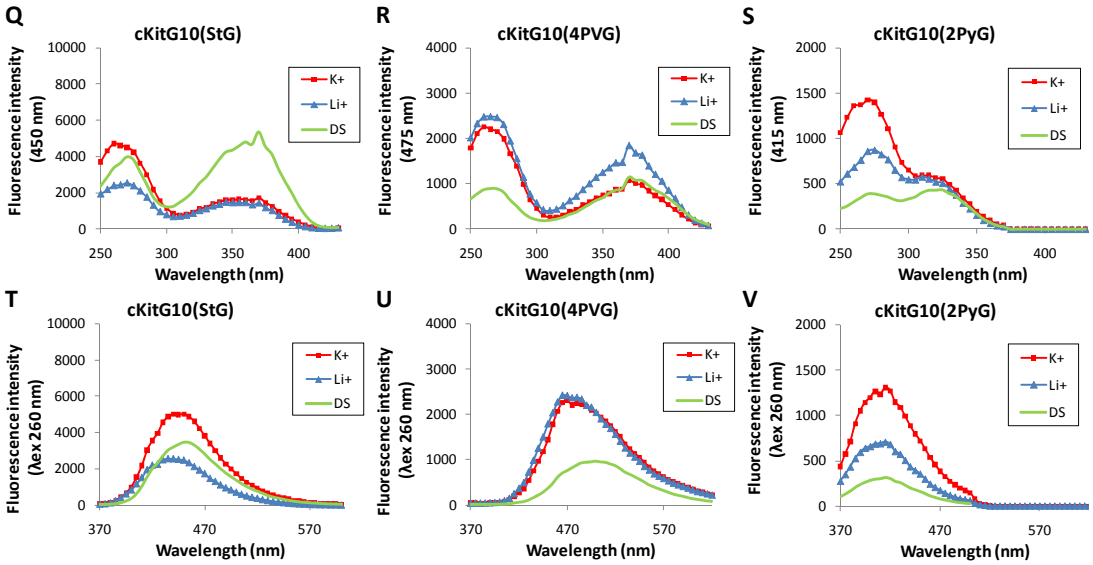

Figure A.5: Excitation spectra of 2 μM of **StG** (A), **4PVG** (B) or **2PyG** monomer (C) in the presence of 100 mM KCl (K^+), 100 mM NaCl (Na^+) or 100 mM LiCl (Li^+). Excitation spectra of hTeloG23(StG) (D), hTeloG23(4PVG) (E), hTeloG23(2PyG) (F), hTeloG9(StG) (J), hTeloG9(4PVG) (K) and hTeloG9(2PyG) (L), cKitG10(StG) (Q), cKitG10(4PVG) (R) and cKitG10(2PyG) (S) in 100 mM KCl (K^+), 100 mM NaCl (Na^+), 100 mM LiCl (Li^+) or 100 mM NaCl double-stranded DNA sample (DS) containing 100 mM NaCl and 1.1 equivalents of the complementary strand. λ_{em} = 450 nm (**StG**), 475 nm (**4PVG**) or 415 nm (**2PyG**). Emission spectra of hTeloG23(StG) (G), hTeloG23(4PVG) (H), hTeloG23(2PyG) (I) hTeloG9(StG) (M), hTeloG9(4PVG) (N) and hTeloG9(2PyG) (P), cKitG10(StG) (T), cKitG10(4PVG) (U) and cKitG10(2PyG) (V) collected using excitation at 260 nm in 100 mM KCl (K^+), 100 mM NaCl (Na^+), 100 mM LiCl (Li^+) or 100 mM NaCl double-stranded DNA sample (DS) containing 100 mM NaCl and 1.1 equivalents of the complementary strand. All samples contained 2 μM of DNA or 8-substituted-2'-deoxyguanosine nucleoside in an aqueous 10 mM cacodylate buffer (pH 7.4).

List of Abbreviations and Symbols

Abbreviations

2AP	2-Aminopurine
2FuG	8-(2-Furyl)-2'-deoxyguanosine
2PyG	8-(2-Pyridyl)-2'-deoxyguanosine
2ThG	8-(2-Thiophene)-2'-deoxyguanosine
3-MI	3-Methylisoxanthopterin
3PVG	(*E*)-8-[2-(Pyrid-3-yl)-ethenyl]-2'-deoxyguanosine
3PyG	8-(3-Pyridyl)-2'-deoxyguanosine
4PVG	(*E*)-8-[2-(Pyrid-4-yl)-ethenyl]-2'-deoxyguanosine
4PyG	8-(4-Pyridyl)-2'-deoxyguanosine
6-MI	6-Methylisoxanthopterin
A	Adenine
ACN	Acetonitrile
AcOEt	Ethyl acetate
C	Cytosine
Calcd	Calculated
CF	Correction factor
DCM	Dichloromethane
DIAD	Diisopropyl azodicarboxylate
DIEA	*N,N*-Diisopropylethylamine
DME	Dimethoxyethane
DMF	*N,N*-Dimethylformamide
DMSO	Dimethyl sulfoxide
DMT	Dimethoxytrityl
DNA	Deoxyribonucleic acid
ESI	Electrospray ionization
FRET	Förster resonance energy transfer
G	Guanine
GMP	Guanosine 5'-monophosphate

Hex	Hexane
HPLC	High-performance liquid chromatography
HR	High resolution
iPr	Isopropyl
MALDI	Matrix-assisted laser desorption/ionization
MS	Mass spectrometry
NBS	*N*-bromosuccinimide
NMR	Nuclear magnetic resonance spectroscopy
PEG	Polyethylene glycol, Avg. MW 200
PhG	8-(Phenyl)-2'-deoxyguanosine
RNA	Ribonucleic acid
StG	(*E*)-8-(2-Phenylethenyl)-2'-deoxyguanosine
T	Thymine
TBDMS	*tert*-Butyldimethylsilyl
THF	Tetrahydrofuran
T_m	Thermal melting temperature
TXPTS	Tris(4,6-dimethyl-3-sulfonato-phenyl)phosphine trisodium salt
UV	Ultraviolet
UV-Vis	Ultraviolet-visible

Symbols

δ	Chemical shift
ε	Molar extinction coefficient
η_t	Energy transfer efficiency
λ_{abs}	Absorption wavelength
λ_{em}	Emission wavelength
λ_{ex}	Excitation wavelength
Φ	Fluorescence quantum yield
τ	Fluorescence life-time

Summary

Nucleic acids are the information carriers of life, encoding all critical components necessary for cellular metabolism and replication. Surprisingly, only 2% of the human genome codes directly for proteins. The remaining 98% is composed of pseudogenes, noncoding functional RNA, introns, tandem repeats, transposons and virus-like elements. An unknown portion of these sequences play regulatory roles in mediating gene expression and other cellular processes. For certain sequences, these functions are likely mediated by the formation of diverse secondary structures such as hairpins, cruciforms, triplexes and quadruplex structures. In particular, certain guanine-rich DNA sequences are known to self-assemble into four-stranded structures called G-quadruplexes that have been proposed to possess important biological functions. Direct evidence for their existence *in vivo,* however, has remained elusive. The development of highly fluorescent guanine analogs that maintain their hydrogen bonding capacity may facilitate the monitoring of G-quadruplex formation *in vitro* and *in vivo*. For this purpose, a small library of 8-(substituted)-2'-deoxyguanosines was synthesized and evaluated. A new synthetic strategy involving O^6 protection of 8-bromo-2'-deoxyguanosine was developed to enable efficient palladium-catalyzed cross-coupling reactions at *C*8.

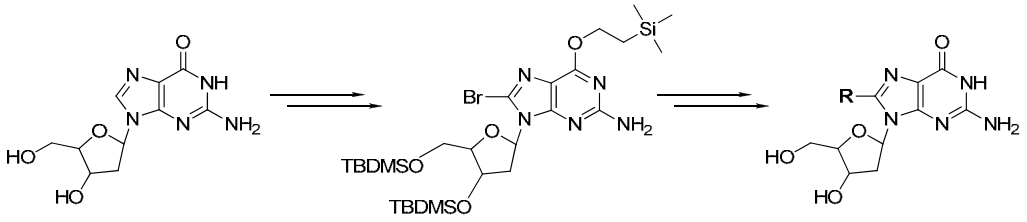

The resulting 8-substituted-2'-deoxyguanosines retain unperturbed *Watson & Crick* and *Hoogsteen* hydrogen bonding faces and are "push-pull" fluorophores that can exhibit environmentally-sensitive quantum yields (Φ = 0.001 – 0.72) due to excited-state proton transfer reactions with bulk solvent.

Among these, 8-(2-pyridyl)-2'-deoxyguanosine (**2PyG**) was identified as a particularly interesting candidate. In contrast to commonly used base analogs such as 2-aminopurine (**2AP**), **2PyG** is not significantly quenched upon titration with guanosine monophosphate (GMP). The corresponding β-cyanoethyl phosphoramidite of **2PyG** was therefore synthesized for incorporation into G-quadruplex and duplex DNA structures. Remarkably, the quantum yield of **2PyG** is generally higher in the context of nucleic acids (Φ = 0.03 - 0.15) as compared to the free nucleoside in water (Φ = 0.02). **2PyG** can be directly incorporated into the *Watson & Crick* base pair of duplex DNA and into the G-tetrads of natively-folded G-quadruplexes with relatively little impact on global structure or stability

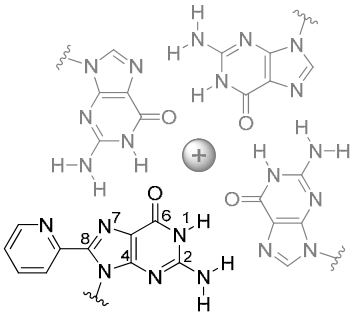

2PyG / G-tetrad
$\phi = 0.07$ $\varepsilon = 25'000\ cm^{-1}M^{-1}$

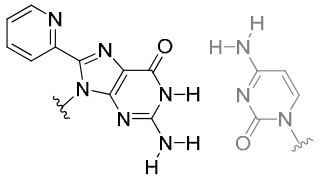

2PyG / C pair in duplex DNA
$\phi = 0.03$ $\varepsilon = 25'000\ cm^{-1}M^{-1}$

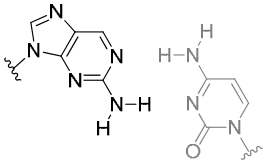

2AP / C pair in duplex DNA
$\phi = 0.002$ $\varepsilon = 5'600\ cm^{-1}M^{-1}$

.

2PyG has enabled the first quantification of DNA-to-probe energy transfer efficiencies (η_t) in G-quadruplexes. These studies revealed highly efficient energy transfer reactions in G-quadruplex structures under conditions of excess salt (η_t = 0.11 – 0.41). In contrast, G-quadruplexes folded using molecular crowding under salt-deficient conditions (40% polyethylene glycol) show little or no energy transfer. To investigate the specific role played by **2PyG** in the unusually efficient energy transfer reactions in G-quadruplexes, 8-(2-phenylethenyl)-2'-deoxyguanosine (**StG**) and 8-[2-(pyrid-4-yl)-ethenyl]-2'-

deoxyguanosine (**4PVG**) phosphoramidites were synthesized and introduced in oligonucleotides to evaluate their ability to report DNA folding and internal energy transfer. Interestingly, **StG** and **4PVG** have similar properties as compared to **2PyG**, including retention of emission efficiency in the context of nucleic acids, minimal disruption of their structures and energy acceptor properties in the context of DNA. In addition, their emission maxima are red-shifted by 35 – 75 nm as compared to **2PyG**. The three fluorescent probes all report that energy transfer efficiencies are highly structure dependent with η_t(duplex) < η_t(single-strand) < η_t(G-quadruplex). These trends are independent of the exact structural features and thermal stabilities of the G-quadruplexes or duplexes containing them.

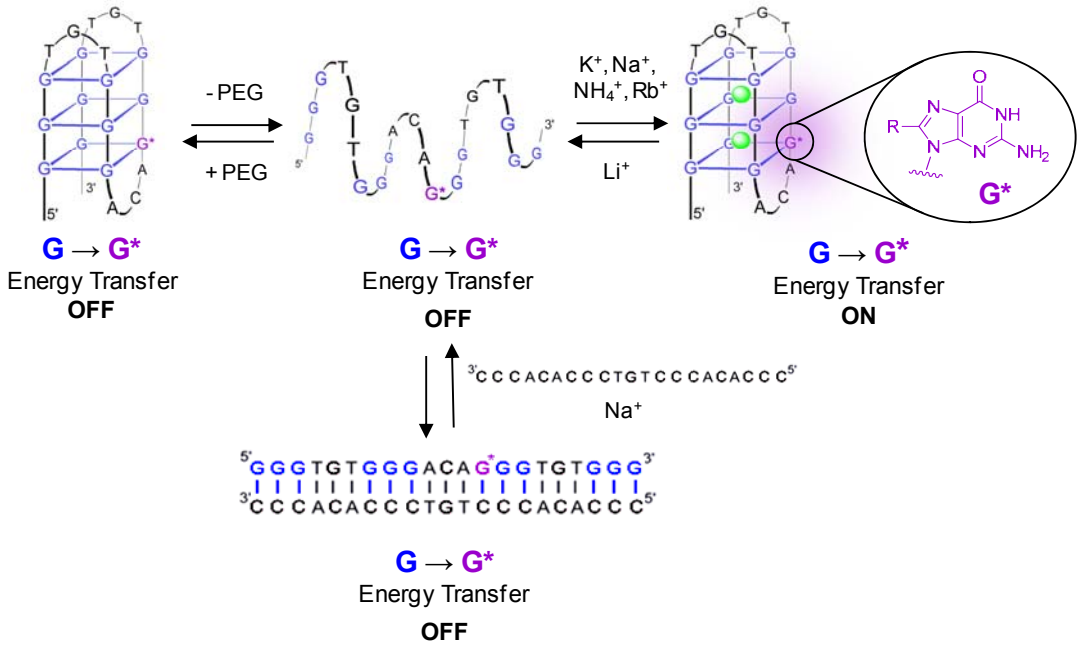

In addition to act as a turn-on fluorescent probe of G-quadruplex folding, **2PyG** exhibits selective binding of Cu(II), Ni(II), Cd(II), and Zn(II) *via* a bidentate effect provided by the *N7* atom of guanine and 2-pyridine group. Changes in nucleoside fluorescence triggered by metals binding to **2PyG** were used to characterize metal binding affinity and specificity. Upon incorporation into folded nucleic acids, **2PyG** selectively binds to Cu(II), Ni(II) and Cd(II) with binding affinities approximately 10- to 1'000-fold higher than unmodified

metal binding sites in DNA. Consistent with *N*7 binding, these affinities depend on the folded state of the oligonucleotide (duplex > G-quadruplex).

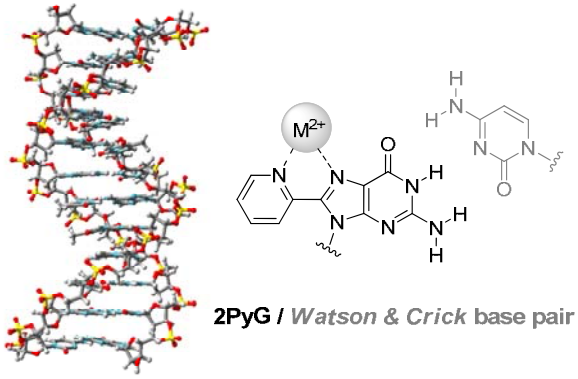

8-Substituted-2'-deoxyguanosines, prepared by the addition of small conjugated groups to the *C*8-position of guanine are powerful and versatile internal fluorescent probes. In the context of DNA, the combination of energy transfer, high probe quantum yield, and high oligonucleotide molar extinction coefficient provides a highly sensitive and reliable readout of DNA folding and G-quadruplex formation *in vitro*. In addition, the incorporation of a single pyridine ring into DNA structures such as in **2PyG** provides site-specific control of metal localization and therefore a new powerful tool for studying the effects of *N*7 metallation on the structure, stability, and electronic properties of nucleic acids.

Zusammenfassung

Nukleinsäuren sind die Informationsträger des Lebens, in denen alle entscheidenden Informationen kodiert sind, die für den Zellstoffwechsel und die Replikation benötigt werden. Erstaunlicherweise werden nur 2% des menschlichen Genoms zur Kodierung von Proteinen genutzt. Die restlichen 98% bestehen aus Pseudogenen, nicht-kodierender funktioneller RNA, Introns, Tandem-Sequenzen, Transposons und Virus ähnlichen Elementen. Ein unbekannter Anteil dieser Sequenzen nimmt eine regulierende Funktion bei der Genexpression und bei weiteren zellulären Prozessen ein. Bei bestimmten Sequenzen werden diese Funktionen wahrscheinlich durch die Bildung diverser sekundärer Strukturen wie Hairpins, Kreuzförmiger, Triplex- und Quadruplexstrukturen ausgelöst. Insbesondere können sich bestimmte guaninreiche DNA Sequenzen eigenständig in viersträngigen Strukturen, sogenannten G-Quadruplexen, anordnen, von welchen man annimmt, dass sie wichtige biologische Funktionen haben. Ein direkter, *in vivo* Beweis dieser Strukturen hat sich bis jetzt jedoch als schwierig erwiesen. Die Entwicklung von stark fluoreszierenden Guanin-derivaten, welche die Fähigkeit zur Wasserstoffbrückenbildung beibehalten, könnte die Beobachtung der Bildung von G-Quadruplexen *in vitro* und *in vivo* ermöglichen. Zu diesem Zweck wurde eine Serie von 8-(substituierten)-2'-Deoxyguanosinen synthetisiert und untersucht. Es wurde eine neue Synthesestrategie entwickelt, bei welcher die O^6-Position von 8-Bromo-2'-deoxyguanosin geschützt wird, um die Palladium-katalysierte Kreuzkupplungsreaktion am *C*8 effizient durchzuführen.

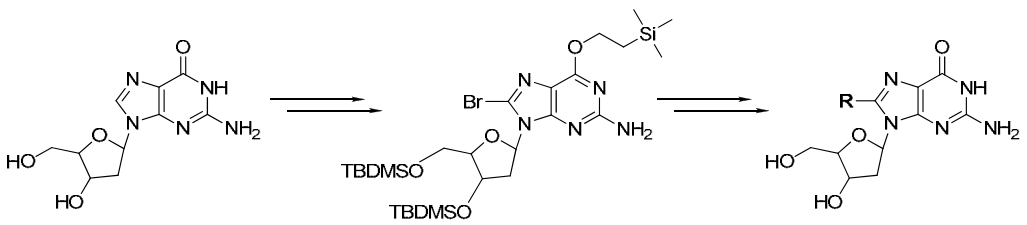

Die so synthetisierten 8-(substituierten)-2'-Deoxyguanosine behalten ihre üblichen *Watson & Crick* und *Hoogsteen* Wasserstoffbrücken-Flächen bei und sind „push-pull" Fluorophore, welche eine umgebungsempfindliche Quantenausbeute (Φ = 0.001 – 0.72) durch Protonenübertragungsreaktionen mit dem Lösungsmittel im angeregten Zustand aufweisen können.

Aus diesen Varianten wurde 8-(2-Pyridyl)-2'-deoxyguanosin (**2PyG**) als besonders vielversprechender Kandidat ermittelt. Im Gegensatz zu den gewöhnlich verwendeten Nukleobasen-Derivaten wie z.B. 2-Aminopurine (**2AP**) wird **2PyG** bei Titration mit Guanosinmonophosphat (GMP) nicht wesentlich gequencht. Das zu **2PyG** korrespondierende β-Cyanoethyl-phosphoramidite wurde deshalb zur Einbindung in G-Quadruplex und Duplex-DNA-Strukturen synthetisiert. Interessanterweise ist die Quantenausbeute von **2PyG** allgemein bei Einbindung in Nukleinsäuren höher (Φ = 0.03 - 0.15) als beim freien Nukleosid in Wasser (Φ = 0.02). **2PyG** kann direkt in die *Watson & Crick* Basenpaare von Duplex-DNA und in die G-Tetraden von natürlich gefalteten G-Quadruplexen eingebaut werden. Dabei ist der Einfluss auf die globale Struktur und Stabilität relativ gering.

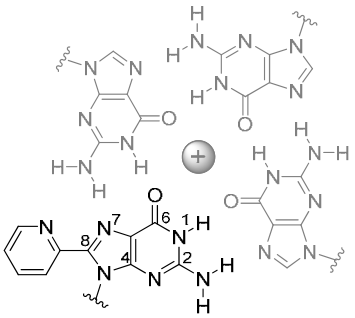

2PyG / G-Tetrad
ϕ = 0.07 ε = 25'000 $cm^{-1}M^{-1}$

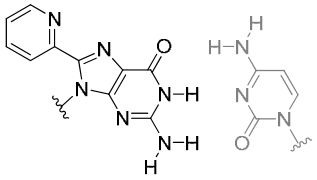

2PyG / C Paar in Duplex DNA
ϕ = 0.03 ε = 25'000 $cm^{-1}M^{-1}$

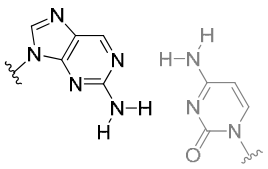

2AP / C Paar in Duplex DNA
ϕ = 0.002 ε = 5'600 $cm^{-1}M^{-1}$

2PyG hat es ermöglicht, erstmals in einer DNA-Testsequenz die Energietransfer-Effizienz (η_t) in G-Quadruplexen quantitativ zu bestimmen. Diese Untersuchung offenbarte unter Salzüberschuss hocheffiziente Energietransferreaktionen in G-Quadruplex-Strukturen (η_t = 0.11 – 0.41). Im Gegensatz dazu zeigen G-Quadruplexe, welche unter salzarmen Bedingungen gefaltet wurden (40% Polyethylenglykol), keinen oder nur sehr geringen Energietransfer. Zur Untersuchung der spezifischen Rolle von **2PyG** bei den ungewöhnlich effizienten Energietransferreaktionen in G-Quadruplexen wurden 8-(2-Phenylethenyl)-2'-

deoxyguanosin (**StG**) und 8-[2-(Pyrid-4-yl)-ethenyl]-2'-deoxyguanosin (**4PVG**) Phosphoramidite synthetisiert und in Oligonukleotide eingebaut, um deren Fähigkeit zum Nachweis von DNA-Faltung und internem Energietransfer zu untersuchen. Erstaunlicherweise haben **StG** und **4PVG** ähnliche Eigenschaften wie **2PyG** einschliesslich des Erhalts der Emissionseffizienz innerhalb von Nukleinsäuren, des minimalen Einflusses auf deren Struktur und der Energieakzeptoreigenschaften innerhalb von DNA. Zusätzlich sind deren Emissionsmaxima im Vergleich zu **2PyG** um 35 – 75 nm in den Rotbereich verschoben. Alle drei Fluoreszenzmarker zeigen mit η_t(duplex) < η_t(single-strand) < η_t(G-quadruplex) eine starke Strukturabhängigkeit der Energietransfereffizienz auf. Diese Tendenzen sind unabhängig von den genauen strukturellen Merkmalen und thermischen Stabilitäten der G-Quadruplexe oder Duplexe, welche diese Marker enthalten.

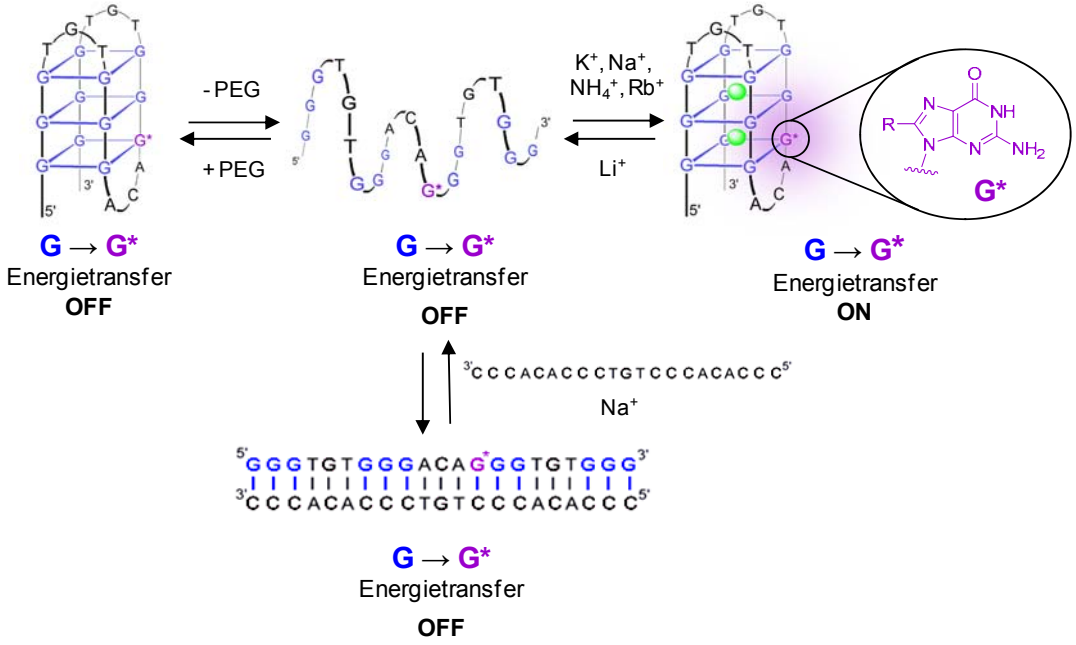

Zusätzlich zu seiner Funktion als Fluoreszenz-Marker für G-Quadruplex-Faltung bindet **2PyG** über einen zweizähnigen Effekt, welcher durch das Guanin-*N*7 und das Pyridinyl-*N*2 Atom ermöglicht wird, selektiv Cu(II), Ni(II), Cd(II), und Zn(II). Veränderungen in der Nukleosid-Fluoreszenz, ausgelöst durch Metallbindungen an **2PyG,** wurden zur Charakterisierung der Metallbindungsaffinität und -spezifität genutzt. Nach Einbindung in

gefaltete Nukleinsäuren bindet **2PyG** selektiv Cu(II), Ni(II) und Cd(II) mit 10- bis 1000-fach stärkerer Bindungsaffinität im Vergleich zu unmodifizierten Metallbindungsstellen in der DNA. Diese Affinitäten hängen, in Übereinstimmung mit der *N*7 Bindung, vom Faltungszustand der Oligonukleotide (Duplex > G-Quadruplex) ab.

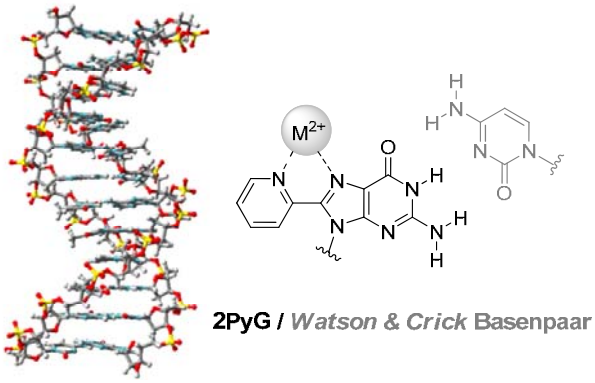

Durch Addition von kleinen konjugierten Gruppen an der *C*8-Position des Guaninmoleküls erhaltene 8-(substituierte)-2'-Deoxyguanosin sind leistungsstarke und vielseitige interne Fluoreszenzmarker. Im DNA-Kontext ermöglicht die Kombination von Energietransfer, hoher Quantenausbeute des Markers und hohem molaren Oligonukleotid-Extinktionskoeffizienten eine hochempfindliche und zuverlässige Anzeige von DNA-Faltung und G-Quadruplex-Bildung *in vitro*. Zusätzlich bietet die Einbindung eines einzelnen Pyridinringes in DNA-Strukturen wie zum Beispiel **2PyG** die Möglichkeit, Metall-Bindungsstellen zu steuern. Damit ergibt sich ein neues, leistungsstarkes Werkzeug zur Untersuchung der Effekte der *N7* Metallkomplexierung auf die Struktur, Stabilität und die elektronischen Eigenschaften von Nukleinsäuren.

Vita

Personal data

Name	**Anaëlle DUMAS**
Date and place of birth	28th February 1984, in Morges
Citizenship	Vuisterens-devant-Romont FR

Education

2002	Maturity, Option Biology & Chemisty, Gymnase de Morges.
2007	Master of Science in Molecular and Biological Chemistry, Swiss Federal Institute of Technology, Lausanne (EPFL). Master thesis in Merck Serono, Geneva: "Synthesis of biologically active 1,2-Benzisoxazoles and 1,2,4-Oxadiazoles derivatives", under the supervision of Prof. Dr. Pierre Vogel (EPFL) and Dr. Cyril Montagne (Merck Serono).
2007 – 2011	University of Zurich, Institute of Organic Chemistry. Ph. D. thesis under the supervision of Prof. Dr. Nathan W. Luedtke: "8-Substituted-2'-Deoxyguanosines as Internal Probes for DNA Folding and Energy Transfer".

Awards and Fellowships

2007	Prix Syngenta Monthey, for the Chemistry Student of the EPFL obtaining the best average for the Master Cycle.
2010	SCS DSM Prize, for the best poster in the section Organic Chemistry, Swiss Chemical Society Fall Meeting (2nd place).
2011	Swiss National Science Foundation Fellowship for Prospective Researchers.

Publications

- Anaëlle Dumas, Nathan W. Luedtke, Cation-Mediated Energy Transfer in G-Quadruplexes Revealed by an Internal Fluorescent Probe, *J. Am. Chem. Soc.*, **2010**, *132*, 18004-18007.

- Anaëlle Dumas, Nathan W. Luedtke, Highly Fluorescent Guanine Mimics for Folding and Energy Transfer Studies, *Nucleic Acid Res.*, **2011**, *39*, 6825-6834.

- Anaëlle Dumas, Nathan W. Luedtke, Fluorescent Properties of 8-(2-Pyridyl)guanine "2PyG" as Compared to 2-Aminopurine in DNA, *ChemBioChem*, **2011**, *12*, 2044-2051.

- Anaëlle Dumas, Nathan W. Luedtke, Site-Specific Control of *N*7-Metal Coordination in DNA Using a Fluorescent Purine Derivative, **2011**, *in review*.

- Nathan W. Luedtke, Anaëlle C. Dumas, 8- and 6,8-Substituted-2'-Deoxyguanosines and uses Thereof, *PCT Intl. Appl.*, **2010**, WO2010028781.

References

1. Watson, J.D. and Crick, F.H.C. Genetical implications of the structure of deoxyribonucleic acid. *Nature,* **1953**, *171*, 964-967.

2. Catasti, P., Chen, X., Mariappan, S.V.S., Bradbury, E.M. and Gupta, G. DNA repeats in the human genome. *Genetica,* **1999**, *106*, 15-36.

3. Patel, D.J., Phan, A.T. and Kuryavyi, V. Human telomere, oncogenic promoter and 5'-UTR G-quadruplexes: Diverse higher order DNA and RNA targets for cancer therapeutics. *Nucleic Acids Res.,* **2007**, *35*, 7429-7455.

4. Qin, Y. and Hurley, L.H. Structures, folding patterns, and functions of intramolecular DNA G-quadruplexes found in eukaryotic promoter regions. *Biochimie,* **2008**, *90*, 1149-1171.

5. Balasubramanian, S., Hurley, L.H. and Neidle, S. Targeting G-quadruplexes in gene promoters: a novel anticancer strategy? *Nat. Rev. Drug Discovery,* **2011**, *10*, 261-275.

6. Wadkins, R.M. Targeting DNA secondary structures. *Curr. Med. Chem.,* **2000**, *7*, 1-15.

7. Elgar, G. and Vavouri, T. Tuning in to the signals: noncoding sequence conservation in vertebrate genornes. *Trends Genet.,* **2008**, *24*, 344-352.

8. Sen, D. and Gilbert, W. Formation of parallel 4-stranded complexes by guanine-rich motifs in DNA and its implications for meiosis. *Nature,* **1988**, *334*, 364-366.

9. Sundquist, W.I. and Klug, A. Telomeric DNA dimerizes by formation of guanine tetrads between hairpin loops. *Nature,* **1989**, *342*, 825-829.

10. Gellert, M., Lipsett, M.N. and Davies, D.R. Helix formation by guanylic acid. *Proc. Natl. Acad. Sci. U S A,* **1962**, *48*, 2013-2018.

11. Hud, N.V.P., J. The role of cations in determining quadruplex structure and stability. In Neidle, S. (ed.), *Quadruplex Nucleic Acids*. RSC Publishing, **2006**, pp. 100-130.

12. Markovitsi, D., Gustavsson, T. and Sharonov, A. Cooperative effects in the photophysical properties of self-associated triguanosine diphosphates. *Photochem. Photobiol.,* **2004**, *79*, 526-530.

13. Gepshtein, R., Huppert, D., Lubitz, I., Amdursky, N. and Kotlyar, A.B. Radiationless transitions of G4 wires and dGMP. *J. Phys. Chem. C,* **2008**, *112*, 12249-12258.

14. Miannay, F.A., Banyasz, A., Gustavsson, T. and Markovitsi, D. Excited states and energy transfer in G-quadruplexes. *J. Phys. Chem. C,* **2009**, *113*, 11760-11765.

15. Mendez, M.A. and Szalai, V.A. Fluorescence of unmodified oligonucleotides: A tool to probe G-quadruplex DNA structure. *Biopolymers,* **2009**, *91*, 841-850.

16. Parkinson, G.N., Lee, M.P.H. and Neidle, S. Crystal structure of parallel quadruplexes from human telomeric DNA. *Nature,* **2002**, *417*, 876-880.

17. Lipps, H.J. and Rhodes, D. G-quadruplex structures: in vivo evidence and function. *Trends Cell Biol.,* **2009**, *19*, 414-422.

18. Todd, A.K., Johnston, M. and Neidle, S. Highly prevalent putative quadruplex sequence motifs in human DNA. *Nucleic Acids Res.,* **2005**, *33*, 2901-2907.

19. Huppert, J.L. and Balasubramanian, S. Prevalence of quadruplexes in the human genome. *Nucleic Acids Res.,* **2005**, *33*, 2908-2916.

20. Eddy, J. and Maizels, N. Gene function correlates with potential for G4 DNA formation in the human genome. *Nucleic Acids Res.,* **2006**, *34*, 3887-3896.

21. Huppert, J.L. and Balasubramanian, S. G-quadruplexes in promoters throughout the human genome. *Nucleic Acids Res.,* **2007**, *35*, 406-413.

22. Cahoon, L.A. and Seifert, H.S. An alternative DNA structure is necessary for Pilin antigenic variation in Neisseria gonorrhoeae. *Science,* **2009**, *325*, 764-767.

23. Hurley, L.H. DNA and its associated processes as targets for cancer therapy. *Nat. Rev. Cancer,* **2002**, *2*, 188-200.

24. Mergny, J.L., Riou, J.F., Mailliet, P., Teulade-Fichou, M.P. and Gilson, E. Natural and pharmacological regulation of telomerase. *Nucleic Acids Res.,* **2002**, *30*, 839-865.

25. Neidle, S. and Parkinson, G. Telomere maintenance as a target for anticancer drug discovery. *Nat. Rev. Drug Discovery,* **2002**, *1*, 383-393.

26. Pennarun, G., Granotier, C., Gauthier, L.R., Gomez, D. and Boussin, F.D. Apoptosis related to telomere instability and cell cycle alterations in human glioma cells treated by new highly selective G-quadruplex ligands. *Oncogene,* **2005**, *24*, 2917-2928.

27. Hurley, L.H., Wheelhouse, R.T., Sun, D., Kerwin, S.M., Salazar, M., Fedoroff, O.Y., Han, F.X., Han, H.Y., Izbicka, E. and Von Hoff, D.D. G-quadruplexes as targets for drug design. *Pharmacol. Ther.,* **2000**, *85*, 141-158.

28. Han, H.Y. and Hurley, L.H. G-quadruplex DNA: a potential target for anti-cancer drug design. *Trends Pharmacol. Sci.,* **2000**, *21*, 136-142.

29. Shay, J.W. and Bacchetti, S. A survey of telomerase activity in human cancer. *Eur. J. Cancer,* **1997**, *33*, 787-791.

30. Siddiqui-Jain, A., Grand, C.L., Bearss, D.J. and Hurley, L.H. Direct evidence for a G-quadruplex in a promoter region and its targeting with a small molecule to repress c-MYC transcription. *Proc. Natl. Acad. Sci. U S A,* **2002**, *99*, 11593-11598.

31. Balasubramanian, S., McLuckie, K.I.E., Waller, Z.A.E., Sanders, D.A., Alves, D., Rodriguez, R., Dash, J., McKenzie, G.J. and Venkitaraman, A.R. G-quadruplex-binding benzo[a]phenoxazines down-regulate c-Kit expression in human gastric carcinoma cells. *J. Am. Chem. Soc.,* **2011**, *133*, 2658-2663.

32. Schaffitzel, C., Berger, I., Postberg, J., Hanes, J., Lipps, H.J. and Pluckthun, A. In vitro generated antibodies specific for telomeric guanine-quadruplex DNA react with Stylonychia lemnae macronuclei. *Proc. Natl. Acad. Sci. U S A,* **2001**, *98*, 8572-8577.

33. Phan, A.T., Luu, K.N. and Patel, D.J. Different loop arrangements of intramolecular human telomeric (3+1) G-quadruplexes in K+ solution. *Nucleic Acids Res.,* **2006**, *34*, 5715-5719.

34. Ambrus, A., Chen, D., Dai, J.X., Jones, R.A. and Yang, D.Z. Solution structure of the biologically relevant g-quadruplex element in the human c-MYC promoter. implications for g-quadruplex stabilization. *Biochemistry,* **2005**, *44*, 2048-2058.

35. Phan, A.T., Kuryavyi, V., Burge, S., Neidle, S. and Patel, D.J. Structure of an unprecedented G-quadruplex scaffold in the human c-kit promoter. *J. Am. Chem. Soc.,* **2007**, *129*, 4386-4392.

36. Jin, R.Z., Gaffney, B.L., Wang, C., Jones, R.A. and Breslauer, K.J. Thermodynamics and structure of a DNA tetraplex - a spectroscopic and calorimetric study of the tetramolecular complexes of d(TG3T) and d(TG3T2G3T). *Proc. Natl. Acad. Sci. U S A,* **1992**, *89*, 8832-8836.

37. Mergny, J.L., Phan, A.T. and Lacroix, L. Following G-quartet formation by UV-spectroscopy. *FEBS Lett.,* **1998**, *435*, 74-78.

38. Phan, A.T. and Mergny, J.L. Human telomeric DNA: G-quadruplex, i-motif and watson-crick double helix. *Nucleic Acids Res.,* **2002**, *30*, 4618-4625.

39. He, F., Tang, Y.L., Wang, S., Li, Y.L. and Zhu, D.B. Fluorescent amplifying recognition for DNA G-quadruplex folding with a cationic conjugated polymer: A platform for homogeneous potassium detection. *J. Am. Chem. Soc.,* **2005**, *127*, 12343-12346.

40. Mergny, J.L. and Maurizot, J.C. Fluorescence resonance energy transfer as a probe for G-quartet formation by a telomeric repeat. *Chembiochem,* **2001**, *2*, 124-132.

41. Nagatoishi, S., Nojima, T., Galezowska, E., Juskowiak, B. and Takenaka, S. G quadruplex-based FRET probes with the thrombin-binding aptamer (TBA) sequence designed for the efficient fluorometric detection of the potassium ion. *Chembiochem,* **2006**, *7*, 1730-1737.

42. Sinkeldam, R.W., Greco, N.J. and Tor, Y. Fluorescent analogs of biomolecular building blocks: design, properties, and applications. *Chem. Rev.,* **2010**, *110*, 2579-2619.

43. Alzeer, J., Vummidi, B.R., Roth, P.J.C. and Luedtke, N.W. Guanidinium-modified phthalocyanines as high-affinity G-quadruplex fluorescent probes and transcriptional regulators. *Angew. Chem., Int. Ed.,* **2009**, *48*, 9362-9365.

44. Xu, L., Zhang, D., Huang, J., Deng, M.G., Zhang, M. and Zhou, X. High fluorescence selectivity and visual detection of G-quadruplex structures by a novel dinuclear ruthenium complex. *Chemical Communications,* **2010**, *46*, 743-745.

45. Alzeer, J. and Luedtke, N.W. pH-Mediated fluorescence and G-quadruplex binding of amido phthalocyanines. *Biochemistry,* **2010**, *49*, 4339-4348.

46. Moreira, B.G., You, Y., Behlke, M.A. and Owczarzy, R. Effects of fluorescent dyes, quenchers, and dangling ends on DNA duplex stability. *Biochem. Biophys. Res. Commun.,* **2005**, *327*, 473-484.

47. Nagatoishi, S., Nojima, T., Juskowiak, B. and Takenaka, S. A pyrene-labeled G-quadruplex oligonucleotide as a fluorescent probe for potassium ion detection in biological applications. *Angew. Chem., Int. Ed.,* **2005**, *44*, 5067-5070.

48. Greco, N.J. and Tor, Y. Furan decorated nucleoside analogues as fluorescent probes: synthesis, photophysical evaluation, and site-specific incorporation. *Tetrahedron,* **2007**, *63*, 3515-3527.

49. Wilson, J.N. and Kool, E.T. Fluorescent DNA base replacements: reporters and sensors for biological systems. *Org. Biomol. Chem.,* **2006**, *4*, 4265-4274.

50. Hawkins, M.E. Fluorescent pteridine nucleoside analogs - A window on DNA interactions. *Cell. Biochem. Biophys.,* **2001**, *34*, 257-281.

51. Hawkins, M.E. Fluorescent pteridine probes for nucleic acid analysis. *Fluorescence Spectroscopy,* **2008**, *450*, 201-231.

52. Srivatsan, S.G. and Tor, Y. Using an emissive uridine analogue for assembling fluorescent HIV-1 TAR constructs. *Tetrahedron,* **2007**, *63*, 3601-3607.

53. Srivatsan, S.G. and Tor, Y. Fluorescent pyrimidine ribonucleotide: Synthesis, enzymatic incorporation, and utilization. *J. Am. Chem. Soc.,* **2007**, *129*, 2044-2053.

54. Salic, A. and Mitchison, T.J. A chemical method for fast and sensitive detection of DNA synthesis in vivo. *Proc. Natl. Acad. Sci. U S A,* **2008**, *105*, 2415-2420.

55. Furman, P.A., Fyfe, J.A., Stclair, M.H., Weinhold, K., Rideout, J.L., Freeman, G.A., Lehrman, S.N., Bolognesi, D.P., Broder, S., Mitsuya, H. *et al.* Phosphorylation of 3'-azido-3'-deoxythymidine and selective interaction of the 5'-triphosphate with human-immunodeficiency-virus reverse-transcriptase. *Proc. Natl. Acad. Sci. U S A,* **1986**, *83*, 8333-8337.

56. Poijarvi-Virta, P. and Lonnberg, H. Prodrug approaches of nucleotides and oligonucleotides. *Curr. Med. Chem.,* **2006**, *13*, 3441-3465.

57. Dunham, M.A., Neumann, A.A., Fasching, C.L. and Reddel, R.R. Telomere maintenance by recombination in human cells. *Nat. Genet.,* **2000**, *26*, 447-450.

58. Sandin, P., Stengel, G., Ljungdahl, T., Borjesson, K., Macao, B. and Wilhelmsson, L.M. Highly efficient incorporation of the fluorescent nucleotide analogs tC and tC(O) by Klenow fragment. *Nucleic Acids Res.,* **2009**, *37*, 3924-3933.

59. Wilhelmsson, L.M. Fluorescent nucleic acid base analogues. *Q. Rev. Biophys.,* **2010**, *43*, 159-183.

60. Srivatsan, S.G., Weizman, H. and Tor, Y. A highly fluorescent nucleoside analog based on thieno[3,4-d] pyrimidine senses mismatched pairing. *Org. Biomol. Chem.,* **2008**, *6*, 1334-1338.

61. Rist, M.J. and Marino, J.P. Fluorescent nucleotide base analogs as probes of nucleic acid structure, dynamics and interactions. *Curr. Org. Chem.,* **2002**, *6*, 775-793.

62. Firth, A.G., Fairlamb, I.J.S., Darley, K. and Baumann, C.G. Sonogashira alkynylation of unprotected 8-brominated adenosines and guanosines: fluorescence properties of compact conjugated acetylenes containing a purine ring. *Tetrahedron Lett.,* **2006**, *47*, 3529-3533.

63. Butler, R.S., Cohn, P., Tenzel, P., Abboud, K.A. and Castellano, R.K. Synthesis, photophysical behavior, and electronic structure of push-pull purines. *J. Am. Chem. Soc.,* **2009**, *131*, 623-633.

64. Ogasawara, S., Saito, I. and Maeda, M. Synthesis and reversible photoisomerization of photoswitchable nucleoside, 8-styryl-2'-deoxyguanosine. *Tetrahedron Lett.,* **2008**, *49*, 2479-2482.

65. Hawkins, M.E., Pfleiderer, W., Mazumder, A., Pommier, Y.G. and Balis, F.M. Incorporation of a fluorescent guanosine analog into oligonucleotides and its application to a real time assay for the HIV-1 integrase 3'-processing reaction. *Nucleic Acids Res.,* **1995**, *23*, 2872-2880.

66. Kimura, T., Kawai, K., Fujitsuka, M. and Majima, T. Monitoring G-quadruplex structures and G-quadruplex-ligand complex using 2-aminopurine modified oligonucleotides. *Tetrahedron,* **2007**, *63*, 3585-3590.

67. Gray, R.D., Petraccone, L., Trent, J.O. and Chaires, J.B. Characterization of a K+-Induced Conformational Switch in a Human Telomeric DNA Oligonucleotide Using 2-Aminopurine Fluorescence. *Biochemistry,* **2010**, *49*, 179-194.

68. Kirk, S.R., Luedtke, N.W. and Tor, Y. 2-Aminopurine as a real-time probe of enzymatic cleavage and inhibition of hammerhead ribozymes. *Bioorg. Med. Chem.,* **2001**, *9*, 2295-2301.

69. Wagenknecht, H.A. Fluorescent DNA base modifications and substitutes: Multiple fluorophore labeling and the DETEQ concept. *Ann. N. Y. Acad. Sci.,* **2008**, *1130*, 122-130.

70. Menacher, F., Rubner, M., Berndl, S. and Wagenknecht, H.A. Thiazole orange and Cy3: Improvement of fluorescent DNA probes with use of short range electron transfer. *J. Org. Chem.,* **2008**, *73*, 4263-4266.

71. Gray, R.D., Petraccone, L., Buscaglia, R. and Chaires, J.B. 2-Aminopurine as a probe for quadruplex loop structures. **2010**, Vol. 608, pp. 121-136.

72. Sandin, P., Wilhelmsson, L.M., Lincoln, P., Powers, V.E.C., Brown, T. and Albinsson, B. Fluorescent properties of DNA base analogue tC upon incorporation into DNA - negligible influence of neighbouring bases on fluorescence quantum yield. *Nucleic Acids Res.,* **2005**, *33*, 5019-5025.

73. Zhao, Y. and Baranger, A.M. Design of an adenosine analogue that selectively improves the affinity of a mutant U1A protein for RNA. *J. Am. Chem. Soc.,* **2003**, *125*, 2480-2488.

74. Hawkins, M.E., Pfleiderer, W., Balis, F.M., Porter, D. and Knutson, J.R. Fluorescence properties of pteridine nucleoside analogs as monomers and incorporated into oligonucleotides. *Anal. Biochem.,* **1997**, *244*, 86-95.

75. Driscoll, S.L., Hawkins, M.E., Balis, F.M., Pfleiderer, W. and Laws, W.R. Fluorescence properties of a new guanosine analog incorporated into small oligonucleotides. *Biophys. J.,* **1997**, *73*, 3277-3286.

76. Gros, J., Rosu, F., Amrane, S., De Cian, A., Gabelica, V., Lacroix, L. and Mergny, J.L. Guanines are a quartet's best friend: impact of base substitutions on the kinetics and stability of tetramolecular quadruplexes. *Nucleic Acids Res.,* **2007**, *35*, 3064-3075.

77. Dumas, A. and Luedtke, N.W. Cation-mediated energy transfer in G-quadruplexes revealed by an internal fluorescent probe. *J. Am. Chem. Soc.,* **2010**, *132*, 18004-18007.

78. Xu, D.G. and Nordlund, T.M. Sequence dependence of energy transfer in DNA oligonucleotides. *Biophys. J.,* **2000**, *78*, 1042-1058.

79. Haran, T.E. and Mohanty, U. The unique structure of A-tracts and intrinsic DNA bending. *Q. Rev. Biophys.,* **2009**, *42*, 41-81.

80. Callis, P.R. Electronic states and luminescence of nucleic-acid systems. *Annu. Rev. Phys. Chem.,* **1983**, *34*, 329-357.

81. Borresen, H.C. On luminescence properties of some purines and pyrimidines - a study by fluorescence spectrophotometry of sites of protonation and of types of lowest excited singlet states. *Acta Chem. Scand.,* **1963**, *17*, 921-929.

82. Saito, Y., Shinohara, Y., Ishioroshi, S., Suzuki, A., Tanaka, M. and Saito, I. Synthesis of environmentally sensitive 2 '-deoxyguanosine containing solvatochromic pyrene fluorophore. *Tetrahedron Lett.,* **2011**, *52*, 2359-2361.

83. Valis, L., Mayer-Enthart, E. and Wagenknecht, H.A. 8-(pyren-1-yl)-2'-deoxyguanosine as an optical probe for DNA hybridization and for charge transfer with small peptides. *Bioorg. Med. Chem. Lett.,* **2006**, *16*, 3184-3187.

84. Wagenknecht, H.A., Wanninger-Weiss, C. and Valis, L. Pyrene-modified guanosine as fluorescent probe for DNA modulated by charge transfer. *Bioorg. Med. Chem.,* **2008**, *16*, 100-106.

85. Saito, Y., Miyauchi, Y., Okamoto, A. and Saito, I. Base-discriminating fluorescent (BDF) nucleoside: distinction of thymine by fluorescence quenching. *Chemical Communications,* **2004**, 1704-1705.

86. Engels, J.W., Forster, U., Lommel, K., Sauter, D., Grunewald, C. and Wachtveitl, J. 2-(1-Ethynylpyrene)-adenosine as a folding probe for RNA-pyrene in or out. *Chembiochem,* **2010**, *11*, 664-672.

87. Seo, Y.J., Ryu, J.H. and Kim, B.H. Quencher-free, end-stacking oligonucleotides for probing single-base mismatches in DNA. *Org. Lett.,* **2005**, *7*, 4931-4933.

88. Kim, B.H., Seo, Y.J. and Lee, I.J. Homoadenine signalling system for SNP typing. *Mol. Biosyst.,* **2009**, *5*, 235-237.

89. Seo, Y.J. and Kim, B.H. Probing the B-to-Z-DNA duplex transition using terminally stacking ethynyl pyrene-modified adenosine and uridine bases. *Chemical Communications,* **2006**, 150-152.

90. Kim, B.H., Seo, Y.J., Lee, I.J. and Yi, J.W. Probing the stable G-quadruplex transition using quencher-free endstacking ethynyl pyrene-adenosine. *Chemical Communications,* **2007**, 2817-2819.

91. Kim, B.H., Seo, Y.J. and Lee, I.J. Detection of structure-switching in G-quadruplexes using end-stacking ability. *Bioorg. Med. Chem. Lett.,* **2008**, *18*, 3910-3913.

92. Matsumoto, K., Shinohara, Y., Bag, S.S., Takeuchi, Y., Morii, T., Saito, Y. and Saito, I. Pyrene-labeled deoxyguanosine as a fluorescence sensor to discriminate single and double stranded DNA structures: Design of ends free molecular beacons. *Bioorg. Med. Chem. Lett.,* **2009**, *19*, 6392-6395.

93. Engels, J.W., Grunwald, C., Kwon, T., Piton, N., Forster, U. and Wachtveitl, J. RNA as scaffold for pyrene excited complexes. *Bioorg. Med. Chem.,* **2008**, *16*, 19-26.

94. Sekine, M., Seio, K., Mizuta, M., Tasaki, K., Tamaki, K. and Ohkubo, A. Hybridization-dependent fluorescence of oligodeoxynucleotides incorporating new pyrene-modified adenosine residues. *Bioorg. Med. Chem.,* **2008**, *16*, 8287-8293.

95. Wagner, C., Rist, M., Mayer-Enthart, E. and Wagenknecht, H.A. 1-Ethynylpyrene-modified guanine and cytosine as optical labels for DNA hybridization. *Org. Biomol. Chem.,* **2005**, *3*, 2062-2063.

96. Hwang, G.T., Seo, Y.J. and Kim, B.H. Pyrene-labeled deoxyuridine and deoxyadenosine: fluorescent discriminating phenomena in their oligonucleotides. *Tetrahedron Lett.,* **2005**, *46*, 1475-1477.

97. Seo, Y.J., Hwang, G.T. and Kim, B.H. Quencher-free molecular beacon systems with two pyrene units in the stem region. *Tetrahedron Lett.,* **2006**, *47*, 4037-4039.

98. Kim, B.H., Seo, Y.J., Rhee, H. and Joo, T. Self-duplex formation of an A(Py)-substituted oligodeoxyadenylate and its unique fluorescence. *J. Am. Chem. Soc.,* **2007**, *129*, 5244-5247.

99. Okamoto, A., Ochi, Y. and Saito, I. Fluorometric sensing of the salt-induced B-Z DNA transition by combination of two pyrene-labeled nucleobases. *Chemical Communications,* **2005**, 1128-1130.

100. Okamoto, A., Kanatani, K., Ochi, Y., Saito, Y. and Saito, I. A novel fluorescent guanine derivative distinguishable of three structures, single strand, duplex, and quadruplex. *Tetrahedron Lett.,* **2004**, *45*, 6059-6062.

101. Saito, I., Saito, Y., Suzuki, A., Imai, K. and Nemoto, N. Synthesis of novel push-pull-type solvatochromic 2 '-deoxyguanosine derivatives with longer wavelength emission. *Tetrahedron Lett.,* **2010**, *51*, 2606-2609.

102. Okamoto, A., Tainaka, K., Tanaka, K., Ikeda, S., Nishiza, K., Unzai, T., Fujiwara, Y. and Saito, I. PRODAN-conjugated DNA: Synthesis and photochemical properties. *J. Am. Chem. Soc.,* **2007**, *129*, 4776-4784.

103. Kimura, T., Kawai, K. and Majima, T. Monitoring of microenvironmental changes in the major and minor grooves of DNA by dan-modified oligonucleotides. *Org. Lett.,* **2005**, *7*, 5829-5832.

104. Kimura, T., Kawai, K. and Majima, T. Probing the microenvironments in the grooves of Z-DNA using dan-modified oligonucleotides. *Chemical Communications,* **2006**, 1542-1544.

105. Ogasawara, S. and Maeda, M. Straightforward and reversible photoregulation of hybridization by using a photochromic nucleoside. *Angew. Chem., Int. Ed.,* **2008**, *47*, 8839-8842.

106. Saito, Y., Matsumoto, K., Takeuchi, Y., Bag, S.S., Kodate, S., Morii, T. and Saito, I. Fluorescence switching of photochromic vinylpyrene-substituted 2 '-deoxyguanosine. *Tetrahedron Lett.,* **2009**, *50*, 1403-1406.

107. Ogasawara, S. and Maeda, M. Reversible photoswitching of a G-quadruplex. *Angew. Chem., Int. Ed.,* **2009**, *48*, 6671-6674.

108. Hocek, M., Vrabel, M., Pohl, R., Votruba, I., Sajadi, M., Kovalenko, S.A. and Ernsting, N.P. Synthesis and photophysical properties of 7-deaza-2 '-deoxyadenosines bearing bipyridine ligands and their Ru(II)-complexes in position 7. *Org. Biomol. Chem.,* **2008**, *6*, 2852-2860.

109. Hocek, M., Vrabel, M., Horakova, P., Pivonkova, H., Kalachova, L., Cernocka, H., Cahova, H., Pohl, R., Sebest, P., Havran, L. *et al.* Base-modified DNA labeled by [Ru(bpy)(3)](2+) and [Os(bpy)(3)](2+) complexes: construction by polymerase incorporation of modified nucleoside triphosphates, electrochemical and luminescent properties, and applications. *Chem.-Eur. J.,* **2009**, *15*, 1144-1154.

110. Seidel, C.A.M., Schulz, A. and Sauer, M.H.M. Nucleobase-specific quenching of fluorescent dyes .1. Nucleobase one-electron redox potentials and their correlation with static and dynamic quenching efficiencies. *J. Phys. Chem.,* **1996**, *100*, 5541-5553.

111. Hawkins, M.E., Pfleiderer, W., Jungmann, O. and Balis, F.M. Synthesis and fluorescence characterization of pteridine adenosine nucleoside analogs for DNA incorporation. *Anal. Biochem.,* **2001**, *298*, 231-240.

112. Wojtuszewski, K., Hawkins, M.E., Cole, J.L. and Mukerji, I. HU binding to DNA: Evidence for multiple complex formation and DNA bending (vol 40, pg 2588, 2001). *Biochemistry,* **2001**, *40*, 4892-4892.

113. Hermann, T. and Parsons, J. Conformational flexibility of ribosomal decoding-site RNA monitored by fluorescent pteridine base analogues. *Tetrahedron,* **2007**, *63*, 3548-3552.

114. Moser, A.M., Patel, M., Yoo, H., Balis, F.M. and Hawkins, M.E. Real-time fluorescence assay for O-6-alkylguanine-DNA alkyltransferase. *Anal. Biochem.,* **2000**, *281*, 216-222.

115. Sanabia, J.E., Goldner, L.S., Lacaze, P.A. and Hawkins, M.E. On the feasibility of single-molecule detection of the guanosine-analogue 3-MI. *J. Phys. Chem. B,* **2004**, *108*, 15293-15300.

116. Singleton, S.F., Roca, A.I., Lee, A.M. and Xiao, J. Probing the structure of RecA-DNA filaments. Advantages of a fluorescent guanine analog. *Tetrahedron,* **2007**, *63*, 3553-3566.

117. Augustyn, K.E., Wojtuszewski, K., Hawkins, M.E., Knutson, J.R. and Mukerji, I. Examination of the premelting transition of DNA A-tracts using a fluorescent adenosine analogue. *Biochemistry,* **2006**, *45*, 5039-5047.

118. Stanley, R.J., Hou, Z.J., Yang, A.P. and Hawkins, M.E. The two-photon excitation cross section of 6MAP, a fluorescent adenine analogue. *J. Phys. Chem. B,* **2005**, *109*, 3690-3695.

119. Ward, D.C., Reich, E. and Stryer, L. Fluorescence studies of nucleotides and polynucleotides .I. Formycin 2-aminopurine riboside 2,6-diaminopurine riboside and their derivatives. *J. Biol. Chem.,* **1969**, *244*, 1228-&.

120. Seela, F. and Becher, G. Synthesis, base pairing, and fluorescence properties of oligonucleotides containing 1H-pyrazolo[3,4-d]pyrimidin-6-amine (8-aza-7-deazapurin-2-amine) as an analogue of purin-2-amine. *Helv. Chim. Acta,* **2000**, *83*, 928-942.

121. Nordlund, T.M., Andersson, S., Nilsson, L., Rigler, R., Graslund, A. and Mclaughlin, L.W. Structure and dynamics of a fluorescent DNA oligomer containing the Ecori recognition sequence - Fluorescence, molecular-dynamics, and NMR-studies. *Biochemistry,* **1989**, *28*, 9095-9103.

122. Jean, J.M. and Hall, K.B. 2-Aminopurine fluorescence quenching and lifetimes: role of base stacking. *Proc. Natl. Acad. Sci. U S A,* **2001**, *98*, 37-41.

123. Fagan, P.A., Fabrega, C., Eritja, R., Goodman, M.F. and Wemmer, D.E. NMR study of the conformation of the 2-aminopurine:cytosine mismatch in DNA. *Biochemistry,* **1996**, *35*, 4026-4033.

124. Sowers, L.C., Fazakerley, G.V., Eritja, R., Kaplan, B.E. and Goodman, M.F. Base-pairing and mutagenesis - Observation of a protonated base pair between 2-aminopurine and cytosine in an oligonucleotide by proton NMR. *Proc. Natl. Acad. Sci. U S A,* **1986**, *83*, 5434-5438.

125. Xu, D.G., Evans, K.O. and Nordlund, T.M. Melting and premelting transitions of an oligomer measured by DNA-base fluorescence and absorption. *Biochemistry,* **1994**, *33*, 9592-9599.

126. Raney, K.D., Sowers, L.C., Millar, D.P. and Benkovic, S.J. A fluorescence-based assay for monitoring helicase Activity. *Proc. Natl. Acad. Sci. U S A,* **1994**, *91*, 6644-6648.

127. Kirk, S.R., Luedtke, N.W. and Tor, Y. 2-aminopurine as a real-time probe of enzymatic cleavage and inhibition of hammerhead ribozymes. *Bioorg. Med. Chem.,* **2001**, *9*, 2295-2301.

128. Marino, J.P. and Zhao, C. Synthesis of HIV-1 Psi-site RNA sequences with site specific incorporation of the fluorescent base analog 2-aminopurine. *Tetrahedron,* **2007**, *63*, 3575-3584.

129. Johnson, N.P., Baase, W.A. and von Hippel, P.H. Low-energy circular dichroism of 2-aminopurine dinucleotide as a probe of local conformation of DNA and RNA. *Proc. Natl. Acad. Sci. U S A,* **2004**, *101*, 3426-3431.

130. Fedoriw, A.M., Liu, H.Y., Anderson, V.E. and deHaseth, P.L. Equilibrium and kinetic parameters of the sequence-specific interaction of Escherichia coli RNA

polymerase with nontemplate strand oligodeoxyribonucleotides. *Biochemistry,* **1998**, *37*, 11971-11979.

131. Strainic, M.G., Sullivan, J.J., Velevis, A. and deHaseth, P.L. Promoter recognition by Escherichia coli RNA polymerase: Effects of the UP element on open complex formation and promoter clearance. *Biochemistry,* **1998**, *37*, 18074-18080.

132. Sullivan, J.J., Bjornson, K.P., Sowers, L.C. and deHaseth, P.L. Spectroscopic determination of open complex formation at promoters for Escherichia coli RNA polymerase. *Biochemistry,* **1997**, *36*, 8005-8012.

133. Nakano, S., Uotani, Y., Uenishi, K., Fujii, M. and Sugimoto, N. DNA base flipping by a base pair-mimic nucleoside. *Nucleic Acids Res.,* **2005**, *33*, 7111-7119.

134. Rachofsky, E.L., Seibert, E., Stivers, J.T., Osman, R. and Ross, J.B.A. Conformation and dynamics of abasic sites in DNA investigated by time-resolved fluorescence of 2-aminopurine. *Biochemistry,* **2001**, *40*, 957-967.

135. Sowers, L.C., Boulard, Y. and Fazakerley, G.V. Multiple structures for the 2-aminopurine-cytosine mispair. *Biochemistry,* **2000**, *39*, 7613-7620.

136. Guest, C.R., Hochstrasser, R.A., Sowers, L.C. and Millar, D.P. Dynamics of mismatched base-pairs in DNA. *Biochemistry,* **1991**, *30*, 3271-3279.

137. Sagher, D. and Strauss, B. Abasic sites from cytosine as termination signals for DNA-synthesis. *Nucleic Acids Res.,* **1985**, *13*, 4285-4298.

138. Stivers, J.T. 2-aminopurine fluorescence studies of base stacking interactions at abasic sites in DNA: metal-ion and base sequence effects. *Nucleic Acids Res.,* **1998**, *26*, 3837-3844.

139. Tor, Y., Tam, V.K. and Kwong, D. Fluorescent HIV-1 dimerization initiation site: Design, properties, and use for ligand discovery. *J. Am. Chem. Soc.,* **2007**, *129*, 3257-3266.

140. Pilch, D.S., Barbieri, C.M. and Kaul, M. Use of 2-aminopurine as a fluorescent tool for characterizing antibiotic recognition of the bacterial rRNA A-site. *Tetrahedron,* **2007**, *63*, 3567-3574.

141. Shandrick, S., Zhao, Q., Han, Q., Ayida, B.K., Takahashi, M., Winters, G.C., Simonsen, K.B., Vourloumis, D. and Hermann, T. Monitoring molecular recognition of the ribosomal decoding site. *Angew. Chem., Int. Ed.,* **2004**, *43*, 3177-3182.

142. Kaul, M., Barbieri, C.M. and Pilch, D.S. Fluorescence-based approach for detecting and characterizing anti biotic-induced conformational changes in ribosomal RNA: Comparing aminoglycoside binding to prokaryotic and eukaryotic ribosomal RNA sequences. *J. Am. Chem. Soc.,* **2004**, *126*, 3447-3453.

143. Marti, A.A., Jockusch, S., Li, Z.M., Ju, J.Y. and Turro, N.J. Molecular beacons with intrinsically fluorescent nucleotides. *Nucleic Acids Res.,* **2006**, *34*, e50.

144. Kelley, S.O. and Barton, J.K. Electron transfer between bases in double helical DNA. *Science,* **1999**, *283*, 375-381.

145. Nordlund, T.M. Sequence, structure and energy transfer in DNA. *Photochem. Photobiol.,* **2007**, *83*, 625-636.

146. O'Neill, M.A., Dohno, C. and Barton, J.K. Direct chemical evidence for charge transfer between photoexcited 2-aminopurine and guanine in duplex DNA. *J. Am. Chem. Soc.,* **2004**, *126*, 1316-1317.

147. Kawai, M., Lee, M.J., Evans, K.O. and Nordlund, T.M. Temperature and base sequence dependence of 2-aminopurine fluorescence bands in single- and double-stranded oligodeoxynucleotides. *J. Fluoresc.,* **2001**, *11*, 23-32.

148. Davis, S.P., Matsumura, M., Williams, A. and Nordlund, T.M. Position dependence of 2-aminopurine spectra in adenosine pentadeoxynucleotides. *J. Fluoresc.,* **2003**, *13*, 249-259.

149. Nordlund, T.M., Xu, D.G. and Evans, K.O. Excitation-energy transfer in DNA - Duplex melting and transfer from normal bases to 2-aminopurine. *Biochemistry,* **1993**, *32*, 12090-12095.

150. Seela, F. and Chen, Y.M. Oligonucleotides containing fluorescent 2'-deoxyisoinosine - Solid-phase synthesis and duplex stability. *Nucleic Acids Res.,* **1995**, *23*, 2499-2505.

151. Wierzchowski, J., WielgusKutrowska, B. and Shugar, D. Fluorescence emission properties of 8-azapurines and their nucleosides, and application to the kinetics of the reverse synthetic reaction of purine nucleoside phosphorylase. *Biochim. Biophys. Acta,* **1996**, *1290*, 9-17.

152. Seela, F., Jiang, D.W. and Xu, K.Y. 8-Aza-2 '-deoxyguanosine: Base pairing, mismatch discrimination and nucleobase anion fluorescence sensing in single-stranded and duplex DNA. *Org. Biomol. Chem.,* **2009**, *7*, 3463-3473.

153. Wierzchowski, J., Ogiela, M., Iwanska, B. and Shugar, D. Selective fluorescent and fluorogenic substrates for purine-nucleoside phosphorylases from various sources, and direct fluorimetric determination of enzyme levels in human and animal blood. *Anal. Chim. Acta,* **2002**, *472*, 63-74.

154. Scott, L.G., Da Costa, C.P. and Fedor, M.J. 8-Azaguanine reporter of purine ionization states in structured RNAs. *J. Am. Chem. Soc.,* **2007**, *129*, 3426-3432.

155. Seela, F. and Lampe, S. Synthesis, base pairing, and structural transitions of oligodeoxyribonucleotides containing 8-aza-2'-deoxyguanosine. *Helv. Chim. Acta,* **1994**, *77*, 1003-1017.

156. Secrist, J.A., Barrio, J.R. and Leonard, N.J. Fluorescent modification of adenosine-triphosphate with activity in enzyme-systems - 1,N6-Ethenoadenosine triphosphate. *Science,* **1972**, *175*, 646-647.

157. Secrist, J.A., Weber, G., Leonard, N.J. and Barrio, J.R. Fluorescent modification of adenosine-containing coenzymes - Biological-activities and spectroscopic properties. *Biochemistry,* **1972**, *11*, 3499-3506.

158. Seela, F., Schweinberger, E., Xu, K., Sirivolu, V.R., Rosemeyer, H. and Becker, E.M. 1,N-6-etheno-2 '-deoxytubercidin and pyrrolo-C: synthesis, base pairing, and fluorescence properties of 7-deazapurine nucleosides and oligonucleotides (vol 63, pg 3471, 2007). *Tetrahedron,* **2007**, *63*, 3471-3482.

159. Kool, E.T., Krueger, A.T., Lu, H.G. and Lee, A.H.F. Synthesis and properties of size-expanded DNAs: Toward designed, functional genetic systems. *Acc. Chem. Res.,* **2007**, *40*, 141-150.

160. Essigmann, J.M., Delaney, J.C., Gao, J.M., Liu, H.B., Shrivastav, N. and Kool, E.T. Efficient replication bypass of size-expanded DNA base pairs in bacterial cells. *Angew. Chem., Int. Ed.,* **2009**, *48*, 4524-4527.

161. Kool, E.T. and Krueger, A.T. Fluorescence of size-expanded DNA bases: Reporting on DNA sequence and structure with an unnatural genetic set. *J. Am. Chem. Soc.,* **2008**, *130*, 3989-3999.

162. Liu, H.B., Gao, J.M. and Kool, E.T. Size-expanded analogues of dG and dC: Synthesis and pairing properties in DNA. *J. Org. Chem.,* **2005**, *70*, 639-647.

163. Liu, H.B., Gao, J.M. and Kool, E.T. Helix-forming properties of size-expanded DNA, an alternative four-base genetic form. *J. Am. Chem. Soc.,* **2005**, *127*, 1396-1402.

164. Liu, H.B., Gao, J.M., Maynard, L., Saito, Y.D. and Kool, E.T. Toward a new genetic system with expanded dimensions: Size-expanded analogues of deoxyadenosine and thymidine. *J. Am. Chem. Soc.,* **2004**, *126*, 1102-1109.

165. Okamoto, A., Tanaka, K., Fukuta, T. and Saito, I. Design of base-discriminating fluorescent nucleoside and its application to T/C SNP typing. *J. Am. Chem. Soc.,* **2003**, *125*, 9296-9297.

166. Okamoto, A., Tanaka, K., Fukuta, T. and Saito, I. Cytosine detection by a fluorescein-labeled probe containing base-discriminating fluorescent nucleobase. *Chembiochem,* **2004**, *5*, 958-963.

167. Reynolds, J.R., Yang, Y.X., Cohn, P., Dyer, A.L., Eom, S.H., Castellano, R.K. and Xue, J.G. Blue-violet electroluminescence from a highly fluorescent purine. *Chem. Mater.,* **2010**, *22*, 3580-3582.

168. Yokoyama, S., Mitsui, T., Kimoto, M., Kawai, R. and Hirao, I. Characterization of fluorescent, unnatural base pairs. *Tetrahedron,* **2007**, *63*, 3528-3537.

169. Hirao, I., Kimoto, M., Mitsui, T. and Yokoyama, S. A unique fluorescent base analogue for the expansion of the genetic alphabet. *J. Am. Chem. Soc.,* **2010**, *132*, 4988-4989.

170. Seela, F., Zulauf, M., Sauer, M. and Deimel, M. 7-substituted 7-deaza-2 '-deoxyadenosines and 8-aza-7-deaza-2 '-deoxyadenosines: Fluorescence of DNA-base analogues induced by the 7-alkynyl side chain. *Helv. Chim. Acta,* **2000**, *83*, 910-927.

171. Knee, J.L., Zhao, Y. and Baranger, A.M. Characterization of two adenosine analogs as fluorescence probes in RNA. *Bioorg. Chem.,* **2008**, *36*, 271-277.

172. Kenfack, C.A., Piemont, E., Ben Gaied, N., Burger, A. and Mely, Y. Time-resolved fluorescent properties of 8-vinyl-deoxyadenosine and 2-amino-deoxyribosylpurine exhibit different sensitivity to their opposite base in duplexes. *J. Phys. Chem. B,* **2008**, *112*, 9736-9745.

173. Gaied, N.B., Glasser, N., Ramalanjaona, N., Beltz, H., Wolff, P., Marquet, R., Burger, A. and Mely, Y. 8-vinyl-deoxyadenosine, an alternative fluorescent nucleoside analog to 2'-deoxyribosyl-2-aminopurine with improved properties. *Nucleic Acids Res.,* **2005**, *33*, 1031-1039.

174. Grotli, M., Dyrager, C., Borjesson, K., Diner, P., Elf, A., Albinsson, B. and Wilhelmsson, L.M. Synthesis and photophysical characterisation of fluorescent 8-(1H-1,2,3-Triazol-4-yl)adenosine derivatives. *Eur. J. Org. Chem.,* **2009**, 1515-1521.

175. Wilhelmsson, L.M., Dierckx, A., Diner, P., El-Sagheer, A.H., Kumar, J.D., Brown, T. and Grotli, M. Characterization of photophysical and base-mimicking properties of a novel fluorescent adenine analogue in DNA. *Nucleic Acids Res.,* **2011**, *39*, 4513-4524.

176. Manderville, R.A., Sun, K.M., McLaughlin, C.K. and Lantero, D.R. Biomarkers for phenol carcinogen exposure act as pH-sensing fluorescent probes. *J. Am. Chem. Soc.,* **2007**, *129*, 1894-1895.

177. Wetmore, S.D., Schlitt, K.M., Millen, A.L. and Manderville, R.A. An indole-linked C8-deoxyguanosine nucleoside acts as a fluorescent reporter of Watson-Crick versus Hoogsteen base pairing. *Org. Biomol. Chem.,* **2011**, *9*, 1565-1571.

178. Dumas, A. and Luedtke, N.W. Fluorescence properties of 8-(2-pyridyl)guanine "2PyG" as compared to 2-aminopurine in DNA. *Chembiochem,* **2011**, *12*, 2044-2051.

179. Dumas, A. and Luedtke, N.W. Highly fluorescent guanosine mimics for folding and energy transfer studies. *Nucleic Acids Res.,* **2011**, *39*, 6825-6834.

180. Saito, Y., Matsumoto, K., Takahashi, N., Suzuki, A., Morii, T. and Saito, I. Design and synthesis of highly solvatochromic fluorescent 2 '-deoxyguanosine and 2 '-deoxyadenosine analogs. *Bioorg. Med. Chem. Lett.,* **2011**, *21*, 1275-1278.

181. Saito, Y., Koda, M., Shinohara, Y. and Saito, I. Synthesis and photophysical properties of 8-arylbutadienyl 2 '-deoxyguanosines. *Tetrahedron Lett.,* **2011**, *52*, 491-494.

182. Kawai, R., Kimoto, M., Ikeda, S., Mitsui, T., Endo, M., Yokoyama, S. and Hirao, L. Site-specific fluorescent labeling of RNA molecules by specific transcription using unnatural base pairs. *J. Am. Chem. Soc.,* **2005**, *127*, 17286-17295.

183. Hirao, I., Hikida, Y., Kimoto, M. and Yokoyama, S. Site-specific fluorescent probing of RNA molecules by unnatural base-pair transcription for local structural conformation analysis. *Nat. Protoc.,* **2010**, *5*, 1312-1323.

184. Hirao, I., Kimoto, M., Mitsui, T., Harada, Y., Sato, A. and Yokoyama, S. Fluorescent probing for RNA molecules by an unnatural base-pair system. *Nucleic Acids Res.,* **2007**, *35*, 5360-5369.

185. Dumas, A. and Luedtke, N.W. Site-specific control of N7-metal coordination in DNA using a fluorescent purine derivative. **2011**, *Submitted*.

186. Shinohara, Y., Matsumoto, K., Kugenuma, K., Morii, T., Saito, Y. and Saito, I. Design of environmentally sensitive fluorescent 2 '-deoxyguanosine containing arylethynyl moieties: Distinction of thymine base by base-discriminating fluorescent (BDF) probe. *Bioorg. Med. Chem. Lett.,* **2010**, *20*, 2817-2820.

187. Birnbaum, G.I., Lassota, P. and Shugar, D. 8-Chloroguanosine - Solid-state and solution conformations and their biological implications. *Biochemistry,* **1984**, *23*, 5048-5053.

188. Dias, E., Battiste, J.L. and Williamson, J.R. Chemical probe for glycosidic conformation in telomeric DNAs. *J. Am. Chem. Soc.,* **1994**, *116*, 4479-4480.

189. Xu, Y. and Sugiyama, H. Formation of the G-quadruplex and i-motif structures in retinoblastoma susceptibility genes (Rb). *Nucleic Acids Res.,* **2006**, *34*, 949-954.

190. Uesugi, S. and Ikehara, M. C-13 Magnetic-resonance spectra of 8-substituted purine nucleosides - Characteristics shifts for syn conformation. *J. Am. Chem. Soc.,* **1977**, *99*, 3250-3253.

191. Stolarski, R., Hagberg, C.E. and Shugar, D. Studies on the dynamic syn-anti equilibrium in purine nucleosides and nucleotides with the aid of H-1 and C-13 NMR-spectroscopy. *Eur. J. Biochem.,* **1984**, *138*, 187-192.

192. He, G.X., Krawczyk, S.H., Swaminathan, S., Shea, R.G., Dougherty, J.P., Terhorst, T., Law, V.S., Griffin, L.C., Coutre, S. and Bischofberger, N. N-2- and C-8-substituted oligodeoxynucleotides with enhanced thrombin inhibitory activity in vitro and in vivo. *J. Med. Chem.,* **1998**, *41*, 2234-2242.

193. Millen, A.L., Churchill, C.D.M., Manderville, R.A. and Wetmore, S.D. Effect of Watson-Crick and Hoogsteen base pairing on the conformational stability of C8-phenoxyl-2 '-deoxyguanosine adducts. *J. Phys. Chem. B,* **2010**, *114*, 12995-13004.

194. Millen, A.L., Manderville, R.A. and Wetmore, S.D. Conformational flexibility of C8-phenoxyl-2 '-deoxyguanosine nucleotide adducts. *J. Phys. Chem. B,* **2010**, *114*, 4373-4382.

195. Millen, A.L., McLaughlin, C.K., Sun, K.M., Manderville, R.A. and Wetmore, S.D. Computational and experimental evidence for the structural preference of phenolic C-8 purine adducts. *J. Phys. Chem. A,* **2008**, *112*, 3742-3753.

196. Western, E.C., Daft, J.R., Johnson, E.M., Gannett, P.M. and Shaughnessy, K.H. Efficient one-step Suzuki arylation of unprotected halonucleosides, using water-soluble palladium catalysts. *J. Org. Chem.,* **2003**, *68*, 6767-6774.

197. Western, E.C. and Shaughnessy, K.H. Inhibitory effects of the guanine moiety on Suzuki couplings of unprotected halonucleosides in aqueous media. *J. Org. Chem.,* **2005**, *70*, 6378-6388.

198. Deng, J.Z., Paone, D.V., Ginnetti, A.T., Kurihara, H., Dreher, S.D., Weissman, S.A., Stauffer, S.R. and Burgey, C.S. Copper-facilitated suzuki reactions: Application to 2-heterocyclic boronates. *Org. Lett.,* **2009**, *11*, 345-347.

199. Billingsley, K.L. and Buchwald, S.L. A general and efficient method for the Suzuki-Miyaura coupling of 2-pyridyl nucleophiles. *Angew. Chem., Int. Ed.,* **2008**, *47*, 4695-4698.

200. Deng, F., Kubin, J. and Testa, A.C. Deuterium isotope effects on the fluorescence of phenylpyridines. *J. Photoch. Photobio. A,* **1997**, *104*, 65-67.

201. Lakowicz, J.R. *Principles of fluorescence spectroscopy*. **1999**, Second ed. Kluwer Academic/Plenum Publishers, New York.

202. Reichardt, C. Solvatochromic dyes as solvent polarity indicators. *Chem. Rev.,* **1994**, *94*, 2319-2358.

203. Sinkeldam, R.W. and Tor, Y. To D or not to D? On estimating the microenvironment polarity of biomolecular cavities. *Org. Biomol. Chem.,* **2007**, *5*, 2523-2528.

204. Wypych, G. *Handbook of solvents*. **2001**. ChemTec Publishing.

205. Lim, K.W., Amrane, S., Bouaziz, S., Xu, W., Mu, Y., Patel, D.J., Luu, K.N. and Phan, A.T. Structure of the human telomere in K+ solution: a stable basket-type G-quadruplex with only two G-tetrad layers. *J. Am. Chem. Soc.,* **2009**, *131*, 4301-4309.

206. Luu, K.N., Phan, A.T., Kuryavyi, V., Lacroix, L. and Patel, D.J. Structure of the human telomere in K+ solution: an intramolecular (3 + 1) G-quadruplex scaffold. *J. Am. Chem. Soc.,* **2006**, *128*, 9963-9970.

207. Li, J., Correia, J.J., Wang, L., Trent, J.O. and Chaires, J.B. Not so crystal clear: the structure of the human telomere G-quadruplex in solution differs from that present in a crystal. *Nucleic Acids Res.,* **2005**, *33*, 4649-4659.

208. Wang, Y. and Patel, D.J. Solution structure of the human telomeric repeat d[AG(3)(T(2)AG(3))3] G-tetraplex. *Structure,* **1993**, *1*, 263-282.

209. Todd, A.K., Haider, S.M., Parkinson, G.N. and Neidle, S. Sequence occurrence and structural uniqueness of a G-quadruplex in the human c-kit promoter. *Nucleic Acids Res.,* **2007**, *35*, 5799-5808.

210. Phan, A.T., Modi, Y.S. and Patel, D.J. Propeller-type parallel-stranded G-quadruplexes in the human c-Myc promoter. *J. Am. Chem. Soc.,* **2004**, *126*, 8710-8716.

211. Yarden, Y., Kuang, W.J., Yangfeng, T., Coussens, L., Munemitsu, S., Dull, T.J., Chen, E., Schlessinger, J., Francke, U. and Ullrich, A. Human protooncogene c-Kit - A new cell-surface receptor tyrosine kinase for an unidentified ligand. *EMBO J.,* **1987**, *6*, 3341-3351.

212. Marcu, K.B., Bossone, S.A. and Patel, A.J. Myc function and regulation. *Annu. Rev. Biochem.,* **1992**, *61*, 809-860.

213. Dang, C.V. c-myc target genes involved in cell growth, apoptosis, and metabolism. *Mol. Cell. Biol.,* **1999**, *19*, 1-11.

214. Petraccone, L., Erra, E., Duro, I., Esposito, V., Randazzo, A., Mayol, L., Mattia, C.A., Barone, G. and Giancola, C. Relative stability of quadruplexes containing different number of G-tetrads. *Nucleosides Nucleotides Nucleic Acids,* **2005**, *24*, 757-760.

215. Bardin, C., Canalia, M. and Leroy, J.L. The formation pathway of tetrameric oligonucleotide structures. *J. Biomol. Struct. Dyn.,* **2007**, *24*, 711-712.

216. Esposito, V., Randazzo, A., Piccialli, G., Petraccone, L., Giancola, C. and Mayol, L. Effects of an 8-bromodeoxyguanosine incorporation on the parallel quadruplex structure [d(TGGGT)](4). *Org. Biomol. Chem.,* **2004**, *2*, 313-318.

217. Virgilio, A., Esposito, V., Randazzo, A., Mayol, L. and Galeone, A. 8-Methyl-2'-deoxyguanosine incorporation into parallel DNA quadruplex structures. *Nucleic Acids Res.,* **2005**, *33*, 6188-6195.

218. Lane, A.N., Chaires, J.B., Gray, R.D. and Trent, J.O. Stability and kinetics of G-quadruplex structures. *Nucleic Acids Res.,* **2008**, *36*, 5482-5515.

219. Rai, P., Cole, T.D., Thompson, E., Millar, D.P. and Linn, S. Steady-state and time-resolved fluorescence studies indicate an unusual conformation of 2-aminopurine within ATAT and TATA duplex DNA sequences. *Nucleic Acids Res.,* **2003**, *31*, 2323-2332.

220. Masiero, S., Trotta, R., Pieraccini, S., De Tito, S., Perone, R., Randazzo, A. and Spada, G.P. A non-empirical chromophoric interpretation of CD spectra of DNA G-quadruplex structures. *Org. Biomol. Chem.,* **2010**, *8*, 2683-2692.

221. Gray, D.M., Wen, J.D., Gray, C.W., Repges, R., Repges, C., Raabe, G. and Fleischhauer, J. Measured and calculated CD spectra of G-quartets stacked with the same or opposite polarities. *Chirality,* **2008**, *20*, 431-440.

222. Balagurumoorthy, P., Brahmachari, S.K., Mohanty, D., Bansal, M. and Sasisekharan, V. Hairpin and parallel quartet structures for telomeric sequences. *Nucleic Acids Res.,* **1992**, *20*, 4061-4067.

223. Chen, C.J. and Russu, I.M. Sequence-dependence of the energetics of opening of AT basepairs in DNA. *Biophys. J.,* **2004**, *87*, 2545-2551.

224. Searle, M.S. and Williams, D.H. On the stability of nucleic-acid structures in solution - Enthalpy entropy compensations, internal rotations and reversibility. *Nucleic Acids Res.,* **1993**, *21*, 2051-2056.

225. Narayanan, M., Kodali, G., Xing, Y.J. and Stanley, R.J. Photoinduced electron transfer occurs between 2-aminopurine and the DNA nucleic acid monophosphates: Results from cyclic voltammetry and fluorescence quenching. *J. Phys. Chem. B,* **2010**, *114*, 10573-10580.

226. Davis, J.T. G-quartets 40 years later: From 5 '-GMP to molecular biology and supramolecular chemistry. *Angew. Chem., Int. Ed.,* **2004**, *43*, 668-698.

227. Neidle, S. and Parkinson, G.N. Quadruplex DNA crystal structures and drug design. *Biochimie,* **2008**, *90*, 1184-1196.

228. Maizels, N. Dynamic roles for G4 DNA in the biology of eukaryotic cells. *Nat. Struct. Mol. Biol.,* **2006**, *13*, 1055-1059.

229. Oganesian, L. and Bryan, T.M. Physiological relevance of telomeric G-quadruplex formation: a potential drug target. *BioEssays,* **2007**, *29*, 155-165.

230. Hershman, S.G., Chen, Q., Lee, J.Y., Kozak, M.L., Yue, P., Wang, L.S. and Johnson, F.B. Genomic distribution and functional analyses of potential G-quadruplex-forming sequences in Saccharomyces cerevisiae. *Nucleic Acids Res.,* **2008**, *36*, 144-156.

231. Luedtke, N.W. Targeting G-quadruplex DNA with small molecules. *Chimia,* **2009**, *63*, 134-139.

232. Sessler, J.L., Sathiosatham, M., Doerr, K., Lynch, V. and Abboud, K.A. A G-quartet formed in the absence of a templating metal cation: A new 8-(N,N-dimethylaniline)guanosine derivative. *Angew. Chem., Int. Ed.,* **2000**, *39*, 1300-1303.

233. Calzolari, A., Di Felice, R., Molinari, E. and Garbesi, A. G-quartet biomolecular nanowires. *Appl. Phys. Lett.,* **2002**, *80*, 3331-3333.

234. Davis, J.T. and Spada, G.P. Supramolecular architectures generated by self-assembly of guanosine derivatives. *Chem. Soc. Rev.,* **2007**, *36*, 296-313.

235. Karimata, H., Miyoshi, D., Fujimoto, T., Koumoto, K., Wang, Z.M. and Sugimoto, N. Conformational switch of a functional nanowire based on the DNA G-quadruplex. *Nucleic Acids Symp. Ser.,* **2007**, 251-252.

236. Borovok, N., Iram, N., Zikich, D., Ghabboun, J., Livshits, G.I., Porath, D. and Kotlyar, A.B. Assembling of G-strands into novel tetra-molecular parallel G4-DNA nanostructures using avidin-biotin recognition. *Nucleic Acids Res.,* **2008**, *36*, 5050-5060.

237. Betancourt, J.E. and Rivera, J.M. Nonpolymeric thermosensitive supramolecules. *J. Am. Chem. Soc.,* **2009**, *131*, 16666-16668.

238. Rivera-Sanchez Mdel, C., Andujar-de-Sanctis, I., Garcia-Arriaga, M., Gubala, V., Hobley, G. and Rivera, J.M. Walking a supramolecular tightrope: a self-assembled dodecamer from an 8-aryl-2'-deoxyguanosine derivative. *J. Am. Chem. Soc.,* **2009**, *131*, 10403-10405.

239. Delaney, S. and Barton, J.K. Charge transport in DNA duplex/quadruplex conjugates. *Biochemistry,* **2003**, *42*, 14159-14165.

240. Chinnapen, D.J.F. and Sen, D. A deoxyribozyme that harnesses light to repair thymine dimers in DNA. *Proc. Natl. Acad. Sci. U S A,* **2004**, *101*, 65-69.

241. Huang, Y.C., Cheng, A.K., Yu, H.Z. and Sen, D. Charge conduction properties of a parallel-stranded DNA G-quadruplex: implications for chromosomal oxidative damage. *Biochemistry,* **2009**, *48*, 6794-6804.

242. Alberti, P., Bourdoncle, A., Sacca, B., Lacroix, L. and Mergny, J.L. DNA nanomachines and nanostructures involving quadruplexes. *Org. Biomol. Chem.,* **2006**, *4*, 3383-3391.

243. Alberti, P. and Mergny, J.L. DNA duplex-quadruplex exchange as the basis for a nanomolecular machine. *Proc. Natl. Acad. Sci. U S A,* **2003**, *100*, 1569-1573.

244. Lubitz, I., Borovok, N. and Kotlyar, A. Interaction of monomolecular G4-DNA nanowires with TMPyP: evidence for intercalation. *Biochemistry,* **2007**, *46*, 12925-12929.

245. O'Neill, M.A. and Barton, J.K. Effects of strand and directional asymmetry on base-base coupling and charge transfer in double-helical DNA. *Proc. Natl. Acad. Sci. U S A,* **2002**, *99*, 16543-16550.

246. Miyoshi, D., Nakao, A. and Sugimoto, N. Molecular crowding regulates the structural switch of the DNA G-quadruplex. *Biochemistry,* **2002**, *41*, 15017-15024.

247. Kan, Z.Y., Yao, Y.A., Wang, P., Li, X.H., Hao, Y.H. and Tan, Z. Molecular crowding induces telomere G-quadruplex formation under salt-dericient conditions and enhances its competition with duplex formation. *Angew. Chem., Int. Ed.,* **2006**, *45*, 1629-1632.

248. Nagatoishi, S., Tanaka, Y. and Tsumoto, K. Circular dichroism spectra demonstrate formation of the thrombin-binding DNA aptamer G-quadruplex under stabilizing-cation-deficient conditions. *Biochem. Biophys. Res. Commun.,* **2007**, *354*, 837-838.

249. Zhou, J., Wei, C.Y., Jia, G.Q., Wang, X.L., Tang, Q., Feng, Z.C. and Li, C. The structural transition and compaction of human telomeric G-quadruplex induced by excluded volume effect under cation-deficient conditions. *Biophys. Chem.,* **2008**, *136*, 124-127.

250. Gabelica, V., Rosu, F., De Pauw, E., Lemaire, J., Gillet, J.C., Poully, J.C., Lecomte, F., Gregoire, G., Schermann, J.P. and Desfrancois, C. Infrared signature of DNA G-quadruplexes in the gas phase. *J. Am. Chem. Soc.,* **2008**, *130*, 1810-1811.

251. Lebreton, P.R., Yang, X., Urano, S., Fetzer, S., Yu, M., Leonard, N.J. and Kumar, S. Photoemission properties of methyl-substituted guanines - Photoelectron and fluorescence investigations of 1,9-dimethylguanine, O-6,9-dimethylguanine, and 9-methylguanine. *J. Am. Chem. Soc.,* **1990**, *112*, 2138-2147.

252. Zhang, Y., Wang, J., Jia, P., Yu, X., Liu, H., Liu, X., Zhao, N. and Huang, B. Two-photon fluorescence imaging of DNA in living plant turbid tissue with carbazole dicationic salt. *Org. Biomol. Chem.,* **2010**, *8*, 4582-4588.

253. Wanninger-Weiss, C., Valis, L. and Wagenknecht, H.A. Pyrene-modified guanosine as fluorescent probe for DNA modulated by charge transfer. *Bioorg. Med. Chem.,* **2008**, *16*, 100-106.

254. Narayanan, M., Kodali, G., Xing, Y.J., Hawkins, M.E. and Stanley, R.J. Differential fluorescence quenching of fluorescent nucleic acid base analogues by native nucleic acid monophosphates. *J. Phys. Chem. B,* **2010**, *114*, 5953-5963.

255. Doudna, J.A. and Cech, T.R. The chemical repertoire of natural ribozymes. *Nature,* **2002**, *418*, 222-228.

256. Muller, J. Functional metal ions in nucleic acids. *Metallomics,* **2010**, *2*, 318-327.

257. Schnabl, J. and Sigel, R.K.O. Controlling ribozyme activity by metal ions. *Curr. Opin. Chem. Biol.,* **2010**, *14*, 269-275.

258. Hud, N. *Nucleic acid-metal ion interactions*. **2008**. RSC Biomolecular Sciences, Springer.

259. Hadjiliadis, N. and Sletten, E. *Metal complex-DNA interactions*. **2009**. John Wiley & Sons.

260. de Silva, A.P. and McClenaghan, N.D. Molecular-scale logic gates. *Chem.-Eur. J.,* **2004**, *10*, 574-586.

261. Richards, A.D. and Rodger, A. Synthetic metallomolecules as agents for the control of DNA structure. *Chem. Soc. Rev.,* **2007**, *36*, 471-483.

262. Seeman, N.C. An overview of structural DNA Nanotechnology. *Mol. Biotechnol.,* **2007**, *37*, 246-257.

263. Fournier, P., Fiammengo, R. and Jaschke, A. Allylic amination by a DNA-diene-iridium(I) hybrid catalyst. *Angew. Chem., Int. Ed.,* **2009**, *48*, 4426-4429.

264. Modi, S., Bhatia, D., Simmel, F.C. and Krishnan, Y. Structural DNA nanotechnology: From bases to bricks, from structure to function. *J. Phys. Chem. Lett.,* **2010**, *1*, 1994-2005.

265. Feringa, B.L., Boersma, A.J., Megens, R.P. and Roelfes, G. DNA-based asymmetric catalysis. *Chem. Soc. Rev.,* **2010**, *39*, 2083-2092.

266. Bandy, T.J., Brewer, A., Burns, J.R., Marth, G., Nguyen, T. and Stulz, E. DNA as supramolecular scaffold for functional molecules: progress in DNA nanotechnology. *Chem. Soc. Rev.,* **2011**, *40*, 138-148.

267. Reiner, B. and Zamenhof, S. Studies on the chemically reactive groups of deoxyribonucleic acids. *J. Biol. Chem.,* **1957**, *228*, 475-486.

268. Lippert, B. Multiplicity of metal ion binding patterns to nucleobases. *Coord. Chem. Rev.,* **2000**, *200*, 487-516.

269. Anastassopoulou, J. Metal-DNA interactions. *J. Mol. Struct.,* **2003**, *651*, 19-26.

270. Jamieson, E.R. and Lippard, S.J. Structure, recognition, and processing of cisplatin-DNA adducts. *Chem. Rev.,* **1999**, *99*, 2467-2498.

271. Lippert, B. *Cisplatin chemistry and biochemistry of a leading anticancer drug*. **1999**. Wiley-VCH.

272. Eastman, A. Interstrand cross-links and sequence specificity in the reaction of cis-dichloro(ethylenediamine)platinum(II) with DNA. *Biochemistry,* **1985**, *24*, 5027-5032.

273. Monjardet-Bas, V., Chottard, J.C. and Kozelka, J. Fast interstrand cross-linking of cisplatin-DNA monoadducts compared with intrastrand chelation: a kinetic study using hairpin-stabilized duplex oligonucleotides. *Chemistry,* **2002**, *8*, 1144-1150.

274. Waalkes, M.P. and Poirier, L.A. In vitro cadmium DNA interactions - Cooperativity of cadmium binding and competitive antagonism by calcium, magnesium, and zinc. *Toxicol. Appl. Pharmacol.,* **1984**, *75*, 539-546.

275. Kasprzak, K.S., Waalkes, M.P. and Poirier, L.A. Antagonism by essential divalent metals and amino-acids of nickel(Ii) - DNA-binding in vitro. *Toxicol. Appl. Pharmacol.,* **1986**, *82*, 336-343.

276. Sayenko, G.N., Babii, A.P. and Bagaveyev, I.A. Change in the UV spectra of Copper-II complexes with native DNA with the ionic strength of solution. *Biophysics,* **1987**, *31*, 451-456.

277. Alex, S. and Dupuis, P. FT-IR and Raman investigation of cadmium binding by DNA. *Inorg. Chim. Acta,* **1989**, *157*, 271-281.

278. Swiatek, J. and Gulanowski, B. Some aspects of lead(II) DNA interactions. *Acta Biochim. Pol.,* **1990**, *37*, 7-20.

279. Sagripanti, J.L., Goering, P.L. and Lamanna, A. Interaction of copper with DNA and antagonism by other metals. *Toxicol. Appl. Pharmacol.,* **1991**, *110*, 477-485.

280. Zhang, L.Z. and Cheng, P. Study of Ni(II) ion-DNA interactions with methylene blue as fluorescent probe. *J. Inorg. Biochem.,* **2004**, *98*, 569-574.

281. Gelagutashvili, E. Interaction of Cu(II) and Cd(II) ions with DNA from Spirulina platensis. *J. Them. Anal. Calorim.,* **2006**, *85*, 491-494.

282. Purugganan, M.D., Kumar, C.V., Turro, N.J. and Barton, J.K. Accelerated electron-transfer between metal-complexes mediated by DNA. *Science,* **1988**, *241*, 1645-1649.

283. Stinner, C., Wightman, M.D., Kelley, S.O., Hill, M.G. and Barton, J.K. Synthesis and spectroelectrochemistry of Ir(bpy)(phen)(phi)(3+), a tris(heteroleptic) metallointercalator. *Inorg. Chem.,* **2001**, *40*, 5245-5250.

284. Ossipov, D., Pradeepkumar, P.I., Holmer, M. and Chattopadhyaya, J. Synthesis of [Ru(phen)(2)dppz](2+)-tethered oligo-DNA and studies on the metallointercalation mode into the DNA duplex. *J. Am. Chem. Soc.,* **2001**, *123*, 3551-3562.

285. Murphy, C.J., Arkin, M.R., Jenkins, Y., Ghatlia, N.D., Bossmann, S.H., Turro, N.J. and Barton, J.K. Long-range photoinduced electron-transfer through a DNA helix. *Science,* **1993**, *262*, 1025-1029.

286. Meade, T.J. and Kayyem, J.F. Electron-transfer through DNA - Site-specific modification of duplex DNA with ruthenium donors and acceptors. *Angew. Chem., Int. Ed. Engl.,* **1995**, *34*, 352-354.

287. Dandliker, P.J., Holmlin, R.E. and Barton, J.K. Oxidative thymine dimer repair in the DNA helix. *Science,* **1997**, *275*, 1465-1468.

288. Krider, E.S., Rack, J.J., Frank, N.L. and Meade, T.J. Automated synthesis of 3 '-metalated oligonucleotides. *Inorg. Chem.,* **2001**, *40*, 4002-4009.

289. Shao, F.W. and Barton, J.K. Long-range electron and hole transport through DNA with tethered cyclometalated iridium(III) complexes. *J. Am. Chem. Soc.,* **2007**, *129*, 14733-14738.

290. Hurley, D.J. and Tor, Y. Metal-containing oligonucleotides: Solid-phase synthesis and luminescence properties. *J. Am. Chem. Soc.,* **1998**, *120*, 2194-2195.

291. Weizman, H. and Tor, Y. Redox-active metal-containing nucleotides: Synthesis, tunability, and enzymatic incorporation into DNA. *J. Am. Chem. Soc.,* **2002**, *124*, 1568-1569.

292. Hurley, D.J. and Tor, Y. Donor/acceptor interactions in systematically modified Ru-II-Os-II oligonucleotides. *J. Am. Chem. Soc.,* **2002**, *124*, 13231-13241.

293. Khan, S.I., Beilstein, A.E., Smith, G.D., Sykora, M. and Grinstaff, M.W. Synthesis and excited-state properties of a novel ruthenium nucleoside: 5-[Ru(bpy)(2)(4-m-4 '-pa-bpy)](2+)-2 '-deoxyuridine. *Inorg. Chem.,* **1999**, *38*, 2411-2415.

294. Hocek, M., Stepnicka, P., Ludvik, J., Cisarova, I., Votruba, I., Reha, D. and Hobza, P. Ferrocene-modified purines as potential electrochemical markers: Synthesis, crystal structures, electrochemistry and cytostatic activity of (ferrocenylethynyl)- and (ferrocenylethyl)purines. *Chem.-Eur. J.,* **2004**, *10*, 2058-2066.

295. Vrabel, M., Pohl, R., Klepetarova, B., Votruba, I. and Hocek, M. Synthesis of 2 '-deoxyadenosine nucleosides bearing bipyridine-type ligands and their Ru-complexes in position 8 through cross-coupling reactions. *Org. Biomol. Chem.,* **2007**, *5*, 2849-2857.

296. Vrabel, M., Pohl, R., Votruba, I., Sajadi, M., Kovalenko, S.A., Ernsting, N.P. and Hocek, M. Synthesis and photophysical properties of 7-deaza-2 '-deoxyadenosines bearing bipyridine ligands and their Ru(II)-complexes in position 7. *Org. Biomol. Chem.,* **2008**, *6*, 2852-2860.

297. Redon, S., Bombard, S., Elizondo-Riojas, M.A. and Chottard, J.C. Platination of the (T(2)G(4))(4) telomeric sequence: A structural and cross-linking study. *Biochemistry,* **2001**, *40*, 8463-8470.

298. Ourliac Garnier, I. and Bombard, S. GG sequence of DNA and the human telomeric sequence react with cis-diammine-diaquaplatinum at comparable rates. *J. Inorg. Biochem.,* **2007**, *101*, 514-524.

299. Bertrand, H., Bombard, S., Monchaud, D., Talbot, E., Guedin, A., Mergny, J.L., Grunert, R., Bednarski, P.J. and Teulade-Fichou, M.P. Exclusive platination of loop adenines in the human telomeric G-quadruplex. *Org. Biomol. Chem.,* **2009**, *7*, 2864-2871.

300. Zhu, S.R., Matilla, A., Tercero, J.M., Vijayaragavan, V. and Walmsley, J.A. Binding of palladium(II) complexes to guanine, guanosine or guanosine 5 '-monophosphate in aqueous solution: potentiometric and NMR studies. *Inorg. Chim. Acta,* **2004**, *357*, 411-420.

301. Noguera, M., Branchadell, V., Constantino, E., Rios-Font, R., Sodupe, M. and Rodriguez-Santiago, L. On the bonding of first-row transition metal cations to guanine and adenine nucleobases. *J. Phys. Chem. A,* **2007**, *111*, 9823-9829.

302. Kiss, A., Farkas, E., Sovago, I., Thormann, B. and Lippert, B. Solution equilibria of the ternary complexes of [Pd(dien)Cl](+) and [Pd(terpy)Cl](+) with nucleobases and N-acetyl amino acids. *J. Inorg. Biochem.,* **1997**, *68*, 85-92.

303. Collier, A. and Wagner, G. A facile two-step synthesis of 8-arylated guanosine mono- and triphosphates (8-aryl GXPs). *Org. Biomol. Chem.,* **2006**, *4*, 4526-4532.

304. Lin, X.J., Shen, Z., Xu, H.J., Li, Y.Z., Zhang, H.T. and You, X.Z. A binuclear tetrahedral zinc(II) complex of 2-(2-pyridyl)benzo[1,2-d;4,5-d ']diimidazole with strong blue fluorescence. *Inorg. Chem. Comm.,* **2004**, *7*, 1167-1169.

305. Yue, S.M., Xu, H.B., Ma, J.F., Su, Z.M., Kan, Y.H. and Zhang, H.J. Design and syntheses of blue luminescent zinc(II) and cadmium(II) complexes with bidentate or tridentate pyridyl-imidazole ligands. *Polyhedron,* **2006**, *25*, 635-644.

306. De la Durantaye, L., McCormick, T., Liu, X.Y. and Wang, S.N. Interaction of 2-(2 '-pyridyl)benzimidazolyl derivative ligands with group 12 metal ions: coordination, structures and luminescence. *Dalton Trans.,* **2006**, 5675-5682.

307. Zhong, C.F., Guo, R.F., Wu, Q. and Zhang, H.L. Design and syntheses of blue luminescent Cu(II) and Zn(II) polymeric complexes with 2-(2 '-pyridyl)benzimidazole derivative ligand. *React. Funct. Polym.,* **2007**, *67*, 408-415.

308. Lan, Y.Q., Li, S.L., Fu, Y.M., Xu, Y.H., Li, L., Su, Z.M. and Fu, Q. d(10)-Metal coordination polymers based on analogue di(pyridyl) imidazole derivatives and 4,4 '-oxydibenzoic acid: influence of flexible and angular characters of neutral ligands on structural diversity. *Dalton Trans.,* **2008**, 6796-6807.

309. Weizman, H. and Tor, Y. Oligo-ligandosides: a DNA mimetic approach to helicate formation. *Chemical Communications,* **2001**, 453-454.

310. Atwell, S., Meggers, E., Spraggon, G. and Schultz, P.G. Structure of a copper-mediated base pair in DNA. *J. Am. Chem. Soc.,* **2001**, *123*, 12364-12367.

311. Carell, T., Tanaka, K., Clever, G.H., Takezawa, Y., Yamada, Y., Kaul, C. and Shionoya, M. Programmable self-assembly of metal ions inside artificial DNA duplexes. *Nat. Nanotechnol.,* **2006**, *1*, 190-195.

312. Switzer, C. and Shin, D.W. A metallo base-pair incorporating a terpyridyl-like motif: bipyridylpyrimidinone center dot Ag(I)center dot 4-pyridine. *Chemical Communications,* **2007**, 4401-4403.

313. Shionoya, M., Takezawa, Y., Maeda, W. and Tanaka, K. Discrete self-assembly of iron(III) ions inside triple-stranded artificial DNA. *Angew. Chem., Int. Ed.,* **2009**, *48*, 1081-1084.

314. Schiemann, O., Clever, G.H., Reitmeier, S.J. and Carell, T. Antiferromagnetic coupling of stacked Cu(II)-salen complexes in DNA. *Angew. Chem., Int. Ed.,* **2010**, *49*, 4927-4929.

315. Sigel, R.K.O., Johannsen, S., Megger, N., Bohme, D. and Muller, J. Solution structure of a DNA double helix with consecutive metal-mediated base pairs. *Nat. Chem.,* **2010**, *2*, 229-234.

316. Mergny, J.L., De Cian, A., Ghelab, A., Sacca, B. and Lacroix, L. Kinetics of tetramolecular quadruplexes. *Nucleic Acids Res.,* **2005**, *33*, 81-94.